Purification of Nitrogen Containing Feedstreams

Mark Leslie Gerrard

A thesis submitted in partial fulfilment of the requirements of The Nottingham Trent University for the degree of Doctor of Philosophy

September 2000

Abstract

Organic nitrogen present in crude oil must be removed before many refining processes can be performed. The continuous drive towards more efficient refineries, combined with a movement toward cleaner, less environmentally polluting fuels is increasing the pressure on existing nitrogen removal technologies. Traditionally nitrogen is removed by hydrotreating over a Co (Ni)-Mo based catalyst which, in the case of naphtha, lowers the nitrogen content from ~ 20 ppm to ~ 0.5 ppm. Further reduction is very difficult to achieve. The use of an adsorbent may be a solution to this problem. With a catalytic process each incremental decrease in nitrogen concentration becomes exponentially more difficult and expensive, whereas with an adsorbent the reverse is true. The ideal adsorbent should be able to selectively adsorb organic nitrogen compounds at a reasonable operating temperature without altering the remaining hydrocarbon stream.

In this work potential adsorbents have been studied using a model system of 10 ppm pyridine in heptane. Experimental conditions have been chosen which approximate to an industrial application. The primary characterisation technique used was FTIR of adsorbed pyridine, in addition to N_2 adsorption, XRD and TEM.

Supported metal sulfates and modified aluminas were found to have low adsorption capacities at the operational temperature of 200 °C; the most effective samples adsorbing 0.2 – 0.3 wt % pyridine. Amorphous silica aluminas have adsorption capacities of up to 0.6 wt %. MCM-41 materials have been shown to have adsorption capacities up to 1.0 wt % and have successfully been regenerated and re-used with only a 10 % reduction in capacity. Zeolite X, mordenite, and ZSM-5 have also been studied. Zeolites in the Na^+ form are ineffective, either because the Na^+ acid sites are not strong enough to retain pyridine under the experimental conditions or because of selective coking. Zeolites in the H^+ or Cu^{2+} forms have high adsorption capacities: up to 2.5 wt %

Acknowledgements

Firstly I would like to thank my supervisors Dr J. S. J. Hargreaves and Professor R. W. Joyner for their continual support throughout my project, as without their guidance none of this would have been possible. I am also very grateful to my industrial supervisors Dr B. P. Williams and Dr N. Young at ICI Katalco for their guidance and encouragement.

I would like to thank Miss N. Goy and Mr G. Richefond: both final year project students working with me, and also Dr M. Stockenhuber for useful discussions about the FTIR work, as well as all other members of the Catalysis Research Centre both past and present

I would also like to thank Dr C. Kiely of the University of Liverpool for performing the electron microscopy in chapter 6.

I am very grateful to my parents, friends and family for their support and encouragement.

I would especially like to thank Sarah for her help, support and understanding throughout this ordeal, and also her family.

I would like also to thank ICI Katalco and the EPSRC for their financial support.
Lastly I would like to thank Pete and Larry in the workshop for almost continually fixing the FTIR cell.

Contents

Chapter 1 Introduction

It is generally accepted that hydrocarbons derive from fossil organic substances synthesised by higher plants on land and by algae and plankton in the ocean, accumulated in depressions, partly modified by the action of bacteria, and known under the generic term of kerogen. Shale oil consists of kerogen imprisoned in sedimentary rocks buried in shallow strata. When these rocks, through geological movements are buried at depths of many thousands of metres they are transformed into conventional crude oil, under the action of temperature, up to 110°C, and pressure. Nitrogen compounds in living matter are mainly amino acids and porphyrin-like molecules. The transformation of these molecules during the genesis of kerogen gives mainly pseudo-polymeric structures containing nitrogen in heterocycles, for the most part aromatic. During the formation of conventional petrol these structures will better resist bond ruptures than the C-S and C-C bonds and will remain in the rocks; the result will be a low nitrogen content (0.1-0.2wt%) in conventional oil [1]. The degradation of this oil by bacteria feeding on alkanes will enrich the relative amount of nitrogen compounds (which explains the variation of nitrogen concentration with the origin of the oil - approximately 0.9wt% for a Caribbean crude [2]). Thermal and high pressure treatments inflicted on coal or oil shale in order to obtain synthetic oils, simulating the natural formation of petrol, will result in many more nitrogen compounds because the higher temperature used to accelerate the natural process, diminishes the resistance of the polymeric structures previously described.

Although there has been very little work carried out on identifying the individual nitrogen compounds in the petrol fraction, it is generally agreed that the nitrogen concentration increases with increasing boiling point of the petroleum fraction. The higher boiling point / higher molecular mass oil fractions contain the higher boiling, higher mass nitrogen compounds. Ledoux [1] determined that the nitrogen compounds found in naphtha (80-160°C), are mainly aniline and alkylanilines with traces of pyridine and quinoline. In this article the total nitrogen concentration in naphtha is quoted as <15ppm. McKetta [3] determined that the nitrogen content of

virgin naphtha is around 0.3-2ppm although in cracked naphtha it will be significantly higher. The exact concentration will depend on the exact boiling range meant by the term 'naphtha' and the source of the crude oil. Nitrogen compounds in oil cause poisoning of catalysts in the refining process and will contribute to NO_x emissions if they are retained in the finished product when it is combusted (gasoline etc.); hence they must be removed. The most general approach for the reduction of nitrogen concentration in oils is hydrodenitrogenation (HDN).

1.1 HDN

This process is carried out in parallel with hydrodesulfurisation (HDS) hydrodeoxygenation (HDO) and hydrodemetallisation (HDM) and the overall technique is known as hydrotreatment. The feedstock is mixed under pressure with hydrogen, heated, then introduced to the top of a fixed bed reactor (generally a trickle bed reactor) onto sulphided $CoMo/Al_2O_3$ or $NiMo/Al_2O_3$ catalyst. The gases and liquids are separated in a high pressure separator and the light gases are recovered (H_2S and NH_3) or recycled (H_2 and hydrocarbons)[1]. The result is that nitrogen is removed as NH_3, sulfur as H_2S, oxygen as H_2O and any metals present coat the catalyst surface. If HDN is a priority in the hydrotreatment process then nickel based systems such as NiW/Al_2O_3 may be preferred because of their higher HDN activity.

The mechanism and kinetics of HDN reactions are not fully understood. Compounds where the nitrogen is not part of an aromatic ring (anilines, amines etc.) undergo HDN easily and therefore have not been widely studied. In the case of heterocyclic aromatic compounds it is generally accepted that the first step is hydrogenation of the aromatic ring (pyridine to piperidine). This is followed by C-N bond fission (hydrogenolysis), but for compounds like quinoline with more than one aromatic ring, the kinetically favoured path begins with hydrogenation of the ring containing the nitrogen [4]. This is most likely followed by hydrogenation of the other ring, forming decahydroquinoline, then C-N bond fission and elimination

of NH_3 [4]. The minor route is C-N bond fission after hydrogenation of the first (N containing) ring. This produces a higher value (aromatic) product, (propyl benzene in the case of quinoline), and less hydrogen is used [4].

For kinetic evaluation many workers have studied HDN using a range of model compounds, catalysts and conditions. To some extent this complicates the matter. For instance, Odebunmi and Ollis [5], in their indole HDN study (250-350°C, 7.0MPa H_2) over a $CoMo/Al_2O_3$ catalyst have found that the hydrogenolysis of indoline is the rate determining step. It should be noted that their catalyst was reduced with H_2 at 400°C prior to sulfiding. The results of Aboul-Gheit and co-workers [6], on a $CoMo/Al_2O_3$ catalyst (350-400°C and 21MPa H_2) indicate that the slowest step in indole HDN is the hydrogenation of indole to indoline. For HDN of more complex molecules there has been some evidence suggesting that hydrogenation may well be the slowest step [7].

1.2 Alternatives to HDN

The difficulty in removing very large concentrations of nitrogen by this method has led many workers to search for an alternative. Their work mainly involves the removal of nitrogen from shale oil and coal tar fractions where effective removal of nitrogen by HDN is most difficult. There have been few studies of conventional naphtha fractions as removal of these low concentrations should be relatively easy. Shale oil typically contains about 2wt% nitrogen (~1wt% in the naphtha fraction) [2]. The effective removal of these quantities of nitrogen requires very severe hydrotreatment conditions. For a Kinetics (U.S.A.) shale oil distillate, the conditions required to reduce nitrogen from 140 ppm to <2 ppm, also reduces the H and C aromaticities by 34% and 29% respectively. This is defined as the amount of C and H in aromatics, as a proportion of the total - from NMR studies), probably

as a result of extensive saturation of mono and diaromatics [8]. Severe hydrotreatment also leads to cracking and coking reactions and increased amounts of low boiling material. The result is a loss in total product yield and value. Many of the nitrogen compounds are themselves valuable if they can be removed and recovered, although this is a long way from being practical.

Most workers in the field have studied possible acidic adsorbents capable of removing the predominantly basic nitrogen compounds. Adsorption on solid $CuCl_2.xH_2O$ has been found to reduce the nitrogen content of shale oil to ~0.2wt% [9], however in this process a large amount (~30%) of the oil was lost and much lower concentrations must be achieved. Extraction with aqueous acid removes basic nitrogen compounds, but serious problems arise owing to emulsion formation and limited ability to remove the less basic compounds [5]. For oil streams with a high nitrogen content it makes sense to use mild hydrotreatment followed by an adsorption step. With HDN the cost of removing each increment of nitrogen increases with decreasing nitrogen concentration, whereas for most adsorbents the reverse is true. Complete removal of nitrogen by HDN requires very vigorous hydrotreatment. Since much of the nitrogen in shale oil (nitriles, aliphatic amines etc.) can be removed under relatively mild conditions, an alternative approach would be to remove all of the sulfur and most of the oxygen and nitrogen by mild hydrotreatment, and to remove the remaining (heterocyclic) nitrogen by a different process such as adsorption. The mechanism of HDN is also important. If hydrogenation is fast and hydrogenolysis is the rate-limiting step, then the nitrogen compounds remaining after hydrotreatment will mostly be fully or partly hydrogenated. Saturated heterocyclics are more basic than their unsaturated (aromatic) equivalents shown by their basic pK_a's (e.g. Pyridine = 5.2, Piperidine =11.2 and Pyrrole = -3.8, Pyrrolidine =11.3) [10], (see below). These pK_a values are for the conjugate acids of the bases in aqueous solution at 25°C. This means that compounds with higher values are more basic. The gas phase basicities however will probably be significantly different from these.

Some of the materials that have been studied as adsorbents are: ion exchange resins [20,21], $CuCl_2.xH_2O$ [9], anhydrous acids on supports [22], metal sulphates on supports [30-34], zeolites [16,17] and amorphous silica aluminas [35].

1.21 Metal Sulfates

Metal sulfates are particularly interesting as they have no intrinsic acidity but develop moderate acidity, in the pK_a range -3 to +7 (depending on the sulfate studied) when partially dehydrated [11]. It has been proposed that the acidic centre is formed by an empty orbital of the metal ion, which appears in an incompletely dehydrated metastable transition structure [11]. These vacant orbitals, and the resulting affinity for electron pairs, account for Lewis acid properties. The Bronsted acidity arises from two sources. One is water co-ordinated to the metal; i.e. the metal tends to attract the oxygen atom, thus freeing a hydrogen ion. The other source is surface water, acidified by the inductive effect of the neighbouring cationic Lewis acid centres. Compression or irradiation can also be used to generate acidity.

In these systems the acidity can be tailored to a specific application because the acid strength is related to the extent of dehydration. For nickel sulfate maximum acidity is achieved by calcining at 350°C to give $NiSO_4.0.5H_2O$. This gives a relatively high number of acid sites at pK_a's around 6.8. Heating to 400°C results in complete dehydration and loss of acidity [11]. These sulfates can be impregnated onto supports such as silica gel to give a high surface area. Metal phosphates also show almost the same range of moderate acidities when treated in a similar manner, and should also be considered, although no literature has been found using these materials.

1.22 Zeolites

Zeolites are highly crystalline aluminosilicates incorporating Al, Si and O in their structures. They are unique in having well defined intra-crystalline cavities or pores with molecular dimensions as part of their structure. Zeolites can be considered to consist of SiO_2 units where Al replaces some of the Si atoms. Each Si atom is tetrahedrally co-ordinated, sharing bridging O atoms with neighbouring Si atoms. When some of the Si species (oxidation state + 4) in the framework are replaced by Al atoms (maximum oxidation state + 3), an excess negative charge is generated. A compensating extra framework source of positive charge must be added [12-14]. Zeolites are therefore ion exchangers and bringing an aqueous salt solution into contact with the zeolite leads to incorporation of cations from the salt into the zeolites, replacing some of the extra framework cations initially present. Ion exchange is the simplest and most important method for modifying the properties of a zeolite. The ion exchange sites are acidic in nature. In the proton form (C) they are Bronsted acids capable of donating a H^+ ion. If the zeolite is dehydrated above 500 °C these sites become Lewis acids (E) capable of accepting electrons [13]. Lewis acid sites can also be created by ion exchange with metal ions such as Cu^{2+}. In this case one Cu^{2+} ion can charge balance two acid sites (F). In this way sites with specific catalytic activity can be created, for instance ZSM-5 zeolites exchanged with Cu^{2+} ions can be used for the selective catalytic reduction of nitrogen oxides, and NO decomposition [15].

The acid strength, number, and nature of acidic sites (Lewis or Bronsted) can all be modified for the specific application either by modifying the aluminium content, pre or post synthesis, or by some other post synthesis treatment such as ion exchange.

(A) Zeolite as synthesised (Na form)

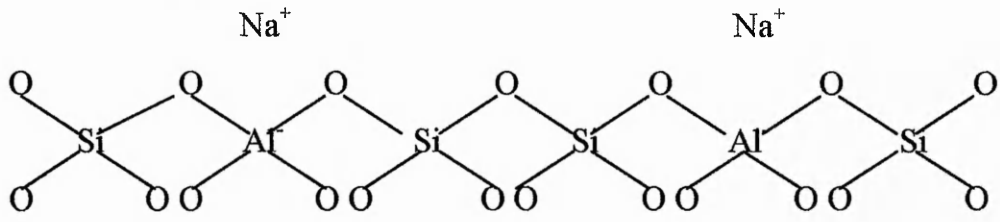

(B) Ammonium ion exchange

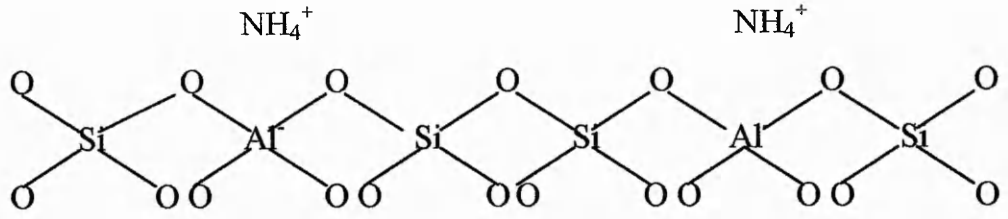

(C) Heating to remove NH_3 – Bronsted form

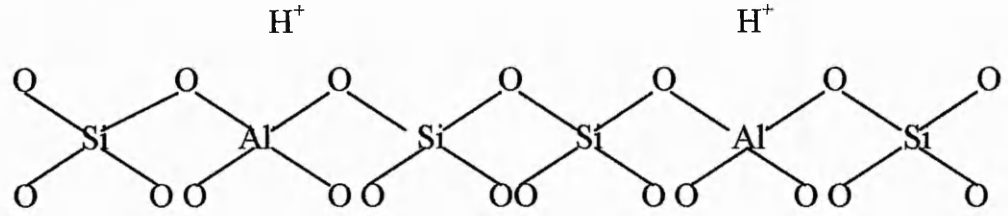

(D) Equilibrium

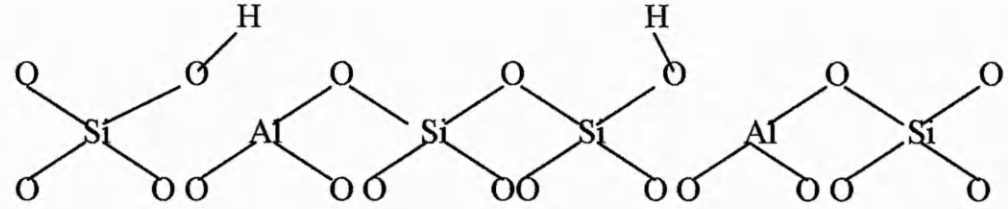

(E) Heating above 500°C $-H_2O$ $+H_2O$

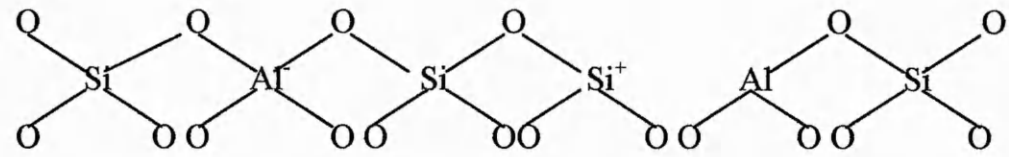

(F) Cu exchanged form

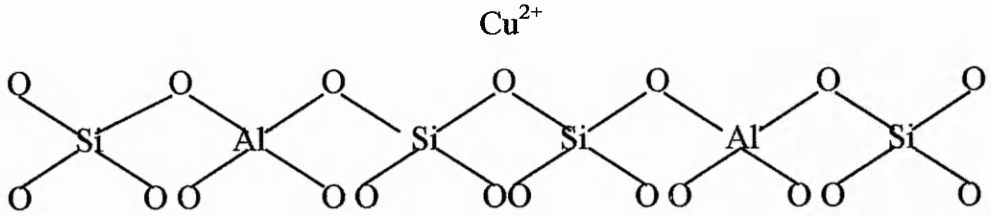

Microporous materials such as zeolites (and AlPO's, SAPO's, etc.) are interesting as adsorbents due to their acidic character, high surface area and high pore volume. The pore structure can also be chosen with the adsorbate in mind. With knowledge of the adsorbate this can be used to predict a material with a suitable pore size. In naphtha, the most likely nitrogen compounds appear to be pyridines and maybe anilines [1], these have dimensions of about 4 - 5Å depending on substitution. Another important consideration is the Si / Al ratio. Zeolites with a low Si / Al ratio are found to be hydrophilic due to a high cation content, whilst zeolites with a high Si / Al ratio are organophilic / hydrophobic, generally have the strongest acid sites, and will selectively adsorb organic molecules [12]. As water is a product of hydrotreatment the high silica zeolites may be more suitable for nitrogen removal from a previously hydrotreated stream, although their adsorption capacities should be lower than high aluminium equivalents, which have more acidic sites. These properties are demonstrated by the zeolites used in the literature (US-Y and ZSM-5) [16,17]. However water is probably easily removed from this stream, and hence high aluminium zeolites, with large numbers of acidic sites may be more effective.

1.23 M41S Materials

The mesoporous molecular sieve MCM-41 has attracted much attention since it was first reported by researchers at Mobil [18,19]. It is a member of a family of materials generically known as M41S. These materials have pores ordered in hexagonal (MCM-41), cubic (MCM-48) or laminar (MCM-50) arrays. The M41S

materials partially fulfil the long held goal of carrying over the activity and well defined structure of zeolites into the mesoporous range. MCM-41 has pores with uniform diameters that can be tailored in the range 1.5 – 10 nm, good thermal stability, a high surface area and acidic sites can be generated by the incorporation of aluminium. These properties uniquely combined in one material make it attractive for various industrial applications. The focus of most interest has been its potential use in refining processes such as fluidised catalytic cracking (FCC) [20,21] and in the manufacture and processing of fine chemicals where fast diffusion of liquids through the pores is beneficial [22,23].

1.23.1 Formation

The materials are synthesised in aqueous solution using surfactant molecules as templates. Several synthesis mechanisms have been proposed for the formation of MCM-41. Microscopy and XRD results are similar to those obtained from surfactant / water liquid crystals or micellar phases [26,27]. This has led Beck et al [19] to propose a direct liquid crystal templating mechanism. The structure being defined by the organisation of surfactant molecules into liquid crystals which serve as templates for the formation of the MCM-41 structure. In other words the first step in the synthesis is the formation of a micellar rod around the surfactant micelle, which in the second step will produce a hexagonal array of rods followed by incorporation of silica or silica-alumina around the rod-like structure. MCM-48 or MCM-50 will be produced if the micellar rods adopt a cubic or laminar arrangement. The authors[19] have not however ruled out the possibility that addition of the silicate results in the ordering of the subsequent silicate encaged surfactant micelles. This relates to the fact that MCM-41 can be formed from a variety of silica / alumina sources, surfactant to silica / alumina ratios and within a broad time / temperature range, whilst liquid crystal structures formed in surfactant solutions are highly sensitive to the overall characteristics of the solution.

Davis et al [28] using 14N NMR spectroscopy, concluded that the liquid crystal phase is not present during the formation of MCM-41, and hence, this phase is not the structure directing agent for the synthesis of the mesoporous material. It is then concluded that M41S materials are formed through a mechanism in which aggregates of cationic surfactant molecules in combination with anionic silicate species form a supramolecular structure. This is further supported by the fact that when short chain quaternary ammonium surfactants with C6 and C8 alkyl chains are used in the synthesis [29], MCM-41 is not formed. The solubility of these species is high, and aggregated structures are not necessary to minimise hydrophobic interactions.

Stucky and co workers [30-37] have developed a model, which makes use of the co-operative organisation of inorganic and organic molecular species into three dimensionally structured arrays. They state that in this model, the properties and structure of a particular system, are not determined by the organic arrays that have long range order, but by the dynamic interplay among ion - pair inorganic and organic species. Different phases can be readily obtained through small variations of controllable synthesis parameters, including mixture composition and temperature. This was proved by examining the structures in the final form and at various stages during the synthesis, by means of Small Angle Neutron Scattering (SANS) [37]. Similar conclusions have been reached by Calabro et al [38] using in situ ATR / FTIR studies of M41S type mesoporous silicate synthesis. Following this mechanism, the criterion of charge density matching at the surfactant / inorganic interfaces governs the assembly process, and consequently the final type of structure generated. This principle methodology can be extrapolated to produce meso-phases with different metal oxides as long as there is charge density matching among the inorganic ions, surfactant and inorganic counter ions.

In the original work, [18,19] and most subsequent work, the mesopore size was altered by changing the chain length of the surfactant molecule and the addition to the synthesis medium of organic molecules, such as 1,3,5-trimethylbenzene [19]. The hydrophobic solvation interactions of the organic playing a key role.

Subsequently alkanes of different chain lengths have also been used to modify the pore size by swelling the surfactant micelle [24]. It has recently been reported that the pore size of these materials can be increased and controlled without the use of such swelling agents[25]. If the composition of the gel and the crystallisation variables are adjusted correctly, the pore size increases with increasing crystallisation time. In this case, [25] from 4.25 nm after 24 h to 7.0 nm after 10 days.

1.23.2 Acidity

In order to produce acidic meso-structured materials, potentially useful for many catalytic applications, aluminium must be incorporated into the walls of M41S materials. Ideally aluminium must be incorporated into to the structure with tetrahedral co-ordination to give useful acidic sites. MCM-41 and MCM-48 materials with walls of silica-alumina have been synthesised where the aluminium is tetrahedrally co-ordinated [28, 39 - 41]. In general it appears from XRD data that the introduction of aluminium into MCM-41 during synthesis decreases the order of the material [39, 42]. This is often accompanied by a spread in the pore size distribution. It has been claimed that in the presence of aluminium, the order can be improved if sodium silicate is used instead of SiO_2 as the silica source [43, 44]. However in these studies a significant amount of Al remains as Al^{VI} and is not incorporated as framework Al^{IV}. Consequently the framework Si / Al ratio is much higher than that given by the chemical analysis. The nature of the aluminium source used can also play an important role in the type of final incorporated species obtained [42]. Contradictory reports have been made as to be preferred Al source for incorporation of tetrahedral aluminium. It seems likely that it is possible to incorporate all of the Al as Al^{IV}, almost regardless of the Al source, if the synthesis conditions are optimised properly [21]. However, for the synthesis of MCM-41 with very low Si / Al ratios, sodium aluminate has most often been used [41, 44, 45]. Borade and Clearfield [45] have synthesised MCM-41 with Si/Al ratios as low as 2, without observing the presence of octahedral aluminium, using sodium aluminate and fumed silica.

Although low Si / Al ratio MCM-41 can be prepared with only tetrahedral aluminium, what is important is the amount of Al^{IV} left after calcination. Calcination at > 500 °C is required to fully de-template MCM-41 and also to activate the material for any catalytic application. It appears that after calcination at these temperatures the NMR peak corresponding to tetrahedral Al decreases, while Al^{VI} is formed. Al^{IV} either becomes distorted or is removed from the framework. Deep hydration of these samples can sometimes restore the tetrahedral aluminium. This is probably due to the restoration of Al^{IV} whose co-ordination was distorted by the heat treatment. Al removed from the framework will remain as Al^{VI}.

Kloetstra et al [46] have observed what they term an 'aluminium rich dense phase' formed with MCM-41 materials. The dense phase has been imaged by TEM, alongside a chaotic MCM-41 phase, for a number of samples with different synthesis routes and Si / Al ratios < 15. The aluminium in the dense phase is tetrahedrally co-ordinated and is not easily seen with X-rays or NMR. This indicates the importance of electron microscopy for characterisation. Energy dispersive X-ray (EDX) elemental analysis shows that the dense phase consumes most of the aluminium in the sample and so the Si / Al ratio of the MCM-41 phase will be significantly higher than the overall composition.

Their moderate acidic strength means they may be suitable for selective adsorption of basic nitrogen compounds, allowing adsorption of the nitrogen bases without activation of hydrocarbons also present. The ease with which relatively small molecules should be able to diffuse through the large pores, and the high pore volume, may also be advantageous for this application. It seems that a very aluminium rich MCM 41 cannot be produced at this time, which would be preferable for an application such as selective adsorption, to provide a very high number of adsorption sites. MCM 41's with Si / Al ratios of greater than 15 may still be useful for such an application.

1.24 Amorphous Silica-Aluminas

Amorphous silica-alumina is an important material as a catalyst for the isomerisation, polymerisation, partial oxidation and catalytic cracking of hydrocarbons, and as a support for metal catalysts [47]. It is one of the primary components in fluidised catalytic cracking (FCC) catalysts. Most commercial FCC catalysts use an active matrix of silica-alumina in combination with ultra-stable Y (US-Y) zeolite. The zeolite has much greater cracking activity than the silica-alumina due to the presence of much stronger Bronsted acid sites, and gives greater selectivity towards desirable gasoline products [48]. However the 7.4Å pore openings of Zeolite Y prevent the cracking of larger molecules inside the pores. It is for this reason that active matrices of silica-alumina are introduced to carry out pre-cracking of the bulkier molecules present in the higher boiling point fractions [49]. As in zeolites, acid sites are generated via substitution of Al^{3+} for Si^{4+} in a structure of SiO_4 tetrahedra, resulting in a charge imbalance. However unlike zeolites the structure is amorphous and the acid sites present are generally weaker than those formed in a crystalline zeolite structure [48].

1.25 Aluminas

Alumina is frequently said to be an acidic catalyst, yet its surface chemistry is vastly different to that of H-zeolites or silica-alumina. The latter have strong to moderate Bronsted acid sites while the surface chemistry of aluminas is centred around Lewis acid base pair sites, accompanied by residual terminal hydroxyls. These terminal hydroxyls may reluctantly function as Bronsted acid sites when this is required by the reaction mechanism [50].

Alumina has several polymorphs. γ-alumina is generally considered to be one of the more active, with a relatively high surface area. γ-alumina is used as a catalyst support, e.g. for catalytic reforming (Pt on γ-alumina) and hydrotreating (Mo – Ni (Co) on γ alumina). At high temperature (c.a. 1000 °C) γ-alumina is converted to

α-alumina, via the δ and θ transitional phases. α-alumina is less active, generally has a much lower surface area and is chemically inert with high thermal stability. It is also widely used as a catalyst support as in the ethylene partial oxidation catalyst.

The acid base properties of aluminas can be extensively modified by chemical treatment [50-57]. The addition of basic metal ions to alumina such as Na^+ and Mg^{2+} decreases the number and strength of acidic sites, and generates basic sites [2-4]. Base metal doped aluminas can be useful as a support for de-hydrogenation catalysts [52]. At low loadings (~0.5 wt %) the base metal cations eliminate strong acid sites and create weak basic sites. As loadings are increased, strong acid sites are removed further, along with acid sites of intermediate strength, and intermediate and strong basic sites are created.

The addition of anions such as F^-, Cl^- and PO_4^{3-} to alumina, increases the number of acid sites [50,51,53-57]. This technique is used commercially in catalytic reforming, where the acidity of the γ-alumina support is increased, and controlled, by the addition of low levels of Cl^- to the feed. Berteau et al [51] have studied aluminas modified by a wide range of ions, and developed the following acidity scale $F^- > SO_4^{2-} > Cl^- > = PO_4^{3-} >$ pure γ-$Al_2O_3 > Mg^{2+} > = Na^+$. In the case of fluoride it has been shown that fluoriding alumina not only increases the number and strength of Lewis acid sites but also generates Bronsted acid sites [50,51,53-55]. The effect of dopants on the acid-base characteristics of alumina is directly related to the electronegativity of the dopant ions. Highly electronegative ions like F^- increase the number and strength of acidic sites, whilst electropositive ions like Na^+ increase the basic nature of the alumina.

Different dopants also have an effect on the surface area and the stability of the alumina. It widely reported that fluoriding alumina decreases the surface area [54,55]. In the case of γ-alumina, fluoride reduces thermal stability, so that conversion to α-alumina will take place at lower temperature, which leads to a further significant loss in surface area. This effect is increased at higher F^-

concentration. By contrast small amounts of cations, such as Na^+ and Mg^{2+}, stabilise γ-alumina so that the conversion to α-alumina requires a higher temperature, and hence the surface area is also stabilised.

It is generally accepted that at low concentrations fluoride replaces surface hydroxyl and oxide groups, whereas at higher fluoride content (~20 wt% +) other phases e.g. aluminium fluoride and aluminium hydroxyfluoride are formed [54,56]. Substitution of hydroxyl and oxide groups takes place up to about 5 - 10 wt % F^- [54]. The generation of Bronsted acid sites, upon fluoriding alumina is attributed to the through lattice inductive effect, brought about by the electronegativity of the fluorine. Fluoride, adjacent to hydroxyls on the surface of the alumina will polarise the lattice, drawing electron density away from the O-H bond making the hydrogen more acidic.

Pure alumina is inactive, or only slightly active, for most acid catalysed hydrocarbon reactions involving skeletal rearrangement [54]. This lack of activity is generally attributed to be absence of protonic sites in the catalyst. In contrast, after incorporation of fluoride, the catalyst possesses enhanced activity, presumably because of the strong protonic sites that are created. Modifying alumina with fluoride has been shown to increase catalytic activity towards a number of acid catalysed reactions. These reactions include cracking, isomerisation, alkylation, polymerisation and disproportionation [54].

1.3 Previous Work

1.31 Ion Exchange Resins

Cronauer et al. [58,59] have used ion exchange resins to denitrogenate fractions of a shale oil which had previously undergone mild hydrotreatment. The six oil fractions studied were in the jet fuel (154 - 271°C) and diesel fuel (271 - 343°C) boiling ranges.

The raw shale oil (1.37 wt% nitrogen) was hydrodenitrogenated at 3 different levels of severity over a commercial catalyst (NM-504, Katalco Corporation). The jet fuel and diesel fractions of these three were then used in ion exchange experiments. The ion exchange resin used was Amberlyst A-15, a macroporous, strongly acidic, cation exchange resin. Chemically, it is a sulphonated, crosslinked styrene /divinylbenzene polymer. It has an exchange capacity of 4.4 meq g^{-1} (milliequivalents per gram), an internal surface area of 100 m^2 g^{-1} and average pore radius of 160Å. This exchange capacity should give Amberlyst A-15 the ability to adsorb 0.062g nitrogen per g dry resin (6.2 wt%) if all the exchange sites are utilised at the ratio of one nitrogen per site. Two other resins were used - Amberlyst XE-397 and Amberlyst XN-1010. These are chemically similar to A-15 but have 1/3 and 3 times the degree of crosslinking, respectively. See table 1.

Table 1.31.1: Ion exchange resin properties from Ref 58.

Resin	Exchange capacity, meq g^{-1}	Capacity utilised, %	Surface area, m^2 g^{-1}	Ave. pore radius, Å	Pore volume, cm^3 g^{-1}	relative cross-linking	D_{eff} cm^2 s^{-1}
XN-1010	3.6	53	200	60	0.46	3	0.30×10^{-8}
A-15	4.4	53	100	160	0.48	1	1.55×10^{-8}
XE-397	4.9	104	66	300	0.50	0.33	0.86×10^{-8}

D_{eff} is the effective intraparticle diffusivity.

It was discovered that the utilisation of sorption capacity of Amberlyst A-15 for nitrogen containing species decreases with increasing boiling range of the shale oil fractions, and increases with a decrease in the nitrogen content (increasing severity of hydrotreatment within a fraction). A two stage processing of shale oil for nitrogen removal appears to be particularly attractive, because the ion exchange process becomes increasingly effective as the nitrogen concentration is reduced.

The shale oil fractions used in these experiments ranged in nitrogen content from 0.09 wt% to 0.50 wt%. Amberlyst A-15 effectively removed nitrogen compounds from these fractions. The percent of the potential resin capacity of 0.062 g g^{-1}resin which is utilised at saturation ranges from a high of 92% (0.057 g g^{-1}resin) for a 0.09 wt% nitrogen jet fuel to a low of 26%(0.016 g g^{-1} resin) for a 0.46 wt% nitrogen diesel fuel. These observations indicate that it is not possible for Amberlyst A-15 to adsorb one nitrogen for each ion exchange site for all of the shale oil fractions studied. Apparently, all of the sorptive sites are not available for ion exchange with all of the nitrogen containing compounds. This lack of efficiency could be caused by steric blocking of adjacent sites by large, adsorbed molecules; the exclusion of some of the larger nitrogen containing molecules from the smaller pores; the fouling and plugging of the resin by some unidentified fraction in the shale oil, or some other change to the resin caused by exposure to the oil.

The Amberlyst XE-397 resin proved to be far superior to either A-15 or XN-1010. The pore size distribution of XE-397 shows the resin to consist of the largest pores, mostly greater than 100Å, and a significant proportion above 500Å. In column operation the integrated adsorption capacity of the Amberlyst XE-397 resin was about 2.5 times that of the Amberlyst A-15 resin. The ion exchange utilisation corresponds to 104% of its theoretical capacity. Therefore it is likely that in A-15 and XN-1010, a mechanism such as pore mouth plugging is making some of the reaction sites unavailable for ion exchange with the nitrogen containing compounds. It appears that effective diffusion within the resin beads is a limiting

factor in their performance. Increasing pore size improves the resin performance by improving the diffusion properties within these resin beads.

If ion exchange resins were applied to the denitrogenation of naphtha, then some improvement in the diffusion properties of the resin may be encountered due to the lower boiling range and RMM of the hydrocarbon/oil. Smaller beads may also help diffusion. Lower boiling oil fractions have been shown to contain lighter and smaller nitrogen compounds, so a very large pore structure will not be as important as with jet fuel or diesel fractions. However, even with complete utilisation of the exchange capacity these resins can only capture about 6% of their own weight of nitrogen.

Another problem could be softening of the resin by components in the naphtha, particularly aromatics, (10-15% in the reformer feed). This point is mentioned in the Prudich et al. paper [58] as a possible reason for the poor performance of the Amberlyst A-15 resin. The better performance of the larger pore resin does not necessarily contradict this theory as a pore constricting affect may not be as pronounced with larger pores. With the relatively high aromatic content of naphtha, this could be a significant problem at elevated temperatures. Cooling of the feed will slow down diffusion and increase costs as the feed must be re-heated to enter the reformer.

1.32 Anhydrous HCl

Audeh from Mobil Research has used anhydrous HCl adsorbed on a support as an adsorbent for removing nitrogen compounds from lubricating oils [60]. The supports used were NaX zeolite and silica / alumina. The author seems to believe that acidity is entirely due to HCl on the surface, however an effect such as chloriding of acidic sites on the support cannot be ruled out. This would increase the strength of acidic sites through an inductive effect. In a typical experiment the

base stock was dehydrated at 100°C over calcined molecular sieves (to prevent hydration of the HCl) before nitrogen removal. Although chloride was not detected in the base stock after denitrogenation, the denitrogenated oil was passed over another bed of calcined molecular sieves to ensure removal of any entrained nitrogen containing hydrochloride or unreacted HCl. In preliminary experiments, it was observed that dehydrated lubricating oil base stock could be partially denitrogenated by anhydrous HCl. By saturating a base stock containing 32 ppm total nitrogen (14 ppm basic) with anhydrous HCl, allowing the mixture to settle for 7 days and filtering, it was possible to reduce the total nitrogen in the stock to 10 ppm. Although not all the nitrogen was removed, more than just the basic nitrogen reacted. Clearly anhydrous HCl in an anhydrous hydrocarbon environment behaves as a stronger acid than aqueous HCl, which only reacts with basic nitrogen compounds [61]. Thus it would seem possible that all nitrogen compounds could be removed with anhydrous HCl. The capacity of the adsorbent could be increased by using a suitable support. As with supporting any acidic agent for adsorption several conditions must be satisfied. Firstly, the HCl must not be leached from the support by water present in the feed. Secondly, the HCl must not lose its adsorption ability toward nitrogen compounds when adsorbed on the support, and also, the adsorbed compounds should preferentially be retained by the solid, even if the hydrochlorides formed are soluble in the oil.

The supports studied were NaX molecular sieves and amorphous silica / alumina (cracking catalyst). These were calcined for 16 h in argon at 350°C - 400°C prior to treatment with anhydrous HCl. NaX molecular sieves adsorb about 16% by weight of HCl. This effectively denitrogenates the base stock reducing the nitrogen content from 32 ppm to <0.2 ppm. The NaX sieves have no denitrogenation activity alone. It was hoped that such a large HCl content would allow denitrogenation of many volumes of oil over a relatively small volume of adsorbent. However, it was observed that denitrogenation efficiency began to decrease after the oil/adsorbent volume ratio exceeded about 30. In molar terms 0.43 mol of HCl was required to remove 0.008 mol of nitrogen. Clearly not all the HCl was available for reaction, possibly because of exclusion of nitrogen

containing molecules from the NaX pores or the reaction of HCl with the molecular sieves. The adsorbent (HCl + support) has an adsorption capacity (for nitrogen compounds) of approximately 0.25wt%. NaX regenerated by removing HCl and calcining at 580°C only has 70% of the capacity of fresh adsorbent for HCl, although it still has denitrogenation abilities equivalent to HCl on fresh NaX. This may be due to some sort of structural collapse, through dealumination by chloride ions. The quantitative efficiency of HCl on NaX is unsatisfactory. For this application the ideal support should have a larger pore size.

Amorphous silica-alumina cracking catalyst has some capacity for denitrogenation without HCl, although this capacity is reduced with regeneration. As a support for HCl it is far superior to NaX. One volume of silica-alumina on which 1wt% HCl is sorbed removes more than 99% of nitrogen from about 32 volumes of oil. After regeneration, the support's capacity for HCl adsorption did not change (1wt%). However, whereas the HCl treated fresh sorbent denitrogenated 32 volumes of oil from 32 ppm nitrogen to 0.2 ppm (99.4% denitrogenation), the HCl treated re-calcined sorbent denitrogenated 112 volumes of the same oil to the same 0.2 ppm nitrogen. The amount of HCl adsorbed was 0.024 mol and the amount of nitrogen removed was 0.022 mol. This represents very efficient use of the HCl adsorbed (almost 1:1 molar ratio). However, with only 1wt% adsorption of HCl on the support the adsorption capacity of the adsorbent (HCl + support) will only be approximately 2-3wt% nitrogen. Other solids tested as supports were zeolon 200H and bauxite, but amorphous silica-alumina cracking catalyst was found to be the support of choice.

The refining of lubricating oils involves relatively small quantities of a high value product. The specifications of some grades such as turbine grade lubricants are very stringent and this technique may be of some use for these products. For the application of supported anhydrous acids to denitrogenation of naphtha, several problems will be encountered. Firstly the necessity for dehydration of the feed stream prior to denitrogenation would be a major problem in a unit with a throughput of 20,000 barrels per day. However in the case of HCl, a small amount

of slippage might be acceptable, if chloride is already added to the reformer feed. A high loss of HCl from the support would interfere with the nitrogen removal. The low adsorption capacity (~2-3 wt%) would require a very large mass of adsorbent if the unit is required to run continuously between shutdowns; according to initial calculations approximately 50 tons for a 6 month run. The regeneration process involves stripping the HCl from the support, calcining the support and then re-adsorbing anhydrous HCl - a relatively costly procedure.

1.33 Zeolites

Ellis and Korth [16] suggest that recent advances in the synthesis of high silica zeolites make them a potential selective adsorbent for the processing of shale oil. The authors propose some advantages of these materials when compared with ion exchange resins:

(1) They are very stable to acid and to high temperature (up to 1100°C).

(2) They are hydrophobic and so will not adsorb water (one of the products of hydrotreatment).

(3) They have a uniform pore size.

(4) They exhibit very rapid intracrystalline diffusion when the molecule being adsorbed has a kinetic diameter only slightly smaller than the diameter of the pore [62]. (This theory however, is not well established).

(5) Their internal surfaces are strongly acidic, which confers a high affinity even for very weakly basic nitrogen heterocycles.

(6) They have a high adsorption capacity (up to ~ 20wt%). (This statement is debatable as high silica zeolites have relatively few acid sites).

(7) Burning off the adsorbed organic compounds can regenerate them very simply.

Their experimental work explored the use of ultrastable zeolite Y (US-Y) a high silica faujasite, for the adsorption of organic nitrogen compounds. A solution of nitrogen compounds in hexane was used, as well as a hydrotreated shale oil from Stuart (Queensland).

The US-Y zeolite (unit cell 2.425nm, SiO_2/Al_2O_3=80, Na_2O=0.03wt%, surface area 780m^2g^{-1}, particle size 0.3-0.5μm) was used to denitrogenate a solution containing 8 aromatic nitrogen compounds, pyridine, quinoline, isoquinoline, indole, acridine, phenanthridine and carbazole (20mg each in 250ml). The adsorption experiments involved mechanical shaking of the model solution with the zeolite for 5 minutes at 20°C. The solution was then analysed by GC. The nitrogen compounds adsorbed on the zeolite were recovered by treatment of the zeolite with HF, neutralised and then analysed by GC.

The total nitrogen concentration of the hexane solution of eight bases was 275ppm wt, similar to the residual nitrogen concentration found previously in shale oils which had been hydrotreated under moderate conditions. Uptake of the model nitrogen compounds from this solution was rapid. Within seconds of contact the yellow colour of acridine appears in the zeolite. With 100mg zeolite mixed with 10ml of the solution >80% of the nitrogen is removed. The model compounds, which were least well adsorbed, were aniline (66%), indole (44%) and carbazole (56%). These are the least basic of the compounds. Quinoline and isoquinoline were both adsorbed >99%. This corresponds to an adsorption of approximately 5wt%. With less zeolite (50mg) none of the compounds are removed as well as before, but the adsorption capacity of the zeolite is better utilised. With more zeolite (200mg) all the compounds are adsorbed to a greater extent, with aniline 95%, indole >99% and carbazole 87%, but this represents very inefficient use of the zeolites' adsorption capacity. With these experiments the contact time of 5 minutes may be insufficient to reach equilibrium, and hence the relative uptake of the nitrogen compounds, may be partly related to diffusion effects.

In a further experiment, increasing amounts of an aromatic hydrocarbon (naphthalene) were added to see how selectively the zeolite would adsorb small quantities of nitrogen heterocycles in the presence of larger concentrations of aromatic hydrocarbons, as would be the case in a hydrotreated shale oil. All nitrogen containing compounds were still adsorbed very efficiently (>99%) except

indole and carbazole (~75%). Nitrogen compounds have a much higher affinity for the zeolite cavities than aromatic hydrocarbons.

A third experiment was conducted to determine whether a large excess of long chain alkanes (the main component of hydrotreated shale oil) would compete with the nitrogen compounds for the adsorption sites in the zeolite. The hexane solution of the eight bases was diluted with hexadecane and analysed by GC before and after exposure to the zeolite. Once again all the bases except indole and carbazole were removed efficiently. When the zeolite was dissolved in HF all the bases except indole were recovered, with a negligible amount of hexadecane. Indole was totally polymerised by the zeolite and/or acid dissolution of the zeolite.

Finally, a shale oil from Stuart (Queensland) which had been subjected to mild hydrotreatment (380°C, 7MPa, 0.4h; residual nitrogen = 2000 ppm wt) was diluted with hexane (to reduce viscosity) and treated with zeolite. As the nitrogen in this solution was distributed over a much greater number of compounds than in the model mixture, the concentrations of individual nitrogen compounds were so low that the GC (using an FID) of the solution before and after treatment differed only slightly. Instead, aqueous acid was used to extract the basic nitrogen compounds before and after treatment with zeolite. The resolved nitrogen compounds comprised mainly of polyalkylanilines and pyridines, >95% of these were removed by the zeolite.

The gas chromatograph of the bases recovered from the zeolite (using HF) was very similar to that of the bases isolated by extraction with aqueous acid. The material recovered from the zeolite only contained small amounts of alkanes, so only minor losses of hydrocarbons would result from the heating of the zeolite to burn off the adsorbed nitrogen compounds before recycling. It is important to note that the adsorption efficiency of zeolite, which had been recycled 5 times, was the same as fresh zeolite, when used with the model system.

The same authors have explored the use of zeolites for the treatment of retort waters, (from the pyrolysis of oil shale) [17]. The water contains a wide variety of dissolved and suspended (emulsified) organic compounds, many of which are highly toxic. The compounds present range from readily biodegradable to highly refractory, the nitrogen and oxygen heterocycles being the most difficult to remove. The disposal of this effluent poses an environmental threat, the basic fraction (nitrogen heterocycles mainly) being of most concern. A number of processes have been examined to remove these compounds from the water, including solvent extraction and adsorption on activated carbon, clays or spent shale [65,66]. These were found to be only partly successful.

In this study, high silica zeolites (US-Y and ZSM-5) were used as adsorbents. The US-Y was the same as used previously and the ZSM-5 had properties :- SiO_2/Al_2O_3 = 280, surface area 780 $m^2 g^{-1}$. Silicalite, ZSM-5 and ZSM-11 have been used previously to adsorb low molecular weight organic compounds from water [65-67]. Dessau [66] has shown from adsorption studies using mixtures of organic liquids that the pore size of these materials (~0.55nm) allows the adsorption of hydrocarbons such as linear alkanes and alkylcyclohexanes etc. but excludes all compounds of higher molecular size. ZSM-5 was found to adsorb the acids present in the water very well but only removed ~40% of the neutrals and bases. The US-Y removed 100% of neutrals and bases but was less efficient at removing the acidic compounds. An explanation for this could be the exclusion of larger nitrogen compounds (multiple ring or highly alkylated) from the ZSM-5 pores (elliptical 0.51-0.56nm). The larger US-Y pores (0.74nm) were able to accommodate these species. A mixture of ZSM-5 and US-Y (2:1) was found to work efficiently. This demonstrates the importance of tailoring pore size as well as acidity to the compounds to be removed.

The use of zeolites as adsorbents for the purification of naphtha streams looks very promising. The resistance to water offered by zeolites with a high silica content makes them ideal for treatment of a previously hydrotreated stream. The wide variety of zeolitic type materials available allows tailoring of acidity and pore size,

either of one material or a mixture, to the properties of the adsorbate to be removed. Their robust nature allows relatively simple regeneration (by heat treatment) without altering their properties, and their potentially high adsorption capacity makes them an obvious choice for future experimental work.

1.34 Metal Sulfates

Mochida et.al. [68-72] have extensively studied coal products, particularly involving the production of high quality coke. Coal tar is recovered when coal is carbonised to coke. The tar is usually distilled forming products such as naphtha, creosote, phenols and pyridine bases (dyestuffs and pharmaceuticals). This was one of the starting points of the chemical industry. The residue of the distillation is known as coal tar pitch and can be carbonised to form carbon blacks. Metal sulfates have been used to remove and recover nitrogen bases from coal tar fractions, including coal tar pitch.

Nickel sulfate has been used to capture and recover nitrogen species present in coal tar pitch [68]. Consecutive extraction with methanol and precipitation with hexane has been shown to concentrate the pyrroles and phenols in the methanol soluble, hexane insoluble fraction of the pitch (M.S.H.I), but most of the basic nitrogen species such as pyridine remain in the methanol insoluble fraction [69]. In Mochida's study nickel sulfate was used to denitrogenate the toluene fraction of the pitch and this was further split into methanol soluble and insoluble fractions. Commercial nickel sulfate was calcined for 4h at 350°C, to generate acidity, before being packed in a glass column. The dried nickel sulfate was found to adsorb basic nitrogen species concentrated in the methanol insoluble fraction. The earliest elutions lost heavier components, which were not necessarily basic. Less soluble and polar species may be removed to some extent by the polar surface of the sulfate. However, the sulfate is rapidly saturated with these compounds and they are not removed from later eluted fractions. It is worthwhile to note that nickel sulfate captured 6 mg g^{-1} basic nitrogen species when 5 g of coal tar pitch was

charged to 30 g of the sulfate. When 150 g of pitch was charged to 150g of sulfate more nitrogen species were adsorbed, 20 mg g^{-1}. Very basic or very polar species seem to be removed beyond the acidity of the nickel sulfate. One problem with using dried sulfates is the relatively low adsorption capacity.

Aluminium sulfate (10 wt%) supported on silica gel has also been used to denitrogenate coal tar fractions [70]. The technique used was simply to stir the adsorbent and tar fractions for 30 minutes. Although relatively successful, adsorption capacity is still relatively low. The study demonstrates the importance of tailoring the properties of the support to the nitrogen compounds being removed as well as tailoring the acidity of the sulfate.

In a more detailed study [71] various loadings of aluminium sulfate on two different silica gel supports were used to denitrogenate crude methyl naphthalene oil (a residue of naphthalene oil from coal tar). Aluminium sulfate is more acidic than nickel sulfate. The supports used had surface area 650 $m^2 g^{-1}$, mean pore size 25Å; and surface area 500 $m^2 g^{-1}$,mean pore size 64Å. These were impregnated with 3-20 wt% aluminium sulfate, which was then calcined at 350°C for 4h in air. The crude methyl naphthalene oil was mixed with various amounts of adsorbent and a solvent (hexane) for 1h. The adsorbent was separated by filtration and the nitrogen compounds recovered with benzene and analysed. The crude methylnaphthalene oil/hexane was also analysed by GC-FID and FTIR.

The support with the larger pores gives more efficient nitrogen removal, with the optimum sulfate loading appearing to be ~5wt%. The larger pores seem to allow the nitrogen compounds better access to the acidic internal surface, especially two ring nitrogen compounds such as quinoline. After impregnation this adsorbent had a surface area of 400 $m^2 g^{-1}$, and pore diameters of 40Å, regardless of the sulfate loadings. With 5% sulfate this gives highly denitrogenated crude methylnaphthalene oil and recovery of quinoline oil. However more than one adsorption step was required to give a very low nitrogen level. The first stage reduced nitrogen content from 2.07wt% to 0.8-1wt% and was only slightly affected

by loading. Further adsorption steps reduce the nitrogen content further but the ratio of adsorbed nitrogen per acidic site decreases to 2.66 from 5.36. It is shown that basic nitrogen compounds are preferentially removed (almost completely). The polar as well as acidic nature of the sulfate helps removal of pyrrolic compounds which were removed quite well although the acid / base interaction is superior to the polar one. The dissolving ability of benzene is sufficient to desorb the nitrogen compounds from the sulfate. The support disperses the sulfate on the surface increasing the acidic strength and number of acidic sites. Crude methylnaphthalene oil contains a lot of quinolines (and alkylated derivatives), hence a support which allows access of these relatively large species to the sulfate surface is preferable. Loadings in excess of 5wt% increases the portion of the sulfate which is useless (not available to nitrogen compounds). Repeated adsorption is more difficult as the remaining species are those which are less easily adsorbed. IR measurements (pyrrolic N-H) support the conclusion that the less basic nitrogen compounds such as indole are not easily removed. The amount and choice of solvent is another important factor. Non polar solvents such as hexane or pentane appear to behave as 'anti-solvents' to expel the polar and basic compounds onto the adsorbent. A fairly large amount of poor solvent is required to overcome the solvent ability of methyl naphthalenes. Solvents such as supercritical propane and CO_2 appear attractive.

Adsorption of nitrogen compounds on supported aluminium sulfate under supercritical CO_2 conditions has been studied [72]. Aluminium sulfate (10wt%) was supported on silica gel (MB-4B, as before). A model methylnaphthalene oil was used in the supercritical extraction experiments, where the adsorbent was in a fixed bed. Supercritical CO_2 (50°C, 80 atmospheres) was flowed at 6 l min^{-1} to carry the feed to the adsorbent bed. After adsorption, higher pressure CO_2 and methanol were used to recover the adsorbed species and regenerate the adsorbent. A GC with an FID detector was used for the analysis.

With a feed rate of 14.5 mg min^{-1} (16wt% quinolines) no nitrogen compounds broke through the bed until 120 minutes (with 3.3g of adsorbent i.e. 0.33g of

$Al_2(SO_4)_3$). In other words 3.3g of adsorbent captured the first 0.3g of nitrogen compounds completely. Breakthrough of nitrogen compounds was fairly rapid after this. The nitrogen compounds were effectively recovered with CO_2 (150 atm.) and then methanol (150 atm.), but the adsorption capacity of the adsorbent slowly decreased with the number of adsorption/desorption cycles.

On suitable supports, metal sulfates may offer a reasonable surface area, and adsorption capacity. One possible problem could be their rehydration by water present in the hydrocarbon (naphtha) stream, especially if the stream has previously been hydrotreated. However it may be possible to overcome this, if the adsorbent can be kept at a high temperature, although this may be undesirable for the adsorption process itself. In the case of nickel sulfate the dehydration temperature for maximum acidity is about 350°C; if the operating temperature can be kept close to this then rehydration may be prevented, and hence metal sulfates (and possibly phosphates) may become viable adsorbents for a feedstream containing water.

1.35 Sud-Chemie adsorbents

Sud-Chemie (Munich) have developed two complementary adsorbents for removal of nitrogen compounds from hydrocarbon streams [73]. The adsorbents are known as 'TRAPIT-N' for liquid phase adsorption and 'TNS Balls' for liquid and vapour phase adsorption. The 'TNS Balls' adsorbent is composed of amorphous aluminium hydrosilicate and the 'TRAPIT-N' adsorbent is aluminium hydrosilicate loaded with 10 wt% sulphuric acid. Both adsorbents have very high adsorption capacities (2 – 3 wt% N for' TNS Balls' and 5 – 6 wt% N for 'TRAPIT-N'), corresponding to approximately 15 wt% and 30 wt% organic nitrogen compounds respectively. 'TNS Balls' can be used for most applications as it is regenerable. Hence two beds of 'TNS Balls' should be installed in parallel operation, one in service, and one in regeneration mode. If higher adsorption capacities are required then 'TRAPIT-N' can be used for more severe poisoning problems, but is limited to liquid phase streams, and is non-regenerable. 'TNS Balls' have been shown to

remove over 90 percent of acetonitrile from a 200 ppm acetonitrile in n-heptane feed at 60°C and 1 atmosphere pressure. Performance improves with time on stream, from about 80% removal initially, to 90% removal after 12 hours and 94% removal after 25 hours. This system models removal of acetonitrile from MTBE synthesis feedstock where it is a well known catalyst poison. 'TRAPIT-N' is effective at removing 5 % pyridine from hexadecane. At 30°C pyridine removal is almost 100 % falling to 97% at 150°C, with adsorption capacities 5.9 wt% N at 30°C falling to around 5.7 wt% N at 150°C. As 'TRAPIT-N' contains sulphuric acid some precautions should be taken. If there is free water in the feedstock to be treated (as there may be for a hydrotreated naphtha), the sulphuric acid may be washed out and corrosion effects may occur. Therefore the use of 'TNS Balls' both on top and on the bottom of the 'TRAPIT-N' bed is mandatory, to pick up free water and stop leaching of sulphuric acid. If this possibility cannot be totally excluded then the inner wall of the reactor should be coated with PTFE. Operating conditions for both adsorbents are 30°C to 135°C (preferably 30 to 60°C) and LHSV < 5 h^{-1} and GHSV < 4000 h^{-1} for 'TNS Balls'. The LHSV limit of 5 h^{-1} is quite low, although the authors state that for 'TRAPIT-N' this limit is determined by the expected on-stream lifetime of one year, and the LHSV does not affect the adsorption capacity or nitrogen cleaned up performance. The limited temperature range is a possible drawback for both systems, although the loss in performance is small at 150°C. If a feedstream must be cooled prior to contact with the adsorbent, and then reheated before a further catalytic process, then significant extra costs may be incurred. 'TRAPIT-N' offers a very high adsorption capacity but the possibility of sulphuric acid leaching from it and the precautions necessary because of this, such as a PTFE lined reactor, make it a less attractive option. 'TNS Balls' has the disadvantage that it requires two beds configured in parallel, one in operation, while the other is regenerated. The limited LHSV may also be a drawback. A further problem for both systems may be the limited operation temperature range. A typical post hydrotreater naphtha stream would be around 185°C. If this temperature must be reduced before the adsorbent bed and then increased before the reformer, expensive energy will inevitably be lost, even with modern, highly efficient heat exchangers in use.

1.4 Conclusions

Many solid acid systems have been studied as adsorbents for removal of nitrogen compounds from oils. Most of these systems have been regarded as successful by the respective experimentalists, as they have removed some or all of the nitrogen compounds. However, properties which would be detrimental to use in a commercial process, such as low adsorption capacity, inability to denitrogenate to very low levels, and problems with rigidity in a high temperature, highly aromatic oil stream (ion exchange resins), have largely been overlooked by the authors. The Sud-Chemie adsorbents look far superior, but are not ideal due to limits in their effective temperature range, LHSV / GHSV (with 'TNS-Balls') and the possible leaching of H_2SO_4.

For a commercial on-line adsorption system, the ideal adsorbents will be required to selectively adsorb high levels of basic nitrogen compounds, at elevated temperature, without activating the hydrocarbon stream and forming 'coke'. For this reason a material of intermediate acidic strength may be advantageous. The 'window' of suitable acid strength will diminish as the temperature is increased. At higher temperatures stronger acid sites will be required to retain pyridine, but activation of the hydrocarbon stream will require a lower acid strength.

The most promising adsorbents appear to be zeolites, MCM-41, aluminas, silica-aluminas, metal sulfates on supports and possibly anhydrous acids on supports. Zeolites have high adsorption capacities, structural integrity and are easily regenerated. MCM-41 offers a moderate acid strength and high pore volumes. Silica aluminas are well known solid acids with lower acid site strength than zeolites. Aluminas can be easily modified to control the nature and strength of acid sites. Metal sulfates on a suitable support may also offer high adsorption capacities, combined with relatively simple regeneration and easily controlled acidity. Anhydrous acids on supports are another possibility provided water in the feed does not pose too much of a problem. In the case of naphtha (the reformer feed) denitrogenation by supported anhydrous HCl may be suitable. Leaching of

small amounts of HCl from the adsorbent would not necessarily be a problem, as chloride can be added to the reformer feed as a promoter.

The nature of the adsorbent (acidity, pore structure etc.) should be chosen with a feedstream in mind. In the case of naphtha most of the nitrogen compounds remaining after hydrotreatment are likely to be single ring aromatics such as pyridine and aniline. Adsorbents with pore diameters greater than about 5Å will adsorb these species, hence ZSM-5 may be effective.

All the literature cited here used mechanical mixing of adsorbent and model feedstream or a gravity fed column, usually at room temperature. These techniques allow a considerable contact time, so it is difficult to assess diffusion kinetics and speed of uptake for the system. There is a strong case for the use of a microreactor with on-line analysis of the exit stream. This would allow the assessment of adsorbents in a far superior manner with respect to an industrial process by using appropriate temperatures, pressures and contact times. Ultimately, a system could be developed that would also allow the study of the breakthrough times for each nitrogen compound in a mixture, and hence assess the relative affinity of each for the adsorbent. Combined analysis of the hydrocarbon components in the stream could verify whether the adsorbent is modifying the nature of the stream in some way. It is important to note that the integrity of the hydrocarbon stream after treatment has not been discussed in any literature found to date.

1.5 Project Objectives

Previous studies in this research area, discussed in this chapter, have used mechanical mixing of adsorbent and model feedstream, or a gravity fed column, usually at room temperature. These techniques allow a considerable contact time, so it is difficult to assess diffusion kinetics and speed of uptake for the system. This study aims to advance this work by introducing the following novel aspects to the experimental approach. :-

- The study of the basic nitrogen adsorption properties of potential adsorbents using a microreactor with on-line analysis of the exit stream. This allows an assessment of the diffusional properties of adsorbents as well as total sorption capacity. It also allows assessment of the ultimate efficiency of the adsorbent at the chosen conditions
- The study of potential adsorbents using a simple, well defined, model system as opposed to complex mixtures of both nitrogen compounds and hydrocarbon matrix. This will allow clear interpretation of the data
- The use of conditions applicable to an industrial system, i.e. basic nitrogen concentrations in the ppm range, operational temperatures around 200°C and high GHSV values (low residence times).
- The use of on-line analysis, capable of identifying any modification to the hydrocarbon component of the model system, or basic nitrogen decomposition products.
- The assessment of a variety of potential adsorbent types under the same, reproducible conditions, instead of studying adsorbents in isolation.

This work also aims to characterise, by experimental means, the acidic and structural properties of adsorbents, and correlate this information with the adsorption data. This should allow identification of which properties are beneficial, and which detrimental, to the selective adsorption process.

The initial aim of the project was to construct and commission a microadsorption apparatus, capable of assessing the basic nitrogen adsorption properties of solid acid materials, under conditions suitable for an industrial application. Concurrent with this was the development of an analytical technique capable of speciating and quantifying organic nitrogen at sub ppm levels. The combined microadsorption / analytical approach should be suitable for use initially with a model system and possibly samples of industrial feeds in the future.

Once suitable experimental apparatus had been commissioned the primary aim of the work was to assess the basic nitrogen adsorption properties of a number of likely solid acid materials. This assessment, combined with characterisation of the differing structural and acidic properties can be used to identify the properties most favourable for selective adsorption of basic nitrogen from a hydrocarbon feedstream.

1.6 References

1) Ledoux, M. J., *Catalysis*, **7**, The Chemistry Society, London, (1988), 125.
2) Satterfield, C. N., Heterogeneous Catalysis in Industrial Practice, 2nd edition, McGraw-Hill Inc., (1991).
3) McKetta, J. J., Petroleum processing handbook, Marcel Dekker Inc (1992).
4) Laine, R. M., *Catal. Rev.-Sci. Eng.*, 1983, **25**, (3) 459.
5) Odebunmi, E.O. and Ollis, D. F., *J.Catal.*, 1983, **80**, 76.
6) Aboul-Gheit, A. K., *Appl. Catal.*, 1985, **16**, 39.
7) Ho, T. C., *Catal. Rev.-Sci. Eng.*, 1988, **30,** (1) , 117.
8) Thomson, L. F. and Holmes, S. A., *Fuel*, 1985, **64** , 9.
9) Choi, H.W. and Dines, M.B., *Fuel*, 1985, **64** 4.
10) Albert, A., Heterocyclic Chemistry (2nd Edition), The Athlone Press, University of London, (1968).
11) Tanabe, K., Solid Acids and Bases, Academic Press Inc.(London), (1970).
12) Studies in Surface Science and Catalysis, Vol. **58**, Elsevier- Amsterdam, 1991.
13) Szostak, R., Molecular Sieves: Principles of Synthesis and Identification, Van Nostrand Reinhold Catalysis Series, (1989).
14) Smart, L. and Moore, E., Solid State Chemistry, (1993), Chapman and Hall.
15) Connerton, J., Joyner, R. W. and Padley, M. B., *J. Chem. Soc. Faraday Trans.*, 1995, **91**(12), 1841.
16) Ellis, J. and Korth, J., *Fuel*, 1994, **73** (10) , 1569.
17) Ellis, J., Korth, J. and Peng, L., *Fuel*, 1995, **74** (6) , 860.
18) Kresge, C. T., Leonowicz, M. E., Roth, W. J., Vartulli, J. C. and Beck, J. S., *Nature* 1992, **359**, 710.
19) Beck, J. S., Vartulli, J. C., Roth, W. J., Leonowicz, M. E., Kresge, C. T., Schmitt, K. D., Chu, C. T.-W., Olson, D. H., Sheppard, E. W., McCullen, S. B., Higgins, J. B. and Schlenker, J. L., *J. Am. Chem. Soc* . 1992, **114**, 10834.

20) Corma, A., Grande, M. S., Gonzales-Alfaro, V. and Orchilles, A. V., *J. Catal.* 1996, **159**, 375.

21) Corma, A., *Chem. Rev.* 1997, **97**, 2373

22) Climent, M. J., Corma, A., Iborra, M. C., Navarro, M. C. and Primo, J., *J. Catal.*1996, **161**, 783.

23) Sayari, A., *Chem. Mater.* 1996, **8**, 1840.

24) Ulagappan, N. and Rao, C. N. R., *J. Chem. Soc., Chem. Commun.* 1996, 2759.

25) Khushalani, D., Kuperman, A., Ozin, G. A., Tanaka, K., Garces, J., Olken, M. M. and Kuperman, A., *Adv. Mater.* 1996, **7**, 842.

26) Winsor, P. A., *Chem. Rev.* 1968, **68**, 1.

27) Ekwall, P., In *Advances in Liquid Crystals*, Brown, G. H., Ed., Academic Press Inc., New York, 1971, 1.

28) Chen, C. Y., Burkett, S. L., Li, H. X. and Davis, M. E., *Microporous Mater.* 1993, **2**, 27.

29) Beck, J. S., Vartulli, J. C., Kennedy, G. J., Kresge, C. T., Roth, W. J. and Schramm, S. E., *Chem. Mater.* 1994, **6**, 1816.

30) Monnier, A., Schuth, F., Huo, Q., Kumar, D., Margolese, D., Maxwell, R. S., Stucky, G. D., Krishnamurty, M., Petroff, P., Firouzi, A., Janicke, M. and Chmelka, B. F., *Science*, 1993, **261**, 1299.

31) Hou, Q., Margolese, D. I., Ciesla, U., Feng, P., Sieger, P., Leon, R., Petroff, P., Schuth, F. and Stucky, G. D., *Nature* 1994, **368**, 317.

32) Ciesla, U., Demuth, D., Leon, R., Petroff, P., Stucky, G., Unger, K. and Schuth, F., *J. Chem. Soc., Chem. Commun.* 1994, 1387

33) Bull, L. M., Kumar, D., Millar, S. P., Besier, T., Janicke, M., Stucky, G. D. and Chmelka, B. F., *Stud. Surf. Sci. Catal.* 1994, **84**, 429.

34) Firouzi, A., Kumar, D., Bull, L. M., Besier, T., Sieger, P., Huo, Q., Walker, S. A., Zasadzinski, J. A., Glinka, C., Nicol, J., Margolese, D. I., Stucky, G. D., and Chmelka, B. F., *Science* 1995, **267**, 1138.

35) Huo, Q., Leon, R., Petroff, P. M. and Stucky, G. D., *Science* 1995, **268**, 1324.

36) Stucky, G. D., Huo, Q., Firouzi, A., Chmelka, B. F., Schacht, S., Voigt-Martin, I. G. and Schuth, F., *Stud. Surf. Sci. Catal.* 1997, **105**, 3.

37) Glinka, C., Nicol, J., Stucky, G. D., Ramli, E., ., Margolese, D. I., and Huo, Q., In *Advances in Porous Materials, Mater. Res. Proc.* Komarneni, S., Smith, D. M. and Beck, J. S., Eds., Materials Research Society, Pittsburgh, PA, 1995, **371**, 47.

38) Calabro, D. C., Valyocsik, E. W. and Ryan, F. X., *Microporous Mater.* 1996, **7**, 243.

39) Corma, A., Fornes, V., Navarro, M. T. and Perez-Pariente, J., *J. Catal.* 1994, **148**, 569.

40) Schmidt, R., Junggreen, H. and Stocker, M., *J. Chem. Soc., Chem. Commun.* 1996, 875.

41) Schmidt, R., Akporiaye, D., Stocker, M. and Ellestad, O. H., *J. Chem. Soc., Chem. Commun.* 1994, 1493.

42) Luan, Z., Cheng, Ch. F., Zhou, W. and Klinowski, J., *J. Phys. Chem.* 1995, **99**, 1018.

43) Janicke, M., Kumar, D., Stucky, G. D. and Chmelka, B. F., *Stud. Surf. Sci. Catal.* 1994, **84**, 243.

44) Schmidt, R., Akporiaye, D., Stocker, M. and Ellestad, O. H., *Stud. Surf. Sci. Catal.* 1994, **84**, 61.

45) Borade, R. B. and Clearfield, A., *Catal. Lett.* 1995, **31**, 267.

46) Kloetstra, K. R., Zandbergen, H. W. and van Bekkum, H., *Catal. Lett.* 1995, **33**, 157.

47) Bisset, A. and Dines, T. J., *J.Chem. Soc. Faraday Trans.* 1997, **93**(8), 1629.

48) Corma, A., Grande, M. S., Gonzales-Alfaro, V. and Orchilles, A. V., *J. Catal.* 1996, **159**, 375.

49) O'Connor, P., Gerritsen, L. A., Pearce, J. R., Desai, P. H., Yanok, S. and Humpries, A., *Hydrocarbon Process. Int.*, 1981, **70**, 76.

50) Engelhardt, J., Onyestyak, G. and Hall, W. K., *J. Catal.* 1995, **157**, 721.

51) Berteau, P., Kellens, M-A. and Delmon, B., *J. Chem. Soc. Faraday Trans.* 1991, **87**(9), 1425.

52) Shen, Jianyi, Cortright, R. D., Yi, Chen, and Dumesic, J. A. *J. Phys. Chem.* 1994, **98**, 8067.

53) Scokart, P. O. and Rouxhet, P. G., *J. Colloid Interface Sci.* 1982, **86**(1), 96.

54) Ghosh, A. K. and Kydd, R. A., *Catal. Rev.-Sci. Eng.* 1985, **27**(4), 539.

55) DeCanio, E. C., Bruno, J. W., Nero, V. P. and Edwards, J. C., *J. Catal.* 1993, **140**, 84.

56) Hegde, R. I. And Barteau, M. A., *J. Catal.* 1989, **120**, 387.

57) Skapin, T. and Kemnitz, E., *Catal. Lett.* 1996, **40**, 241.

58) Prudich, M. E., Cronauer, D. C. and Marcelin, G., *Separation Science and Technology*, 1987, **22** (2&3), 889.

59) Cronauer, D. C., Young, D. C., Solash, J., Seshadri, K. S. and Danner, D.A. *Ind. Eng. Chem. Process Des. Dev.*, 1986, **25**, 756.

60) Audeh, C. A., *Ind. Eng. Chem. Prod. Res. Dev.*, 1983, **22**, 276.

61) Richter, F. P., Ceaser, P. D., Meisel, S. L. and Offenhauer, R. D., *Ind. Eng. Chem.*, 1952, **44**, 2601.

62) Derouane, E. G., Andre, J. M. and Lucas, A. A., *J. Catal*, 1988, **110**, 58.

63) Zhu, S., Bell, P. R. F. and Greenfield, P. F., *Wat. Res.*, 1988, **22**, 1331.

64) Riley, R.G., Garland, T.R., Soisaki, K., Mann, D.L. and Wildung, R.E., *Environ. Sci. Technol.*, 1981, **15**, 697.

65) Lin, Y.S. and Ma, Y.H. in Zeolites: Facts, Figures, Future (Eds P.A. Jacobs and R.A. van Santen), Elsevier, Amsterdam, (1989).

66) Dessau, R.M. in Absorption and Ion Exchange with Synthetic Zeolites', Symposium Series No. 135 (Ed. W.H. Flank), American Chemical Society, Washington, DC, (1980), 123.

67) Chorley, S.R., Crittenden, D.B. and Kolaczkowski, S.T., 'Advances in Water Treatment and Environmental Management', (Eds. G. Thomas and R. King), Elsevier, London, (1991), 181.

68) Mochida, I., Fei, Y.Q., Sakanishi, K., Usuba, H. and Miura, K., *Chem. Lett.*, 1990, **4**, 515.

69) Fei, Y.Q., Sakanishi, K., Sun, Y.N., Yamashita, R. and Mochida, I., *Fuel*, 1990, **69**, 261.

70) Mochida, I., Fei, Y.Q., Sakanishi, K., Korai, Y., Usuba, H. and Miura, K., *Carbon,* 1992, **30** (2), 241.

71) Sakanishi, K., Sun, Y.N., Mochida, I. and Hidehiko, U., *Fuel Processing Technology*, 1992, **32**, 143.

72) Sakanishi, K., Obata, H., Mochida, I. and Sakaki, T., *Abstracts of Papers of the American Chemical Society,* 1994, **208** (1), 50.

73) Sud Chemie publication.

Chapter 2 Experimental

2.1 Preparations

2.11 Preparation of supported metal sulfates

Three types of silica were used to support the metal sulfates.

1. Acros - used for chromatography

BET Surface area : 700 $m^2 g^{-1}$ * Mesh 0.06 - 0.20 mm Pore diameter 40Å

2. Davisil grade 645

BET Surface area : 240 $m^2 g^{-1}$ * Mesh 0.15 - 0.25 mm Pore diameter 150Å

3. Fumed silica

Surface area : 390 ± 40 $m^2 g^{-1}$ Mesh 0.007 μm Non - porous

* Experimental surface area

Two metal sulfates were added to the silica by impregnation.

1. Aluminium sulfate $Al_2(SO_4)_3$, BDH > 99.8%

2. Nickel sulfate $NiSO_4$, Pronalys AR > 99%

3wt%, 6wt% and 12wt% samples were made for each metal sulfate on each different silica giving 18 samples.

Metal sulfate	ACROS	DAVISIL	FUMED
$Al_2(SO_4)_3$	3, 6, 12wt%	3, 6, 12wt%	3, 6, 12wt%
$NiSO_4$	3, 6, 12wt%	3, 6, 12wt%	3, 6, 12wt%

The samples were prepared using the incipient wetness impregnation technique. Firstly the amount of solvent (in this case water) required to form a homogeneous paste with a given amount of the silica gel is determined experimentally for each of the gels. This is known as the point of incipient wetness - when the solvent fills the pores and just covers the external surface of the gel. In the second step the appropriate amount of the sulfate is dissolved in this volume of water and the solution is added to the gel, forming a similar paste. The paste is then dried in an oven. As the solvent only just fills the pores, and coats the surface, the sulfate should be left well dispersed on the pore walls, and external surface of the silica, when the solvent is removed.

2.12 Preparation of MCM 41

Samples of MCM 41 have been prepared following the procedure in ref. (1) with Si / Al ratios between 8 and 25. Amounts of sodium aluminate ($Na_2Al_2O_4$, Riedel-de Haen) between 0.77 and 2.4 grams were stirred with 90 mls of distilled water, and 30 grams cetyl-trimethyl ammonium bromide (Lancaster 98%) in a polypropylene bottle for one hour. Between 1.0 and 1.3 grams of NaOH, such that $2< Na_2O / Al_2O_3 <3$, and 120 mls distilled water were then added with continued stirring. When all the NaOH pellets had dissolved, 12.3 grams of fumed silica was added, and after a further two hours stirring the bottle was sealed and placed in an oven, at 90°C for 48 hours. After cooling to room temperature the solids were collected by filtration and washed with distilled water, and then ethanol, to remove part of the template. After drying overnight at 100°C, the residual template was removed by calcining in static air for 12 hours, at 550°C, after ramping from room temperature, at 0.7°C min^{-1}.

2.13 Preparation of Amorphous Silica-Aluminas

A series of 5 amorphous silica-aluminas were prepared with different alumina content according to the established procedure in ref. (2). The five samples had SiO_2 / Al_2O_3 molar ratios of 90:10, 75:25, 50:50, 25:75 and 10:90. HNO_3 was added dropwise to required amounts of water glass (Na_2SiO_3 – Fisher scientific) until the silicate solution gelled (pH 9.8). The gel was aged for 1 hour at room temperature. A requisite amount of $Al(NO_3)_3.9H_2O$ (Fisher > 98%) as demanded by the SiO_2 / Al_2O_3 ratio was dissolved in distilled water and mixed with the silica gel. The mixture was stirred for 10 minutes and 8M NH_4OH solution added dropwise until a pH of about 6. 35 ml of 1M NH_4NO_3 (Janssen chimica) solution was then added with stirring and the pH was increased from 6 to 7 using 8M NH_4OH. The precipitate was aged for 3 h at 25°C and 4 h at 45°C. The sample was then dried for 6 h at 75°C and 16 h at 120°C, then calcined at 550°C for 10 h. The samples were gently ground prior to triple ion exchange with 1M NH_4NO_3 and then calcined for a further 16 h at 550°C.

2.14 Modified Aluminas

γ-Alumina (Alfa) was fluorided by incipient wetness impregnation of NH_4F (BDH >99%). Requisite amounts of NH_4F were used to give fluoride loadings of 1 wt% and 14 wt%, representing the two extremes of fluoride loadings generally used to increase the acidity of aluminas[3]. The impregnated samples were dried overnight at 100 °C. Both the unmodified and fluorided aluminas were calcined for 16 h in static air, at either 600 °C or 1000 °C prior to FTIR and microadsorption examination.

2.15 Zeolites

Fig 2.15.01 The parent zeolite samples studied in this work

Sample	Si / Al	Supplier
H-Mordenite	12.5	Catal Ltd (Sheffield, UK)
Na-Mordenite	6.4	Catal Ltd (Sheffield, UK)
H-ZSM-5	25	Catal Ltd (Sheffield, UK)
H-ZSM-5	15	Catal Ltd (Sheffield, UK)
13X	< 2	UOP

2.15.1 Ion Exchange

All zeolite and MCM-41 ion exchanges were conducted at room temperature in aqueous solution. Unless otherwise stated 2g of zeolite was exchanged for 4 h with 500 ml 0.05M $Cu(NO_3)_2$ (Aldrich >99.8 %) or NH_4NO_3 (BDH 99.9 %)(with stirring). In some cases the zeolite was multiple exchanged. The samples were then dried at 60 °C for 16 h and 90 °C for 4 h.

2.16 Calcination

All calcinations were performed for 4 hours in static air.

Zeolite and MCM-41 samples were activated before use by calcination at 500 °C, except 13X which was calcined at 300°C. Calcinations were performed with a shallow sample bed, and a 5 °C min^{-1} temperature ramp from room temperature. Supported metal sulfate samples were calcined before use at 350°C, which should give a relatively high number of acid sites [4].

2.2 Techniques

2.21 BET Surface Area Measurement

The knowledge of the total surface area of a material is important in catalysis. Physical adsorption of a gas such as N_2 is a convenient method of measurement. The surface area can be deduced from the adsorption isotherm, which is the volume of an inert gas adsorbed as a function of equilibrium pressure. Isotherms have certain characteristic shapes that reflect the nature of the solid and the adsorption process. At least five types of isotherm have been identified [5].

Fig 2.21.1 The five types of physical adsorption isotherm[5].

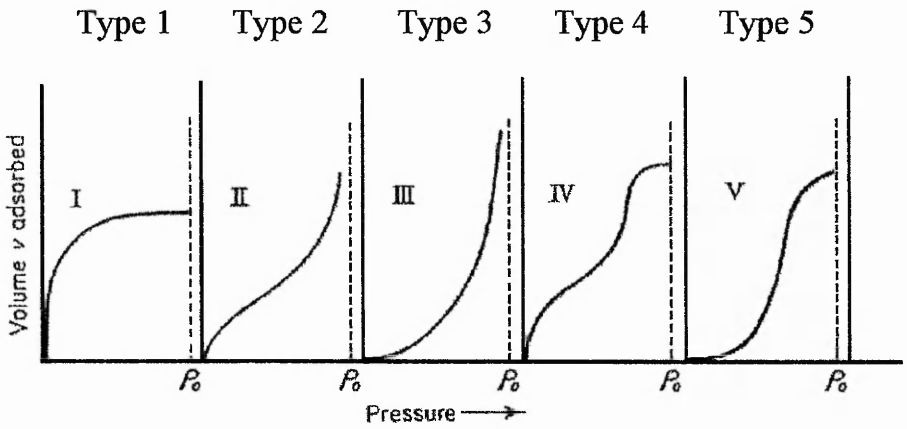

P is the equilibrium pressure and Po is the saturated vapour pressure of the adsorbent gas at the temperature of the measurement.

Type 1 isotherms are characteristic of microporous* materials with pore diameters of no more than a few molecular diameters. Type 2 isotherms are given by non-porous materials. Type 3 isotherms are characteristic of non-porous and macroporous materials, when adsorbate / adsorbent interactions are weak. Type 4

is characteristic of mesoporous* materials and type 5 is given by mesoporous or microporous materials when the adsorbate / adsorbent interactions are weak [5].

* Micropores are defined as < 2nm

Mesopores are defined as > 2nm and < 50nm

To determine the surface area from the 'raw' isotherm requires a mathematical procedure to linearise the experimental isotherm in such a way that the volume can be deduced. The Brunauer, Emmett and Teller approach referred to as the B. E. T. equation, which is generally only applicable to type II isotherms (non-porous) and type IV isotherms (mesoporous), in the P/Po range 0.05 to 0.3, is used in this experiment.

The B.E.T. equation

$$\frac{P}{V(P_o-P)} = \frac{1}{V_m C} + \frac{(C-1)P}{V_m C P_o}$$

V is the volume of gas adsorbed at equilibrium pressure P, Vm is the volume necessary to form a monolayer and Po is the saturated vapour pressure of the adsorbent gas at the temperature of the measurement. C is a constant which describes the difference between the heats of adsorption of the first monolayer and subsequent monolayers with a value normally between 2 and 500. The heats of adsorption of monolayers after the first are more characteristic of a condensation than physical adsorption. A straight line is obtained by plotting P/V(Po-P) against P/Po. The slope is given by (C-1)/VmC and the intercept by 1/VmC. The monolayer volume, Vm, can be determined by the reciprocal of the sum of the intercept and gradient. Then by knowing the cross-sectional area of an adsorbed

molecule (taken to be 16.2Å^2 for N_2) and the mass of the sample, the specific surface area can be deduced.

The nitrogen adsorption experiments were performed on a computer controlled volumetric instrument, at liquid nitrogen temperature (77 K), making the Po term equal to atmospheric pressure.

2.22 F.T.I.R Fourier Transform Infra Red Spectroscopy

2.22.1 Theory

Absorption of electromagnetic radiation in the IR region of 5000-200cm^{-1}, causes transitions between vibrational and rotational energy levels of molecules. Since the gross-selection rule for infra-red spectroscopy is that a change in dipole moment must occur, only those transitions which give rise to such a change can be observed. The vibrating bond has a certain intrinsic vibrational frequency dependent on the effective mass and force constant, this oscillation frequency can be shown by (i). The equation is converted into wavenumbers (cm^{-1}) which is the unit usually employed, by dividing by the velocity of light c (eqn. ii). The positions of the bands in the spectra are related to the strength of bond vibration and also masses of the atoms involved in the vibration.

(i) $$\nu = \frac{1}{2\pi}\sqrt{\frac{k}{\mu}} \quad \text{Hz}$$

(ii) $$\bar{\nu} = \frac{1}{2\pi c}\sqrt{\frac{k}{\mu}} \quad \text{cm}^{-1}$$

k = bond force constant, μ = effective mass,

$\bar{\nu}$ = wavenumber, c = velocity of light

An F.T.I.R. spectrophotometer's optical system is very simple, and is based on the 'Michelson interferometer'. The interferometer requires two mirrors, an infrared light source, an infrared detector and a beamsplitter.

Fig 2.22.11 The Michelson Interferometer Optical System [16].

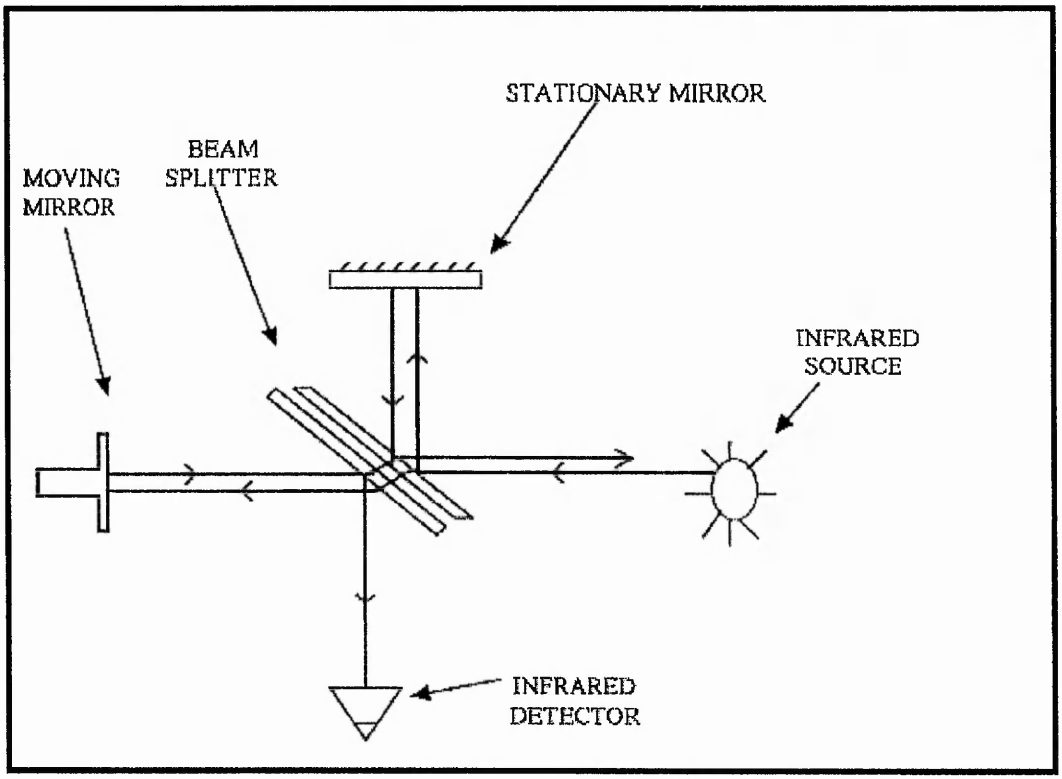

The beamsplitter is the heart of the interferometer; it reflects about 50% of an incident light beam and at the same time transmits the remaining 50%. One part of the split light beam travels to a moving mirror while the other part travels to a stationary mirror. The two mirrors reflect the light beams back to the beamsplitter where they recombine. In practice, the sample can be placed between the beamsplitter and either the moving or stationary mirror. At the beamsplitter, half of the recombined light is transmitted to the detector and the other half is reflected toward the infrared source. When the two light beams recombine at the beamsplitter, they can interfere constructively or destructively; hence an interference pattern is generated. This interference pattern varies with the displacement of the moving mirror along its axis and is detected by the infrared

detector as variations in the infrared intensity level. [37]. The interference pattern or interferogram can be converted into an infrared spectrum using Fourier transform mathematics.

FTIR was chosen for this type of study as it offers many advantages over conventional dispersive IR systems.

1. Multiplex advantage (Felgett's advantage). All frequencies are collected simultaneously, increasing the speed of analysis.

2. Throughput advantage (Janquinot advantage). The power of the radiation reaching the detector is much greater than in a dispersive instrument as there are fewer optical elements. No slits are required to attenuate radiation, so sample sizes are larger. Much greater signal-to-noise ratios are observed.

3. Conne's advantage. Extremely high wavelength accuracy and precision. This makes signal averaging possible which leads to improved signal-to-noise ratios.

High signal to noise ratios are important when the IR beam is passed through a solid undiluted disc of sample and a substantial amount of intensity is lost.

Infrared absorption spectroscopy is one of the most powerful tools available to the chemist for identifying pure organic and inorganic compounds because, with the exception of a few homonuclear compounds such as O_2, N_2 and Cl_2, all molecular species absorb infrared radiation [6]. Furthermore with the exception of chiral molecules in the crystalline state, each molecular species has a unique infrared absorption spectrum. Thus an exact match between the spectrum of a compound of known structure and an analyte unambiguously identifies the latter [6]. As well as identification of compounds, infrared spectroscopy can be used as a surface characterisation technique, through the study of adsorbed probe molecules. All kinds of probe molecules have been used with infrared, including bases such as NH_3 and pyridine, as well as CO, CO_2, nitrogen oxides, alkenes, alcohols and acids

[7]. Bases such as NH_3 and pyridine are often used to probe acid sites in materials like metal oxides [7]. In the case of pyridine a useful distinction can be made between pyridine chemisorbed on a Lewis acid site and pyridine chemisorbed on a Bronsted acid site, and hence the relative proportion of each can be assessed. The band assignments for these states are well understood [8-15].

Interaction between a lone pair orbital of pyridine and a Lewis acid centre results in the 8a normal vibration mode of pyridine being observed in the range 1590 – 1615 cm^{-1}, while the 19b normal mode is found between 1440 and 1465 cm^{-1}. Interaction with the proton of a Bronsted site results in the formation of a pyridinium ion, shifting these bands, respectively, to 1638 – 1642 cm^{-1} and 1545 – 1540 cm^{-1}. The 19a normal mode is observed at 1490 cm^{-1} for both Lewis and Bronsted sites interacting with pyridine. Indications of acid strength may also be gained by measurements after evacuation at different temperatures.

When solid acids, such as zeolites, are involved in cracking of hydrocarbons, a highly carbonaceous material known as 'coke' is deposited on them. This is partly due to the inherent hydrogen deficiency of the cracked product. The deposition of 'coke', generates an absorption band at around 1585 cm^{-1} in the infrared spectrum [17,18]. This makes infrared an ideal technique for monitoring coke formation.

The exact nature of cracking and coking reactions on solid acid catalysts has been a subject of discussion for many decades [19,20]. Early studies favoured Lewis centres for the initiation of cracking reactions [21]. Later work, particularly with zeolites, using techniques such as infra-red spectroscopy showed that Bronsted sites are probably the seat of catalytic activity [22-24]. More recent studies have shown a direct correlation between the numbers of strong Bronsted sites and activity in cracking of linear alkanes [25-27]. Abbott et. al.[19] have studied the cracking of n-octane on H-mordenite, concluding that the dominant cracking processes leading to formation of acyclic alkanes and alkenes take place on Bronsted sites. However, formation of aromatics and coke, associated with hydrogen transfer and cyclisation processes, is enhanced by the presence of Lewis sites on the catalyst surface. Whilst there is no evidence that Lewis sites are

directly involved in simple cracking reactions, they may participate directly, or indirectly, in processes leading to aromatics and coke. Coking therefore appears to be driven by interplay between strong Bronsted and Lewis sites, the exact nature of which is still not fully understood.

In this project a Mattson Polaris FTIR spectrometer has been used in conjunction with an in-situ vacuum transmission cell, to study pyridine and heptane adsorption on solid acid materials. This gives information on the number, and nature of acid sites, as well as the samples propensity to activate a hydrocarbon and generate coke. This can then be correlated with their performance as adsorbents for pyridine from a model hydrocarbon system.

2.22.2 Equipment

The main body if the in-situ transmission cell consisted of a 316 stainless steel cylinder with a diameter of 105 mm and a length of 64 mm. The aluminium sample holder was simply two pieces of circular aluminium, with their elliptical centres removed, to allow the infra-red beam through, and two keyhole shapes removed near the edges. The sample was sandwiched between the aluminium pieces, and secured by means of two tightening screws, so that it was visible in the centre of the holder. The sample holder was fixed in the cell by means of placing the keyholes over two screws set in the internal wall of the cell and then rotating to secure in position. A 'K type' thermocouple was screwed into the body of the cell, with the temperature sensing tip just touching the sample, held within the aluminium holder. The thermocouple was connected to a Eurotherm temperature controller, coupled to a variac voltage supply controller. The combination of the Eurotherm controller and variac enabled a more accurate control of the temperature of the cell and the sample disc. Heat was supplied by four 600 Watt cartridge heaters, placed through the main body of the cell, and controlled by the Eurotherm. Modification of the input voltage by the variac protected the heating rods from 'burning out'.

The ends of the in-situ cell contained two calcium fluoride windows with diameter 35 mm and thickness 4 mm. To prevent the windows from expanding and cracking at high temperatures, the windows were cooled, by water passing through channels in the end sections of the cell, encircling the windows. The flowing water also prevented the overheating of the vacuum tight viton seals between the main body and the ends of the cell.

The in-situ cell was connected to a vacuum dosing line. The dosing line made use of a diffusion pump 'backed' by a rotary pump, and could maintain a vacuum of 10^{-3} mbar in the cell throughout the experiment. A complex arrangement of valves allowed the cell to be isolated, dosed with pyridine (or heptane), evacuated straight

to the rotary pump, or evacuated to the diffusion pump at appropriate times in the experiments.

Fig2.22.21 Schematic of the In-Situ Fourier Transform Infrared Cell

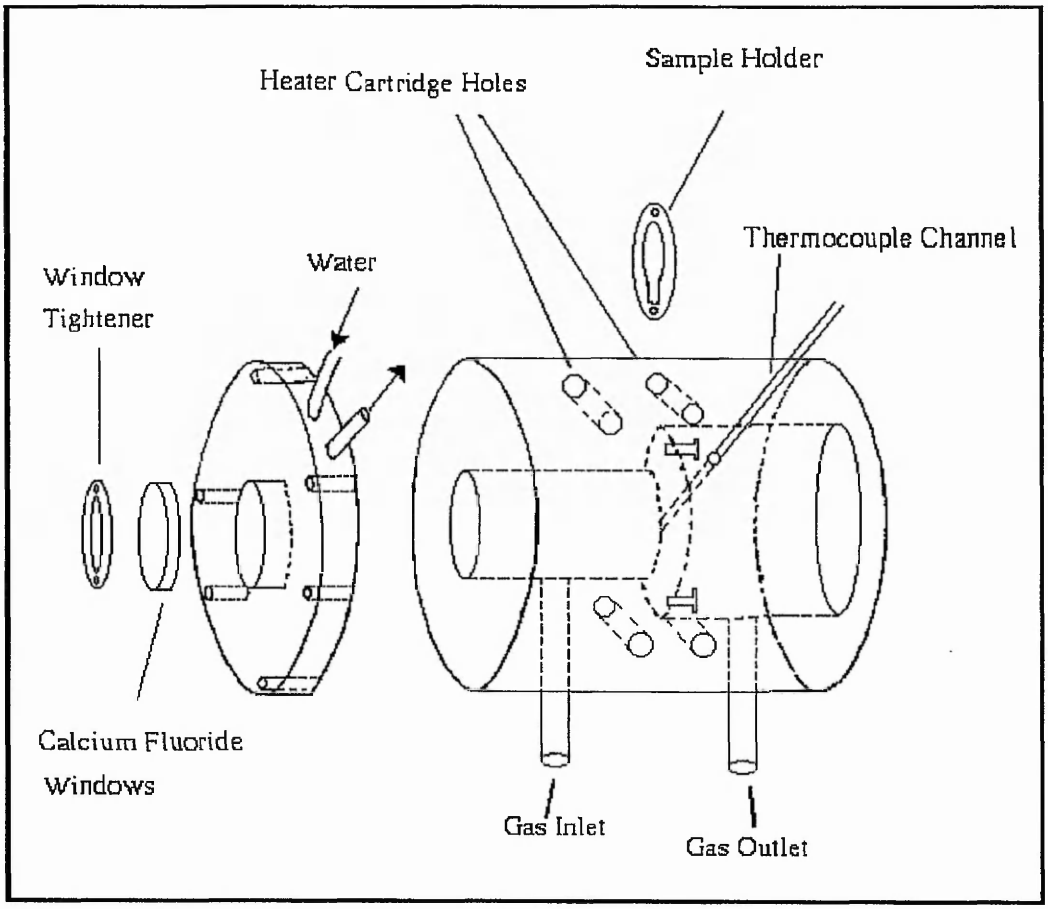

2.22.3 Procedure

After calcination, each sample was placed in a desiccator until cool and then gently ground using a mortar and pestle if necessary. A small amount of sample < 0.02g was pressed into a self-supporting wafer of 13 mm diameter at 15 MN m^{-2}. XRD analysis of pressed zeolites showed that this pressure does not damage the lattice and Gusev et.al[19] have established that the MCM-41 structure is not affected by mechanical compression below ~ 80 MN m^{-2}. Gentle grinding can improve the quality of the wafer when using samples which are difficult to press, and hence results in better spectra.

The disc was then carefully mounted in the sample cell. The cell was sealed, evacuated and heated to between 200°C and 350°C for 1.5 hours to activate the sample. Once cooled to room temperature, the cell was placed in the cell holder between the two fixed mirrors in the instrument. The instrument was then sealed and allowed to purge with dried, purified air, to remove water and CO_2 as these may interfere with the spectra. A second background spectrum was recorded with the beam passing through the cell, but missing the sample disk, for reference. The cell was then adjusted inside the instrument to align the sample disc in the beam. A sample spectrum was recorded.

At this stage excess pyridine vapour was admitted into the cell and allowed to equilibrate for 10 minutes at room temperature. The cell was opened to vacuum to remove the excess pyridine and an infra red spectrum was taken after 30 minutes evacuation. The cell was heated to 100°C and after 30 minutes a second spectrum was recorded. After 100°C, spectra were taken after 30 minutes at 150, 200, 250, 300 and 350°C.

The FTIR experiments with heptane were conducted in a similar way, except that heptane was dosed onto the sample at each temperature for 10 minutes. The sample was then evacuated for 30 minutes before each spectrum was taken

The heptane pre-activation experiments used in chapter 7 were performed by letting heptane vapour interact with the sample for 20 minutes, in the FTIR cell, at 350 °C. This was preceded by the usual activation at 350 °C for 1.5h. The cell was then evacuated and cooled to room temperature before a standard pyridine adsorption FTIR experiment was performed. This is designed to speciate which types of acid site are responsible for coke formation.

2.22.4 Normalisation of the absorption bands

Unless otherwise stated the tabulated experimental FTIR band areas have been normalised using the lattice overtone bands in the spectra. These overtone bands are usually found at ca. 1870 cm^{-1} and 1980 cm^{-1}, but can move ± 30 wavenumbers depending on the sample studied. The overtone bands effectively provide an accurate internal standard for the amount of sample in the IR beam so the same absorption band area should be generated regardless of the thickness of the sample disc.

2.22.5 Extinction coefficients

In order to calculate the ratio of Lewis to Bronsted sites from FTIR spectra, knowledge of the integrated molar extinction coefficients of the V_{19b} pyridine absorption bands is required. The absolute extinction coefficients are not required, only the ratio of the two. In this work the ratio (Lewis ~ 1450cm^{-1} / Bronsted ~ 1545 cm^{-1}) of 1.33 reported by Emeis[29] is used. However it is recognised that the results may be subject to significant systematic error as Borade et al[13] and Lefrancois and Malbois[30] have earlier reported values of 1.54 and 1.15 respectively.

2.23 Microadsorption studies

2.23.1 Procedure

For all the microadsorption studies, 0.1 g of sample was used. The sample was first pressed using 15 MN m^{-2} pressure into a disc, which is then broken up and sieved. The sieving fraction used in the experiments was between 0.25 mm and 0.425 mm. The pelleted sample was then packed between two plugs of silica wool, in the centre of a 4 mm i.d., 6 mm ø.d. silica tube, forming a bed approximately two centimetres in length. This gave an aspect ratio (bed length to bed diameter) of approximately 5:1, a bed diameter to particle diameter ratio of greater than 10:1 and a bed length to particle diameter ratio of greater than 50:1. These values should ensure plug flow conditions through the bed, and hence provide reliable results. The tube was placed in a tube furnace, with the bed in the central, isothermal zone. The samples were then activated at 350°C for 1.5 hours in a flow of helium, and cooled to the operational temperature of 200°C. The feed was 15 ppm pyridine in heptane, introduced via a Kontron 422 HPLC pump at 0.375 ml min^{-1} of liquid, corresponding to 58 ml min^{-1} gas phase at STP. Helium was also added as a diluent at a flow rate of 29 ml min^{-1} STP, regulated by a Brooks 5850 mass flow controller, making the gas phase concentration of pyridine 10 ppm. This total flow of 87 ml min^{-1} gave a GHSV of approximately 21000 h^{-1}, depending on the exact bed length. After microadsorption, analysis was performed by an ATI Unicam 610 gas chromatograph, fitted with a nitrogen / phosphorus (flame thermionic) detector capable of measuring levels of organic nitrogen below 1 ppm, and a Spectra Physics SP4290 integrator. A 4 metre, quarter inch diameter, stainless steel column with OV 101 stationary phase was used for the separation, which was performed isothermally at 135°C. Trace heating of all lines kept the feed and microadsorber exit stream in the gas phase throughout, and GC sampling was performed with a 6 port gas sampling valve and 1 ml sample loop. Once pumping of the feed was in progress, the adsorber exit stream was sampled at regular intervals by the 6 port valve and injected onto the column. The frequency

of this procedure was determined by the ca.15 minutes taken for the chromatographic analysis. The time taken for the pyridine in the feed to saturate the adsorption capacity of the bed and breakthrough into the exit stream can then be assessed. A plot of pyridine concentration in the exit stream against time, (T_0 being the initial introduction of the feed) can be made for each sample.

Fig 2.23.1 Schematic of the microadsorption apparatus

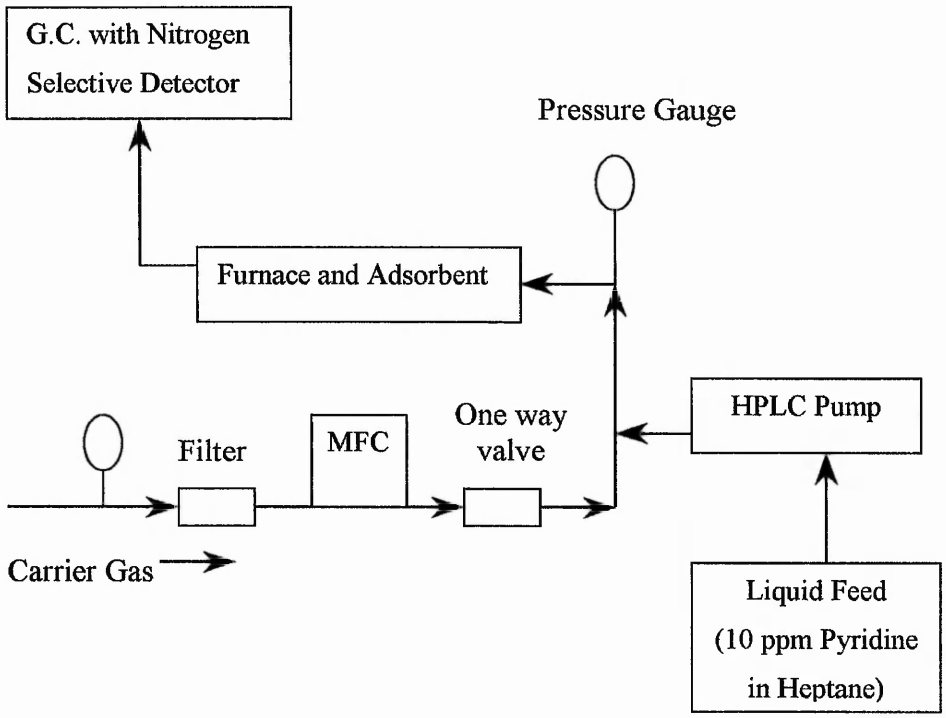

2.23.2 Breakthrough time

For comparison of the different samples the 50 % breakthrough time has been used, i.e. the time at which 50 % of the feed concentration of pyridine breaks through the adsorbent bed. It is recognised that for an adsorption application 50 % breakthrough would be unacceptable, however the author believes that this value is a better representation of the sample performance. As the profile of breakthrough is generally close to symmetrical the 50 % breakthrough time is representative of the total adsorption capacity. This value and not the initial or final breakthrough

points therefore best describe the effect of scaling up the process. In other words, if the size of the adsorbent bed were doubled, the 50 % breakthrough time would be expected to double.

2.23.21 Breakthrough time reproducibility

Fig 2.23.21 Multiple microadsorption experiments for H-ZSM-5 #3

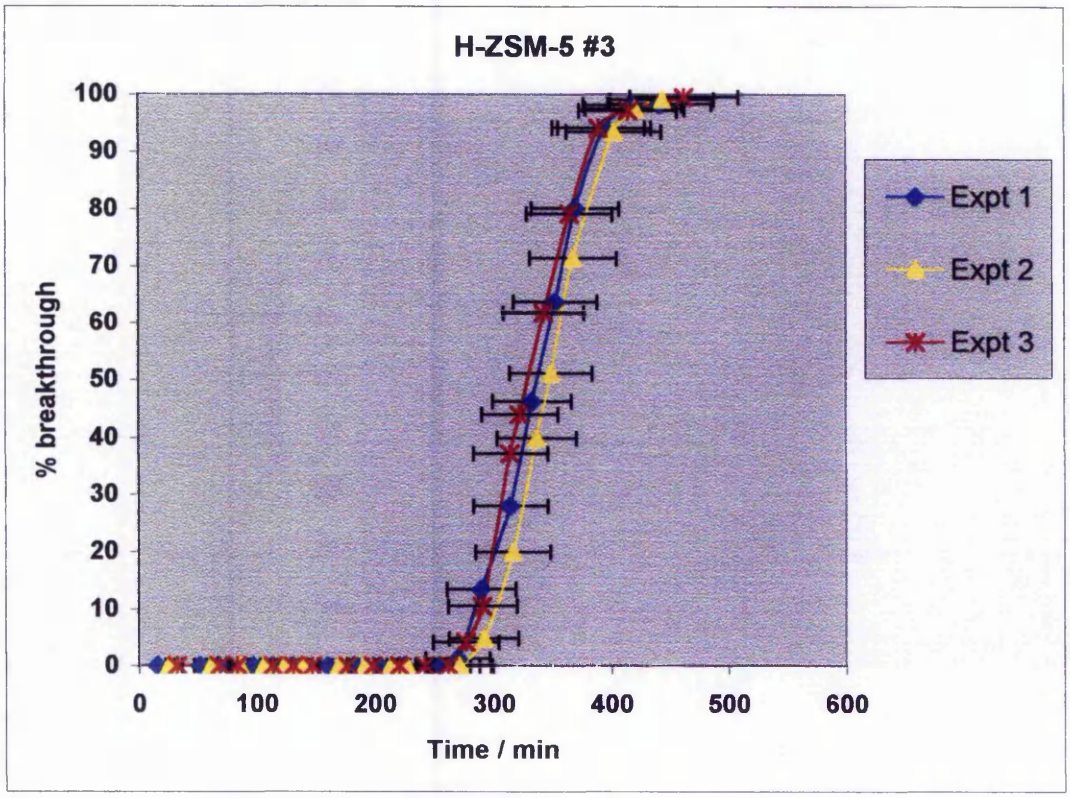

Fig 2.23.21 shows the pyridine breakthrough profiles for 3 microadsorption experiments on H-ZSM-5 #3. It demonstrates the high level of reproducibility in the microadsorption experiments. The 50% breakthrough times for the 3 experiments vary from 325 minutes to 345 minutes. The error bars on the graph represent errors of ± 10% of the x-axis values (time). The 3 experimental runs all fall well within these error bars, indicating that a ± 10% error approximation is more than sufficient to evaluate the 50% breakthrough times.

2.23.3 Regeneration

The ability of potentially interesting adsorbents to be regenerated and re-used has also been studied. After the completion of a microadsorption experiment, the model feed flow was stopped and the sample was left for 1 h under a flow of helium carrier gas, at the operational temperature of 200 °C. After this time no pyridine was detectable by G.C. The temperature was then raised in 50°C increments, dwelling for 60 min at each new temperature, up to a maximum temperature of 650 °C. Desorption of pyridine was monitored by G.C. at each temperature. After 60 min at each temperature pyridine desorption was reduced almost to the detection limits of the analytical technique (~ 0.2 ppm). As the temperature was increased to the next increment, fresh pyridine was desorbed. At temperatures above 500 °C, desorption of pyridine was significantly reduced. At the maximum temperature of 650 °C, only a very small amount of pyridine desorption was observed immediately after this temperature had been attained. Although it is possible that a small amount of pyridine may remain, the temperature was not increased further, because this might damage the adsorbent. Although the possibility of pyridine decomposition cannot be excluded, no evidence of decomposition products was observed by the G.C. analysis.

2.24 Powder X-Ray Diffraction (XRD)

The powder X-ray diffraction pattern can be used as a fingerprint for the identification of many compounds. Diffraction occurs when the angle of incidence of X-rays, satisfies the Bragg equation :

Equation 2.24.1

$$n\lambda = 2d \sin\theta$$

Where n = a small integer

λ = wavelength of X-ray source

d = separation between planes in crystal

θ = angle of incidence of X-rays

Reflections from the pattern can be compared to those in a standard powder diffraction file, enabling structure identification. The presence of different phases can also be determined. Measurements were performed using a Philips 3510 diffractometer with a Cu Kα source, wavelength 1.5418 Å. A scan range of $5° < 2\theta > 80°$ was used, with step size 0.02° and counting time of 0.5 s. The pattern obtained by rotating the sample through an angle θ while the detector is rotated through 2θ.

2.25 Transmission Electron Microscopy (TEM)

Transmission electron microscopy is a useful technique, which can be employed to examine sample morphology. In the case of MCM-41 high resolution TEM can be used to image the pore structure, and verify the presence of the MCM-41 phase.

The high resolution micrographs presented in this thesis were obtained by Dr C. J. Kiely at the University of Liverpool.

2.3 References

1) Kloetstra, K. R., Zandbergen, H. W. and van Bekkum, H., *Catal. Lett.* 1995, **33**, 157.
2) Rajagopal, S., Grimm, T. L., Collins, D. J. and Miranda, R., *J. Catal.* 1992, **137**, 453.
3) Ghosh, A. K. and Kydd, R. A., *Catal. Rev.-Sci. Eng.* 1985, **27**(4), 539.
4) Tanabe, K., Solid Acids and Bases, Academic Press Inc.(London), (1970).
5) Gregg and Sing, Adsorption Surface Area and Porosity, 2nd edition (1982), Academic Press.
6) Skoog, D. A., West, D. M. and Holler, F.J., Fundamentals of Analytical Chemistry, 5th ed., (1988), Saunders College Publishing.
7) Kung, M. C. and Kung, H. H., *Catal. Rev.-Sci. Eng.*, 1985, **27**(3), 425.
8) Connerton, J., Joyner, R. W. and Padley, M. B., *J. Chem. Soc. Faraday Trans.*, 1995, **91**(12), 1841.
9) Parry, E. P., *J. Catal*, 1963, **2**, 371.
10) Basila, M. R., Kantner, T. R. and Rhee, K. H., *J. Phys. Chem.*, 1964, **68** (11), 3197.
11) Cannings, F. R., *J. Phys. Chem.*, 1968, **72** (13), 4691.
12) Lercher, J. A. and Rumplmayr, G., *Zeitschrift fur Physikalische Chemie Neue Folge*, Bd. 1985, **146**, 113.
13) Borade, R. B., Adnot, A. and Kaliaguine, S., *J. Chem. Soc. Faraday Trans.*, 1990, **86** (23), 3949.
14) Abbot, J. and Guerzoni, F. N., *Applied Catalysis A: General*, 1992, **85**, 173.
15) Connell, G. and Dumesic, J. A., *J. Catal.*, 1986, **102**, 216.
16) Mattson Polaris FTIR manual.
17) Studies in Surface Science and Catalysis, 1991, Vol **58**, Elsevier – Amsterdam

18) Blackmond, D. G., Goodwin Jr, J. G. and Lester, J. E., *J. Catal.*, 1982, **78**, 34.

19) Abbot, J. and Guerzoni, F. N., *Appl. Catal. A: General*, 1992, **85**, 173.

20) Hansford, R. C., *Adv. Catal.*, 1952, **4**, 1.

21) Milliken, Jr., T. H., Mills, G. A. and Oblad, A. G., *Faraday Discuss.*, 1950, **8**, 279.

22) Hopkins, P. D., *J. Catal.*, 1968, **12**, 325.

23) Ward, J. W., *J. Catal.*, 1968, **11**, 238.

24) Benisi, H. A., *J. Catal.* 1967, **8**, 368.

25) Borade, R. B., Hedge, S. G., Kulkasni, S. B. and Ratnasamy, P., *Appl. Catal.*, 1984, **13**, 27.

26) Klyachko, A. L., Kapustin, G. I., Brueva, T. R. and Rubenstein, A. M., *Zeolites*, 1987, **7**(2), 119.

27) Haag, W. O., Lago, R. M. and Weisz, P. B., *Nature (London)*, 1984, **309**, 589.

28) Gusev, Y. G., Feng, X., Bu, Z., Haller, G. L. and O'Brien, J. A., *J. Phys. Chem.*, 1996, **100** (6), 1985.

29) Emeis, C. A., *J. Catal*, 1993, **141**, 347.

30) Lefrancois, M. and Malbois, G., *J. Catal.*, 1971, **20**, 350.

Chapter 3 Supported Metal Sulfates

3.1 Introduction

Metal sulfates are interesting materials as they have no intrinsic acidity, but develop acid sites of moderate strength when partially dehydrated[1]. Although this acidity is not intrinsic, in the sense that the sulfates must be carefully pre-treated, it is not the result of impurities. In the case of nickel sulfate, optimum acidity is generated by calcining at 350 °C, to give $NiSO_4$. $0.5H_2O$. Heating at 400 °C results in total dehydration and the acidity is lost[1].

Many metal sulfates, heat-treated at optimum temperatures, have been used as solid catalysts for various acid catalysed reactions[2]. These include polymerisation, de-polymerisation, hydration, esterification and isomerisation[2].

Metal sulfates have been extensively studied as potential acidic adsorbents for basic nitrogen compounds[3-7]. Basic nitrogen has successfully been removed from coal tar fractions,[3-5] and methylnaphthalene oil,[6,7] at room temperature.

The moderate acidity of partially dehydrated metal sulfates may allow selective adsorption of basic nitrogen compounds at realistic operational temperatures (200°C) without any unwanted side reactions such as cracking and coking. In addition regeneration may be a simple single step process. Heating to 400 °C will dehydrate the sulfate, destroying the acidity, and releasing the adsorbed bases.

3.2 Results

Only twelve of the series of eighteen supported metal sulfate samples will be discussed. The six samples supported on fumed silica proved impossible to press into a self-supporting wafer for FTIR analysis, or into pellets for the microadsorption studies

3.21 BET Surface areas

Fig 3.21.1 BET surface areas of supported metal sulfates and supports

Sample	BET surface area m^2g^{-1}	Sample	BET surface area m^2g^{-1}
As received ACROS (calcined)	700	As received Davisil (calcined)	240
ACROS + H_2O (calcined)	405	Davisil + H_2O (calcined)	200
3 wt% $Al_2(SO_4)_3$ ACROS	650	3 wt % $Al_2(SO_4)_3$ Davisil	229
6 wt% $Al_2(SO_4)_3$ ACROS	654	6 wt % $Al_2(SO_4)_3$ Davisil	238
12 wt% $Al_2(SO_4)_3$ ACROS	638	12 wt % $Al_2(SO_4)_3$ Davisil	222
3 wt % $NiSO_4$ ACROS	577	3 wt% $NiSO_4$ Davisil	224
6 wt % $NiSO_4$ ACROS	558	6 wt% $NiSO_4$ Davisil	235
12 wt % $NiSO_4$ ACROS	510	12 wt% $NiSO_4$ Davisil	231

The surface areas of the ACROS silica gel supported sulfates are all significantly higher than the Davisil supported materials. This is because of the high intrinsic surface area of the ACROS gel itself.

The blank impregnation (H_2O only) and 350 °C calcination has led to a decrease in the surface areas of both the gels, but the ACROS gel is particularly effected and has lost ~ 40 % of its original surface area.

When the gels are impregnated with sulfate this seems to stabilise the surface area. The surface areas of the sulfate samples are all higher than the equivalent blank impregnation. The surface areas of the ACROS supported samples appear to be reduced slightly at the higher sulfate loadings (12 wt %). This is not the case for the Davisil supported samples which all have similar surface areas regardless of sulfate composition.

3.22 F.T.I.R. and microadsorption studies

3.22.1 ACROS silica gel impregnated with H_2O

Fig 3.22.11 FTIR - Pyridine region and tabulated band areas

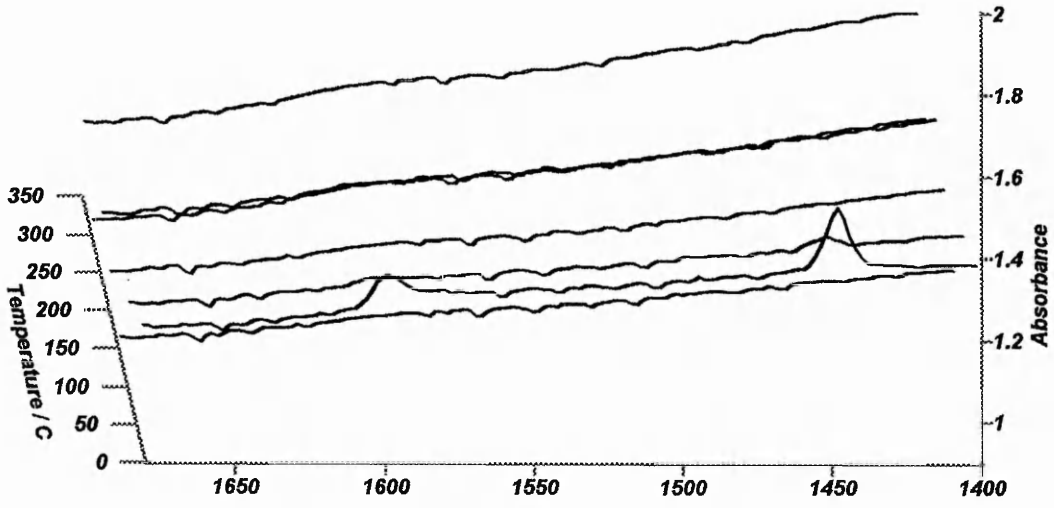

	Temperature / C	25	100	150	200	250	300	350
Assignment	cm^{-1}							
Physisorbed	1446	5.13	0.77					
Lewis	1455							
L + B	1492							
Bronsted	1547							
Physisorbed	1598	2.72	0.46					
Lewis	1623							
Bronsted	1639							

3.22.2 Davisil silica gel impregnated with H_2O

Fig 3.22.21 FTIR - Pyridine region and tabulated band areas

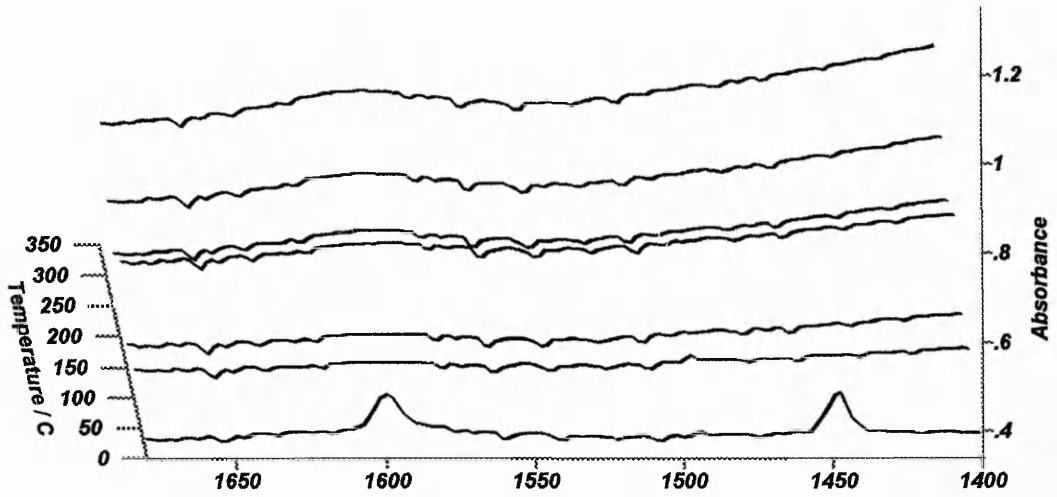

Absorbance / Wavenumber (cm-1)
File #10 = N014M#1 @ 25

	Temperature / C	25	100	150	200	250	300	350
Assignment	cm^{-1}							
Physisorbed	1446	1.41						
Lewis	1455							
L + B	1492							
Bronsted	1547							
Physisorbed	1598	1.71						
Lewis	1623							
Bronsted	1639							

The only pyridine observed in the FTIR pyridine spectra of the blank impregnated silica gels (Figs 3.22.11 and 3.22.21) is physically adsorbed pyridine at room temperature. It is clear that neither of the silicas possess any intrinsic acidity, so any acid sites observed in the supported samples are due to the sulfate component, although some type of support effect may be operative.

3.22.3 3 wt % $Al_2(SO_4)_3$ on Davisil silica gel

Fig 3.22.31 FTIR - Pyridine region and tabulated band areas

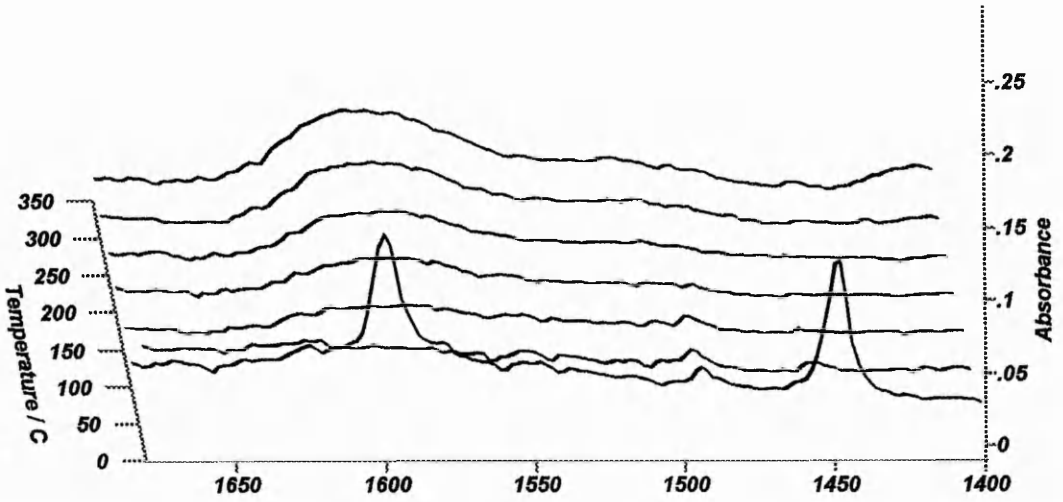

Absorbance / Wavenumber (cm-1)
File # 1 = N002M#1 @ 25

	Temperature / C	25	100	150	200	250	300	350
Assignment	cm-1							
Physisorbed	1446	1.52	0.09					
Lewis	1455	0.1	0.09	0.01				
L + B	1492	0.17	0.1	0.07				
Bronsted	1547							
Physisorbed	1598	1.47						
Lewis	1623							
Bronsted	1639							

Fig 3.22.31 shows that the 3 wt % $Al_2(SO_4)_3$ on Davisil gel sample has very few acid sites. The Lewis and Bronsted bound pyridine bands are not observed, but a small combined band is seen at 1490 cm^{-1} at temperatures below 200 °C

The pyridine FTIR spectra of 3 wt % $NiSO_4$ on ACROS gel (Fig 3.22.41) demonstrates that this sample has a higher density, of stronger acid sites, than 3 wt % $Al_2(SO_4)_3$ on Davisil. There is very little evidence of Bronsted acid sites, but the Lewis bound pyridine band is clearly visible even at 250 °C.

3.22.4 3 wt% $NiSO_4$ on ACROS silica gel

Fig 3.22.41 FTIR - Pyridine region and tabulated band areas

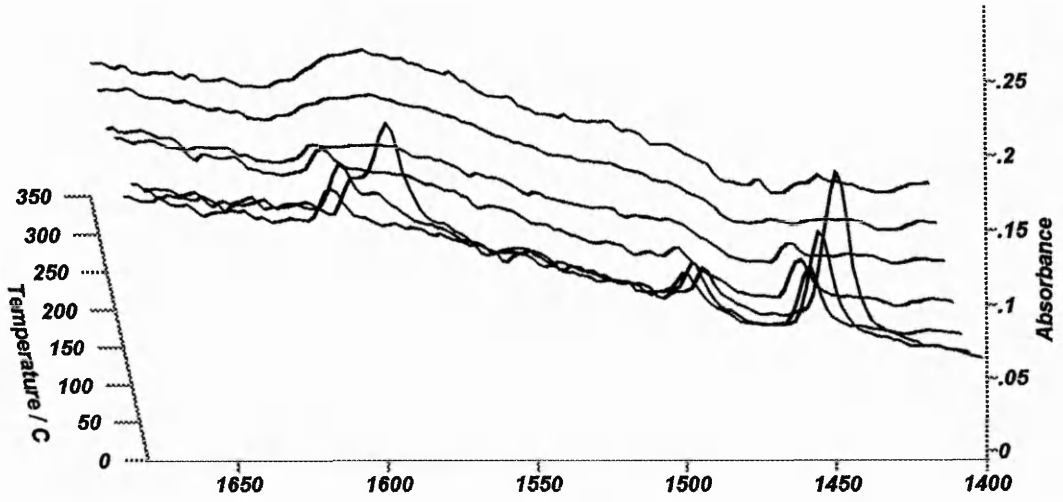

Absorbance / Wavenumber (cm-1)
File # 3 = N003M#1 @ 25

	Temperature / C	25	100	150	200	250	300	350
Assignment	cm^{-1}							
Physisorbed	1446	1.07						
Lewis	1450	0.89	1.13	0.57	0.37	0.12		
L + B	1490	0.30	0.34	0.30	0.12			
Bronsted	1540	0.09						
Physisorbed	1598	1.43	0.13					
Lewis	1610	0.18	0.36	0.35	0.21	0.05		
Bronsted	1639							

This is a trend that is observed throughout the series of twelve samples (mostly not shown here for brevity). The ACROS silica gel appears to be the better of the two supports, with both sulfates showing larger numbers of stronger sites when supported on it. This is possibly because of its higher surface area. The nickel sulfate is the most acidic (greater site density and strength) of the two sulfates. This might be because the 350 °C activation temperature is better suited to generating acid sites in the $NiSO_4$ than in the $Al_2(SO_4)_3$.

3.22.5 6 wt% $Al_2(SO_4)_3$ on ACROS silica gel

Fig 3.22.51 FTIR - Pyridine region and tabulated band areas

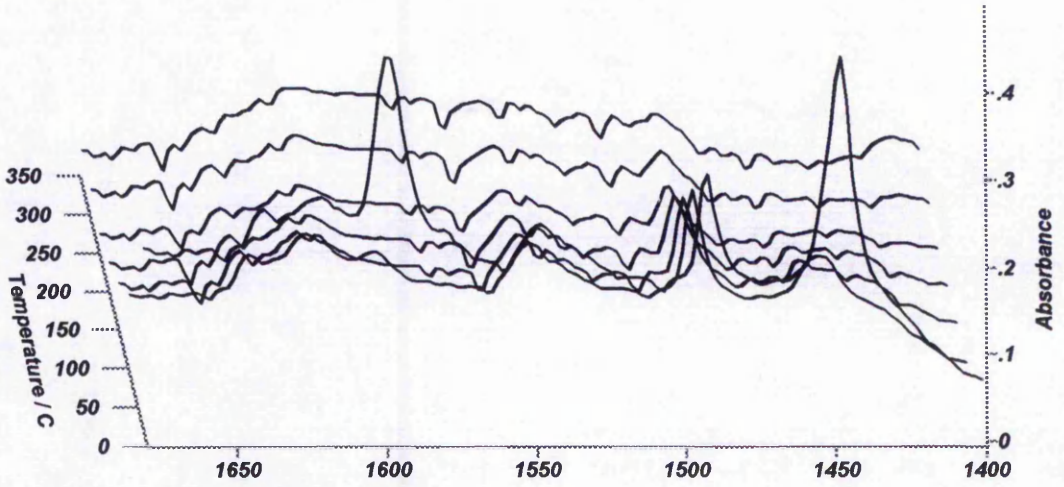

Absorbance / Wavenumber (cm-1)
File # 8 = N008M#7 @ 350

	Temperature / C	25	100	150	200	250	300	350
Assignment	cm^{-1}							
Physisorbed	1446	6.73	1.83					
Lewis	1450							
L + B	1490	2.48	2.29	1.72	1.42	1.03	0.57	
Bronsted	1540	1.01	2.13	0.75	0.57	0.34	0.23	
Physisorbed	1598	4.87	0.44					
Lewis	1610	0.68	0.80					
Bronsted	1639	0.39	0.36	0.29	0.23	0.18	0.13	

Fig 3.22.52 Microadsorption breakthrough vs time

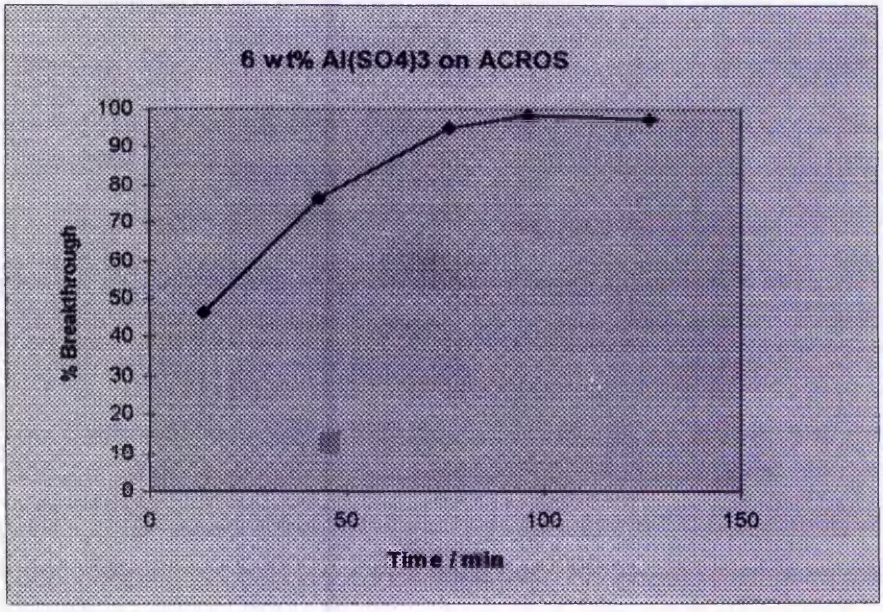

The number of acidic sites present on the materials increases with sulfate loading, as might be expected. Fig 3.22.51 shows the pyridine FTIR spectra of the 6 wt% $Al_2(SO_4)_3$ on ACROS silica gel. Although the aluminium sulfate is the least acidic of the two sulfates at these conditions, there are significantly more acid sites present than in either of the 3 wt % sulfate on ACROS samples. This is simply due to the higher loading of sulfate. At these higher loadings it is more easily observed that aluminium sulfate tends to generate Bronsted acid sites whereas the nickel sulfate generates predominantly Lewis acid centres.

In the microadsorption experiment (Fig 3.22.52) the 50 % breakthrough point for the 6 wt% $Al_2(SO_4)_3$ on ACROS sample is reached after approximately 15 minutes, which is around the time of the first G.C. injection.

As the ACROS silica appears to be the most effective support, the number of acid sites increases with sulfate loading, and $NiSO_4$ appears to be the most acidic sulfate at these conditions; the 12 wt % $NiSO_4$ supported on ACROS silica gel sample is expected to have a highest density of strong acid sites, and be the best performer in the microadsorption experiment.

Fig 3.22.61 shows that it does contain a large number of Lewis acid sites, as well as a smaller number of Bronsted sites. Fig 3.22.62 shows that in the microadsorption experiment, 50 % pyridine breakthrough is observed after 50 – 55 minutes, which is the best basic nitrogen adsorption performance of any of the samples in this series. This corresponds to adsorption of 0.28 wt % at the 50 % breakthrough point.

3.22.6 12 wt % $NiSO_4$ on ACROS silica gel

Fig 3.22.61 FTIR - Pyridine region and tabulated band areas

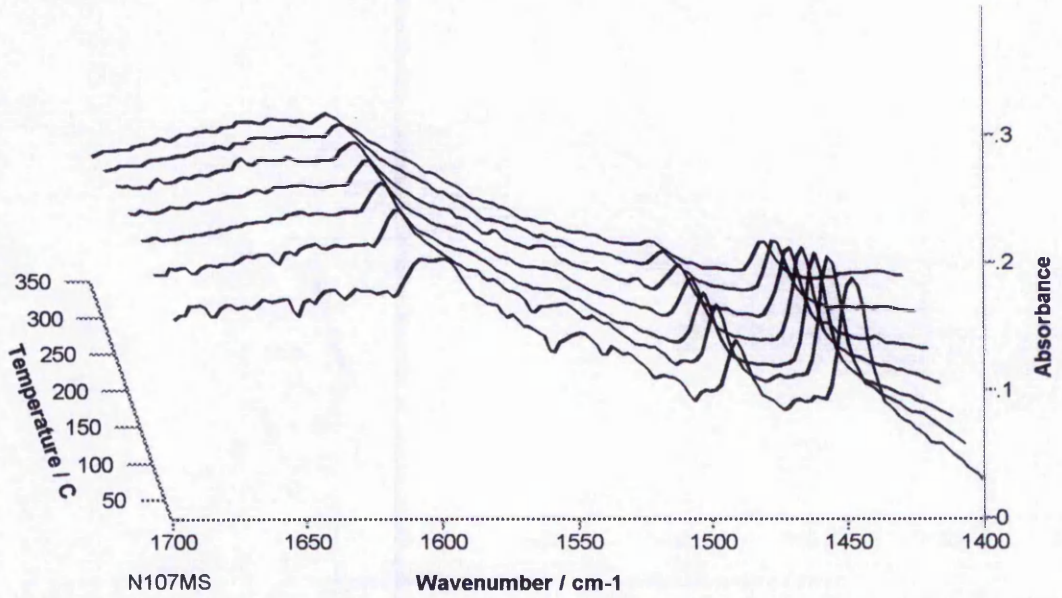

	Temperature / C	25	100	150	200	250	300	350
Assignment	cm-1							
Physisorbed	1446	2.03						
Lewis	1450	9.64	8.76	7.65	6.22	4.78	3.27	1.83
L + B	1490	2.75	2.91	2.71	2.31	1.83		
Bronsted	1540	0.80	0.48	0.24	0.24	0.32	0.16	
Physisorbed	1598	3.19						
Lewis	1610	3.19	2.87	2.31	1.67	1.12	0.72	0.32
Bronsted	1639							

Fig 3.22.62 Microadsorption breakthrough vs time

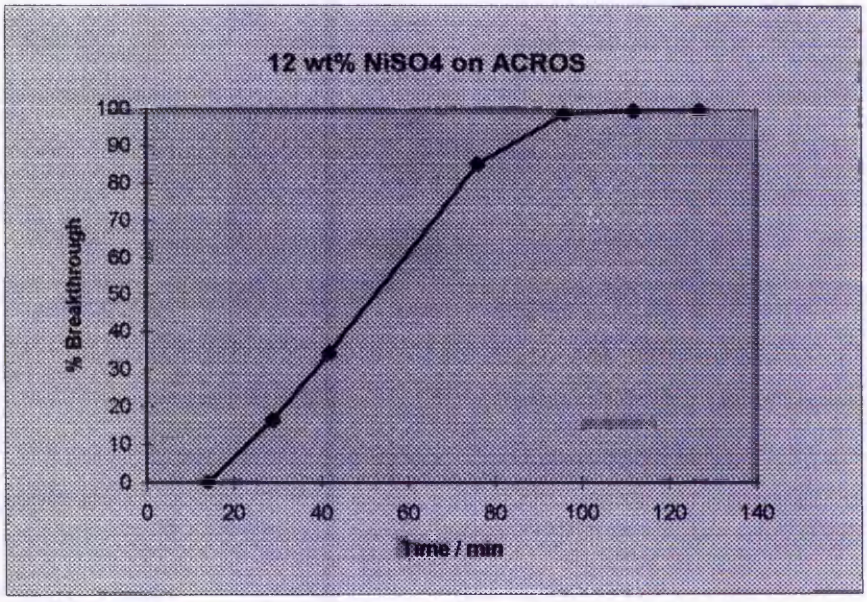

Fig 3.22.63 FTIR -OH Region

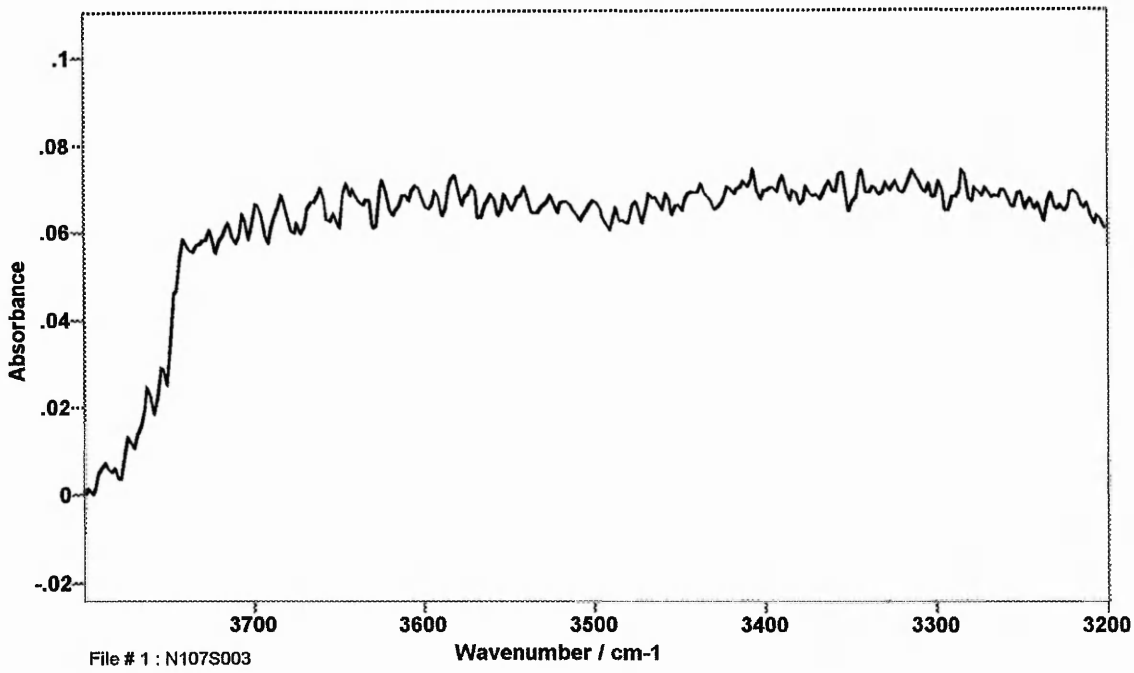

Fig 3.22.63 shows the -OH region of the FTIR spectra for the 12 wt% $NiSO_4$ on Acros sample, which is typical for this series of samples. The only feature observed in the –OH region, for all the samples in this series, was a band at 3741 cm^{-1}. This band is assigned to terminal silanol groups and is typical of the silica supports [8,9].

3.3 Summary and Discussion

An important feature of the supported metal sulfate materials is that the silica supports are devoid of acid sites before the sulfate impregnation. If a blank impregnation is performed (using distilled water) then this fails to generate acid sites in the silica, although it does reduce the surface area. The acid sites are therefore not a feature of the impregnation process itself (wetting and drying) but are directly related to the presence of the sulfate phase.

Fig 3.31 Pyridine Temperature Programmed Desorption Profiles for the supported metal sulfate samples.

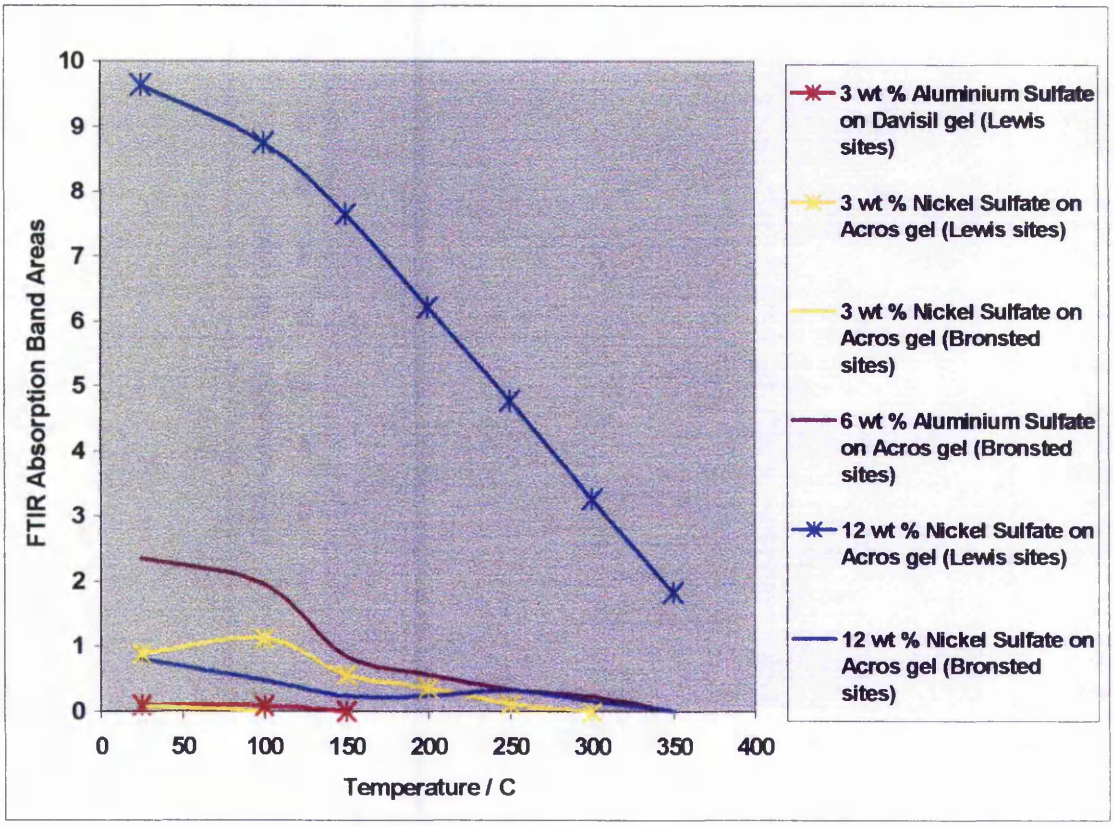

Fig 3.31 shows the pyridine desorption profiles for the supported metal sulfate samples studied. The most striking feature is the large number of Lewis acid sites on the Acros supported 12 wt% $NiSO_4$ sample. There is significant desorption of pyridine with each temperature increment indicating that these sites have a wide range of strengths, but are generally weak. Pyridine has desorbed from approximately 80% of these sites at 350°C. There is also a much smaller number

of Bronsted sites present on this sample, which have a more uniform strength distribution. Most of these Bronsted sites retain pyridine at 250 °C, although desorption is swift above this temperature and there is no Bronsted bound pyridine at 350 °C, indicating few strong Bronsted sites. It can be seen that the samples with a lower loading of sulfate have fewer acidic sites.

The 3 wt% $NiSO_4$ on Acros sample is similar to the 12 wt% $NiSO_4$ on Acros sample in that there are far more Lewis sites than Bronsted, but the numbers of both types of site are reduced by around an order of magnitude. Interestingly this difference in the numbers of acid sites is far greater than the difference in sulfate loading which is only a factor of 4. The 12 wt% $NiSO_4$ on Acros sample appears to generate more acid sites per unit amount of sulfate. This is the opposite of the expected result. A lower loading might be expected to give a better dispersion of the sulfate and generate more sites per unit mass of sulfate. The origin of this effect is unknown but one possibility could be a sulfate-support interaction which inhibits the generation of acidic sites. At low sulfate loading most of the sulfate will be in close proximity to the support. As the sulfate loading is increased, possibly giving thicker layers of sulfate on the support, then the effect would be less pronounced as the active sulfate surface is further away from the support. The strength distribution of the Lewis sites is also similar, with steady desorption with increasing temperature. The number of Bronsted sites is too small to assess the desorption profile, but the Lewis / Bronsted ratio appears similar for both $NiSO_4$ on Acros samples (~ 10:1 at room temperature).

The Aluminium sulfate samples possess a smaller number of acidic sites. The 3 wt% $Al_2(SO_4)_3$ on Davisil sample exhibits only a very small number of Lewis sites from which pyridine desorbs at low temperature (< 150°C). The 6 wt% $Al_2(SO_4)_3$ on Acros sample is more typical of $Al_2(SO_4)_3$ samples. It has a larger number of exclusively Bronsted sites. These Bronsted sites have a broad distribution of acid site strength and pyridine desorbs progressively with increasing temperature until complete desorption is achieved below 350°C. In this case there is a particularly pronounced desorption around 150°C.

From the pyridine FTIR spectra and microadsorption performance the three factors affecting the number of acid sites appear to be :-

- the type of metal sulfate used
- the nature of the support used
- and the sulfate loading

The nickel sulfate samples possess predominantly Lewis acid centres, whereas the aluminium sulfate samples demonstrate mostly Bronsted type centres. Both types of site appear to be effective for selective adsorption of pyridine. The total number of acid sites is higher for the nickel sulfate samples compared to aluminium sulfate samples with the same sulfate loading. Consequently the $NiSO_4$ based samples perform better in the microadsorption experiments. The differences in both the Lewis / Bronsted distribution and in acid site density may be a result of intrinsic properties of the two sulfates, or because the 350°C dehydration temperature chosen for this work may be better suited to the $NiSO_4$. 350°C is known to be a good dehydration temperature for generating acid sites in $NiSO_4$[1]. The optimum temperature for $Al_2(SO_4)_3$ is similar, but has not been as accurately documented [1].

The choice of the support material is another important factor influencing the performance of the metal sulfates. In this case both sulfates demonstrated a greater number of acid sites and performed better in the microadsorption study when supported on the Acros silica gel. The most striking differences between the two gels are their pore sizes and surface areas. The Acros gel has a mean pore diameter of ca. 40Å and a surface area of 700 m^2g^{-1}. The Davisil grade 645 gel has much larger pores with a mean diameter of 150Å and a surface area of 240 m^2g^{-1}. The particle sizes are also slightly different (Acros 0.06 – 0.2 mm and Davisil 0.15 – 0.25 mm). The simplest explanation for the increased numbers of acid sites, when Acros gel is used as the support, is that the higher surface area of this gel gives greater dispersion of the sulfate, and hence greater sulfate surface

area. This is probably the most likely explanation. However, the possibility of a differing support – sulfate interaction for the two silicas cannot be ruled out. Another difference between the two gels may arise in the drying process. As the two supports have very different pore sizes and hence pore curvatures, as well as slightly different particle sizes, the nature of the drying process may also differ. This may affect the way that the sulfate is deposited and dispersed on the support and hence the sulfate surface available for adsorption.

As the loading of both the sulfates is increased, there is an increase in the numbers of acid sites observed by pyridine FTIR and a concomitant increase in the 50% breakthrough times in the microadsorption experiments. As acidity is due to the sulfate, and not the support, this effect is consistent with an increase in the sulfate / support ratio. However, improving the performance by increasing the sulfate loading will have limits. As the sulfate loading increases, the regions of the sulfate phase will become larger. Therefore a smaller proportion of the sulfate will be at a surface, and hence available to an adsorbing molecule. Further to this, the pores will become progressively narrower, decreasing the available sulfate surface and leading to pore clogging. For these reasons, increasing the sulfate loading will only lead to an improvement in adsorption capacity up to an optimum loading. Above this, a decrease in performance may be observed due to pore clogging and a general reduction in surface area.

The optimum value for sulfate loading will be dependent upon the nature of the support. Supports with a relatively small number of narrow pores would be expected to have quite a low optimum loading as pore filling and clogging will occur with a relatively small amount of sulfate present. Supports with a larger number of wider pores will be able to accommodate a much larger loading before access to the sulfate surface becomes a problem. In the case of the Acros silica gel the surface areas for both the 12 wt% sulfate samples are reduced slightly compared to the respective 3 and 6 wt% samples (Fig 3.21.1). This could suggest that the sulfate loading is reaching a level where the pore diameters are being restricted. If this is the case, higher sulfate loadings will reduce the pore size and

surface area further, possibly leading to occlusion of the pores. Hence a 12 wt% sulfate loading may be close to the optimum for the Acros gel. The Davisil silica gel, which has much larger pores, shows no such loss in surface area at 12 wt% sulfate loading. This suggests that the optimum loading for this support may be substantially higher than that for the Acros gel. The C constants, from the BET analysis of the N_2 adsorption isotherms, for all these samples, are very similar, and are substantially less than 100. This indicates that the reduction in pore size caused by impregnation of the sulfate has not introduced significant microporous character into any of the samples. The BET isotherm model is therefore applicable to these samples.

3.4 Conclusions

The supported metal sulfate samples studied generally only contain small numbers of weak acid sites. This limits their usefulness as adsorbents for selective removal of pyridine. The most effective sample studied was the 12 wt % $NiSO_4$ on Acros sample, for which the microadsorption 50% pyridine breakthrough time was ~ 50 – 55 minutes. This sample also had the greatest number of acid sites visible by pyridine FTIR, which has proven to be an effective characterisation technique for studying acid sites in these materials.

Several factors influence the acid site density and hence microadsorption performance. These include the type of silica support, the loading of the sulfate, and the type of sulfate used. The Acros silica gel is the most effective of the two silica supports studied. Differences in pore size, particle size and sulfate – support interactions cannot be discounted, but the higher surface area of the Acros gel is probably the primary factor influencing performance. As might be expected the sulfate loading is another important factor. Increasing the sulfate loading increases the number of acid sites generated, regardless of the support, or sulfate used. The $NiSO_4$ has proven to be the most effective sulfate, although it is possible that the pre-treatment conditions used in this work are better suited to $NiSO_4$ than $Al_2(SO_4)_3$. Optimisation of these conditions for $Al_2(SO_4)_3$ may improve its performance and restore parity with $NiSO_4$.

The most effective sample was the sample with all these factors in its favour, i.e. 12 wt% $NiSO_4$ on Acros.

The three major factors influencing acid site density can all be optimised, which should lead to significant improvement microadsorption performance. Although this may still only allow relatively low adsorption capacities, in comparison with some other types of material, the potential ease with which these samples can be regenerated makes them worthy of further study.

3.5 References

1) Tanabe, K., Solid Acids and Bases, Academic Press Inc.(London), (1970).

2) Tanabe, K. and Takeshita, T., *Advances in catalysis*, 1967, **17**, 315.

3) Mochida, I., Fei, Y. Q., Sakanishi, K., Usuba, H. and Miura, K., *Chem. Lett.*, 1990, **4**, 515.

4) Y.Q. Fei, K. Sakanishi, Y.N. Sun, R. Yamashita and I. Mochida, *Fuel*, **69** (1990), 261.

5) Mochida, Y.Q. Fei, K. Sakanishi, Y. Korai, H. Usuba and K. Miura, Carbon, **30** (2) (1992), 241.

6) K. Sakanishi, Y.N. Sun, I. Mochida and U. Hidehiko, Fuel Processing Technology, **32** (1992), 143.

7) K. Sakanishi, H. Obata, I. Mochida and T. Sakaki, Abstracts of Papers of the American Chemical Society, **208** (1) (1994), 50.

8) Chakraborty, B. and Viswanathan, B., *Catalysis Today*, 1999, **49**, 253.

9) Weglarski, J., Datka, K., He, H. and Klinowski, *J. Chem. Soc., Faraday Trans.*, 1996, **92**(24), 5161.

Chapter 4 Amorphous Silica-Aluminas

4.1 Introduction

Amorphous silica-alumina is an important material as a catalyst for the isomerisation, polymerisation, partial oxidation and catalytic cracking of hydrocarbons, and as a support for metal catalysts [1]. The activity of silica-alumina as an acid catalyst is dependent on the Al:Si ratio, typically in the range 0.1 to 0.25 for most applications. Like most acidic materials composed of silica and alumina, acidity is generated via substitution of Al^{3+} for Si^{4+} in the structure of SiO_4 tetrahedra, resulting in a charge imbalance. A vacant site is generated at the aluminium atom, which can accept electrons (Lewis site). The four fold co-ordination of aluminium demanded by the silica structure can also be achieved by interaction with H_2O, giving Al-OH where the complementary protons are donated to neighbouring oxygen atoms, or approaching base molecules (a Bronsted site).

In this study a series of five Silica-alumina samples has been prepared according to the procedure of Rajagopal et. al. [2]. The samples have alumina contents of 10, 25, 50, 75 and 90 wt%, and are designated SA10 to SA90 respectively.

4.2 Results

4.21 B.E.T. Surface areas

Fig 4.21.1 B.E.T. Surface areas of the silica-alumina samples

Sample	Name	B.E.T. Surface Area (m^2g^{-1})
SiO_2-Al_2O_3 (90%:10%)	SA10	361
SiO_2-Al_2O_3 (75%:25%)	SA25	349
SiO_2-Al_2O_3 (50%:50%)	SA50	291
SiO_2-Al_2O_3 (25%:75%)	SA75	255
SiO_2-Al_2O_3 (10%:90%)	SA90	246

The data in Fig 4.21.1 shows that as a general trend, the BET surface area decreases as the alumina content is increased. This effect has been documented [2], and the surface areas observed are typical for these types of materials [1-5].

4.22 F.T.I.R. and Microadsorption studies

4.22.1 SA10

Fig 4.22.11 F.T.I.R. - Pyridine region and tabulated band areas

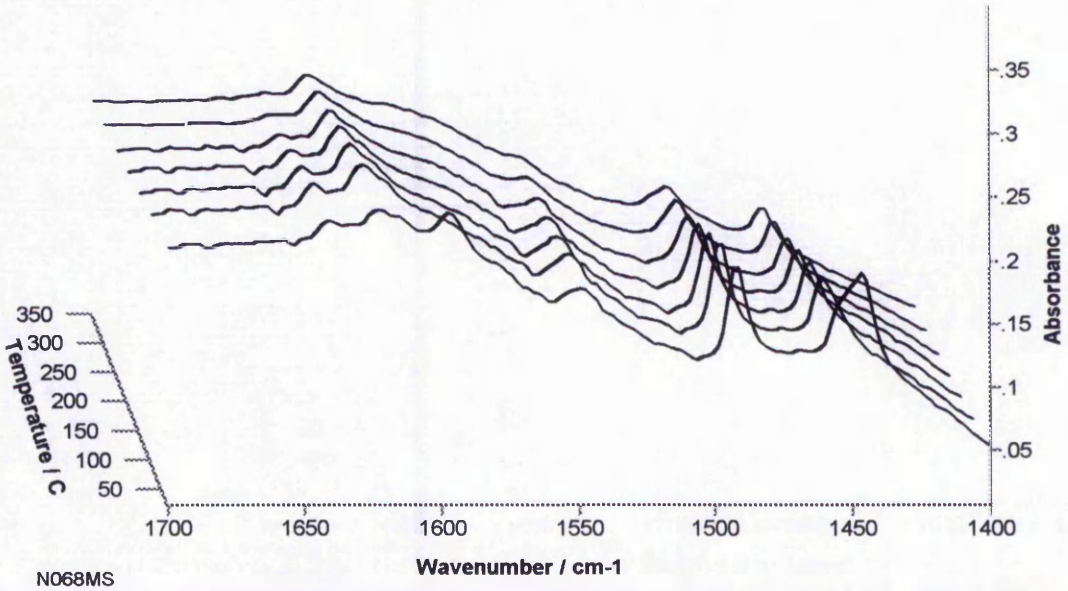

N068MS

	Temperature / C	25	100	150	200	250	300	350
Assignment	cm-1							
Physisorbed	1446	0.48	0.05					
Lewis	1455	0.59	0.51	0.4	0.3	0.23	0.22	0.21
L + B	1492	0.58	0.59	0.52	0.44	0.4	0.27	0.18
Bronsted	1547	0.18	0.22	0.2	0.14	0.11	0.09	0.04
Physisorbed	1596	0.2						
Lewis	1619	0.19	0.22	0.23	0.23	0.22	0.2	0.16
Bronsted	1639	0.06	0.05	0.05	0.05	0.03		

Fig 4.22.12 Microadsorption breakthrough vs time

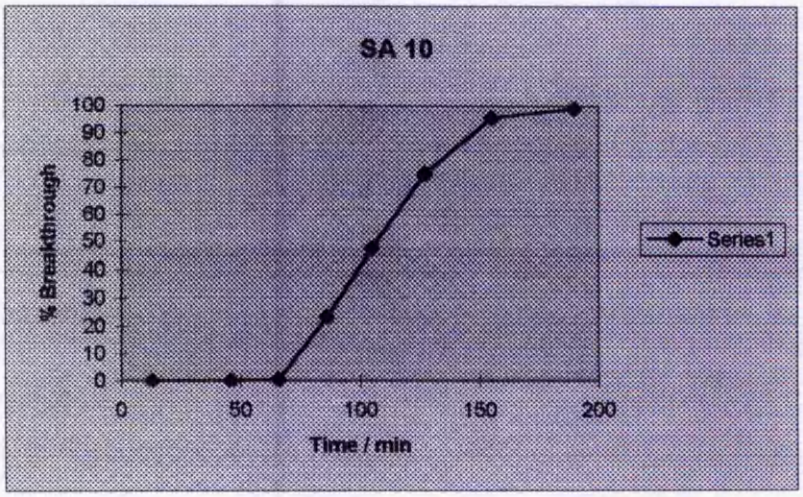

4.22.2 SA25

Fig 4.22.21 F.T.I.R. – Pyridine region and tabulated band areas

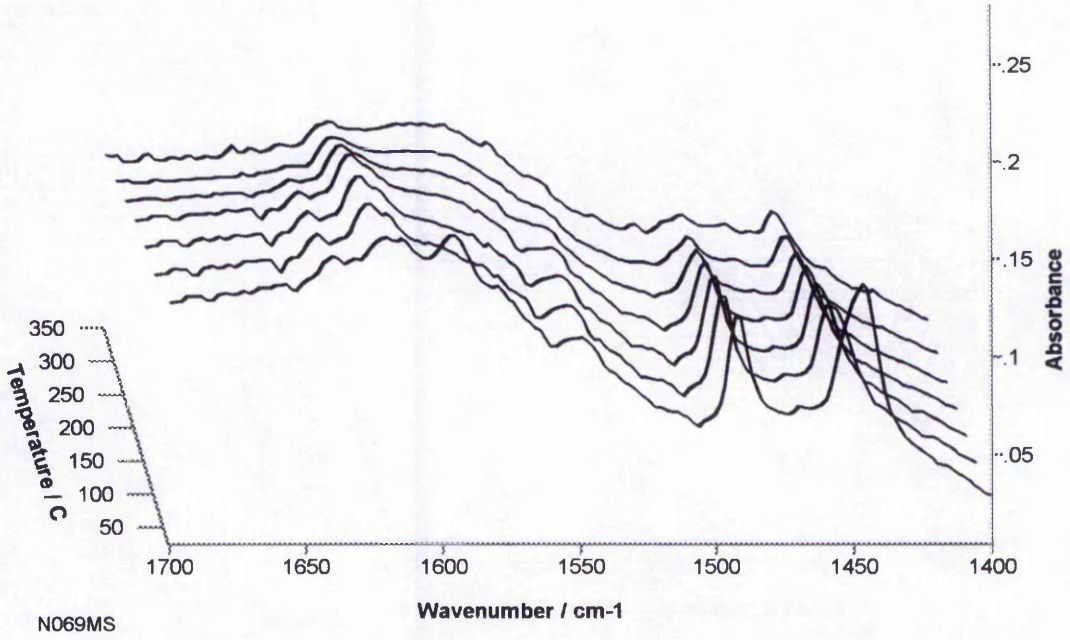

	Temperature / C	25	100	150	200	250	300	350
Assignment	cm-1							
Physisorbed	1446	0.46	0.06					
Lewis	1453	0.61	0.5	0.42	0.34	0.29	0.25	0.21
L + B	1492	0.48	0.39	0.34	0.28	0.22	0.11	0.05
Bronsted	1547	0.13	0.14	0.08	0.08	0.03	0.02	
Physisorbed	1595	0.15						
Lewis	1617	0.15	0.23	0.24	0.24	0.19	0.12	0.08
Bronsted	1639	0.05	0.05	0.04	0.03	0.01		

Fig 4.22.22 Microadsorption breakthrough vs time

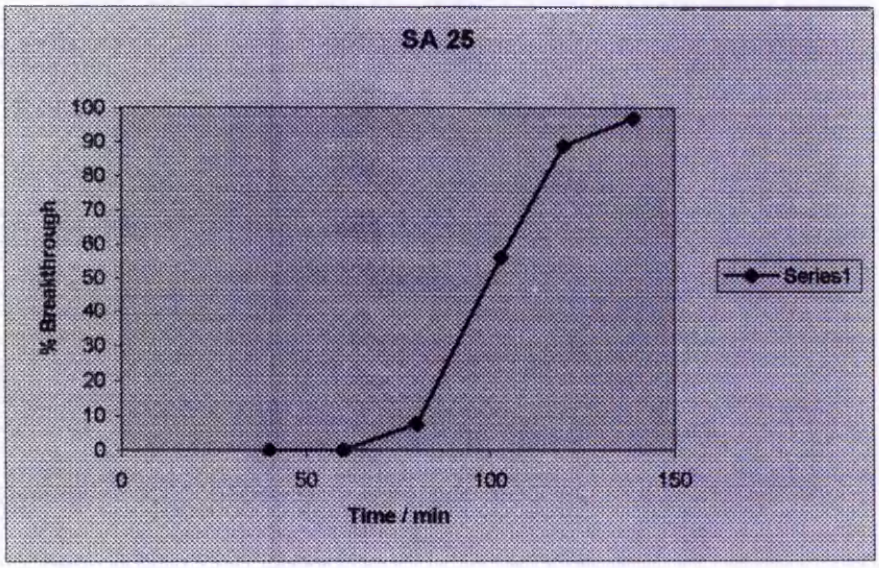

4.22.3 SA50

Fig 4.22.31 F.T.I.R. – Pyridine region and tabulated band areas

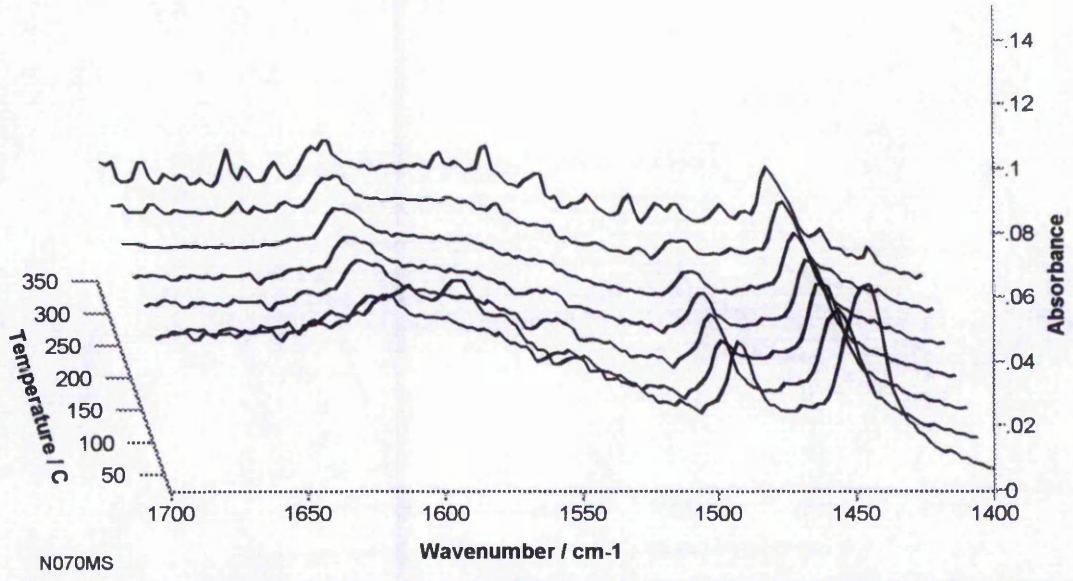

	Temperature / C	25	100	150	200	250	300	350
Assignment	cm-1							
Physisorbed	1446	0.2						
Lewis	1452	0.5	0.4	0.32	0.25	0.23	0.18	0.16
L + B	1492	0.21	0.16	0.13	0.1	0.07	0.04	
Bronsted	1548	0.04	0.03	0.02				
Physisorbed	1598	0.09						
Lewis	1613	0.06	0.05	0.03				
Bronsted	1639							

Fig 4.22.32 Microadsorption breakthrough vs time

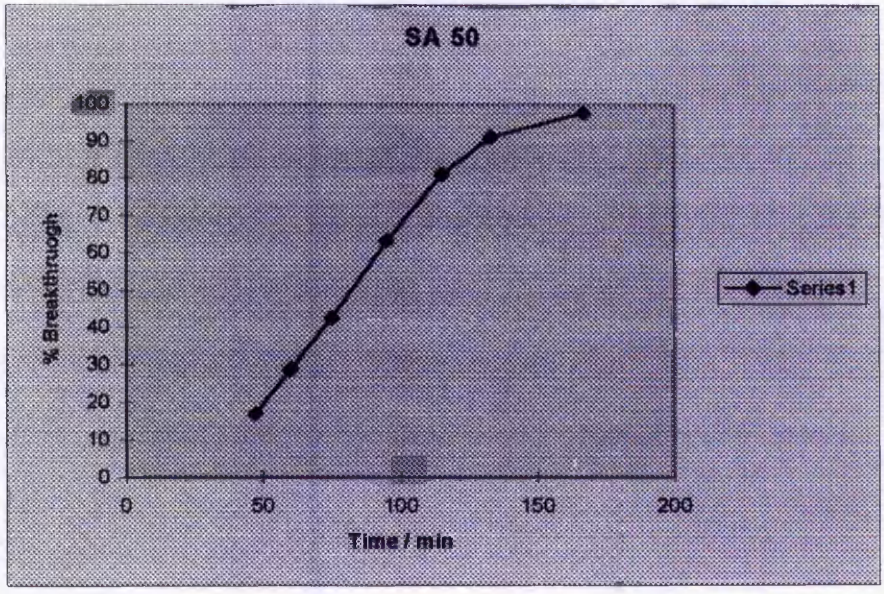

4.22.4 SA75

Fig 4.22.41 F.T.I.R. – Pyridine region and tabulated band areas

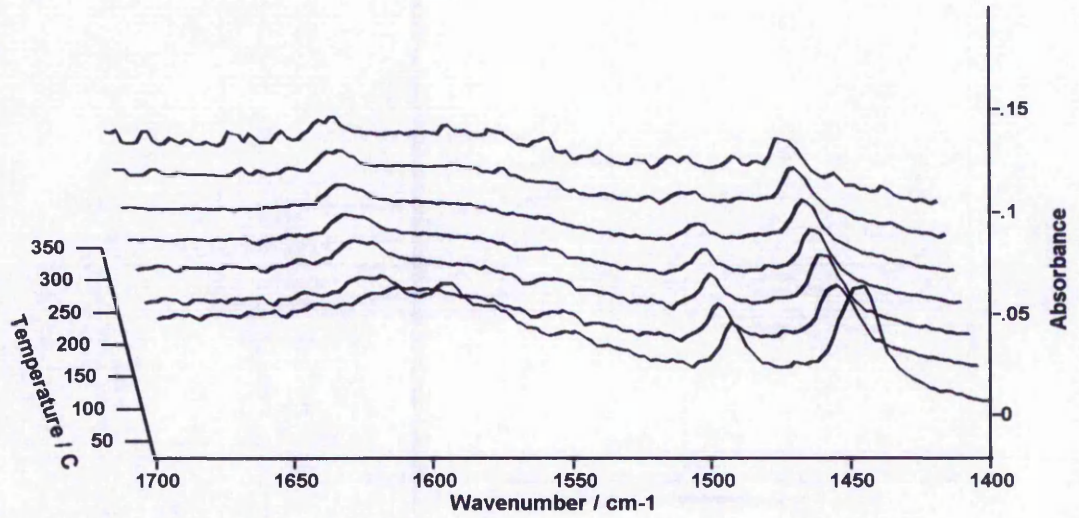

N074MS

	Temperature / C	25	100	150	200	250	300	350
Assignment	cm-1							
Physisorbed	1446	0.17						
Lewis	1452	0.39	0.31	0.2	0.17	0.15	0.11	0.1
L + B	1492	0.16	0.12	0.1	0.07	0.05	0.02	
Bronsted	1547	0.03	0.02	0.01				
Physisorbed	1598	0.05						
Lewis	1623	0.04	0.03	0.02	0.01			
Bronsted	1639							

Fig 4.22.42 Microadsorption breakthrough vs time

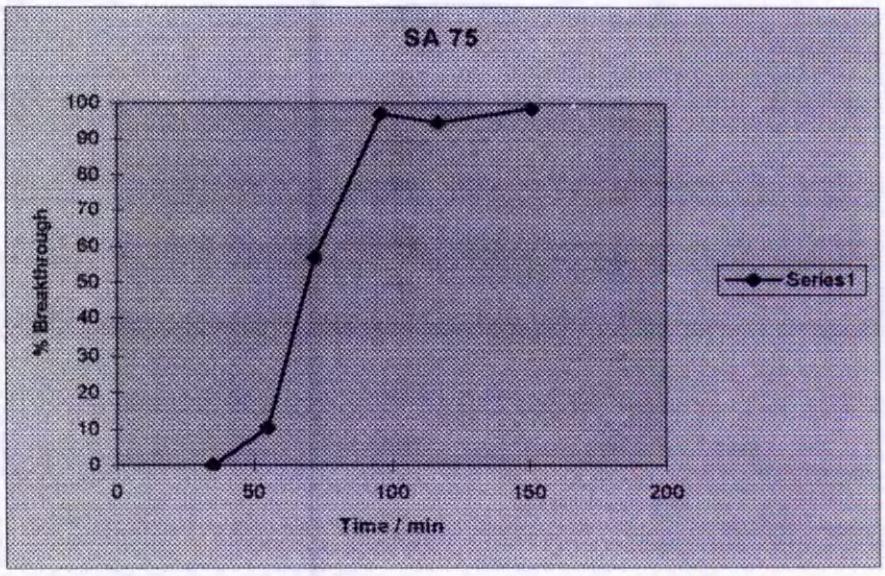

4.22.5 SA90

Fig 4.22.51 F.T.I.R. – Pyridine region and tabulated band areas

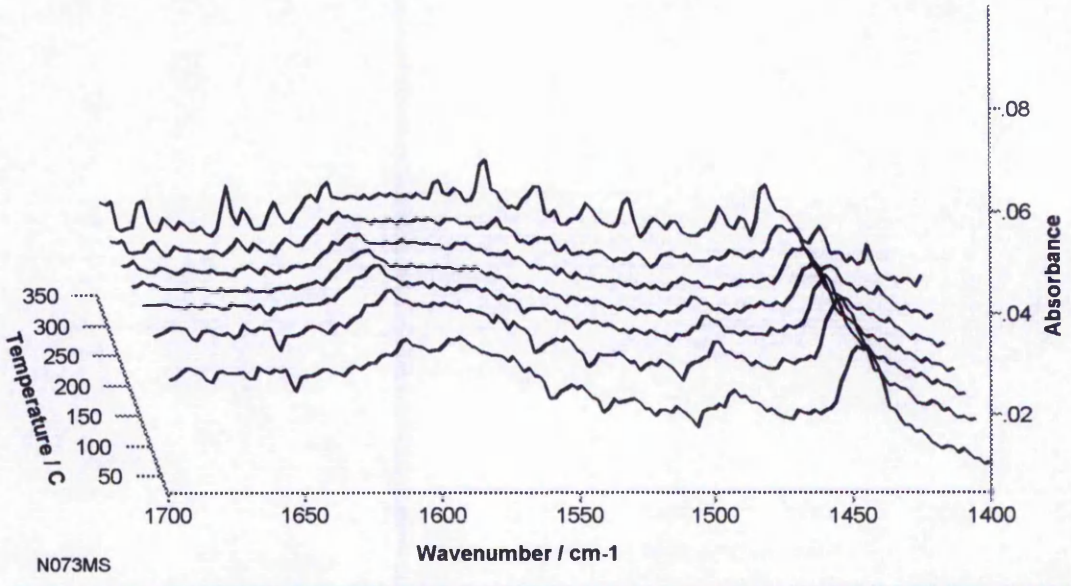

	Temperature / C	25	100	150	200	250	300	350
Assignment	cm-1							
Physisorbed	1446							
Lewis	1450	0.21	0.18	0.12	0.11	0.09	0.07	0.05
L + B	1492	0.02	0.02	0.02	0.01	0.01		
Bronsted	1547							
Physisorbed	1598	0.02						
Lewis	1612	0.02	0.02	0.03	0.03	0.02		
Bronsted	1639							

Fig 4.22.52 Microadsorption breakthrough vs time

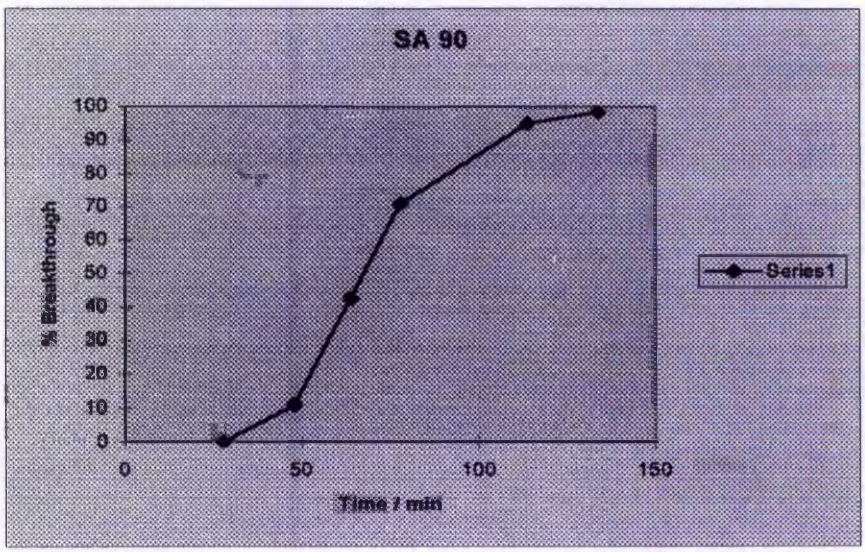

4.3 Discussion

Before discussing the FTIR results it should be noted that the absorption band areas have not been normalised using lattice overtone bands. In the absence of suitable overtone bands the mass of the sample disc has been used. This method is less accurate, so some caution should be used in comparing the band areas of different samples.

The spectra of adsorbed pyridine on amorphous silica-alumina show that most of the samples studied possess both Lewis and Bronsted sites. This is in agreement with other studies [3-8]. In the range studied, the numbers of both types of sites decrease with increasing alumina content. For the high alumina samples (SA90 and SA75) the absorption bands are so small that differentiation between absorption bands and the background signal is very difficult.

Fig 4.3.1 shows the pyridine desorption profiles for Lewis sites on the silica-alumina samples. For all five samples approximately 30 % of the sites observed at 25 °C retain pyridine at 350 °C. The shapes of the desorption profiles vary through the series. Moving from SA90 to SA50 the average strength of site appears to increase. The SA90 and SA75 samples both have a large desorption at 150 °C. The SA50 sample does not have this feature, although both the SA75 and SA50 samples have a small plateau in desorption at 200 – 250 °C, with desorption continuing at 300 °C +. The SA75 desorption therefore resembles the SA90 sample below 200 °C and the SA50 sample above this temperature. This may indicate that two distinct types of weak Lewis site are operating. The SA90 sample containing predominantly one type of site, whilst the SA50 Lewis sites are predominantly the other, slightly stronger type. The intermediate SA75 sample therefore contains both types of site, and the desorption profile is a hybrid of the two neighbouring samples in the series.

Fig 4.3.1 Pyridine Temperature Programmed Desorption Profiles for Amorphous Silica-aluminas (Lewis acid sites)

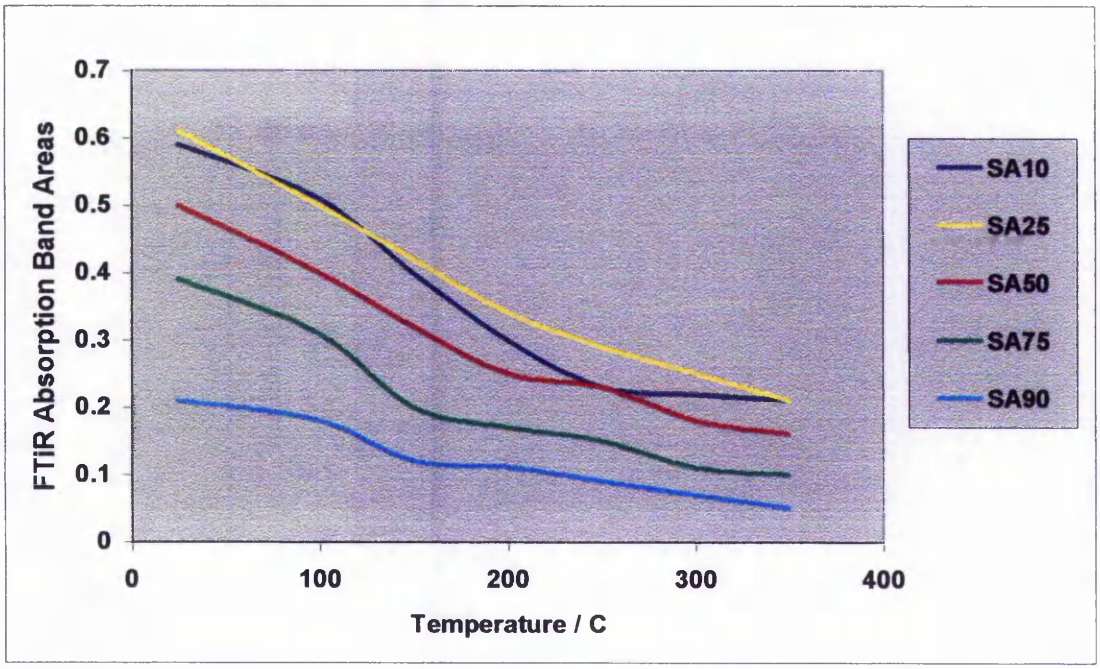

The desorption profiles for the high silica SA25 and SA10 samples do not possess either of these characteristics, although with the SA10 sample there is a plateau in desorption between 250 and 350 °C. These two samples have almost identical amounts of pyridine desorbed at both 25 °C and 350 °C. However, between these temperatures, the desorption profiles are very different. There is much greater pyridine desorption between 100 °C and 250 °C on the SA10 sample, although the pyridine retained at 250 °C is stable up to 350 °C. The SA25 sample by comparison desorbs pyridine steadily with each temperature increment up to 350 °C. These observations suggest that the total number of Lewis acid sites on the two samples is very similar (observed at 25°C). The numbers of strong Lewis sites capable of retaining adsorbed pyridine at 350°C is also almost identical. However, the intermediate strength sites contributing to the shape of the desorption profiles are very different. The Lewis sites on SA25 have a wide range of strengths giving the desorption profile a 'straight line' slope as the temperature is increased. The intermediate sites on SA10 appear to have a narrower strength distribution centred on weaker sites. Pyridine is desorbed from these sites at or

below 250°C leaving only the strong Lewis sites with adsorbed pyridine. This means there is no further desorption of pyridine from Lewis sites between 250 and 350 °C.

In general, increasing the Al_2O_3 content seems to decrease the strength as well as quantity of acid sites. Further evidence for a decrease in strength comes from the position of the V_{19b} (~1450 cm^{-1}) and V_{8a} (~1620 cm^{-1}) Lewis bands. There is a gradual shift to lower frequency with increasing aluminium, from 1455 cm^{-1} and 1619 cm^{-1} for SA10, to 1450 cm^{-1} and 1612 cm^{-1} for SA90. A possible reason for this shift is a change in co-ordination environment of the aluminium ions, an effect that has been observed on silica-aluminas [11]. Pyridine adsorbed on octahedrally co-ordinated aluminium cations exhibits a band at 1615 cm^{-1}, and that on tetrahedral aluminium at 1624 cm^{-1} [12]. Tetrahedral aluminium species are more acidic than octahedral aluminium [13], and thus interact with pyridine more strongly, causing the bands to shift to higher frequency. The shift in these bands therefore shows that the population of tetrahedral Al decreases with increasing alumina content. Hence the ratio of strong (tetrahedral) Lewis sites to weak (octahedral) Lewis sites decreases with increasing alumina, and the Lewis bands shift to lower frequency. The decrease in tetrahedral aluminium with increasing alumina has been documented [11].

Fig 4.3.2 shows the desorption of pyridine from Bronsted acid sites on the silica-alumina samples. It is immediately evident that for all the samples there are far fewer Bronsted sites than Lewis sites. Like the Lewis sites shown in Fig 4.3.1, the primary trend is of increasing numbers of sites with decreasing alumina content. For the SA90 sample no Bronsted sites can be observed by pyridine FTIR even at room temperature. The SA75 and SA50 samples have a small number of weak Bronsted sites from which pyridine desorbs below 200°C. The SA25 and SA10 samples have larger numbers of Bronsted sites with a broad distribution of strengths. Bronsted bound pyridine is not completely removed from SA25 until the temperature is raised to 350°C. The SA10 sample, which has the greatest number of sites, also has the largest number of strong Bronsted sites. It is the only

sample with Bronsted sites strong enough to retain adsorbed pyridine at 350°C. From Fig 4.3.2 approximately 20% of the sites observed at 25°C are strong enough to retain pyridine at 350°C.

Fig 4.3.2 Pyridine Temperature Programmed Desorption Profiles for Amorphous Silica-aluminas (Bronsted acid sites)

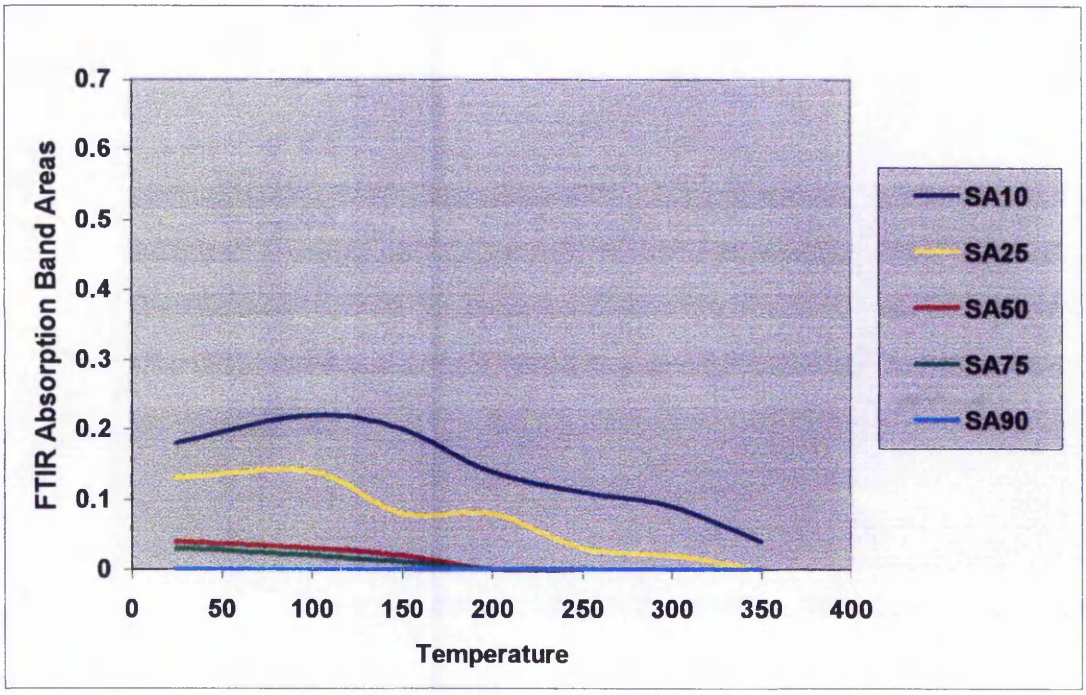

The –OH region of the silica-alumina FTIR spectra exhibit one well defined absorption band at 3741 cm^{-1}. This is typical of amorphous silica in which it is assigned to non acidic silanol groups terminating the particles. The size of the 3741 cm^{-1} band is related to the composition of the material. As the alumina content is increased the band becomes less intense, and is not observed at all in SA75 and SA90. Fig 4.3.3 shows the reappearance of the band in SA10 as the temperature is increased. The band behaves in the same way in SA25 and SA50, but with much lower intensities. No other OH bands are observed, probably because of the low outgasing temperature. The band at 3741 cm^{-1} behaves in an

unusual manner. The intensity is suppressed upon the addition of pyridine, and recovers as pyridine is desorbed (Fig 4.3.3). The recovery mirrors the combined desorption of both the physically adsorbed pyridine and the Bronsted bound pyridine.

Fig 4.3.3 SA10 FTIR -OH region

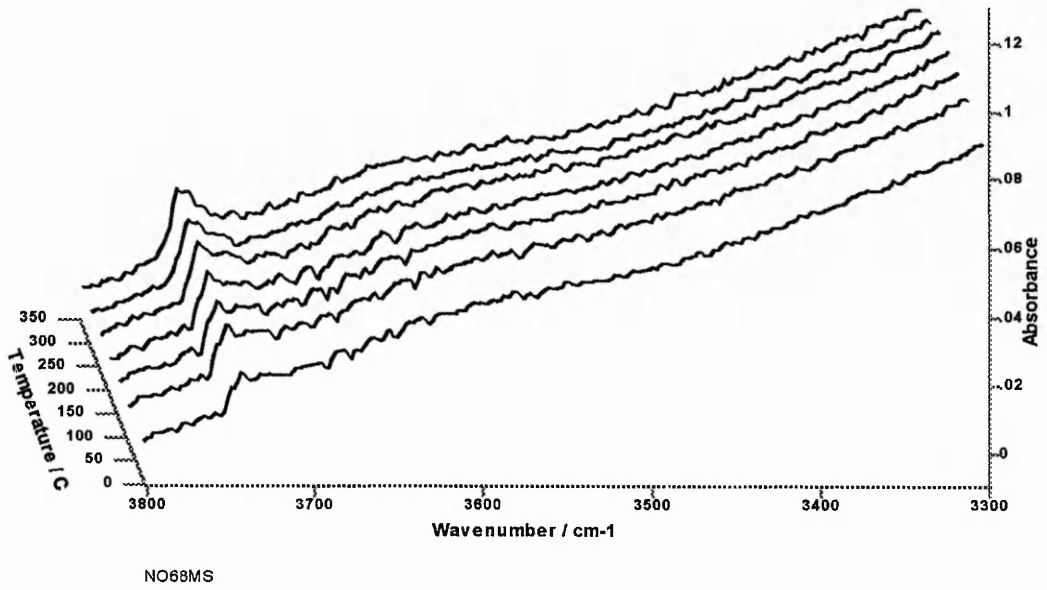

There are two possible explanations for this effect. Firstly the 3741 cm^{-1} band is a composite band comprising a contribution from acidic Bronsted O-H as well as non-acidic silanol groups. Alternatively some of the terminal O-H groups interact with pyridine adsorbed on Bronsted and/or Lewis acid sites, reducing the intensity of the OH band at 3741 cm^{-1} while the pyridine is present. The later explanation appears much more likely, and Chen et. al. [14] have come to similar conclusions based on pyridine adsorption on D_2O exchanged Al-MCM-41.

Fig 4.3.4 Band areas at 200 °C and 50% breakthrough times for Silica-aluminas

Sample	Lewis band ~1450 cm^{-1}	Bronsted band ~1545 cm^{-1}	Lewis / Bronsted Ratio[a]	50 % Breakthrough / min
SA10	0.3	0.14	1.61	~ 105
SA25	0.34	0.08	3.20	~ 100
SA50	0.25	-	-	~ 80
SA75	0.17	-	-	~ 70
SA90	0.11	-	-	~ 65

(a) Normalised using relative molar extinction coefficients

Fig 4.3.4 shows the integrated, normalised band areas for the five samples at 200 °C, along with the Lewis / Bronsted ratios and 50 % breakthrough times. It can be seen that the Lewis / Bronsted ratio increases with increasing alumina i.e. the reduction in the number of Bronsted sites is greater than the reduction in Lewis sites. At 200 °C the area of the 1545 cm^{-1} Bronsted band is negligible for materials with > 50 % alumina. It is possible that as the alumina content increases the structure becomes more like that of alumina itself, which exhibits only Lewis acidity [5,9,10], instead of a structure with aluminium incorporated into a silica lattice, generating both Lewis and Bronsted sites.

As the numbers of acidic sites (of both types), acidic strength, and the BET surface area increase with silica content, it is perhaps not surprising that microadsorption performance improves in parallel with these trends. The 50% breakthrough point for SA90 occurred at approximately 70 minutes (Fig 4.3.4) and was the shortest time observed for this series of samples. The maximum was for SA10 where the 50% breakthrough occurred at approximately 105 minutes. This corresponds to approximately 0.4 wt % pyridine adsorption on SA90 and 0.6 wt % on SA10.

However, if the 50% breakthrough times are plotted alongside the BET surface areas (Fig 4.3.5) then it can be seen that the correlation between the two is extremely good. The reduction in the number of acidic sites accessible to pyridine, as the alumina content increases, will be partly due to the corresponding loss in surface area.

Fig 4.3.5 BET surface area vs 50% breakthrough time for the five silica – alumina samples

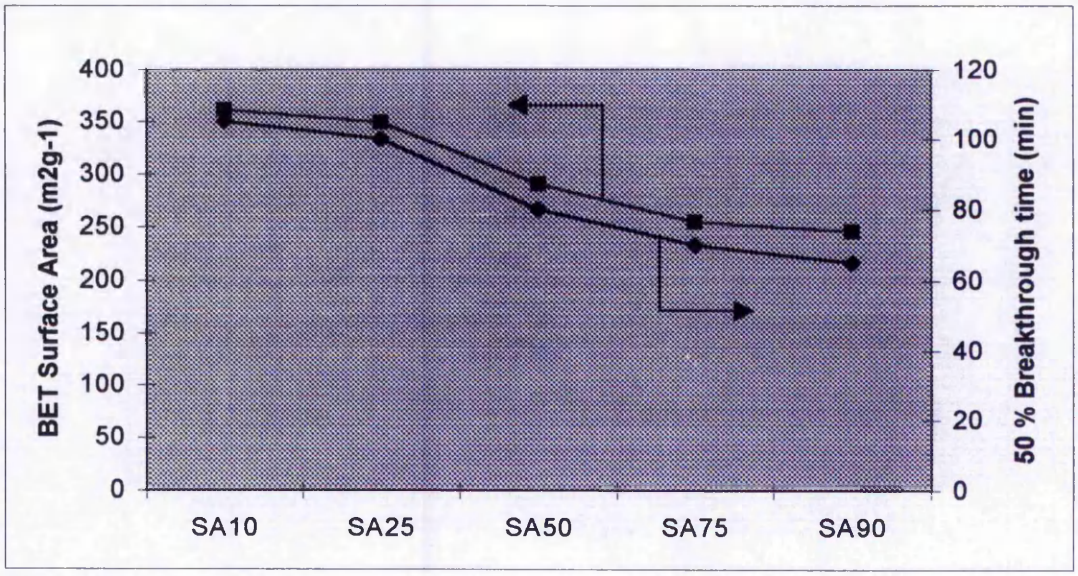

However the reduction in both the Lewis and Bronsted band areas with increasing Al_2O_3 is much larger than can be explained by the loss in surface area alone. In addition both types of acidic site appear to become weaker as well as less numerous as the alumina content is increased. Despite these effects the reduction in adsorption capacity is little more than the reduction in surface area. This indicates that surface area may be the single most important factor effecting the microadsorption performance. If this is the case then higher surface area silica-aluminas may offer a significant improvement in performance

4.4 Conclusions

Amorphous silica-aluminas have been shown to be moderately successful as selective adsorbents for pyridine. Samples with 10 and 25 % Al_2O_3 have adsorption capacities of ~0.6 wt%. Higher alumina samples have reduced numbers of both Bronsted and Lewis acid sites. The reduction in the number of Bronsted sites is particularly striking, indicating that as the Al_2O_3 content is increased, the structure becomes increasingly like that of alumina, which generally displays only Lewis acidity. In addition, increasing incorporation of alumina reduces the mean acid site strength and lowers BET surface area. The surface area appears to one of the most important factors influencing the microadsorption performance. The correlation between surface area and breakthrough time is very good, although the surface area increases by ~40% across the series, but the breakthrough time increases by ~60%. The silica rich, high surface area, samples have the strongest acid sites and highest acid site density. This explains why they adsorb more pyridine per unit area of surface.

The correlation between microadsorption performance and surface area suggests that if higher surface area silica-aluminas can be synthesised, they might show considerably improved adsorption capacities. For this reason MCM-41 appears to be promising, as it can be considered a very high surface area silica-alumina.

In addition to maximising the surface area, optimisation of the SiO_2 / Al_2O_3 ratio is another area worthy of further study. Silica-aluminas are only effective with relatively low Al_2O_3 content, as this allows substitution of Al into a SiO_2 framework. In this study the performance of samples with 10 and 25 % Al_2O_3 has been almost identical (within experimental error). This may mean that the optimum composition lies somewhere between these two values. A more finely tuned study, focusing on this region of composition, may yield improvements in adsorption capacity.

4.5 References

1) Bisset, A. and Dines, T. J., *J.Chem. Soc. Faraday Trans.* 1997, **93**(8), 1629.

2) Rajagopal, S., Grimm, T. L., Collins, D. J. and Miranda, R., *J. Catal.* 1992, **137**, 453.

3) Basila, M. R., Kantner, T. R. and Rhee, K. H., *J. Phys. Chem.* 1964, **68**, 3197.

4) Basila, M. R. and Kantner, T. R., *J. Phys. Chem.* 1966, **70**, 1681.

5) Riseman, S. M., Massoth, F. E., Dhar, G. M. and Eyring, E. M., *J. Phys. Chem.* 1982, **86**, 1760.

6) Parry, E. P., *J. Catal.* 1963, **2**, 371.

7) Eischens, R. P. and Pliskin, W. A., *Advan. Catal.* 1958, **10**, 1.

8) Emeis, C. A., *J. Catal.* 1993, **141**, 347.

9) Ghosh, A. K. and Kydd, R. A., *Catal. Rev.-Sci. Eng.* 1985, **27**(4), 539.

10) Engelhardt, J., Onyestyak, G. and Hall, W. K., *J. Catal.* 1995, **157**, 721.

11) Leonard, A., Suzuki, S., Fripiat, J. J. and De Kimpe, C., *J. Phys. Chem.* 1964, **68**, 2608.

12) Connell, G. and Dumesic, J. A., *J. Catal.* 1986, **102**, 216.

13) Knözinger, H., in "Catalysis by acids and bases" (B. Imelic, C. Naccache, G. Goudurier, Y. B. Taarit and J. C. Vardine, Eds) p. 111, Elsevier, Amsterdam, 1995.

14) Chen, L.Y., Ping, Z., Chuah, G.K., Jaenicke, S. and Simon, G., *Microporous and Mesoporous Materials,* 1999, **27**, 231.

Chapter 5 Aluminas and Modified Aluminas

5.1 Introduction

Alumina has many different crystallographic forms. Two of the most commonly discussed are γ-alumina and α-alumina. γ-Alumina is considered a high surface area, highly active form of alumina whereas α-alumina is a highly crystalline; low surface area, low activity form. α-Alumina is formed by high temperature (ca. 1000°C) treatment of other alumina phases, including the γ phase, which converts to the α phase via the δ and θ transitional phases. Both γ-alumina and α-alumina are widely used as catalyst supports. γ-Alumina is used in processes where support acidity is important e.g. catalytic reforming (Pt on γ-alumina) where the γ-alumina support is chlorided to increase acidity. α-Alumina is chosen when the support must be thermally stable at high temperatures and / or chemically inert.

Unlike silica-aluminas or zeolites, aluminas do not possess Bronsted acid sites – only a low density of Lewis acid sites is generally observed. However the acidic properties of aluminas can be extensively modified by simple chemical procedures [1-9]. This versatility may make aluminas useful adsorbents for the selective removal of basic nitrogen compounds because their acidity can be tailored to suit the operational conditions. The addition of fluoride to aluminas has been shown to increase the strength of existing Lewis acid sites and introduce Bronsted acid sites[1,2,4-9].

5.2 Results and Discussion

5.21 B.E.T. Surface areas

Fig 5.21.1 B.E.T. Surface area of the five alumina samples

Sample[a]	Name	B.E.T. Surface Area (m^2g^{-1})
γ-Al_2O_3 (600°C)	Al-600	82
γ-Al_2O_3 (1000°C)[b]	Al-1000	5
1wt%F^- γ-Al_2O_3 (600°C)	F1-Al-600	78
1wt%F^- γ-Al_2O_3 (1000°C)[b]	F1-Al-1000	4
14wt%F^- γ-Al_2O_3 (600°C)	F14-Al-600	69

a) Temperatures in brackets refer to calcination temperatures

b) Samples calcined at 1000°C can be considered to be α-Al_2O_3

The B.E.T. surface area results in Fig 5.21.1 show that the most significant factor affecting the surface area is calcination temperature. The surface areas of both the aluminas calcined at 1000 °C are in single figures and are over an order of magnitude smaller than any of the samples calcined at 600 °C. Fluoriding the aluminas also seems to have an effect. Within the series of samples calcined at 600 °C, the addition of a small amount of fluoride (~ 1 wt%) leads to a small reduction in the surface area, as compared to the unmodified sample. The addition of greater amounts of fluoride leads to a more significant loss of surface area, and at 14 wt% F^- the surface area has been reduced by ~ 16 %. Both the effect of high temperature treatment, and fluoride loading are consistent with previous reports [5,6].

5.22 F.T.I.R. and Microadsorption studies

5.22.1 Al-600

Fig 5.22.11 F.T.I.R. - Pyridine Region and tabulated band areas

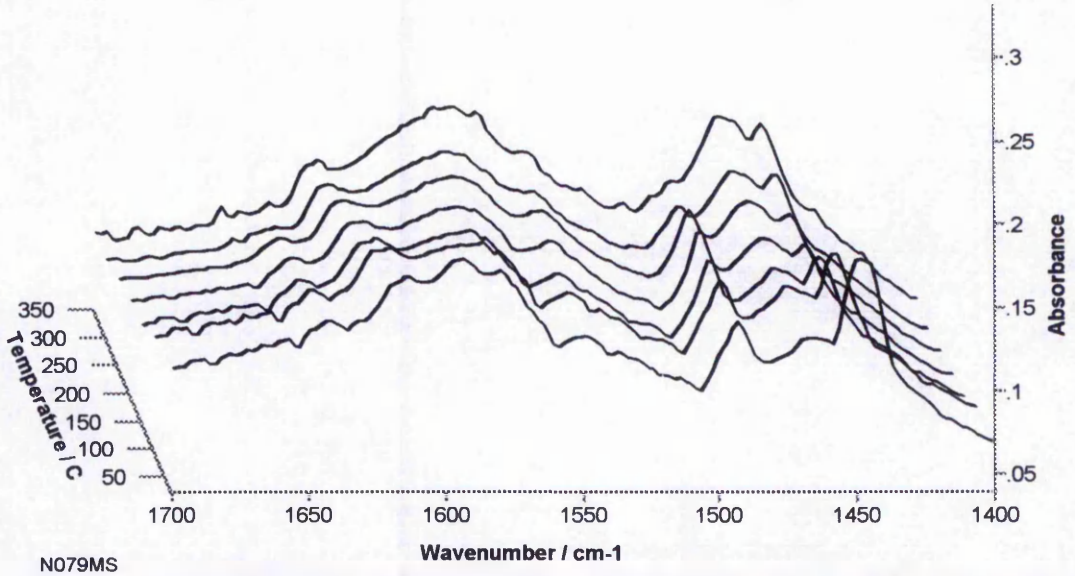

N079MS

	Temperature / C	25	100	150	200	250	300	350
Assignment	cm-1							
Physisorbed	1446	0.75						
Lewis	1450		0.39	0.2	0.08	0.07	0.12	0.08
L + B	1492	0.27	0.28	0.27	0.25	0.2	0.09	0.01
Bronsted	1547	0.07	0.08	0.07	0.08	0.08	0.03	0.02
Physisorbed	1598	0.12						
Lewis	1614	0.11	0.14	0.14	0.14	0.14	0.13	0.13
Bronsted	1641	0.06	0.07	0.07	0.07	0.06	0.02	

Fig 5.22.12 Microadsorption breakthrough vs time

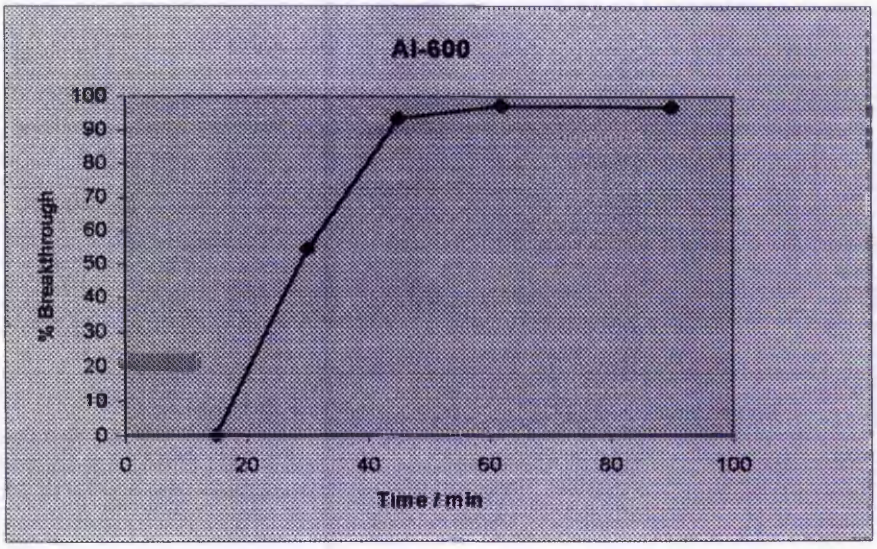

For the unmodified γ-alumina, Al-600 sample, the FTIR spectra of adsorbed pyridine (Fig 5.22.11) show the presence of pyridine bound to both Lewis and Bronsted acid sites (1450 cm^{-1} and 1547 cm^{-1} respectively). This is unexpected as most reports [1,2,5,6,9] suggest that unmodified alumina does not possess hydroxyls acidic enough to protonate pyridine. The bands assigned to bronsted bound pyridine are significantly smaller than the equivalent Lewis bands, and even after the different extinction coefficients are considered, it is clear that there are significantly more Lewis sites.

When the unmodified alumina is calcined at 1000 °C, to convert it to α-Al_2O_3 the BET surface area is reduced significantly, from 82 m^2g^{-1} to 5 m^2g^{-1}. The only pyridine bands observed are the 'Lewis' bands at 1450cm^{-1} and 1608 cm^{-1} (Fig 5.22.21), and the 'combined band' at 1492 cm^{-1}. All these bands are very small, and no pyridine is observed at temperatures above 150 °C. The high temperature treatment has shifted the ν_{8a} Lewis band to 1608 cm^{-1} from 1614 cm^{-1} in the Al-600 sample. This shift to lower frequency indicates a reduction in the strength of the Lewis acid sites. The reduction in acid strength is also evidenced by the complete desorption of pyridine at or below 200 °C. The reduction in the number of acidic sites is probably associated with the loss of surface area – acid sites are a surface phenomenon. The reduction in acid site strength however, suggests that α-Al_2O_3 is inherently less active than γ-Al_2O_3.

5.22.2 Al-1000

Fig 5.22.21 F.T.I.R. - Pyridine Region and tabulated band areas

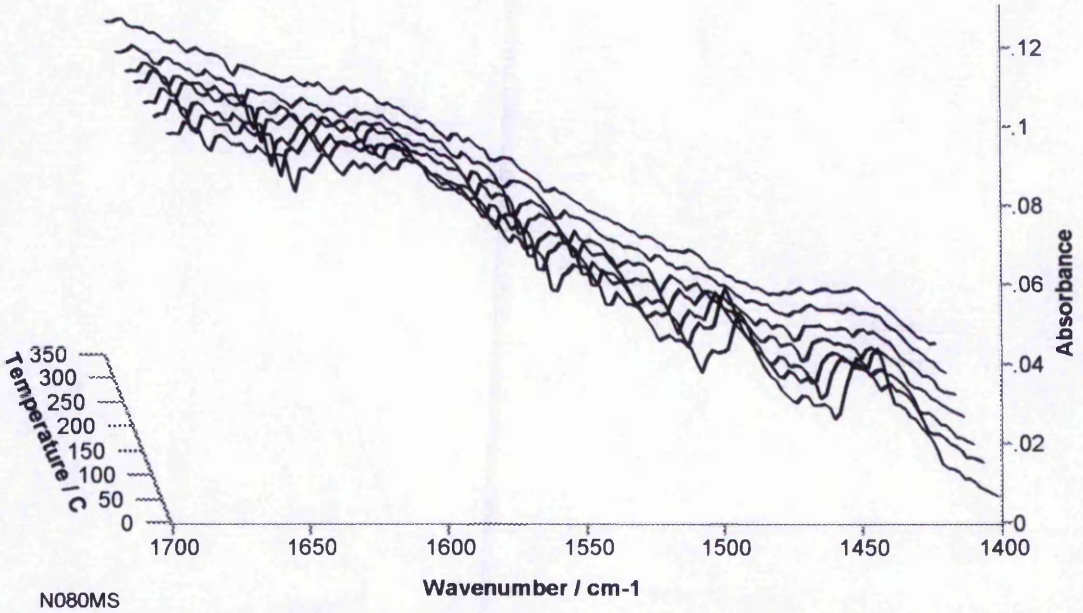

N080MS

	Temperature / C	25	100	150	200	250	300	350
Assignment	cm-1							
Physisorbed	1446	0.15						
Lewis	1450	0.1	0.08	0.04				
L + B	1492	0.1	0.08	0.04				
Bronsted	1547							
Physisorbed	1598							
Lewis	1608	0.03	0.02	0.01				
Bronsted	1639							

Fig 5.22.22 Microadsorption breakthrough vs time

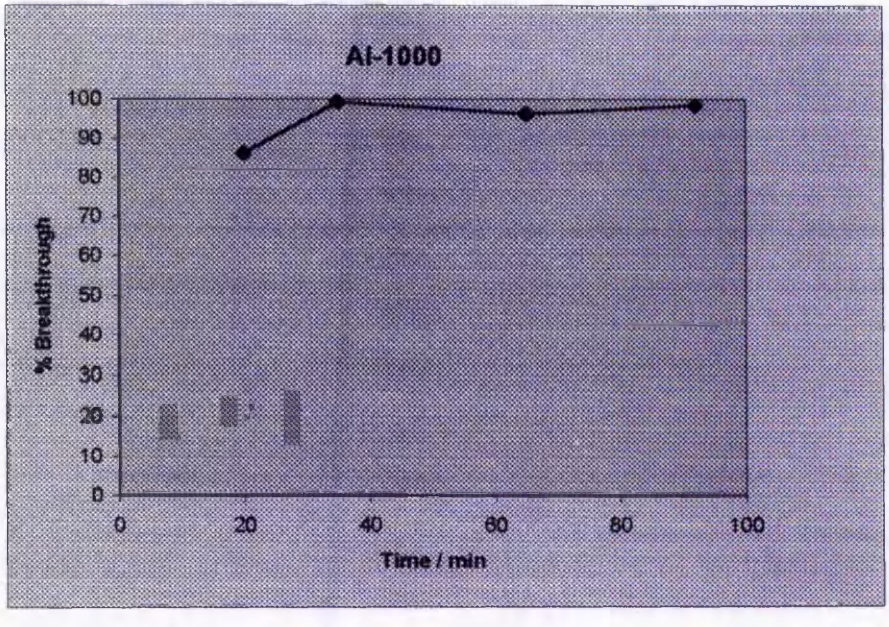

5.22.3 F1-Al-600

Fig 5.22.31 F.T.I.R. - Pyridine Region and tabulated band areas

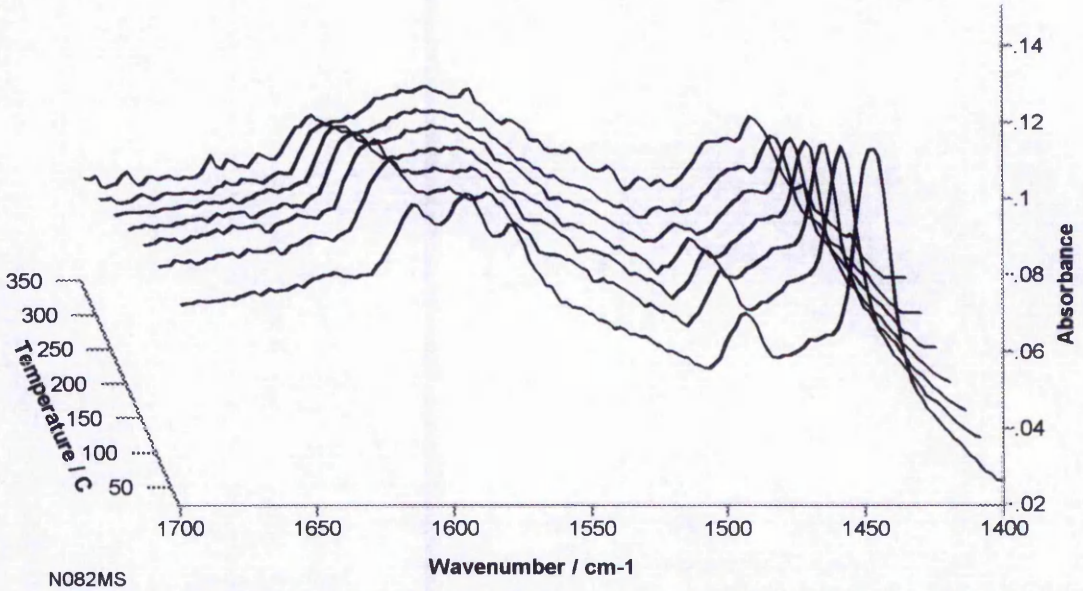

N082MS

	Temperature / C	25	100	150	200	250	300	350
Assignment	cm-1							
Physisorbed	1446	0.21						
Lewis	1450	0.58	0.46	0.34	0.25	0.185	0.14	0.09
L + B	1492	0.16	0.11	0.08	0.05	0.02		
Bronsted	1547							
Physisorbed	1598	0.1	0.01					
Lewis	1614	0.11	0.19	0.19	0.16	0.13	0.1	0.04
Bronsted	1639							

Fig 5.22.32 Microadsorption breakthrough vs time

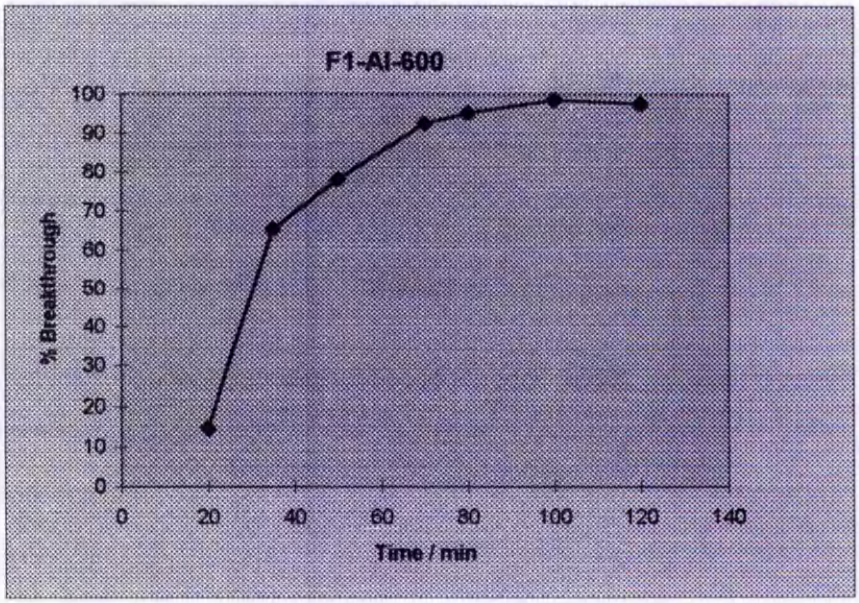

The addition of 1 wt % F^- to γ-Al_2O_3 gives rise to a pyridine FTIR spectra which is very similar to the unmodified γ-Al_2O_3. However there are no bands in the spectra assigned to Bronsted bound pyridine. One of the effects of adding small amounts of fluoride to alumina is reported to be the generation of strong Bronsted sites [1,2,4-6]. Fluoride substitutes for hydroxyls on the surface, reducing the total number of hydroxyls, but increasing the strength of those that remain [5]. The reduction in the total number of hydroxyls, combined with the loss of surface area upon fluoriding, may explain why Bronsted bound pyridine bands are not observed in the fluorided sample. Alternatively a loading of 1 wt % F^- may not be sufficient to generate an observable number of Bronsted sites. It should be noted, that with these alumina samples, levels of pyridine adsorption are generally low. Identification and quantification of these weak bands can therefore be difficult. The addition of fluoride to alumina is also reported to increase the strength of Lewis acid sites [4,5]. In this respect the addition of 1 wt % F^- does appear to be partially effective. A strong absorption band is observed at 1450 cm^{-1} (Lewis bound pyridine). The number of Lewis sites appears to be increased compared to the unmodified sample, however the strength of these sites does not appear to have altered significantly. The band is centred at 1450 cm^{-1} for both samples and the profile of desorption with increasing temperature is similar.

When the calcination temperature of the fluorided alumina is increased, to 1000°C, the reduction in surface area is similar to that observed with high temperature treatment of the unmodified aluminas. The fluoride reduces the thermal stability of the γ-Al_2O_3 phase and catalyses the transformation to α-Al_2O_3. This results in lower surface areas, for both the fluorided samples, as compared to the unmodified samples treated at the same temperature. The pyridine FTIR spectra show only small amounts of adsorbed pyridine at low temperature. At room temperature, as well as a small physically adsorbed band at 1446 cm^{-1}, there is a small Lewis bound pyridine band observed at 1450 cm^{-1}, which is removed as the temperature is raised to 200 °C.

5.22.4 F1-Al-1000

Fig 5.22.41 F.T.I.R. - Pyridine Region and tabulated band areas

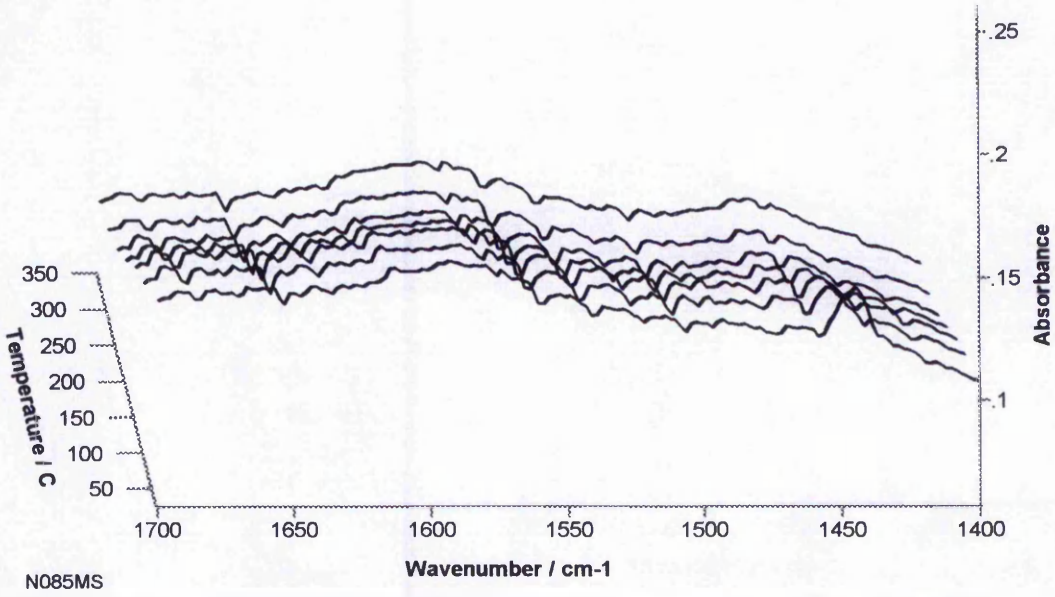

	Temperature / C	25	100	150	200	250	300	350
Assignment	cm-1							
Physisorbed	1446	0.06						
Lewis	1450	0.05	0.045	0.02				
L + B	1492							
Bronsted	1547							
Physisorbed	1598							
Lewis	1623							
Bronsted	1639							

Fig 5.22.42 Microadsorption breakthrough vs time

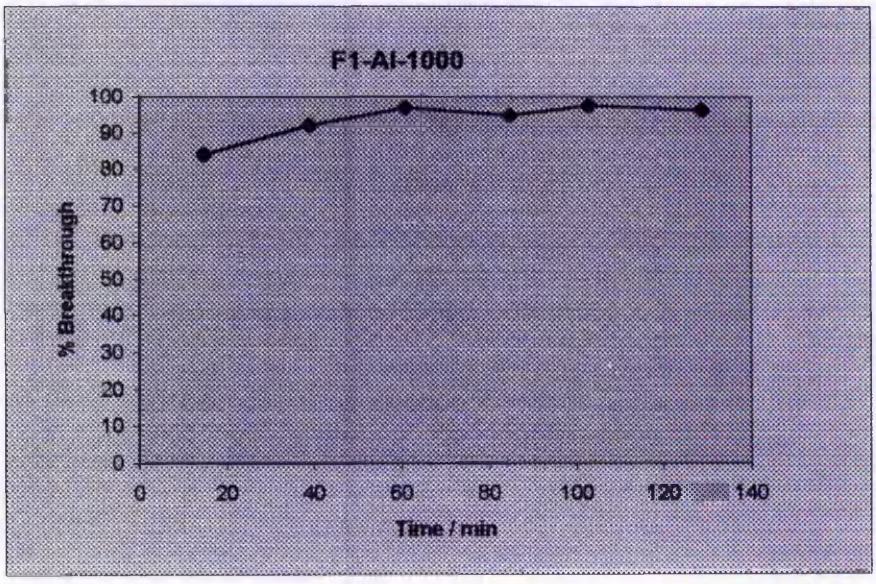

5.22.5 F14-Al-600

Fig 5.22.51 F.T.I.R. - Pyridine Region and tabulated band areas

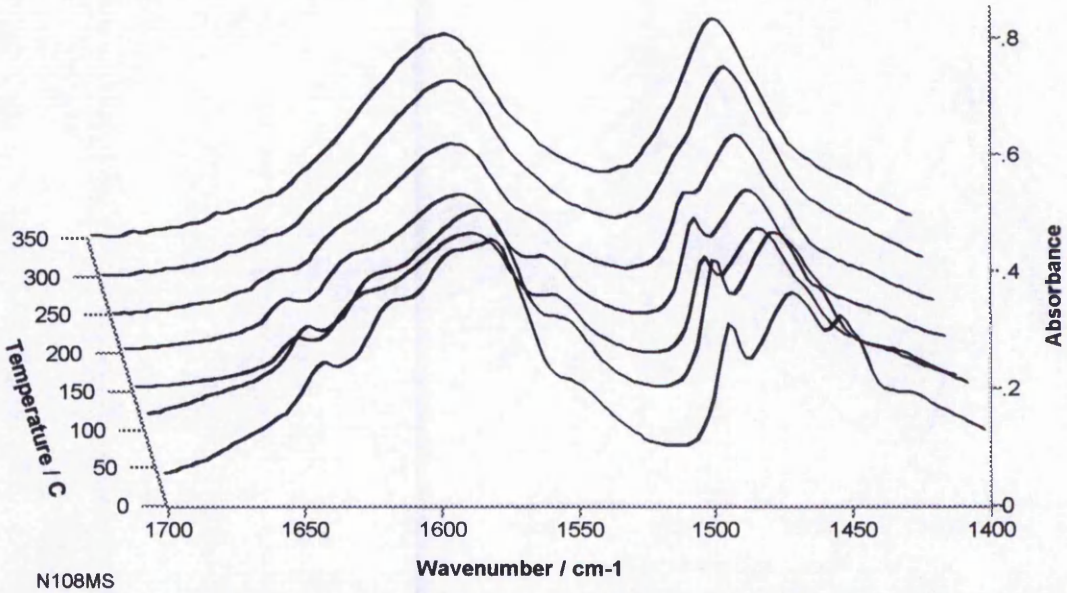

N108MS

	Temperature / C	25	100	150	200	250	300	350
Assignment	cm-1							
Physisorbed	1446	0.1						
Lewis	1452	0.2	0.025	0.02	0.015	0.01		
L + B	1492	0.44	0.43	0.245	0.08			
Bronsted	1547	0.1	0.145	0.14	0.04			
Physisorbed	1595	0.105						
Lewis	1618	0.18	0.17	0.16	0.155	0.06		
Bronsted	1642	0.165	0.15	0.13	0.095	0.05		

Fig 5.22.52 Microadsorption breakthrough vs time

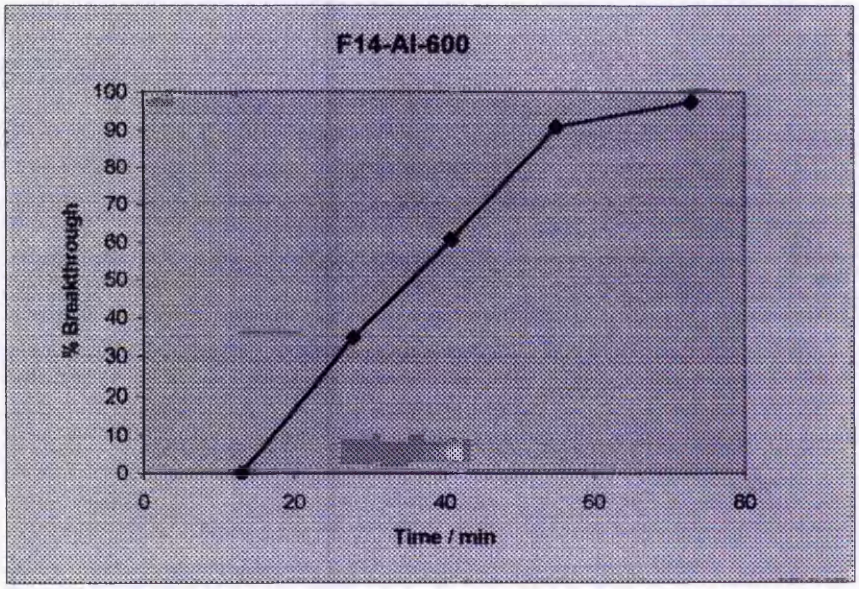

Increasing the loading of fluoride on γ-Al_2O_3 to 14 wt % introduces significant changes to the spectra of adsorbed pyridine (Fig 5.22.51). Bronsted sites have been generated which retain pyridine up to temperatures around 250 °C. It seems likely that the 1 wt % F^- γ-Al_2O_3 did not have observable numbers of Bronsted sites because the F^- loading was not sufficient. The high fluoride level also appears to have an effect on the Lewis sites present. The wavenumber of the Lewis bound pyridine band has moved from 1450 cm^{-1} in the other alumina samples to 1452 cm^{-1} indicating a stronger interaction with the pyridine. Fig 5.22.51 also exhibit unusual background bands at ~ 1470 cm^{-1} and 1580 cm^{-1}. The precise nature of these bands is unknown, but as these spectra are not 'difference' spectra (differential spectra) they may well be some sort of structural feature generated by the high F^- levels. The band at ~1470 cm^{-1} makes observation of the Lewis bound pyridine band at 1452cm^{-1} difficult at higher temperatures. However the ν_{8a} Lewis band at 1618 cm^{-1} shows that significant amounts of pyridine are retained at temperatures up to 250 °C.

For all the alumina samples the –OH region of the FTIR spectra are found to be devoid of the five hydroxyl stretch vibrations found by Peri et. al.[10,11] between 3800 and 3700 cm^{-1}. Their absence can be attributed to the low outgasing temperature (350 °C) employed in the sample pre-treatment, since these bands were observed to remain unresolved until pre-treatment temperatures above 500°C.

5.3 Summary

Fig 5.3.1 Band areas at 200°C and 50% breakthrough times for the Aluminas.

Sample	Lewis ~1614 – 1618 cm^{-1}	Lewis ~1450 cm^{-1}	Bronsted band ~1545 cm^{-1}	Lewis / Bronsted Ratio[a]	50 % Breakthrough / min
Al-600	0.14	0.08	0.08	0.75	~30
Al-1000	-	-	-	-	<20
F1-Al-600	0.16	0.25	-	-	~30
F1-Al-1000	-	-	-	-	<10
F14-Al-600	0.15	0.015	0.04	0.28	~35

(a) 1545 cm^{-1} and 1450 cm^{-1} bands normalised using relative molar extinction coefficients

Fig 5.3.1 summarises the pyridine band areas at 200°C, and the 50 % breakthrough times for the five alumina samples. Figs 5.3.2 and 5.3.3 show the pyridine desorption profiles from Lewis and Bronsted sites respectively. The two samples calcined at 1000 °C (Al-1000 and F1-Al-1000) do not retain any pyridine observable by FTIR at 200 °C, and in the microadsorption experiments pyridine breakthrough is almost immediate. At lower temperatures small amounts of Lewis bound pyridine are observed, but there is no evidence of any Bronsted sites.

The three samples treated at 600 °C retain similar amounts of pyridine at 200 °C and have similar microadsorption 50 % breakthrough times. The 1614 / 1618 cm^{-1} band areas are included because the 1450 cm^{-1} band is difficult to measure accurately, particularly for F14-Al-600. Although these samples have similar amounts of adsorbed pyridine at 200°C, the nature and strength distributions of these sites are different. The F1-Al-600 sample has no Bronsted sites, but the most Lewis sites, although approximately 80% of Lewis bound pyridine desorbs below 350°C. The Al-600 sample has fewer weak Lewis sites, but a similar number of strong Lewis sites, and also has a small number of Bronsted sites that

appear to be relatively strong. These Bronsted sites seem to be of uniform strength. There is no desorption below 250°C, but then about 2/3 of the pyridine is removed by 300°C. The unusual desorption profile of Lewis bound pyridine is probably the result of the difficulty in measuring the 1450 cm^{-1} band accurately. The F14-Al-600 sample does not appear to have a large number of acid sites in the pyridine FTIR experiment, although the number of Lewis sites is more significant if the 1614-1618 cm^{-1} band is used. The Lewis sites are very weak, and most of the pyridine adsorbed to these sites desorbs below 100°C. The Bronsted sites are also weak, and pyridine is completely removed by 250°C.

Fig 5.3.2 Pyridine Temperature Programmed Desorption Profiles for the alumina samples (Lewis acid sites)

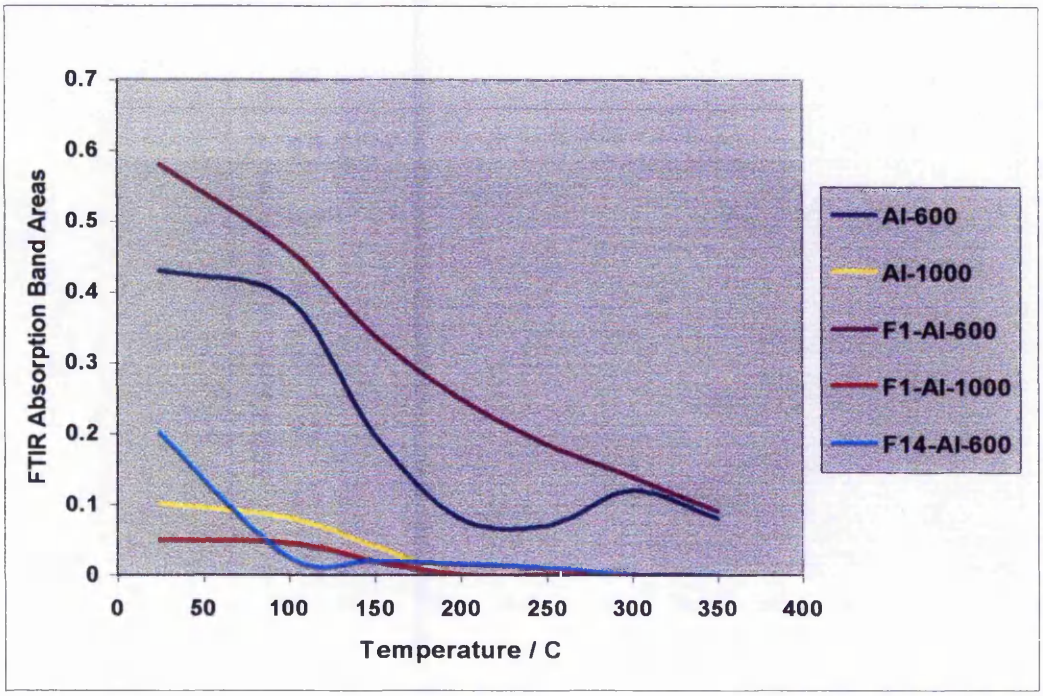

Fig 5.3.3 Pyridine Temperature Programmed Desorption Profiles for the alumina samples (Bronsted acid sites)

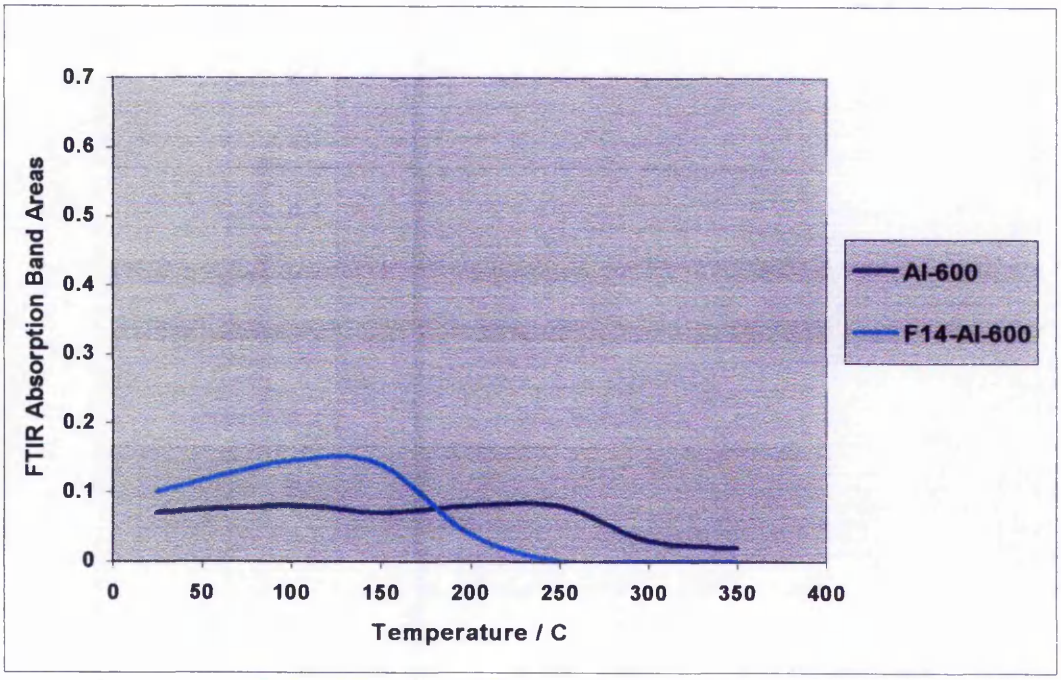

5.4 Conclusions

The effect of fluoriding the alumina is unclear. The addition of 1wt% F^- has increased the number of weak Lewis sites, but removed the few Bronsted sites that were initially present. Increasing the fluoride loading to 14 wt% has introduced weak Bronsted sites, but has dramatically reduced the number of Lewis sites, (especially strong Lewis sites). These changes in the nature and strength distribution of acid sites have had little effect on the microadsorption performance.

By far the most significant variable is the BET surface area, which is primarily dictated by the calcination temperature. The samples calcined at 600°C, with surface areas of 70 – 80 m^2g^{-1} have 50% pyridine breakthrough times around 30 minutes. The samples calcined at 1000°C, with surface areas around 5 m^2g^{-1} were much less effective.

The 50 % breakthrough time of 35 minutes for F14-Al-600 corresponds to pyridine adsorption of ~ 0.2 wt % at the 50 % breakthrough point. This is much lower than some other materials tested in this study. Even with optimisation of the fluoride levels, to generate a higher acid site density and strength, it appears unlikely that aluminas will become a viable adsorbent for basic nitrogen species.

5.5 References

1) Engelhardt, J., Onyestyak, G. and Hall, W. K., *J. Catal.* 1995, **157**, 721.

2) Berteau, P., Kellens, M-A. and Delmon, B., *J. Chem. Soc. Faraday Trans.* 1991, **87**(9), 1425.

3) Shen, Jianyi, Cortright, R. D., Yi, Chen, and Dumesic, J. A. *J. Phys. Chem.* 1994, **98**, 8067.

4) Scokart, P. O. and Rouxhet, P. G., *J. Colloid Interface Sci.* 1982, **86**(1), 96.

5) Ghosh, A. K. and Kydd, R. A., *Catal. Rev.-Sci. Eng.* 1985, **27**(4), 539.

6) DeCanio, E. C., Bruno, J. W., Nero, V. P. and Edwards, J. C., *J. Catal.* 1993, **140**, 84.

7) Hegde, R. I. And Barteau, M. A., *J. Catal.* 1989, **120**, 387.

8) Skapin, T. and Kemnitz, E., *Catal. Lett.* 1996, **40**, 241.

9) Riseman, S. M., Massoth, F. E., Dhar, G. M. and Eyring, E. M., *J. Phys. Chem.* 1982, **86**, 1760.

10) Peri, J. B. and Hannan, R. B., *J. Phys. Chem.*, 1960, **64**, 1526.

11) Peri, J. B., *J. Phys. Chem.*, 1965, **69**, 211.

Chapter 6 MCM-41

6.1 Introduction

Since its discovery in 1992 by researchers at Mobil[1,2] the mesoporous molecular sieve MCM-41 has been the subject of considerable research as an acidic catalyst[3-6]. Little work has focused on its use as an acidic adsorbent. The material has uniform pores of diameter 15 – 100 nm, ordered in a hexagonal array (Fig 6.1.01). This pore size makes it particularly suitable for the treatment of large molecules. The acid sites generated by substitution of aluminium into the structure are not as strong as the acid sites present in zeolites[3,4]. This may be a disadvantage for some acid catalysed reactions, but for selective adsorption applications it could be very favourable. The moderate acid strength may be sufficient to adsorb basic nitrogen compounds at 200°C without activating the hydrocarbon matrix and generating coke.

In this study five MCM-41 samples with different Si / Al ratios have been synthesised according to the preparation in reference 11. The Si / Al ratios quoted refer to the gel composition during synthesis, but this is generally a reasonable approximation to that of the samples produced [7-10].

Fig 6.1.01 Schematic of the hexagonal array of pores in MCM-41.

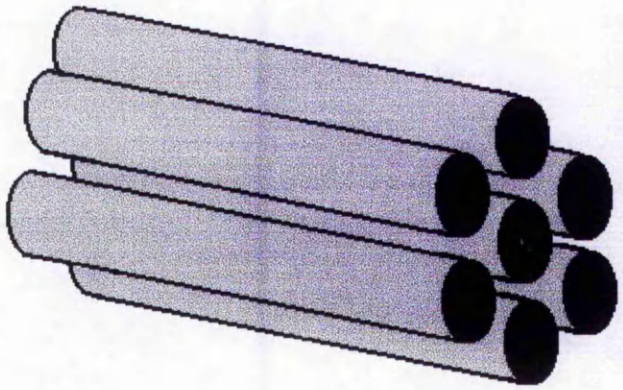

6.2 Results and Discussion

6.21 Introduction and T.E.M.

Electron microscopy (Figs 6.21.1-3) shows the samples to be made up of irregular crystallites of approximately 50nm. The micrographs show all samples in the series have a chaotic arrangement of pores – most clearly seen in Fig 6.21.3 at 100,000X magnification. This is consistent with other T.E.M. studies on Al containing samples [11,12]. The pores essentially run parallel to one another, as in a 'genuine' MCM-41, but do not have the hexagonal symmetry shown in Fig 6.1.01. As the hexagonal arrangement of pores is one of its defining features, none of these samples are true MCM-41 materials (or MCM-48 / MCM-50). The 'aluminium rich dense phase' observed by Kloetstra et al,[11] is not observed, only the chaotic 'MCM-41' phase is present. The samples discussed here will still be designated MCM-41, partly for simplicity and partly because this designation is consistently used in the literature for such materials. The chemical properties should be very similar to a 'genuine' aluminosilicate MCM-41, with the same Al content, as the structure and composition of the pore walls should be the same. Only the arrangement of the pores differs. The less well ordered pore structure may account in part for the lower surface areas of Al containing materials, but as this can be measured, results can be normalised accordingly. The performance for the selective adsorption of pyridine should not be affected by the chaotic arrangement of pores and pyridine is too small a molecule, in comparison to the typical pore size, for its adsorption to be affected by any spread in the pore size distribution.

Fig 6.21.1 Electron micrograph of MCM-41 (Si / Al = 25)

60,000 times magnification 7.5mm = 100nm

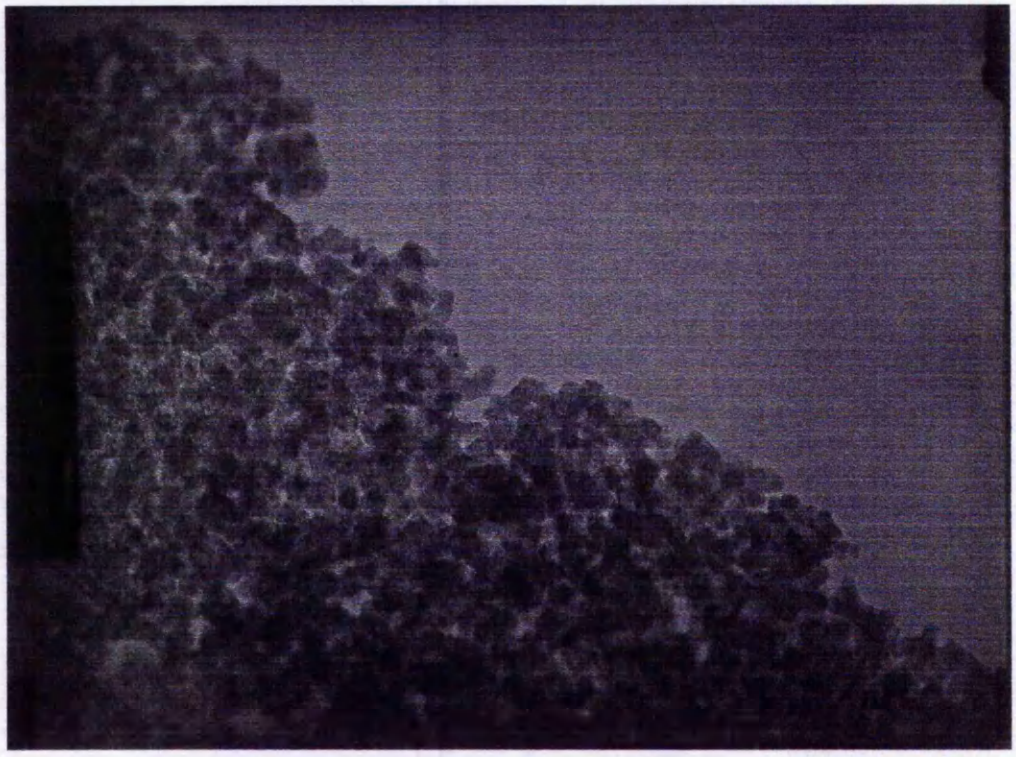

Fig 6.21.2 Electron micrograph of MCM-41 (Si / Al = 8)

80,000 times magnification 10mm = 100nm

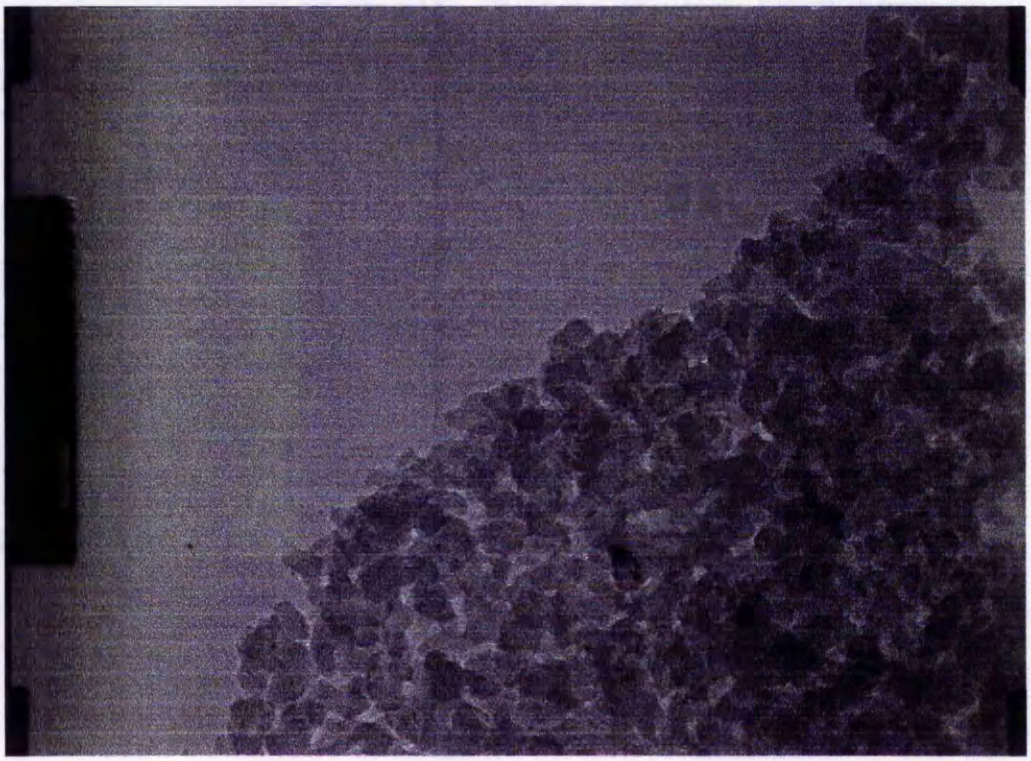

Fig 6.21.3 Electron micrograph of MCM-41 (Si / Al = 25)

100,000 times magnification **8mm = 50nm**

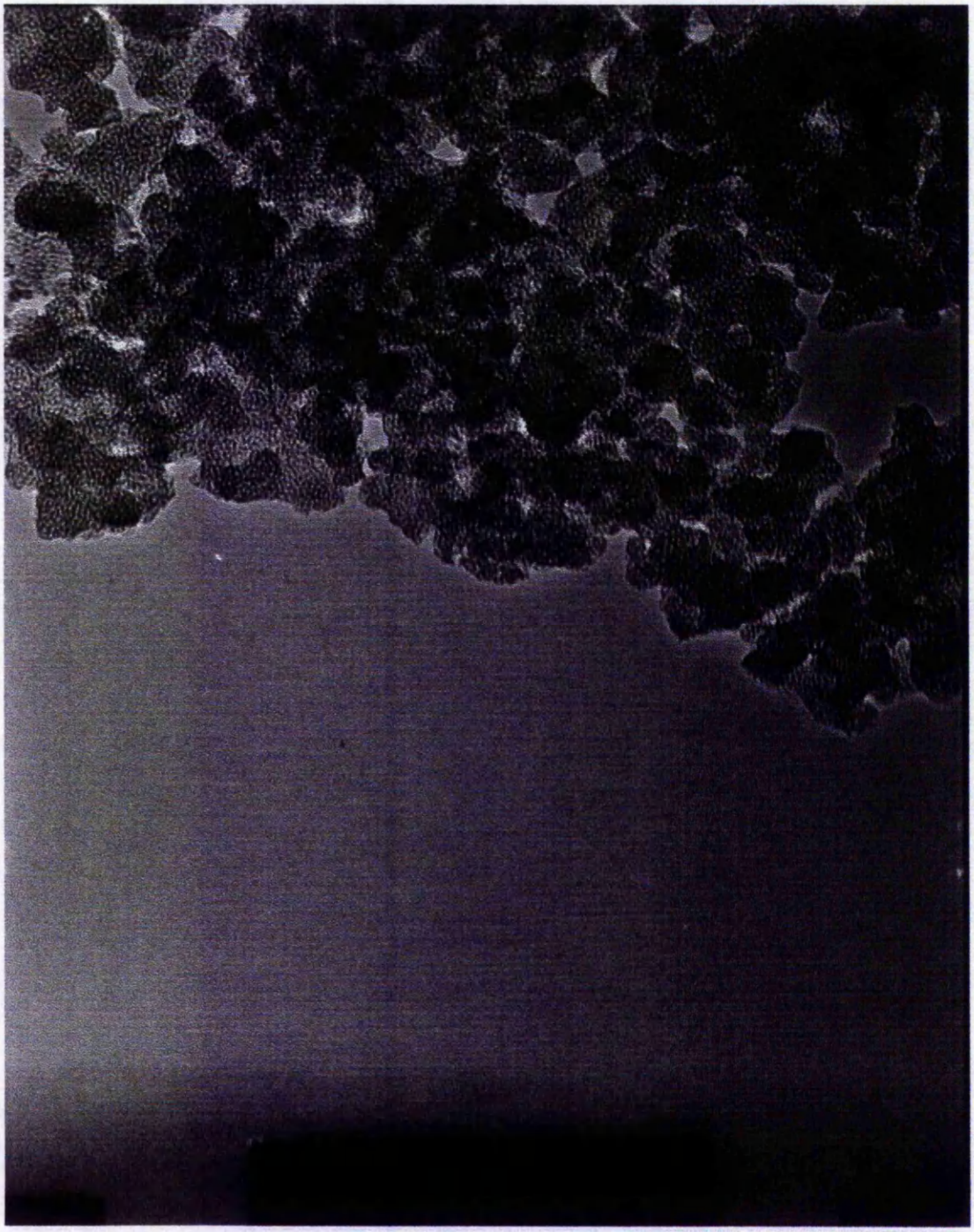

6.22 N_2 adsorption isotherms and B.E.T. surface areas

Fig 6.22.1 B.E.T. surface areas for MCM-41 samples

SAMPLE	B.E.T. Surface Area ($m^2 g^{-1}$)
MCM-41 (SiO_2)[a]	680
MCM-41 (Si / Al = 8)	710
MCM-41 (Si / Al = 12) [a]	669
MCM-41 (Si / Al = 15)	810
MCM-41 (Si / Al = 18)	835
MCM-41 (Si / Al = 25)	877
H-MCM-41 (Si / Al = 8) [b]	631
H-MCM-41 (Si / Al = 8) ex adsorption [c]	659

(a) Prepared in different batches

(b) After NH_4^+ exchange and calcination at 450°C for 16h

(c) After two microadsorption experiments with regeneration in between

The BET surface areas for the MCM-41 samples (Fig 6.22.1) show a general reduction with increasing aluminium content, which is consistent with most reports [9,13,14]. The values observed correspond well with the values reported by Kloetstra et al [11] whose synthesis procedure is followed. When aluminium is incorporated into MCM-41 the structure becomes less ordered, leading to the chaotic pore structure observed by TEM. The surface areas are reduced accordingly and this effect appears to increase with increasing aluminium content. The sample with Si / Al = 12 is the only inconsistency in this trend, but it is worthwhile to note that this sample was prepared in a different batch to the other samples. NH_4^+ ion exchange and calcination at 450°C leads to a significant reduction in the surface area, from 710 $m^2 g^{-1}$ to 631 $m^2 g^{-1}$. Either the aqueous ion exchange or the thermal treatment has caused a degradation of the structure. Several reports [7,12] have shown this procedure to remove aluminium from the framework. The aluminium is not removed in the ion

exchange stage, but in the calcination, despite the fact that the sample has already been calcined at a higher temperature to remove the template. It is possible that the very small H^+ cations, created in the calcination step, cannot efficiently satisfy the negative electric charge on the framework, at these elevated temperatures [12]. As a result the mesoporous structure partly collapses.

Fig 6.22.2 N_2 adsorption isotherms for MCM-41 (Si / Al = 8)

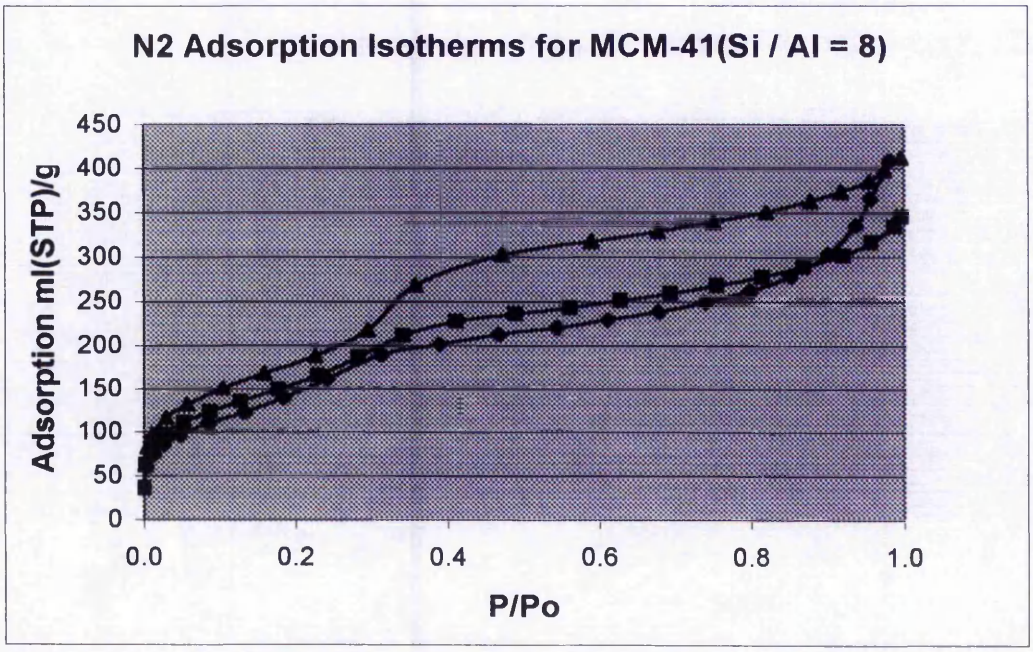

▲ Before NH_4^+ exchange; ■ After NH_4^+ exchange and calcination (H-MCM-41); ◆ H-MCM-41 after two microadsorption experiments with regeneration in between.

The N_2 adsorption isotherms for the Si / Al = 8 samples are all typical type IV shapes (mesoporous). Ion exchange and calcination has the effect of reducing the uptake of nitrogen for the full range of P / Po values. Adsorption in the mesopore filling region (P / Po = 0.30 – 0.40) is particularly suppressed, indicating a loss of definition in the pore structure. Adsorption is reduced further, for most P / Po values, after two microadsorption experiments

separated by a regeneration step. At P / Po values > 0.9 the isotherm for the regenerated sample shows a sharp increase in adsorption. Adsorption in this region can be attributed to filling of very large pores as the pressure approaches Po. Macropores may be formed as the walls between the pores collapse, so that several mesopores may combine to form one macropore [12]. This is most likely to occur during the regeneration step, where the sample was heated to 650°C.

6.23 F.T.I.R and microadsorption studies

6.23.1 MCM-41 (SiO_2)

Fig 6.23.10 F.T.I.R. – Pyridine region and tabulated band areas

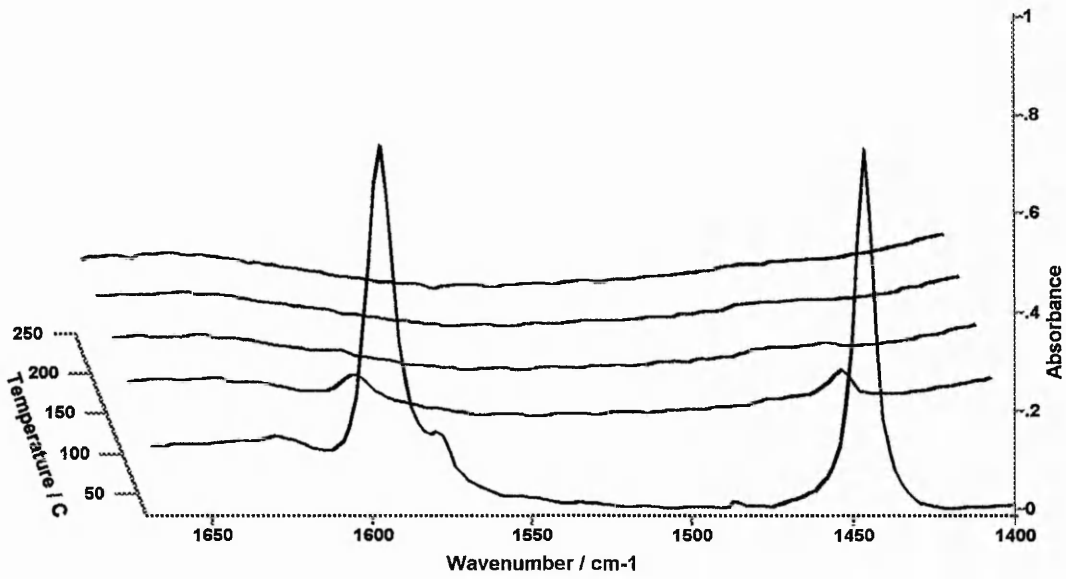

File #11 = N042MS#2 @ 100

	Temperature / C	25	100	150	200	250	300	350
Assignment	Band (cm^{-1})							
Physisorbed	1446	33.35	2.09	0.24				
Lewis	1455							
L + B	1492							
Bronsted	1547							
Physisorbed	1598	31.55	2.14	0.19				
Lewis	1623							
Bronsted	1639							

Fig 6.23.11 F.T.I.R. – OH region

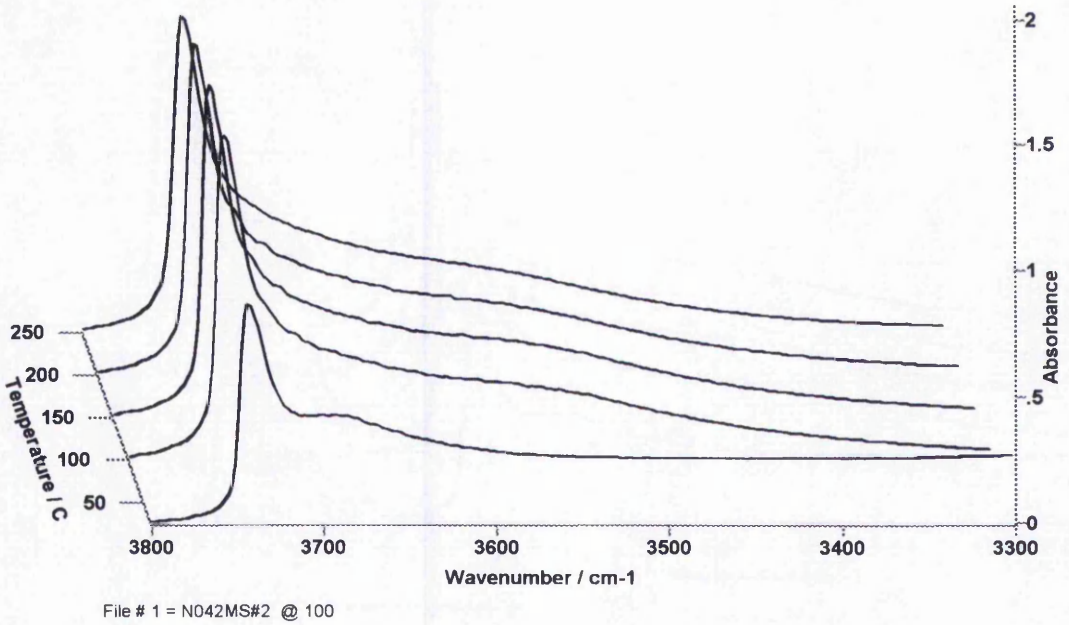

Fig 6.23.12 Comparison of the 3740 cm^{-1} (-OH) band with the 1446 cm^{-1} (physically adsorbed pyridine) band at each temperature.

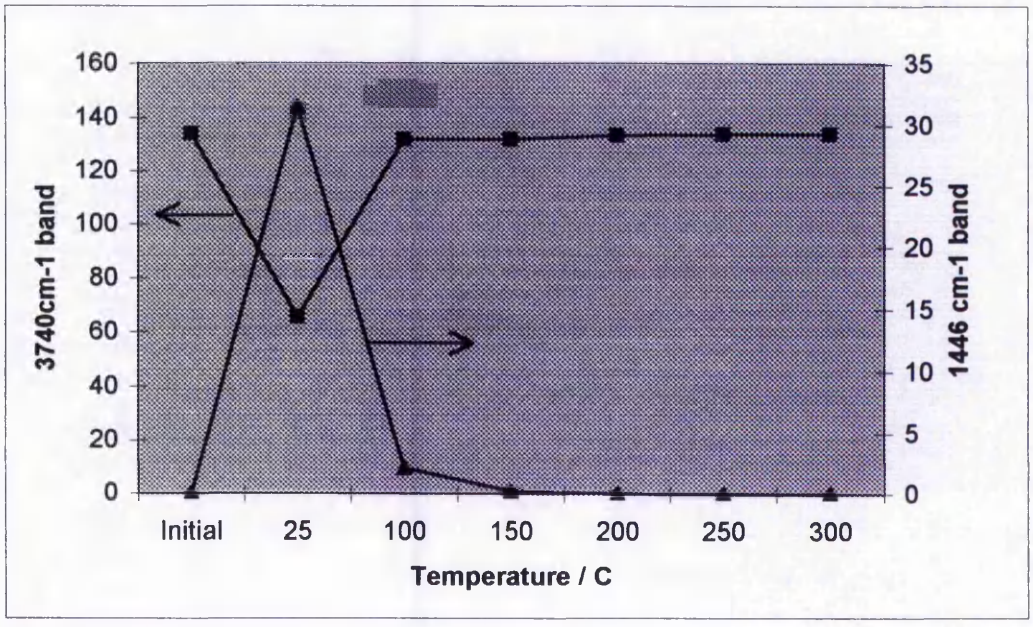

▲ - 1446 cm^{-1} band. ■ - 3740 cm^{-1} band

N.B. 'Initial' is spectrum before dosing pyridine.

The FTIR spectra of adsorbed pyridine on MCM-41 are fairly easy to interpret for the 1670 cm^{-1} – 1400 cm^{-1} pyridine region. The bands observed are the same as for other solid acid materials and the band assignments are well documented. The V_{19b} ring vibration for Bronsted bound pyridine (pyridinium ion) is seen at ~1545 cm^{-1} whilst the same vibration for Lewis bound pyridine is at ~1455 cm^{-1}. V_{8a} vibrations are also observed at ~1639 cm^{-1} and ~1622 cm^{-1} for Bronsted and Lewis bound pyridine respectively.

The interpretation of the OH region of the spectra is more difficult. The one well defined absorption band in this region is at 3740 cm^{-1}. It is typical of amorphous silica, and is assigned to isolated non acidic silanol groups [9,10,16-21], although Kosslick et al [19] assign it to silanol groups within the pores, due to its high intensity, whilst all other authors assign it to silanols terminating the particles [9,10,16-18,20,21]. The other features in this part of the spectra are generally broad and of weak intensity, making it difficult to differentiate bands from the background. Different studies have produced different apparent bands, and the assignments are not always consistent. A band at ~ 3715 cm^{-1} has been assigned to internal silanol groups [9,18] and internal silanol groups at defect sites due to interrupted Si-O-Si linkages [9]. A band at 3660 cm^{-1} is assigned to hydroxy groups on octahedral, extra-framework aluminium [9,18,20,21]. A feature at 3530 – 3555 cm^{-1} is assigned to H-bonded silanol groups [9,18,20], probably internal [18,20]. Most authors have failed to observe an acidic OH band although Kosslick et al [19] assign an absorbance at 3605 cm^{-1} to bridging acidic hydroxy groups Si-O(H)-Al.

The spectra of the pure silica and Si / Al = 25 samples exhibit an additional band in the hydroxyl region at room temperature. This band at ~3690 cm^{-1} is only visible when there is a large amount of physically adsorbed pyridine present, and could be due to silanol groups hydrogen bonded with pyridine.

All the MCM-41 samples studied here show significant amounts of physically adsorbed pyridine at room temperature. This is probably related to the very high surface areas of these materials. The 1598 and 1446 cm^{-1} bands are of very high intensity. A shoulder is visible on the 1598 cm^{-1} band at 1580 cm^{-1}, which is also assigned to physically adsorbed pyridine. It is much less intense than either of the other two physically adsorbed bands, and is only visible in these samples where a large amount of physically adsorbed pyridine is observed. In all cases this pyridine is weakly bound and desorbs as the temperature is increased. Most is removed by 100°C, and the tiny amount visible at 150°C, in some of the spectra, would probably be removed if a longer equilibration time was allowed. For the pure silica sample (Fig 6.23.1) the physically adsorbed pyridine is all that is visible in this region, and the spectra are featureless at higher temperatures.

The spectra of all the aluminium containing samples exhibit absorption bands assigned to pyridine chemisorbed to both Bronsted and Lewis sites. In all cases desorption of Bronsted bound pyridine (1548 cm^{-1}) is seen at relatively low temperatures. The size of this band decreases regularly, with increasing temperature, above 100°C, although some pyridine is still seen bound to these sites at 350°C, for all the samples. This indicates that the Bronsted sites present have a considerable range of strengths, although they are generally weak. From the spectra it is expected that very few Bronsted sites, in any of the samples, will retain pyridine at temperatures in excess of 350°C. The Lewis sites by comparison are much stronger. The size of the 1455 cm^{-1} Lewis band appears to decrease at 100 and 150°C for all the samples, and then remain almost constant to 350°C. It is, however, difficult to measure the band at the lower temperatures because of the proximity of the physically adsorbed band at 1446 cm^{-1}. The band does not visibly shrink, and so the initial reduction in the measured area may be due to difficulties integrating the band area accurately. In any case a large proportion of the Lewis sites retain pyridine at 350°C.

The size of both the Lewis and Bronsted adsorbed pyridine bands increase through the series of samples with increasing aluminium incorporation. This indicates that increasing the amount of aluminium in the samples increases the number of acid sites generated. The microadsorption breakthrough times follow the same trend. As the aluminium content is increased, and the number of acid sites increases, the breakthrough time also increases. The Si / Al = 25 sample has the least acid sites and a breakthrough time of 120 minutes. The Si / Al = 8 samples has the most acid sites and the breakthrough time is increased to 150 minutes.

6.23.2 MCM-41 (Si/Al =8)

Fig 6.23.20 F.T.I.R. – Pyridine region and tabulated band areas

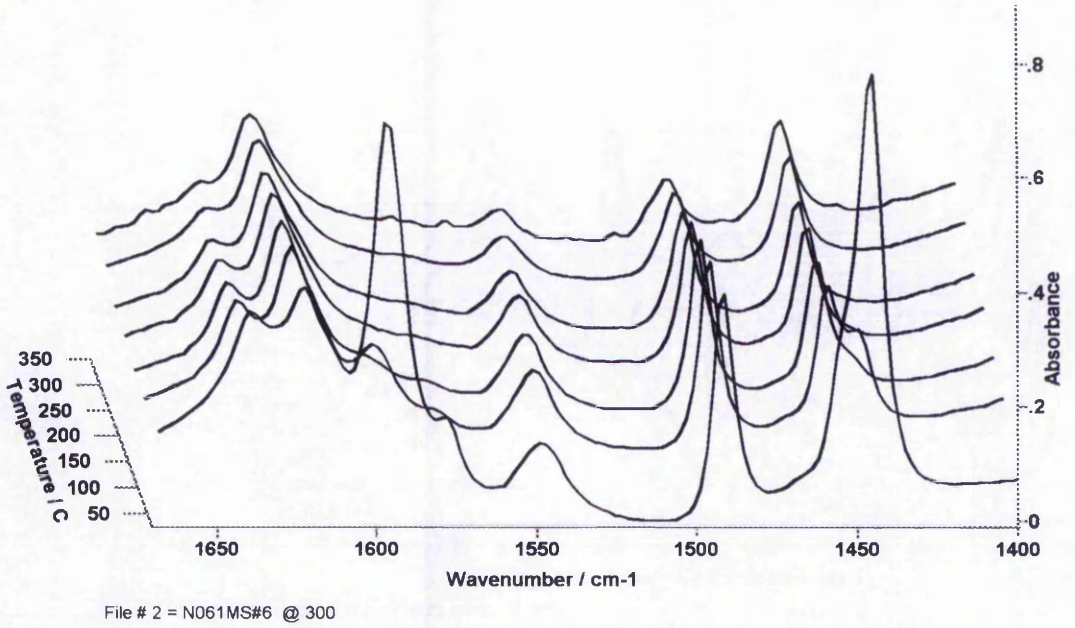

N.B. Very small additional bands at 350°C are due to H_2O vapour in the FTIR instrument.

	Temperature / C	25	100	150	200	250	300	350
Assignment	Band (cm-1)							
Physisorbed	1446	37.31	5.35	0.16				
Lewis	1455	13.92	13.38	12.31	9.69	9.64	9.64	9.31
L + B	1490	17.45	14.13	12.90	10.97	9.37	7.49	5.19
Bronsted	1548	7.82	8.46	7.98	6.58	5.46	3.59	2.19
	1577	1.05	0.30	0.21	0.11			
Physisorbed	1598	25.59	2.73	0.24				
Lewis	1621	4.44	8.73	10.06	10.28	10.28	9.96	9.64
Bronsted	1639	3.75	3.32	2.62	1.87	1.43	0.82	0.43

Fig 6.23.21 microadsorption breakthrough vs time

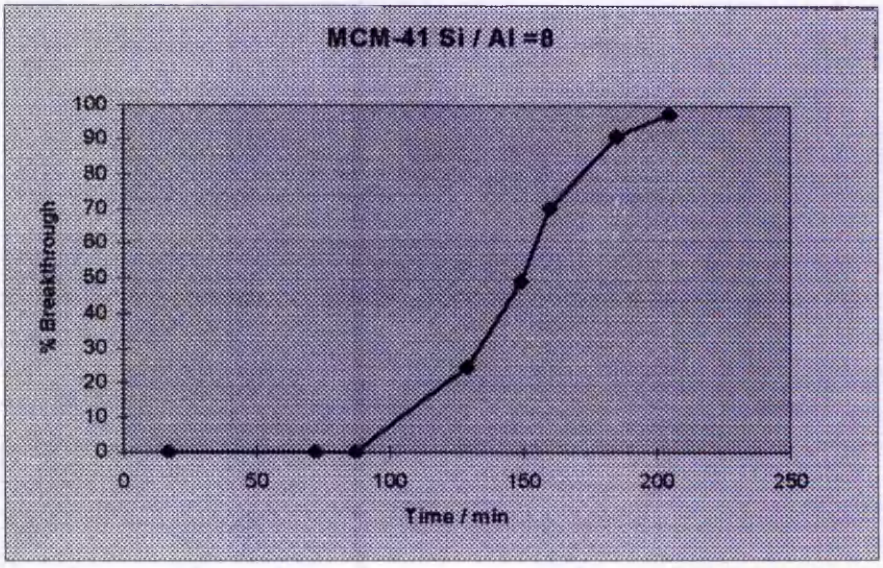

Fig 6.23.22 F.T.I.R. – OH region

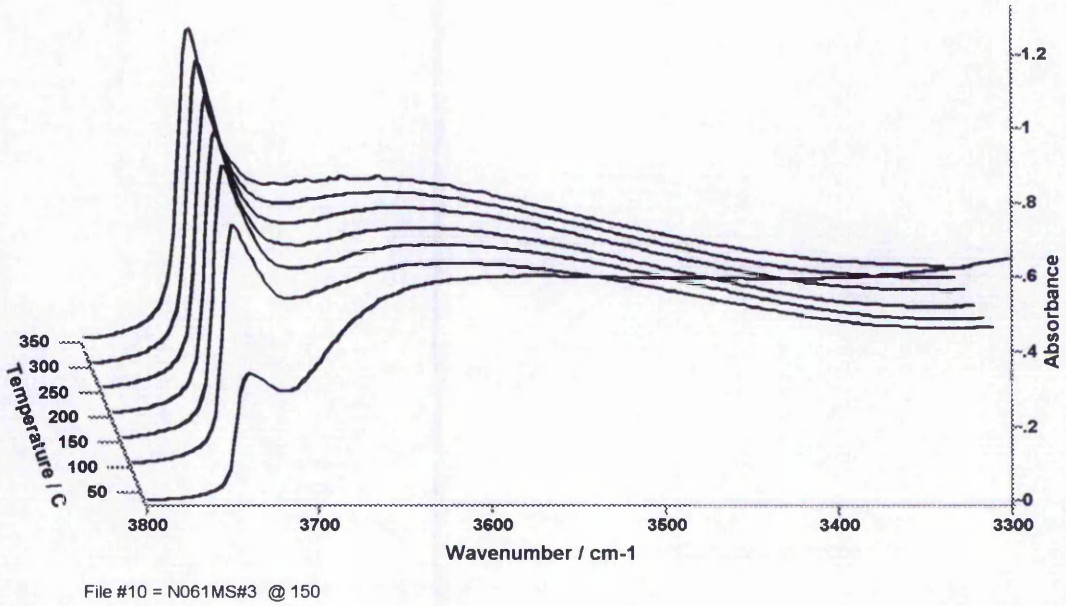

Fig 6.23.23 Comparison of the 3740 cm^{-1} (-OH) band with the 1446 cm^{-1} (physically adsorbed pyridine) band and 1548 cm^{-1} (bronsted) band at each temperature.

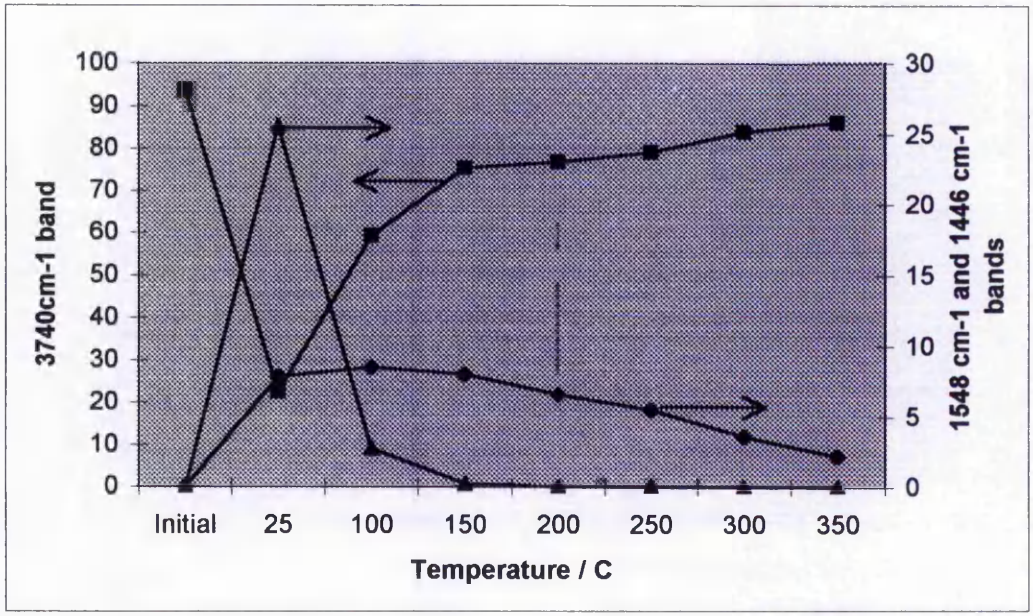

▲ - 1446 cm^{-1} band. ■ - 3740 cm^{-1} band. ◆ - 1548 cm^{-1} band.
N.B. 'Initial' is spectrum before dosing pyridine.

6.23.3 MCM-41 (Si/Al=12)

Fig 6.23.30 F.T.I.R. – Pyridine region and tabulated band areas

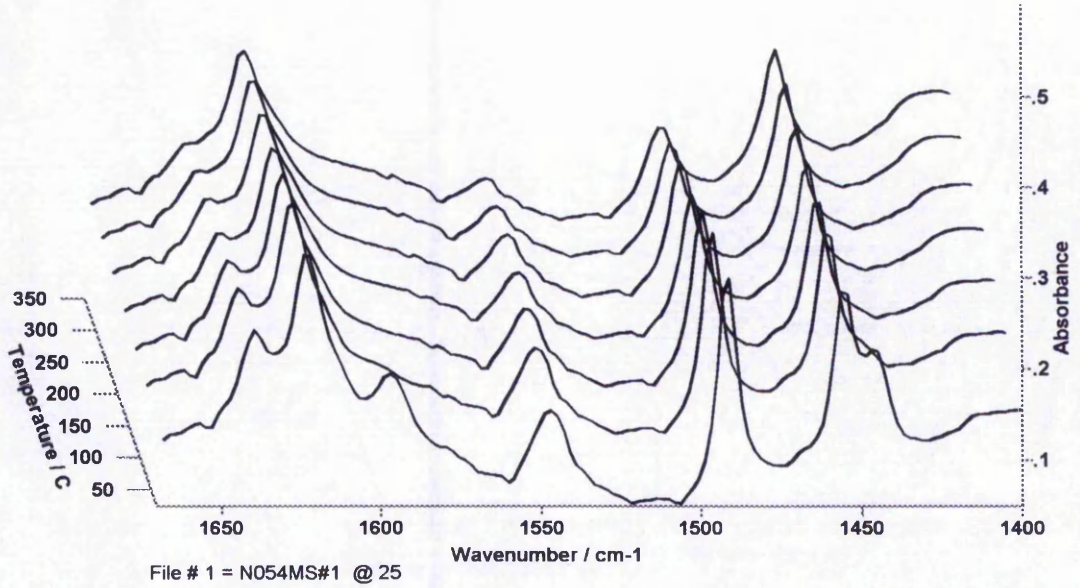

	Temperature / C	*25*	*100*	*150*	*200*	*250*	*300*	*350*
Assignment	Band (cm^{-1})							
Physisorbed	1446	1.53						
Lewis	1455	13.75	9.54	7.87	7.52	7.82	8.01	8.00
L + B	1492	12.89	11.34	10.63	8.96	8.91	7.52	5.86
Bronsted	1547	8.82	8.26	7.54	5.84	6.16	4.91	3.81
	1577	0.20						
Physisorbed	1598	3.31						
Lewis	1623	8.91	10.66	10.10	10.31	10.20	9.18	9.16
Bronsted	1639	2.08	1.94	1.34	0.96	0.98	0.55	0.31

Fig 6.23.31 microadsorption breakthrough vs time

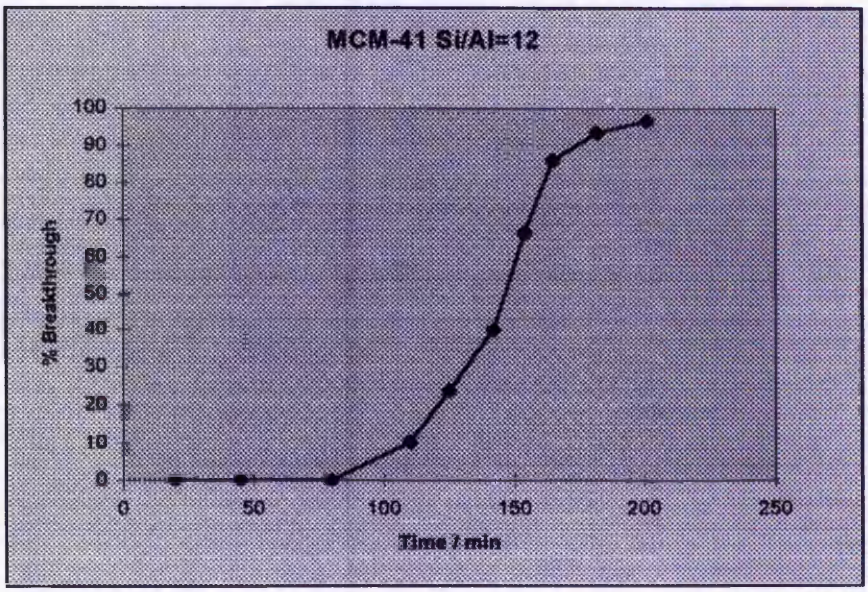

Fig 6.23.32 F.T.I.R. MCM-41 (Si/Al=12) – OH region

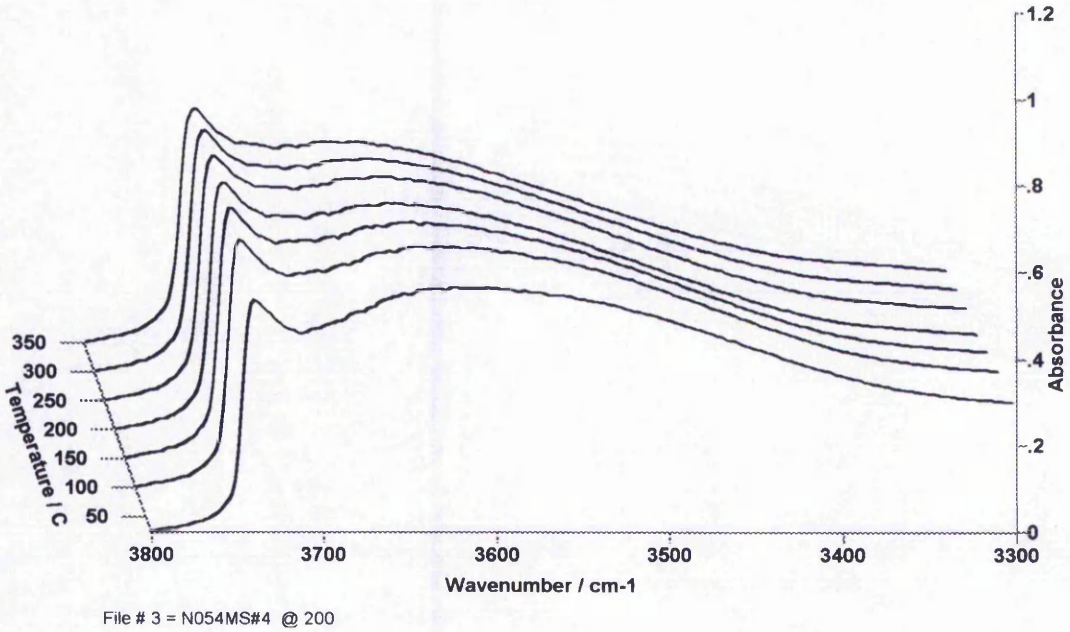

Fig 6.23.33 Comparison of the 3740 cm^{-1} (-OH) band with the 1446 cm^{-1} (physically adsorbed pyridine) band and 1547 cm^{-1} (bronsted) band at each temperature.

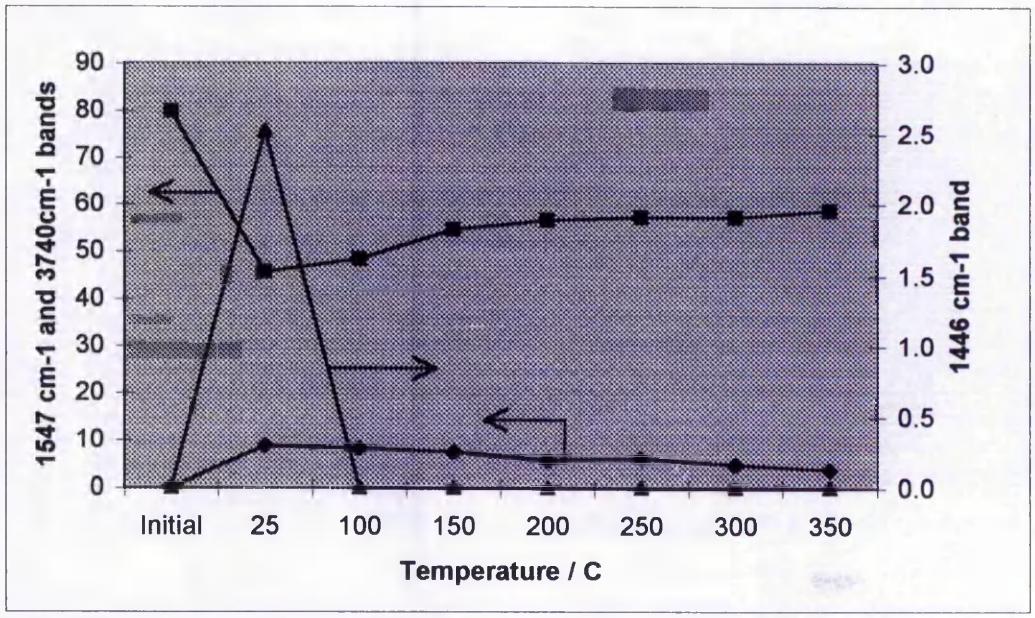

▲ - 1446 cm^{-1} band. ■ - 3740 cm^{-1} band. ◆ - 1547 cm^{-1} band.
N.B. 'Initial' is spectrum before dosing pyridine.

6.23.4 MCM-41 (Si/Al=15)

Fig 6.23.40 F.T.I.R– Pyridine region and tabulated band areas

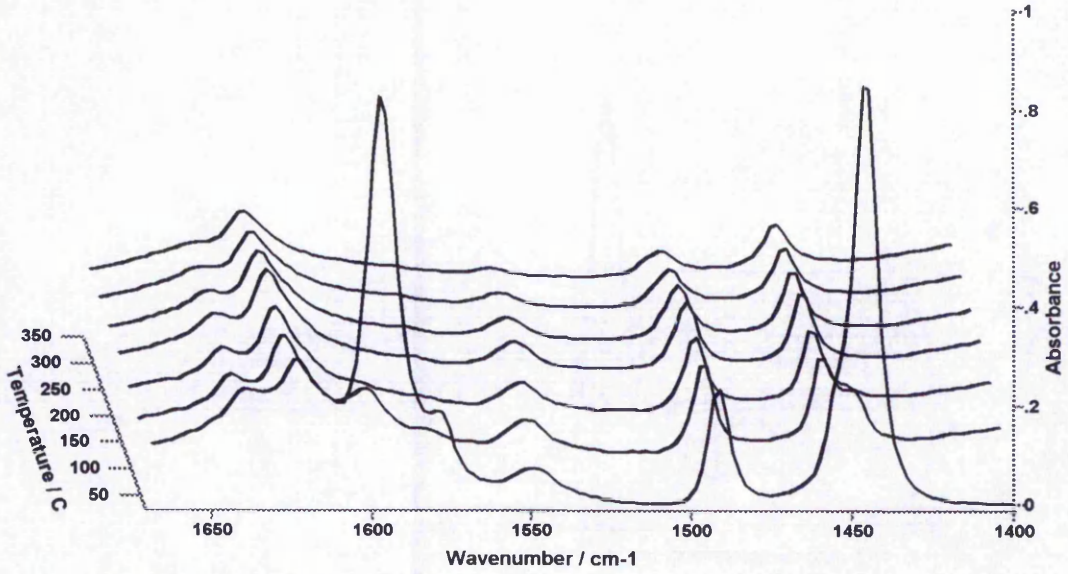

File # 9 = N062MS#7 @ 350

	Temperature / C	25	100	150	200	250	300	350
Assignment	Band (cm^{-1})							
Physisorbed	1446	50.97	2.68					
Lewis	1455	13.41	13.41	9.39	8.05	7.44	6.51	6.04
L + B	1490	12.47	9.73	8.18	7.71	6.51	4.83	3.22
Bronsted	1548	3.35	4.69	4.02	4.02	3.22	1.81	0.87
	1577	1.81	0.27	0.13				
Physisorbed	1598	42.45	2.55					
Lewis	1621	4.40	7.44	7.38	8.05	7.51	6.84	6.44
Bronsted	1639	1.61	1.68	1.48	1.34	0.91	0.54	0.38

6.23.41 microadsorption breakthrough vs time

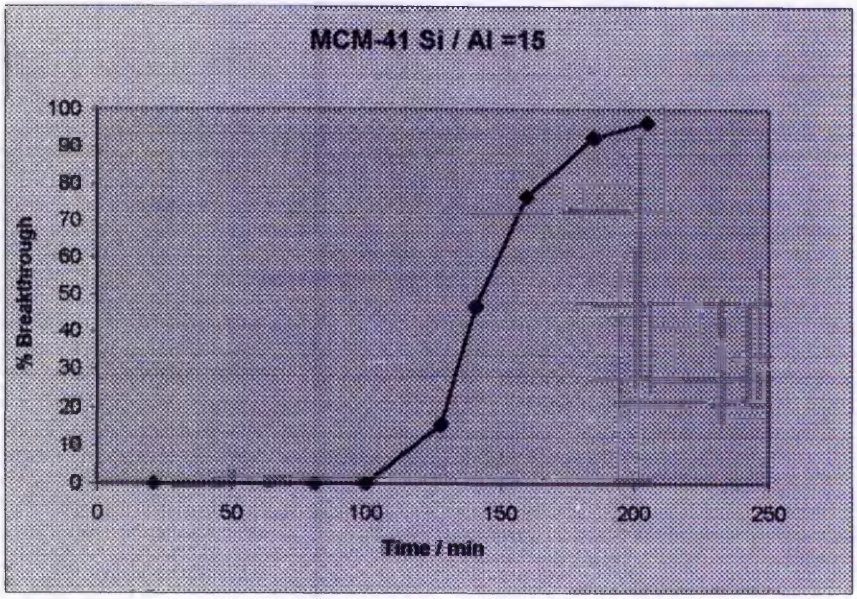

Fig 6.23.42 F.T.I.R. MCM-41 (Si/Al=15) – OH region

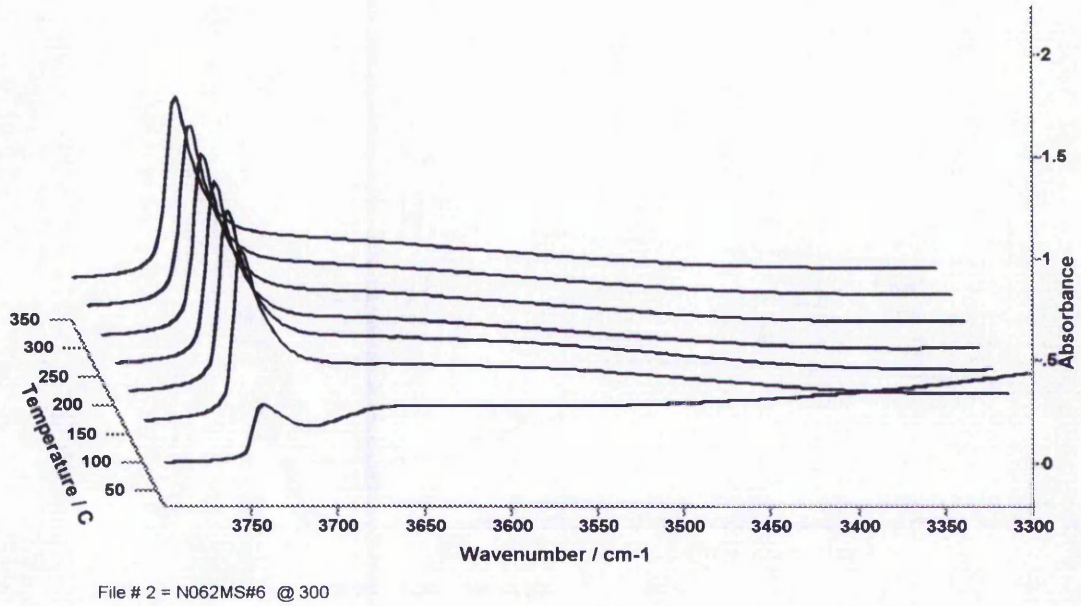

Fig 6.23.43 Comparison of the 3740 cm^{-1} (-OH) band with the 1446 cm^{-1} (physically adsorbed pyridine) band and 1548 cm^{-1} (bronsted) band at each temperature.

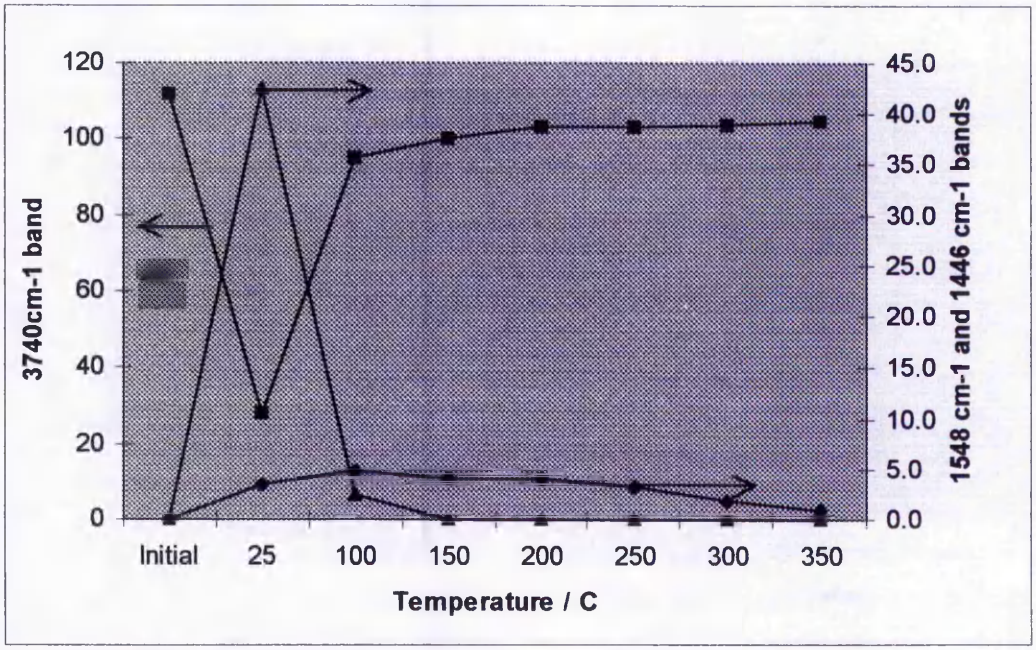

▲ - 1446 cm^{-1} band. ■ - 3740 cm^{-1} band. ◆ - 1548 cm^{-1} band.

N.B. 'Initial' is spectrum before dosing pyridine.

6.23.5 MCM-41 (Si/Al=18)

Fig 6.23.50 F.T.I.R – Pyridine region and tabulated band areas

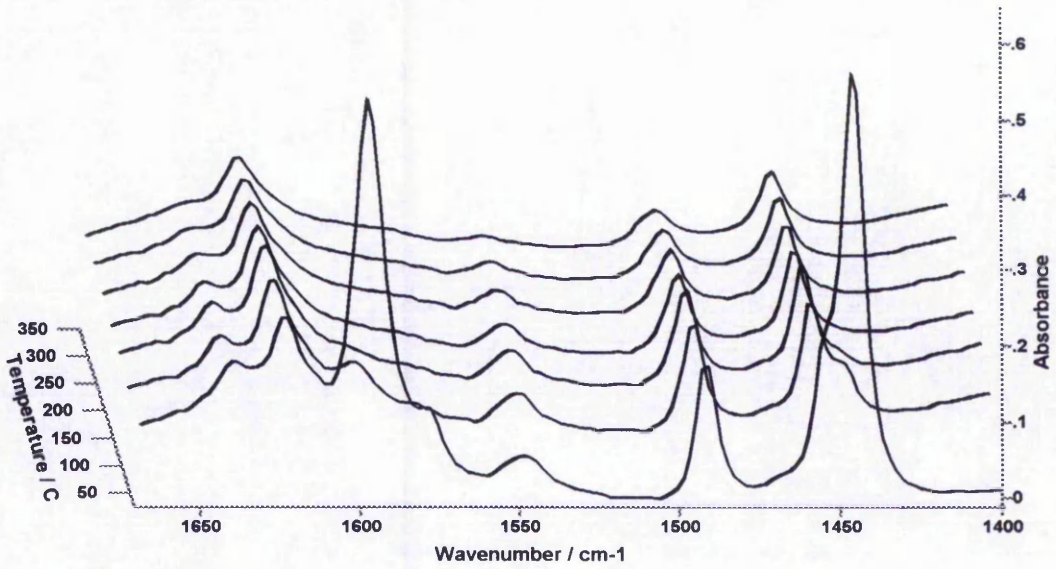

File # 1 = N063MS#4 @ 200

	Temperature / C	25	100	150	200	250	300	350
Assignment	Band (cm^{-1})							
Physisorbed	1446	37.40	1.57					
Lewis	1455	15.75	13.54	10.31	8.46	6.93	6.69	6.46
L + B	1490	11.50	8.74	8.11	6.85	5.91	4.88	3.54
Bronsted	1548	3.00	3.78	3.61	2.60	2.05	1.42	0.76
	1577	1.10	0.24					
Physisorbed	1598	30.94	1.73					
Lewis	1621	4.80	7.95	8.50	7.87	7.40	7.24	6.77
Bronsted	1639	1.97	1.50	1.32	1.02	0.75	0.47	0.28

Fig 6.23.51 microadsorption breakthrough vs time

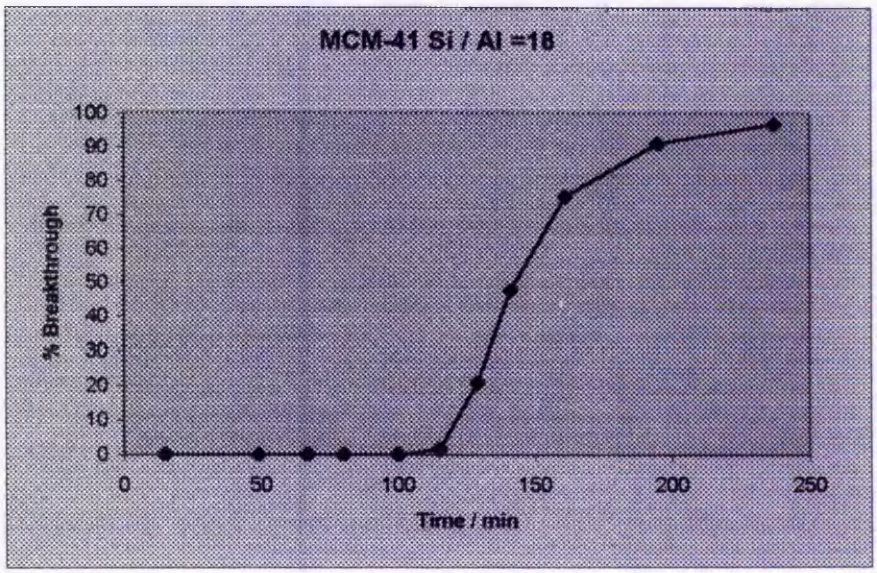

Fig 6.23.52 F.T.I.R. MCM-41 (Si/Al=18) – OH region

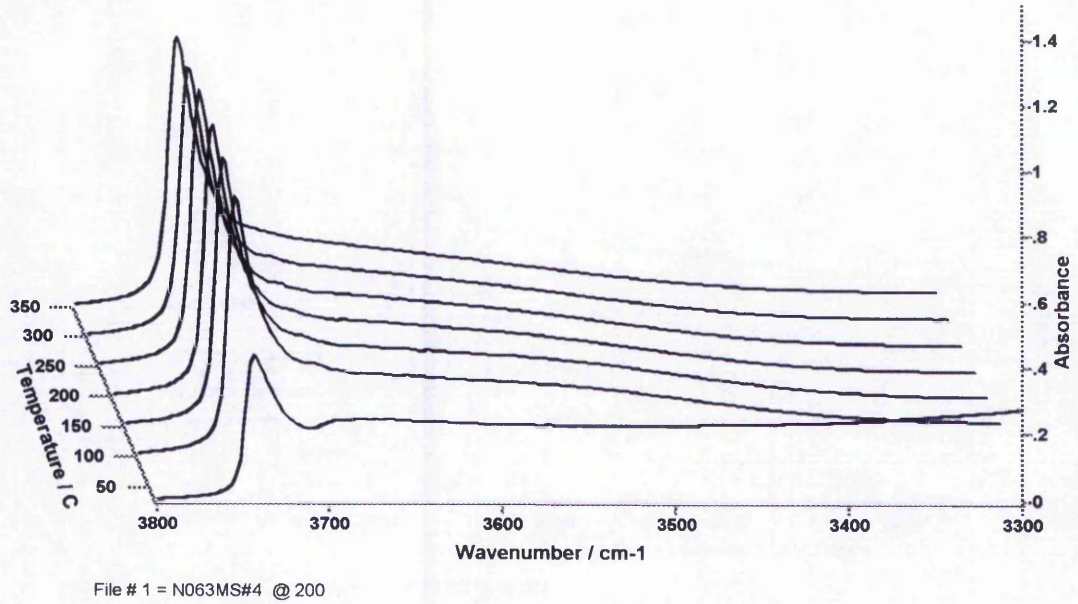

Fig 6.23.53 Comparison of the 3740 cm^{-1} (-OH) band with the 1446 cm^{-1} (physically adsorbed pyridine) band and 1548 cm^{-1} (bronsted) band at each temperature.

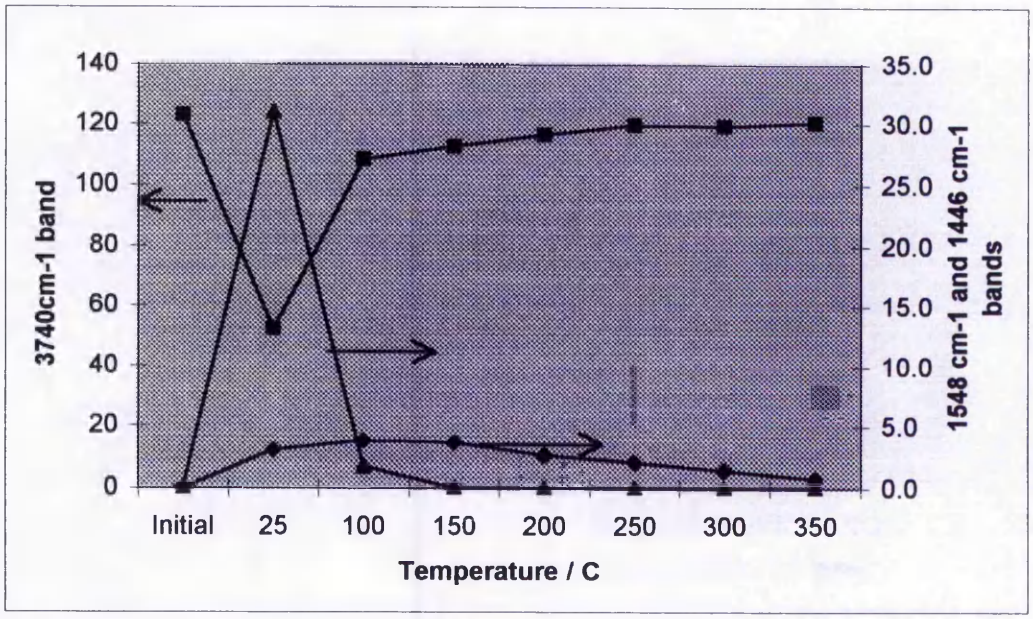

▲ - 1446 cm^{-1} band. ■ - 3740 cm^{-1} band. ◆ - 1548 cm^{-1} band.
N.B. 'Initial' is spectrum before dosing pyridine.

6.23.6 MCM-41 (Si/Al=25)

6.23.60 F.T.I.R– Pyridine region and tabulated band areas

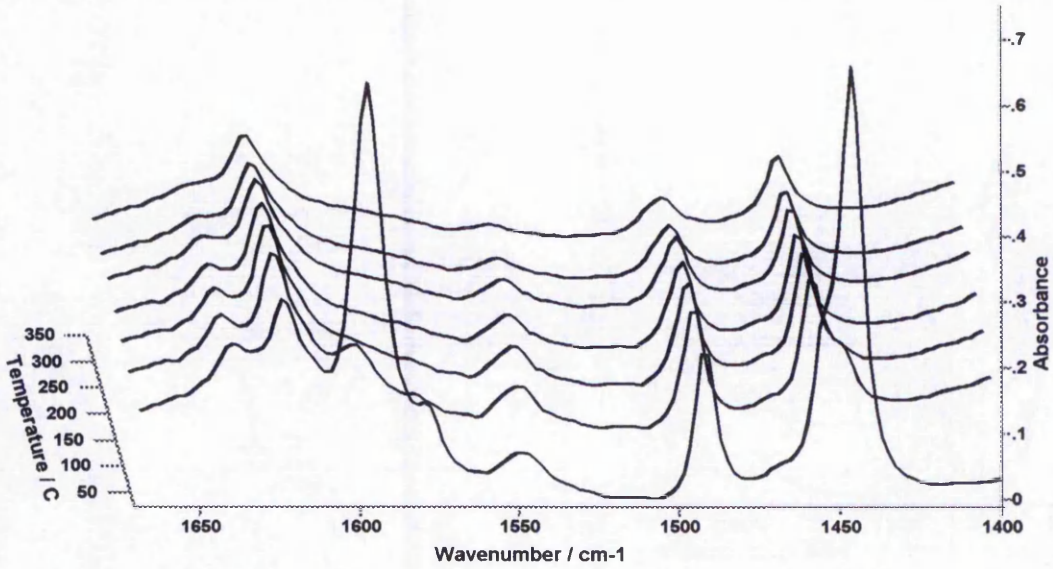

File # 2 = N064MS#7 @ 350

	Temperature / C	25	100	150	200	250	300	350
Assignment	Band (cm^{-1})							
Physisorbed	1446	23.87	1.02					
Lewis	1455	13.20	10.92	8.02	6.65	5.74	5.28	5.03
L + B	1490	8.94	6.96	6.15	5.43	4.47	3.66	2.95
Bronsted	1548	2.79	3.20	2.97	2.59	1.93	1.14	0.66
	1577	0.89	0.20					
Physisorbed	1598	23.72	1.83					
Lewis	1623	3.76	6.35	6.86	6.55	6.09	5.74	5.03
Bronsted	1639	1.32	1.22	1.08	0.87	0.64	0.39	0.25

Fig 6.23.61 microadsorption breakthrough vs time

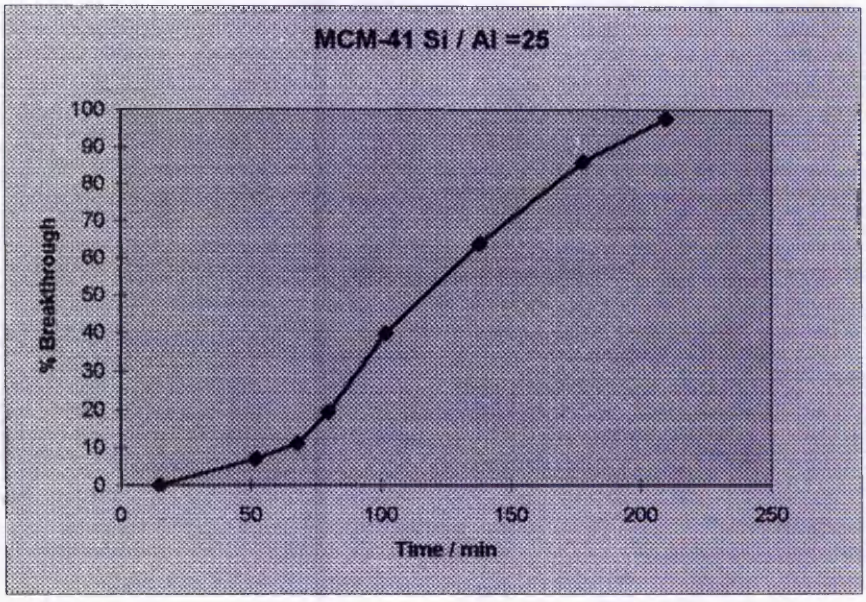

Fig 6.23.62 F.T.I.R. MCM-41 (Si/Al=25) – OH region

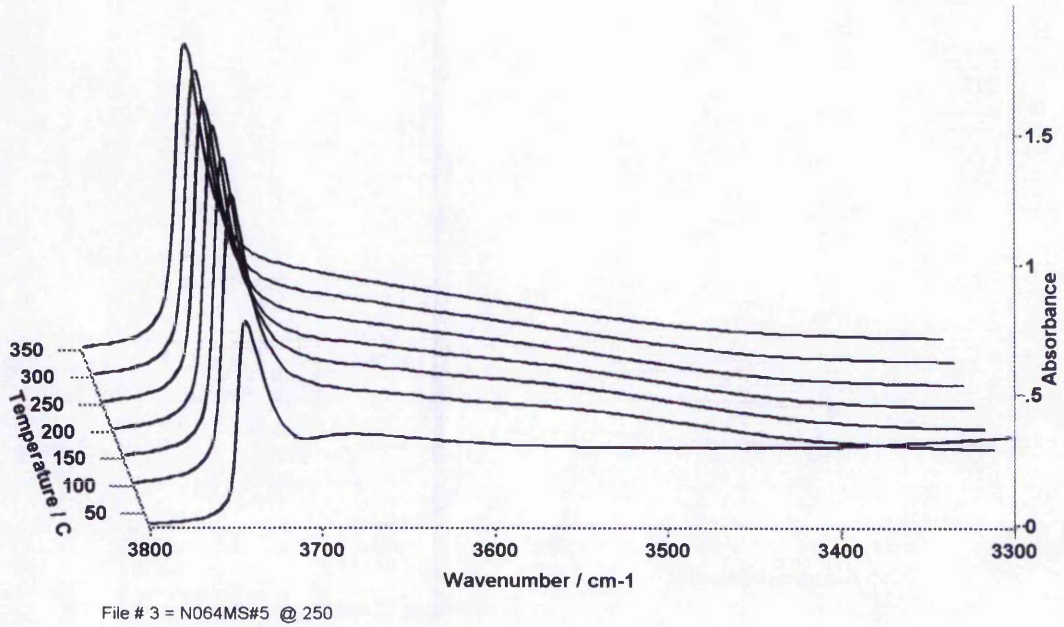

Fig 6.23.63 Comparison of the 3740 cm^{-1} (-OH) band with the 1446 cm^{-1} (physically adsorbed pyridine) band and 1548 cm^{-1} (bronsted) band at each temperature.

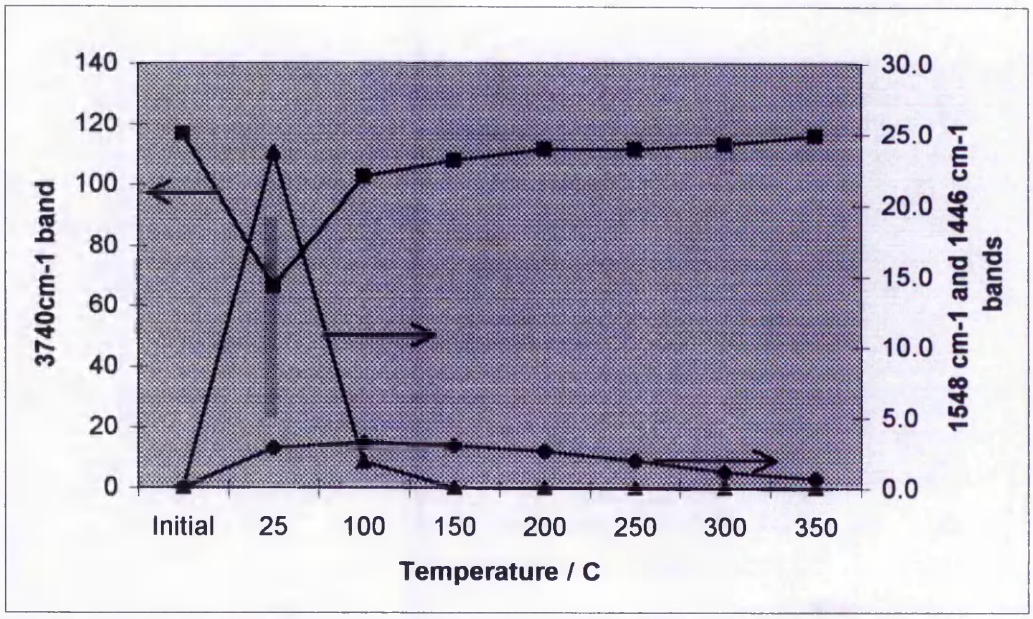

▲ - 1446 cm^{-1} band. ■ - 3740 cm^{-1} band. ◆ - 1547 cm^{-1} band.
N.B. 'Initial' is spectrum before dosing pyridine.

6.23.7 H-MCM-41 (Si/Al=8)

Fig 6.23.70 F.T.I.R – Pyridine region and tabulated band areas

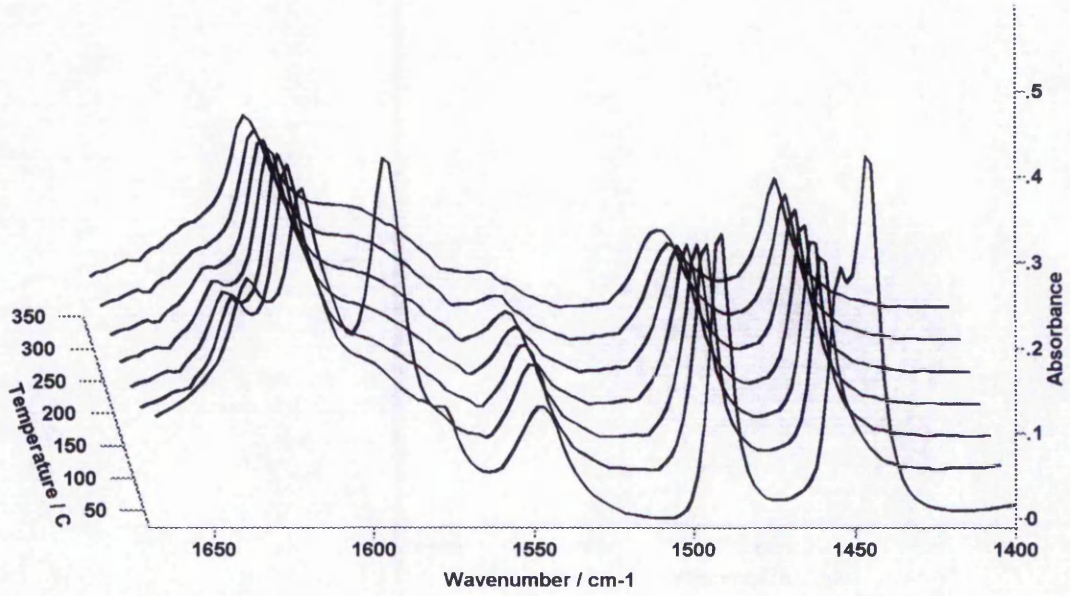

File # 1 = N095MS#2 @ 100

	Temperature / C	25	100	150	200	250	300	350
Assignment	Band							
Physisorbed	1446	23.30						
Lewis	1455	20.01	17.73	14.94	13.58	12.15	11.08	10.36
L + B	1490	20.94	17.73	16.15	14.08	11.87	9.86	8.22
Bronsted	1547	11.01	9.79	8.43	6.22	4.07	2.00	0.93
	1577	0.79	0.07					
Physisorbed	1598	17.66	0.42					
Lewis	1623	11.22	16.44	16.08	15.23	14.58	12.08	10.86
Bronsted	1639	3.86	2.93	2.00	1.37	0.79	0.29	0.18

Fig 6.23.71 microadsorption breakthrough vs time

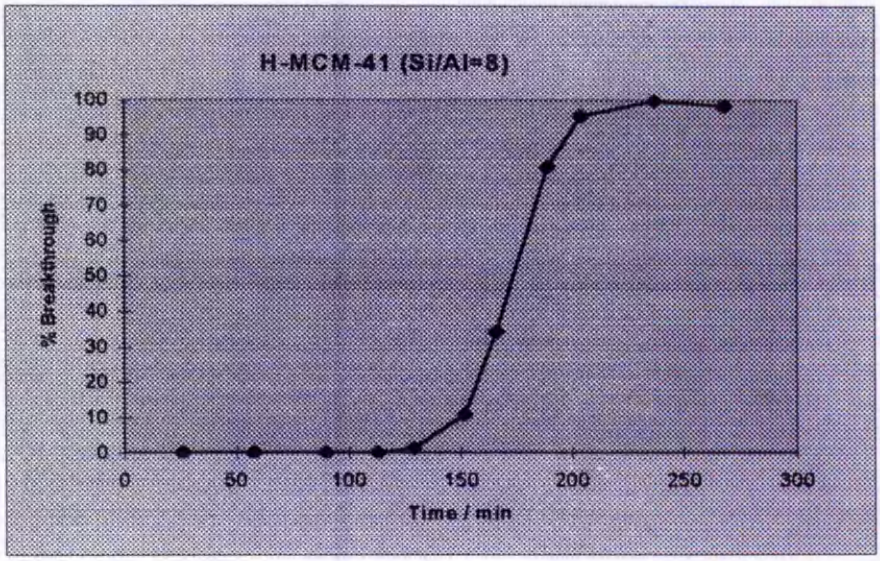

Fig 6.23.72 F.T.I.R. H-MCM-41 (Si/Al=8) – OH region

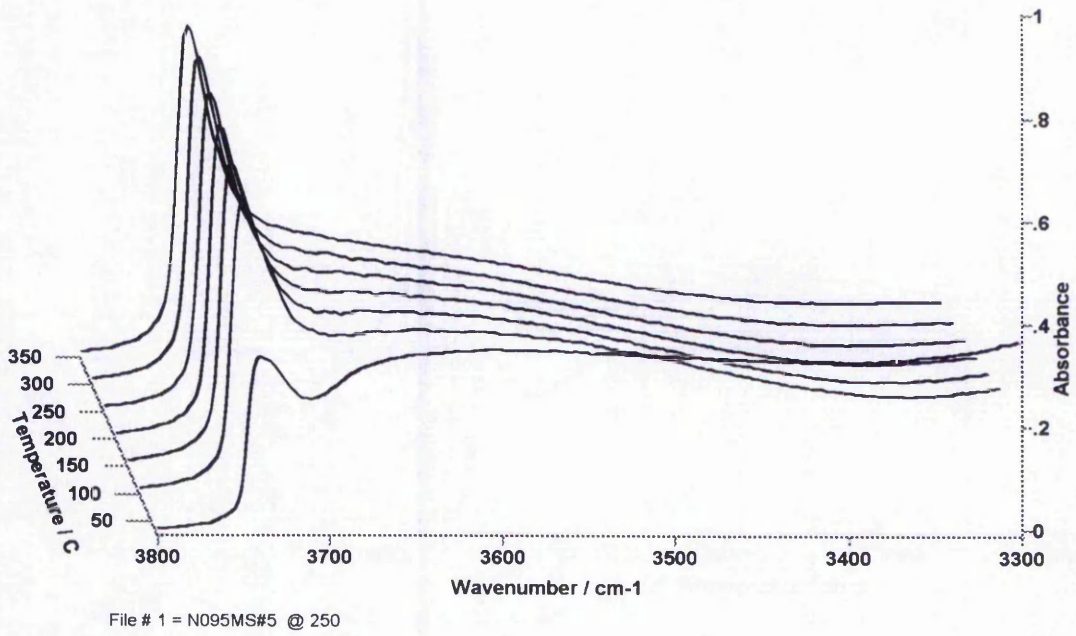

Fig 6.23.73 Comparison of the 3740 cm^{-1} (-OH) band with the 1446 cm^{-1} (physically adsorbed pyridine) band and 1547 cm^{-1} (bronsted) band at each temperature.

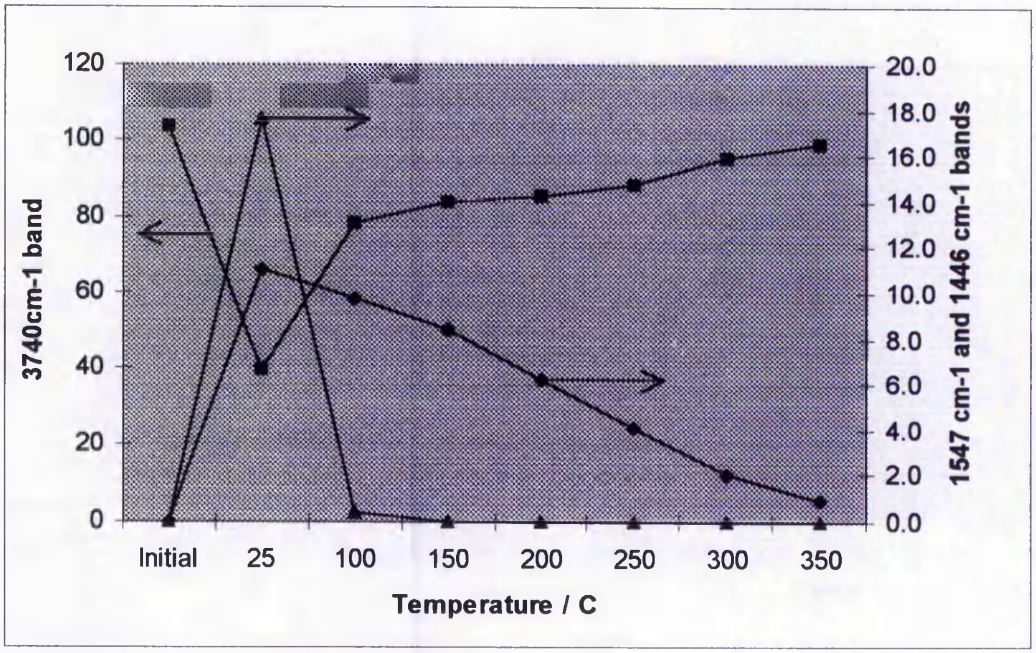

▲ - 1446 cm^{-1} band. ■ - 3740 cm^{-1} band. ◆ - 1547 cm^{-1} band.
N.B. 'Initial' is spectrum before dosing pyridine.

The major effect of ammonium exchange and calcination on the Si/Al = 8 sample has been to increase the number of Lewis sites. The amount of Bronsted bound pyridine, observed in the FTIR spectra has increased, but only at low temperature. Below 150°C this sample has more pyridine accessible Bronsted and Lewis sites than any of the other MCM-41s. At higher temperatures (>200°C) there appear to be less active Bronsted sites than before the ion exchange. The increase in the total number of acid sites may be a result of removal of extra-framework material during the ion exchange. This might leave behind only the high quality component in the original sample. However, from the B.E.T. results (fig 6.22.1) and N_2 adsorption isotherms (fig 6.22.2) it can be seen that the ion exchange procedure has a detrimental effect on the integrity of the MCM-41 structure, reducing both mesoporosity and surface area. As Bronsted sites can be assigned to 'framework' Al and Lewis sites to 'extra-framework' Al [10,16], then the ion exchange procedure may remove Al from the framework. Hence the number of 'extra-framework' Lewis sites increases, although this does not explain the increase in the numbers of Bronsted sites or the decrease in the average strength of Bronsted sites. Alternatively if Lewis sites are a result of the dehydration of Bronsted sites during the calcination step, and strong Bronsted sites are preferentially dehydrated, then this may explain the weak nature of the remaining Bronsted sites.

6.23.8 H-MCM-41 (Si/Al=8) Ex Rig / Regeneration / Rig

Fig 6.23.80 F.T.I.R. – Pyridine region and tabulated band areas

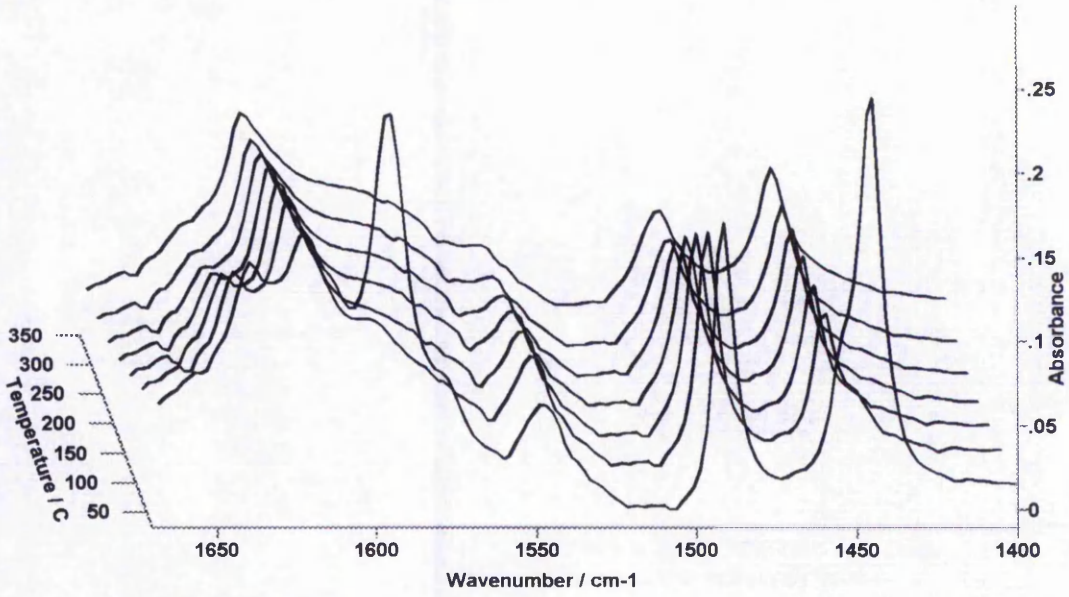

File # 2 = N096MS#7 @ 350

	Temperature / C	25	100	150	200	250	300	350
Assignment	Band							
Physisorbed	1446	44.77	2.27					
Lewis	1455	20.45	18.41	16.93	16.70	16.59	15.91	15.68
L + B	1490	32.27	27.27	25.00	22.27	19.32	15.91	14.09
Bronsted	1547	11.82	12.27	10.93	7.95	5.45	2.50	1.82
	1577	1.23						
Physisorbed	1598	30.45	1.66					
Lewis	1621	8.02	16.59	18.86	19.55	17.95	17.50	15.23
Bronsted	1639	5.68	4.34	3.52	2.50	1.14	0.68	0.45

Fig 6.23.81 microadsorption breakthrough vs time

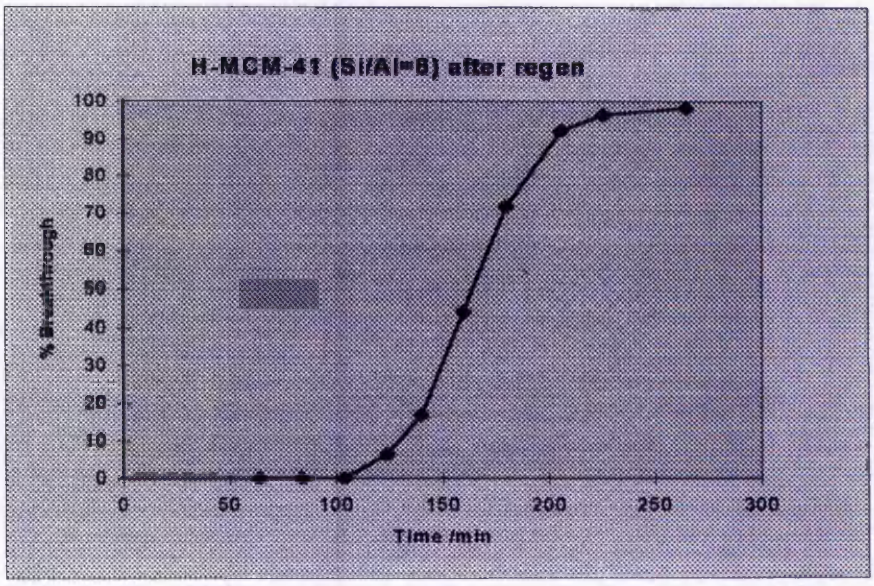

Fig 6.23.82 F.T.I.R. H-MCM-41 (Si/Al=8) Ex Rig / Regeneration / Rig - OH region

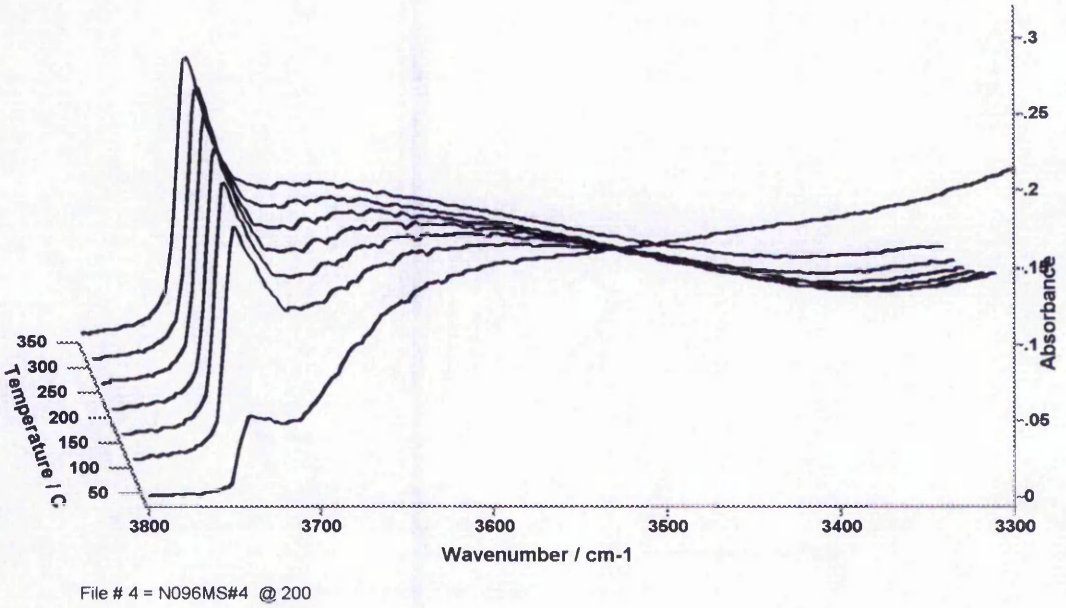

Fig 6.23.83 Comparison of the 3740 cm^{-1} (-OH) band with the 1446 cm^{-1} (physically adsorbed pyridine) band and 1547 cm^{-1} (bronsted) band at each temperature.

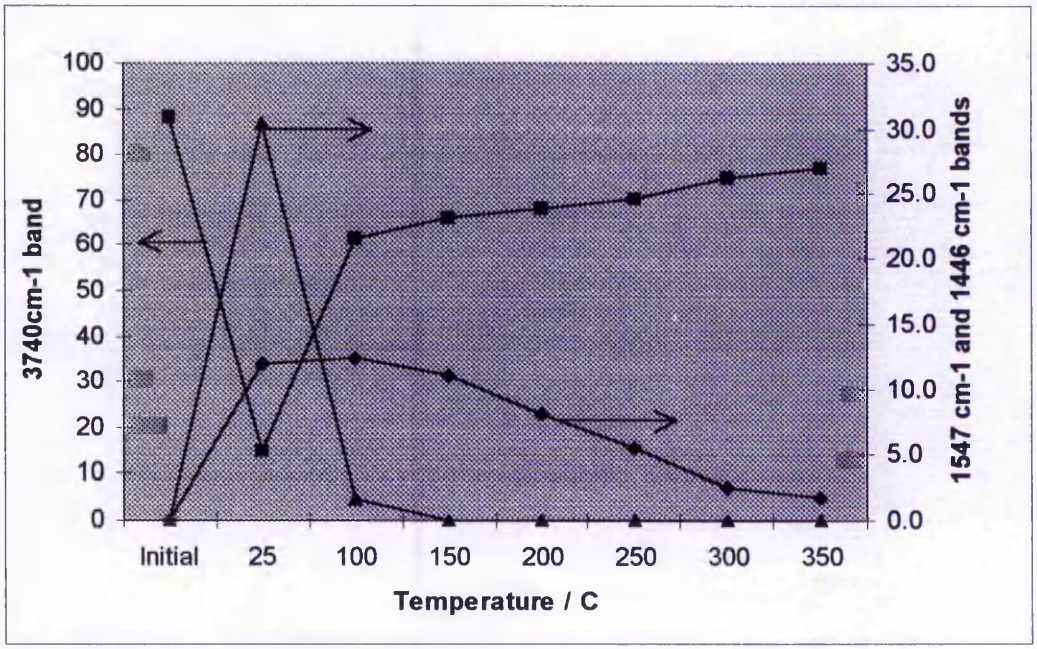

▲ - 1446 cm^{-1} band. ■ - 3740 cm^{-1} band. ◆ - 1547 cm^{-1} band.
N.B. 'Initial' is spectrum before dosing pyridine.

The regeneration procedure on the H-MCM-41 (Si / Al = 8) sample has essentially been successful. The sample was re-used and continued to remove pyridine from the model system. The FTIR pyridine spectra after two microadsorption experiments with a regeneration step in between show no sign of a coke band at 1585 cm^{-1}. On the first microadsorption run the 50 % breakthrough point was at 175 minutes. On the second run it was only reduced slightly to 165 minutes. The loss in performance can be explained by the partial collapse in the structure seen in the nitrogen adsorption isotherms (Fig 6.22.2), although the BET surface area appears to have increased. If MCM-41 could be regenerated at a slightly lower temperature e.g. 550 °C then might limit the structural degradation and make the material perfectly re-usable

Fig 6.23.100 F.T.I.R. MCM-41 (Si/Al=12) – Heptane coking experiment

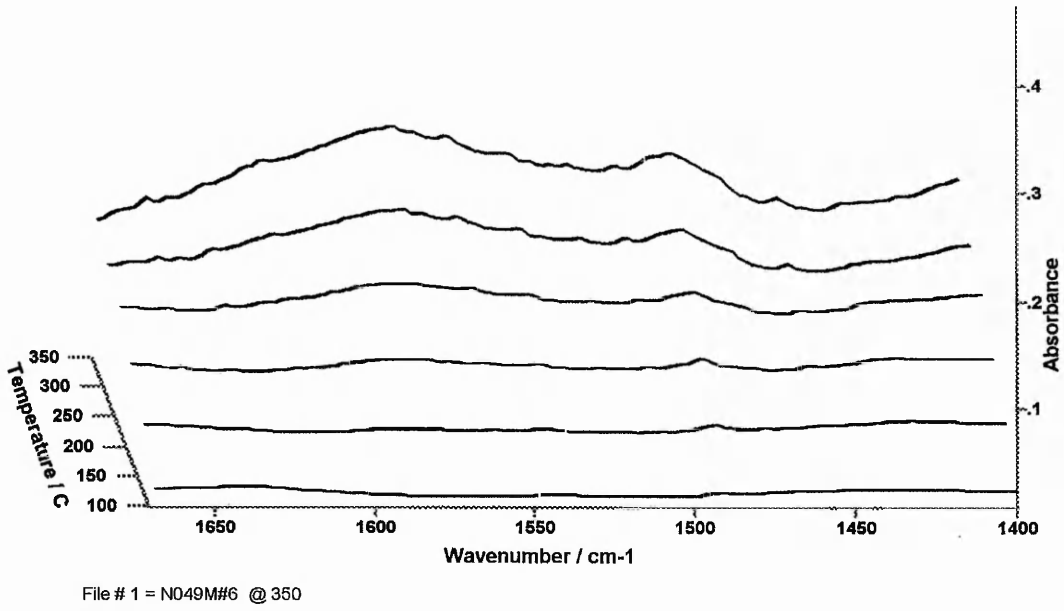

Fig 6.23.100 shows the spectra of MCM-41 (Si / Al = 12) interacting with heptane. It can be seen from the pyridine FTIR experiments, that the acidic strength of all the Al-MCM-41 samples is very similar. The interaction of the Si / Al = 12 sample with heptane should therefore be representative for all the Al-MCM-41 samples here. The spectra show very little coke formation (~

1585 cm^{-1}) even at 350°C. Weak absorption at 1490 cm^{-1} and 1455 cm^{-1} can be assigned to pyridine contamination in the IR cell from previous experiments. The broad feature at ~ 1575 cm^{-1} might be assigned to coke formation although this is usually observed at slightly higher wavenumbers. The band is relatively small even at 350°C and is not really apparent at 200°C - the temperature of the microadsorption experiments. In addition, the FTIR spectra of the Si / Al = 8 sample, after two microadsorption experiments separated by a regeneration (fig 6.23.80), show no evidence of a coke absorption band.

The FTIR band at 3741 cm^{-1} has been noted to behave in an unusual manner. In all the samples studied here the intensity of the band is significantly reduced upon the introduction of pyridine. It is not clear if this effect is caused by the physical adsorption of pyridine on the non-acidic silanol groups, or by the acidic character of some of the groups in MCM-41 which give rise to the 3741 cm^{-1} band. The latter explanation seems unlikely however, as the effect is observed for purely siliceous MCM-41 as well as aluminium containing samples. The band should therefore return to its original size with desorption of the physically adsorbed pyridine. For the pure silica MCM-41 this is found to be the case, and the reappearance of the 3741 cm^{-1} band mirrors perfectly the decrease in the 1446 cm^{-1} (physically adsorbed pyridine) band, as the temperature increases (fig 6.23.12). Once all the physically adsorbed pyridine has been removed (100 - 150°C) the 3741 cm^{-1} band returns to its original size (before the introduction of pyridine), and it remains at this size as the temperature is increased further. For the Al-MCM-41 samples the 3741 cm^{-1} band does not return fully to its original size when all the physically bound pyridine has been removed. It continues to grow as the temperature is raised further. Figs 6.23.(2-8)3 show the areas for the bands at 3741 cm^{-1}, 1446 cm^{-1} (physically adsorbed pyridine) and 1545 cm^{-1} (bronsted bound pyridine). It can be seen that the increase in the 3741 cm^{-1} band mirrors not only the desorption of physically adsorbed pyridine, but also the desorption of Bronsted bound

pyridine. The 3741 cm^{-1} band approaches its original intensity as the 1545 cm^{-1} band approaches zero intensity.

There are two possible explanations for this effect. Firstly the 3741 cm^{-1} band is a composite band comprising a contribution from acidic bronsted O-H as well as non-acidic silanol groups. Alternatively some of the terminal O-H groups interact with pyridine adsorbed on Bronsted and/or Lewis acid sites, reducing the intensity of the OH band at 3741 cm^{-1} while the pyridine is present. The later explanation appears more likely, and Chen et. al. [13] have come to similar conclusions based on pyridine adsorption on D_2O exchanged Al-MCM-41.

Fig 6.23.101 Band areas at 200°C and 50% breakthrough times for the MCM-41 samples

Si / Al ratio	Lewis (1455 cm^{-1})	Lewis / Bronsted Ratio (a)	Bronsted (1548 cm^{-1})	50% Breakthrough time (min)
8	9.69	1.11	6.58	~150
12	7.52	0.98	5.84	~145
15	8.05	1.50	4.02	~145
18	8.46	2.44	2.60	~140
25	6.65	1.93	2.59	~120
8 (b)	13.58	1.60	6.22	~175
8 (c)	16.7	1.58	7.95	~165

(a) Normalised using relative molar extinction coefficients from ref 15
(b) H^+ exchanged via NH_4^+
(d) Sample 8(b) after 2 adsorption experiments with regeneration in between

Fig 6.23.101 shows the integrated, normalised, band areas for the 1455 cm^{-1} Lewis and 1548 cm^{-1} Bronsted bands at 200°C, for all of the aluminium containing samples. Also shown is the Lewis / Bronsted ratio, normalised using the ratio of the extinction coefficients (L/B = 1.33) from Ref 15. This shows the relative numbers of each type of site. It can be seen that for all but the Si/Al = 12 sample there are greater numbers of Lewis sites than Bronsted. As a general trend the numbers of both Lewis and Bronsted sites decrease with increasing Si/Al ratio. The reduction in Lewis sites is less significant, leading to an increase in the Lewis to Bronsted ratio. The breakthrough times follow the same trend - decreasing with increasing Si / Al ratio, and consequent reduction in acid sites.

Fig 6.23.102 The correlation between the intensity of pyridine absorption bands at 200°C and 50 % Breakthrough times.

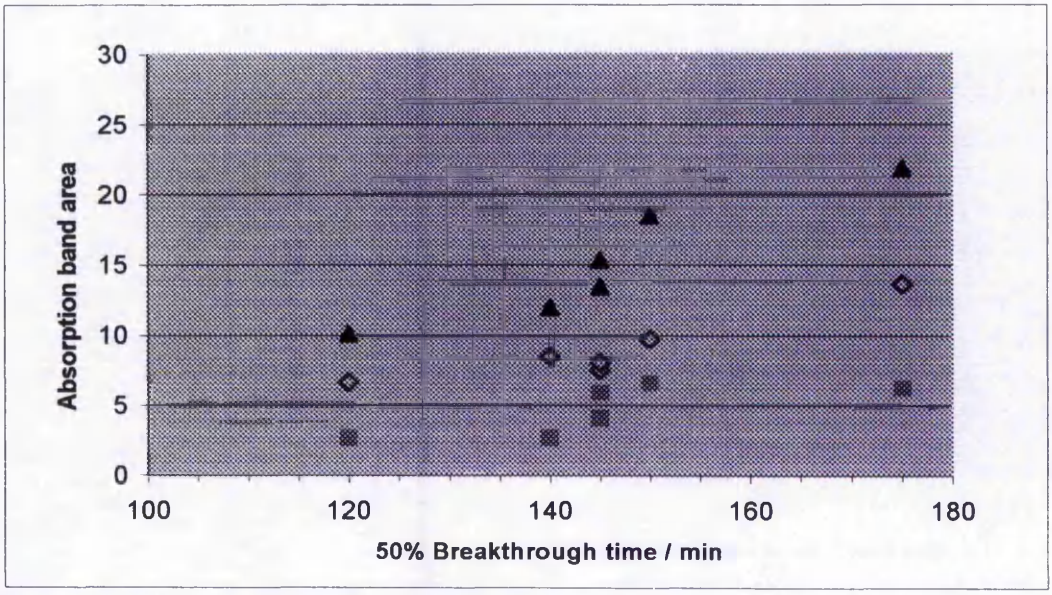

▩ - Bronsted bound pyridine band at 1547 cm^{-1}.

◇ - Lewis bound pyridine band at 1455 cm^{-1}.

▲ - 1547 cm^{-1} + 1455 cm^{-1} bands (normalised using relative molar extinction coefficients) i.e. total acid sites

As Lewis sites are the most numerous, and in general, are significantly stronger than the Bronsted sites, it seems likely that the Lewis sites play the most important role in the performance of MCM-41 as an adsorbent for pyridine. However it can be seen in Fig 6.23.102 the relationship between breakthrough time and the 1546 cm^{-1} Bronsted band is reasonably good, although not perfect or linear. The correlation between the 1455 cm^{-1} Lewis band and breakthrough time is slightly better, although again not perfect, or linear. However the best correlation in Fig 6.23.102 is that between 50 % breakthrough times and the combined 1547 cm^{-1} and 1455 cm^{-1} bands i.e. the total number of acid sites. This shows that both Lewis and Bronsted sites make an important contribution towards the pyridine adsorption capacity.

6.3 Summary

Fig 6.3.01 Pyridine Temperature Programmed Desorption Profiles for MCM-41s (Lewis sites)

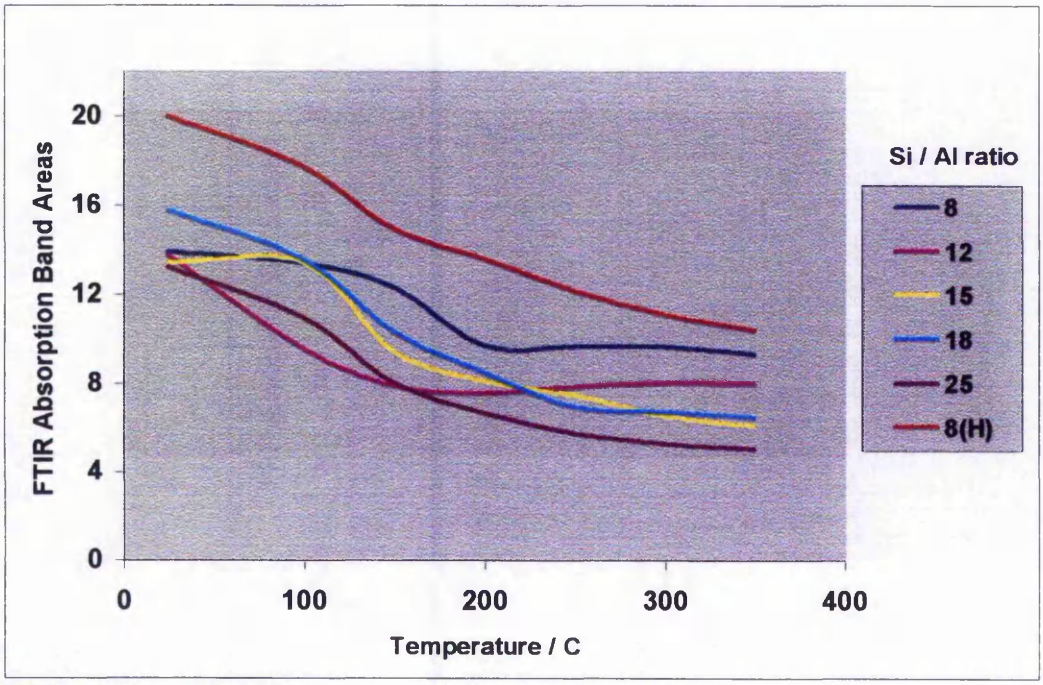

8(H) H^+ exchanged via NH_4^+

The desorption profiles, of pyridine from Lewis acid sites are similar for all the MCM-41 samples. Unexpectedly the samples with the highest aluminium content have the greatest proportion of strong Lewis sites. Approximately 70% of Lewis sites in the Si / Al = 8 sample retain pyridine at 350°C. In the Si / Al = 12 sample this figure is around 60%, and the remaining samples continue this trend, with the Si / Al = 25 sample retaining around 40%. The total number of Lewis sites also increases with aluminium content. The effect of NH_4^+ exchange and calcination on the Si / Al = 8 sample (8(H)), has been to increase the number of Lewis acid sites. This is opposite to what might generally be expected, as this procedure should introduce H^+ Bronsted sites.

The profiles of pyridine desorption from Bronsted sites (Fig 6.3.02) show a similar trend. The number of Bronsted acid sites increases with aluminium content. The strength distribution of these sites is similar for most of the

samples. There is steady desorption with each temperature increment, and approximately 30 – 40 % of Bronsted sites retain pyridine at 350°C.

Fig 6.3.02 Pyridine Temperature Programmed Desorption Profiles for MCM-41s (Bronsted sites)

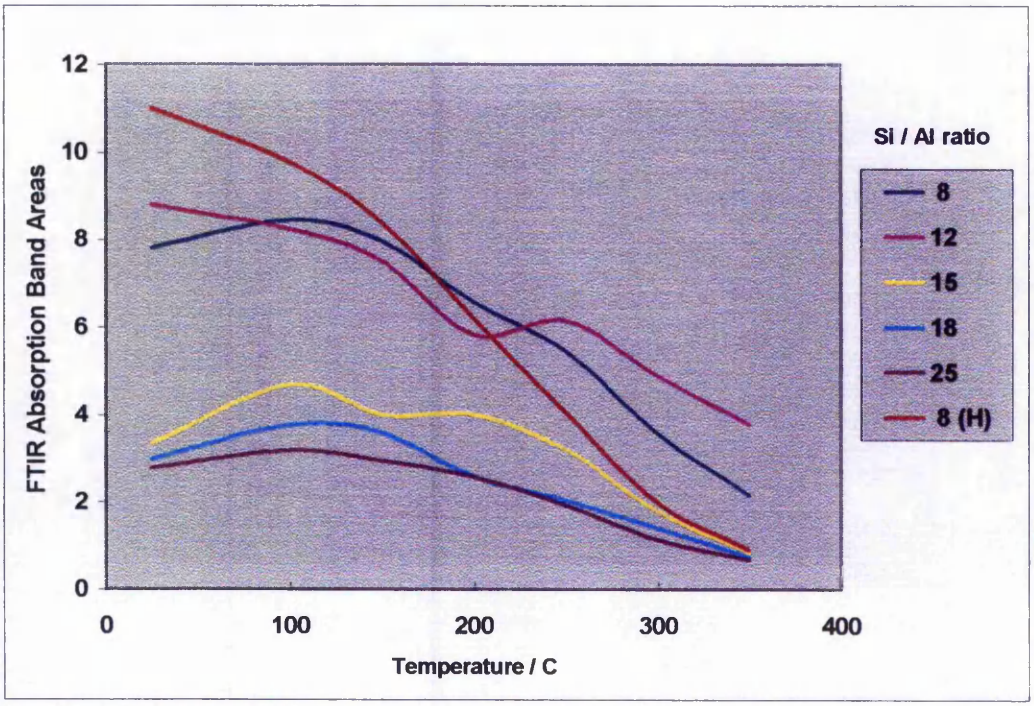

8(H) H^+ exchanged via NH_4^+

The principal exception to this rule is the ion exchanged sample. As with the Lewis sites, the total number of Bronsted sites has increased after the ion exchange, but the number of strong Bronsted sites has decreased. Only around 10% of the Bronsted bound pyridine is observed at 350 °C. The total number of strong Bronsted sites is equivalent to the Si / Al = 25 or 18 samples. It is unclear why the number of Lewis and weak Bronsted sites has increased, but the number of strong Bronsted sites has been reduced.

The results of the microadsorption experiments are consistent with the pyridine FTIR spectra. The 50% breakthrough times increase with increased aluminium incorporation. The BET surface areas, which are reduced with increasing

aluminium content, do not appear to be a significant factor in the microadsorption performance. The 50% breakthrough time improves through the series of samples from 120 minutes for Si / Al = 25 to 150 minutes for Si / Al = 8. The increase in acid site density observed upon ion exchange is also represented in the breakthrough data, and the breakthrough time for Si / Al = 8 improves from 150 minutes to 175 minutes. This is the best performance of any MCM-41 sample studied. Although both Lewis and Bronsted sites appear active for selective pyridine adsorption (Fig 6.23.102), it seems likely that in this sample the Lewis sites are most important due to the weak nature of the Bronsted sites

There is no evidence that any of the MCM-41 samples form coke during the microadsorption experiments. The heptane FTIR spectra of the Si /Al = 12 sample exhibit no coke band, and the N_2 adsorption isotherm of the ion exchanged sample, after two microadsorption experiments with a regeneration step, show only a small reduction on the pore volume. In addition the ion exchanged H-MCM-41 sample was successfully regenerated and re-used with only a small reduction in the breakthrough time in the second microadsorption run.

6.4 Conclusions

The MCM-41 materials studied here show some potential for selective adsorption of basic nitrogen compounds, although considerable improvements are required if they are to become a viable solution. They seem to achieve the goal of a material of intermediate acidic strength; strong enough to retain pyridine at the chosen temperature, but not strong enough to activate the hydrocarbon stream and consequently become covered with coke. Acid site density and breakthrough times increase with increasing aluminium content, despite a reduction in the BET surface areas. NH_4^+ ion exchange and calcination also improves microadsorption performance by increasing the number of Lewis acid sites, although the number of strong Bronsted sites is reduced. The large mesopores allows pyridine to diffuse through the structure freely, even when N_2 adsorption isotherms show the pore volume to be reduced by the ion exchange procedure. The best breakthrough time of 175 minutes corresponds to an adsorption capacity of approximately 1.0 wt%. After successful regeneration and re-use this material was slightly less effective on the second run. The regeneration (at 650°C) has also partly collapsed the mesoporous structure. Further regeneration procedures would almost certainly result in increased structural collapse leading to the failure of the adsorbent. Regeneration in an oxygen containing gas stream may regenerate the adsorbent at a lower temperature, by burning off the adsorbed bases, instead of desorbing in an inert flow. However, with this approach, care must be taken that the exotherm of reaction does not cause localised areas of very high temperature.

For these materials to be useful the adsorption capacity must be increased significantly and / or samples must be engineered so that they can undergo frequent regeneration without a loss in performance. Both these improvements may be possible. The structure and stability of aluminium containing MCM-41's are inferior to purely siliceous MCM-41. If future developments in the synthesis of these materials can improve the structure of aluminium containing samples then their resistance to high temperature regeneration may be improved. At the same time incorporation of greater amounts of aluminium may improve their adsorption capacity.

6.5 References

1. Kresge, C. T., Leonowicz, M. E., Roth, W. J., Vartulli, J. C. and Beck, J. S., *Nature* 1992, **359**, 710.
2. Beck, J. S., Vartulli, J. C., Roth, W. J., Leonowicz, M. E., Kresge, C. T., Schmitt, K. D., Chu, C. T.-W., Olson, D. H., Sheppard, E. W., McCullen, S. B., Higgins, J. B. and Schlenker, J. L., *J. Am. Chem. Soc* . 1992, **114**, 10834.
3. Corma, A., Grande, M. S., Gonzales-Alfaro, V. and Orchilles, A. V., *J. Catal.* 1996, **159**, 375.
4. Corma, A., *Chem. Rev.* 1997, **97**, 2373
5. Climent, M. J., Corma, A., Iborra, M. C., Navarro, M. C. and Primo, J., *J. Catal.*1996, **161**, 783.
6. Sayari, A., *Chem. Mater.* 1996, **8**, 1840.
7. Luan, Z., Cheng, C-F., He, H. and Klinowski, J., *J. Phys. Chem.* 1995, **99**, 10590.
8. Mokaya, R., Jones, W., Luan, Z., Alba, M.D. and Klinowski, J., *Catal. Lett.*, 1996, **37**, 113.
9. Chakraborty, B. and Viswanathan, B., *Catalysis Today*, 1999, **49**, 253.
10. Weglarski, J., Datka, K., He, H. and Klinowski, *J. Chem. Soc., Faraday Trans.*, 1996, **92**(24), 5161.
11. Kloetstra, K. R., Zandbergen, H. W. and van Bekkum, H., *Catal. Lett.* 1995, **33**, 157.
12. Luan, Z., He, H., Zhou, W., Cheng, C-F. and Klinowski, J., *J. Chem. Soc., Faraday Trans.*, 1995, **91**(17), 2955.
13. Chen, L.Y., Ping, Z., Chuah, G.K., Jaenicke, S. and Simon, G., *Microporous and Mesoporous Materials,* 1999, **27**, 231.
14. Sun, Y., Yue, Y. and Gao, Z., *Applied Catal. A: General,* 1997, **161**, 121.
15. Emeis, C.A., *J.Catal.*, 1993, **141**, 347.
16. Corma, A., Fornes, V., Navarro, M. T. and Perez-Pariente, J., *J. Catal.* 1994, **148**, 569.
17. Borade, R. B. and Clearfield, A., *Catal. Lett.* 1995, **31**, 267.

18. Jentys, A., Pham, N. H. and Vinek, H., *J. Chem. Soc., Faraday Trans.*, 1996, **92**(17), 3287.

19. Kosslick, H., Landmesser, H. and Fricke, R., *J. Chem. Soc., Faraday Trans.*, 1997, **93**(9), 1849.

20. Jentys, A., Kleestorfer, K. and Vinek, H., *Microporous and Mesoporous Materials*, 1999, **27**, 321.

21. Di Renzo, F., Chiche, B., Fajula, F., Viale, S. and Garrone, E., *Stud. Surf. Sci. Catal.*, 1996, **101**, 851.

Chapter 7 Zeolites

7.1 Introduction

Zeolites are highly crystalline alumino-silicates, which contain very well defined intracrystalline cavities or pores, with molecular dimensions. There are many different structural types, with different pore arrangements and properties. The structures consist of SiO_4 tetrahedra, where Al replaces some of the Si. Since Al^{3+} is occupying a Si^{4+} location this leads to an excess negative charge on the lattice, which is counterbalanced by a cation near the lattice surface. These cations are generally acidic, and this is the cause of the high catalytic activity zeolites have for a wide range of reactions. If the counterbalancing cation is H^+ then these can act as Bronsted acid sites, i.e. the proton is labile and can be donated to an incoming base molecule. The zeolite is said to be in the H or Bronsted form. If the counterbalancing cation is a metal ion i.e. Na^+, Cu^{2+} etc. then these are capable of acting as Lewis acid sites (electron pair acceptors). The counter-balancing cations are ion-exchangeable, hence acidity and activity can be easily tailored for a specific application, usually by ion-exchanging in aqueous solution.

Zeolite structures can by classified according to their pore dimensions. Zeolites with an 8 membered ring pore opening are classified as 'small pore'. The 8 membered ring comprises of 8 Si or Al atoms bridged by 8 O atoms. Zeolites with 10 and 12 membered pore openings are classified as medium and large pore respectively. The materials studied here are medium pore (ZSM-5) and large pore (mordenite and zeolite X) zeolites. Small 8 membered ring systems would not be expected to accommodate pyridine easily.

7.11 Mordenite

The main pore channels in mordenite are 7.4 Å in diameter, and run in only one direction through the structure. The mordenite structure also contains smaller pores with 8 membered openings. The two types of pore can be seen in Fig 7.11.01. The smaller pores run parallel to the larger pores and the two pore types are interconnected through 'side pockets' which are also made up of 8 membered rings. The pore structure and connecting 'side pockets' can be seen in Fig 7.11.02. Pyridine is too large to enter either the side-pockets or the secondary pores so the structure is effectively one dimensional, with respect to the diffusion of a pyridine molecule.

Fig 7.11.01 The mordenite structure viewed along the axis of the pores.

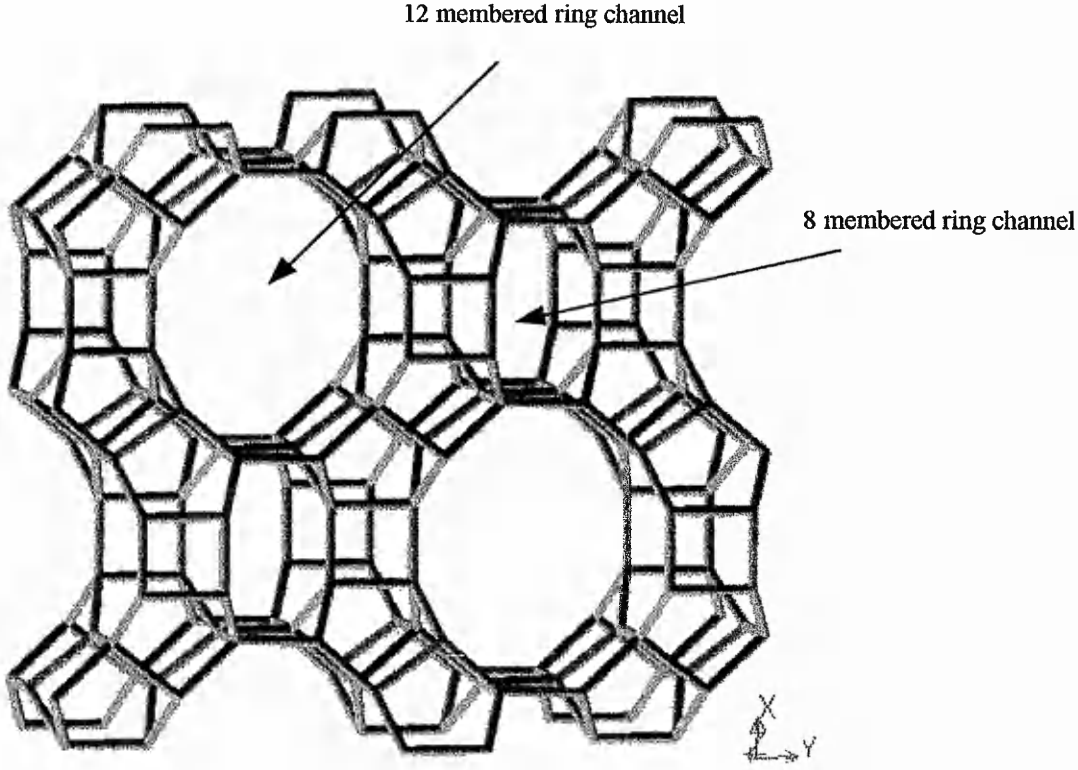

Fig 7.11.02 The pore structure of mordenite

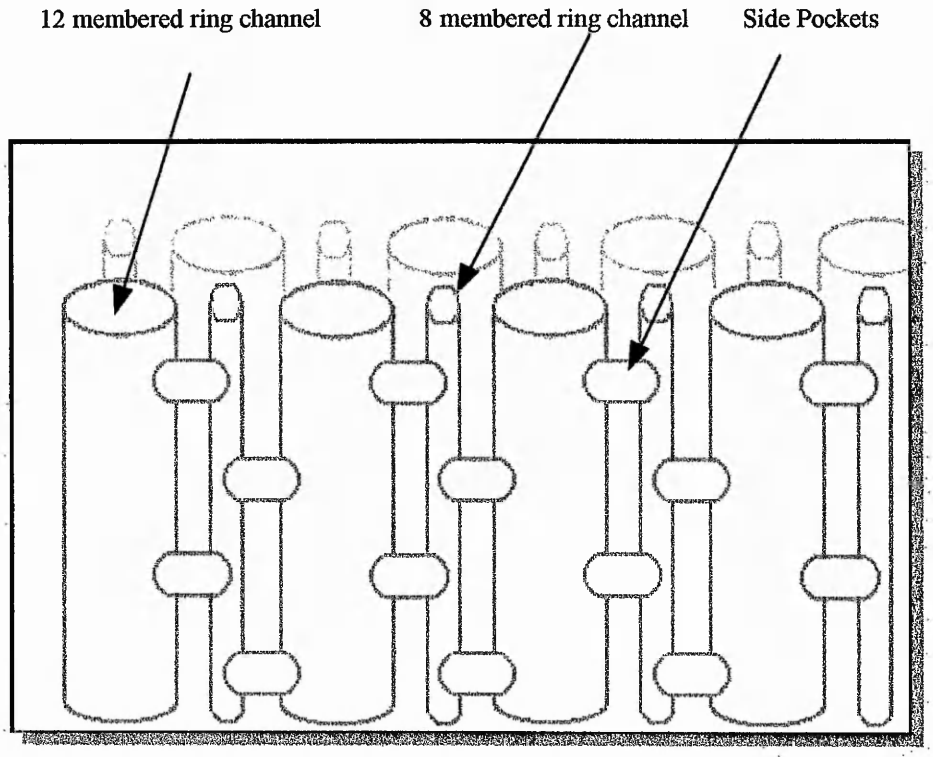

7.12 ZSM-5

ZSM-5 has the MFI crystallographic structure, which is built up of five sided blocks called pentasil units. The MFI structure is only formed with relatively low aluminium content, and there is a pure silica analogue of ZSM-5 called silicalite-1. ZSM-5 is a highly porous material and throughout its structure it has an intersecting two-dimensional pore structure. It has two types of pores, both formed by 10-membered oxygen rings. The first of these pores is straight and elliptical in cross section. The second pores intersect the straight pores at right angles, in a zig-zag pattern and are circular in cross section. The straight channels have dimensions of 5.1 Å x 5.6 Å and the zig-zag pores have a diameter of ~5.5 Å. This unique two-dimensional pore structure allows a molecule to move from

one point in the structure to anywhere else in the particle. As pyridine can enter both types of pore it can diffuse through the structure in any direction.

ZSM-5 is mainly used commercially for hydrocarbon interconversion, for example meta-xylene to para-xylene, or the methanol to gasoline (MTG) process. It is especially useful for such reactions because it is highly resistant to coke formation. For the MTG process it is the pores created by these 10-oxygen rings, along with the zig-zag pores intersecting them, that are essential to the formation of products that are desirable components of gasoline. An 8-oxygen ring zeolite will not produce molecules with 6 or more carbons, molecules of this size will not fit into the small pores of these zeolites. The large pores of a 12-oxygen ring zeolite produce large amounts of C-11 and C-12 compounds, which are undesirable products for gasoline. The structure of ZSM-5 and the pore system are shown in Figs 7.12.01 and 7.12.02

Fig 7.12.01 The ZSM-5 structure viewed along the axis of the straight, elliptical pores.

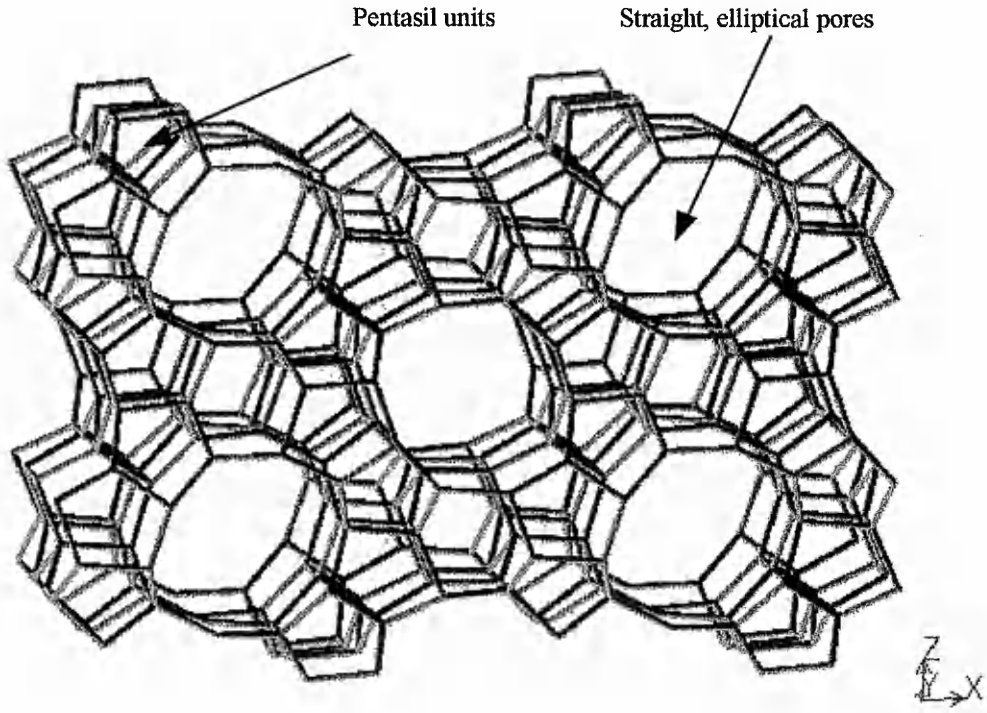

Fig 7.12.02 The pore structure of ZSM-5

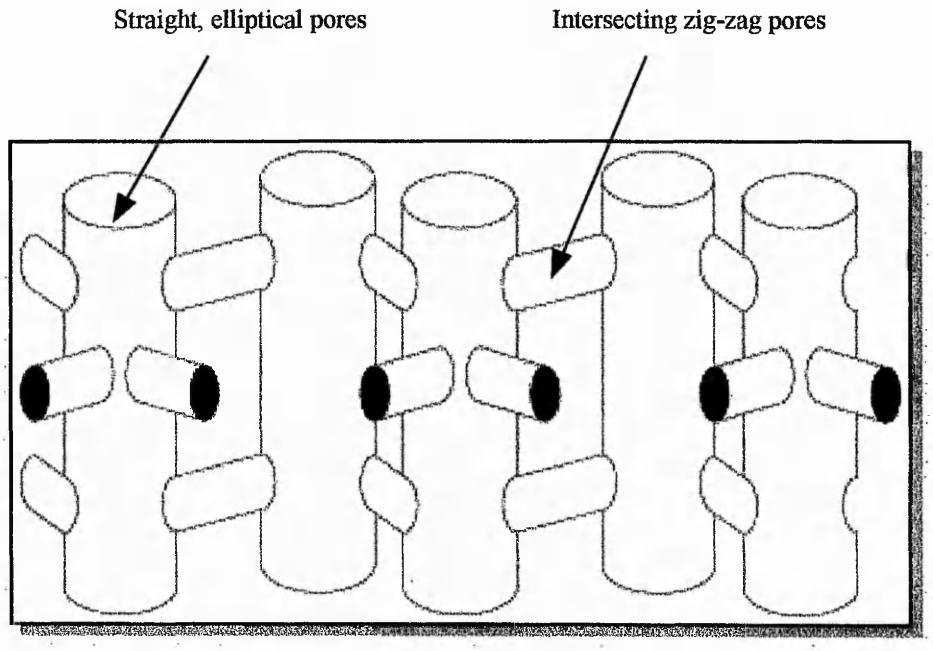

7.13 Zeolite X

Zeolite X is one of a family of zeolites, which share the faujasite crystallographic structure. The faujasite structure is only formed with a large amount of aluminium (Si / Al < 5). Zeolite X is defined as having a Si / Al ratio of < 2. Faujasites have a three dimensional pore structure made up of cavities called 'supercages' of ~ 12 Å diameter. The cavity is surrounded by ten sodalite cages (truncated octahedra) connected on their hexagonal faces, and are connected by 12 membered ring openings of 7.4 Å diameter, called 'windows'. The pores run perpendicular to each other in the x, y, and z planes. Diffusion through the pores is limited to molecules smaller than these 7.4 Å openings. The arrangement of sodalite cages and supercages is shown in Figs 7.13.01 and 7.13.02.

Fig 7.13.01 The arrangement of sodalite units forming a 7.4 Å window and supercage.

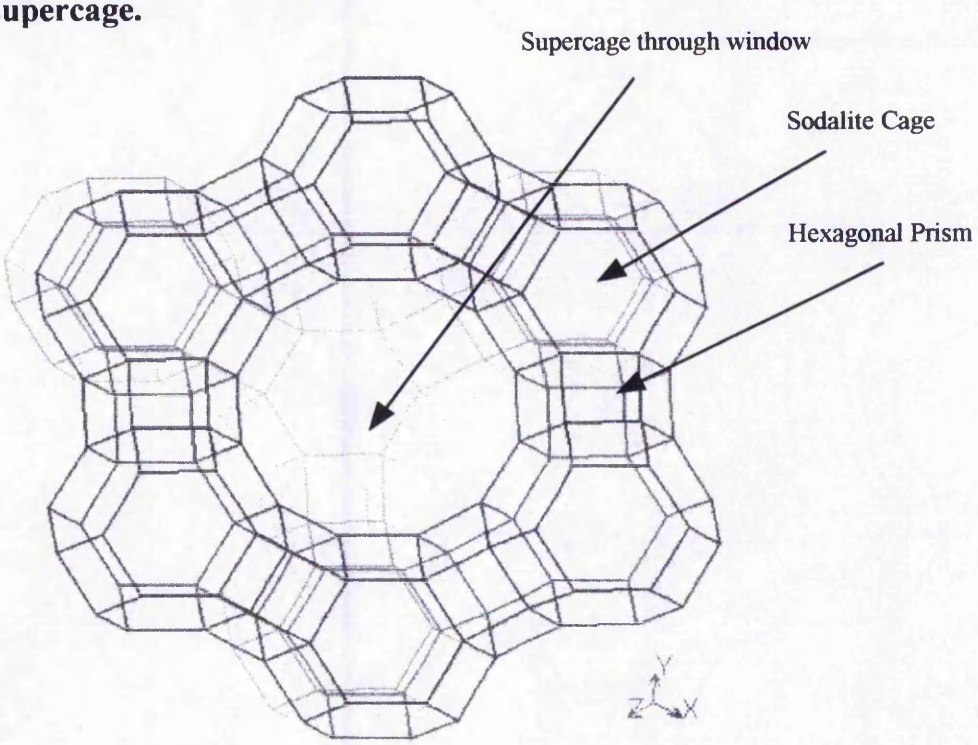

Fig 7.13.02 The pore structure of faujasite

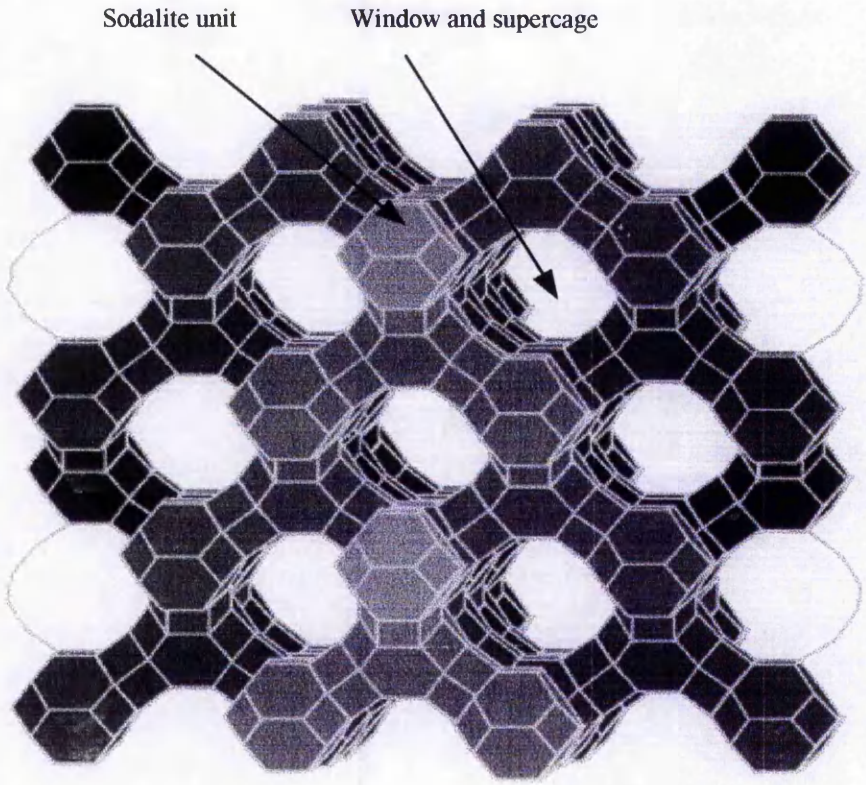

7.2 Results

7.21 Mordenites

Fig 7.21.01 Mordenites studied in this work

Sample	Si / Al ratio	Name
H-Mordenite[a]	12.5	H-MOR-12.5
Cu-H-Mordenite	12.5	Cu-H-MOR-12.5
Na-Mordenite[a]	6.4	Na-MOR-6.4
Cu-Na-Mordenite	6.4	Cu-Na-MOR-6.4 #1
Cu-Na-Mordenite[b]	6.4	Cu-Na-MOR-6.4 #2
H-Mordenite[c]	6.4	H-MOR-6.4

(a) The Parent Mordenites

(b) Double ion exchanged with 0.3M $Cu(NO_3)_2$

(c) Double ion exchanged with 0.3M NH_4NO_3

7.21.1 H-MOR-12.5

Fig 7.21.11 FTIR - Pyridine region and tabulated band areas

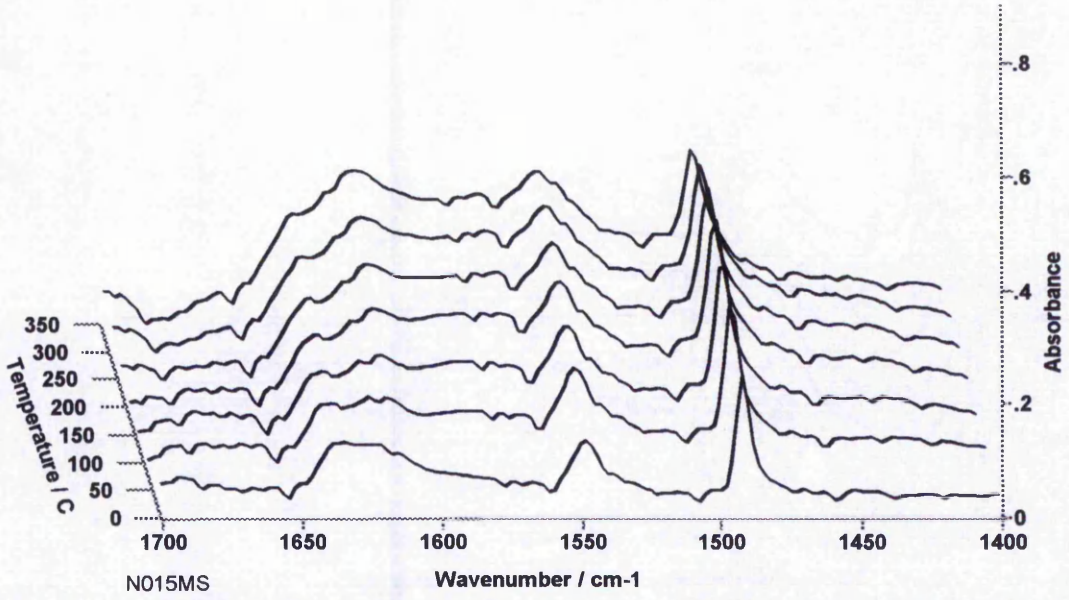

	Temperature / C	25	100	150	200	250	300	350
Assignment	cm-1							
Physisorbed	1446							
Lewis	1450							
L + B	1492	8.52	9.96	10.65	10.82	10.36	9.79	8.98
Bronsted	1546	6.56	7.31	6.33	5.01	4.66	4.61	4.61
Physisorbed	1598							
Lewis	1610							
Bronsted	1633	1.84	2.07	2.01	1.73	1.67	1.73	1.73

Fig 7.21.12 Microadsorption breakthrough vs time

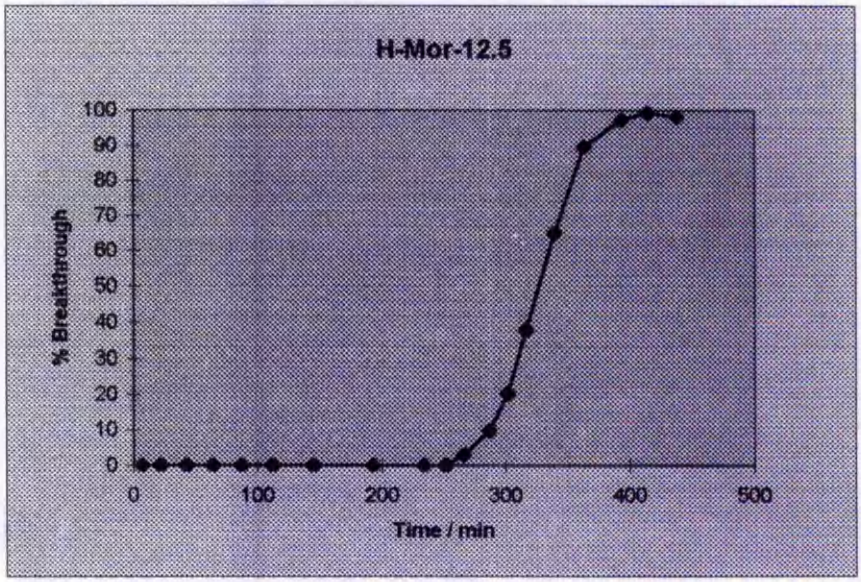

Fig 7.21.13 FTIR - Heptane coking experiment

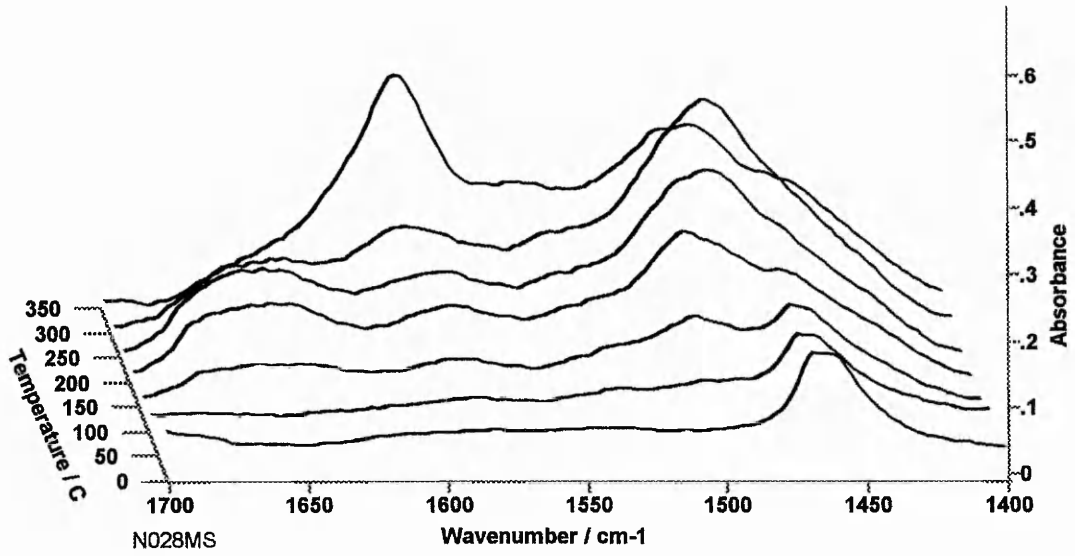

Fig 7.21.14 FTIR – OH Region

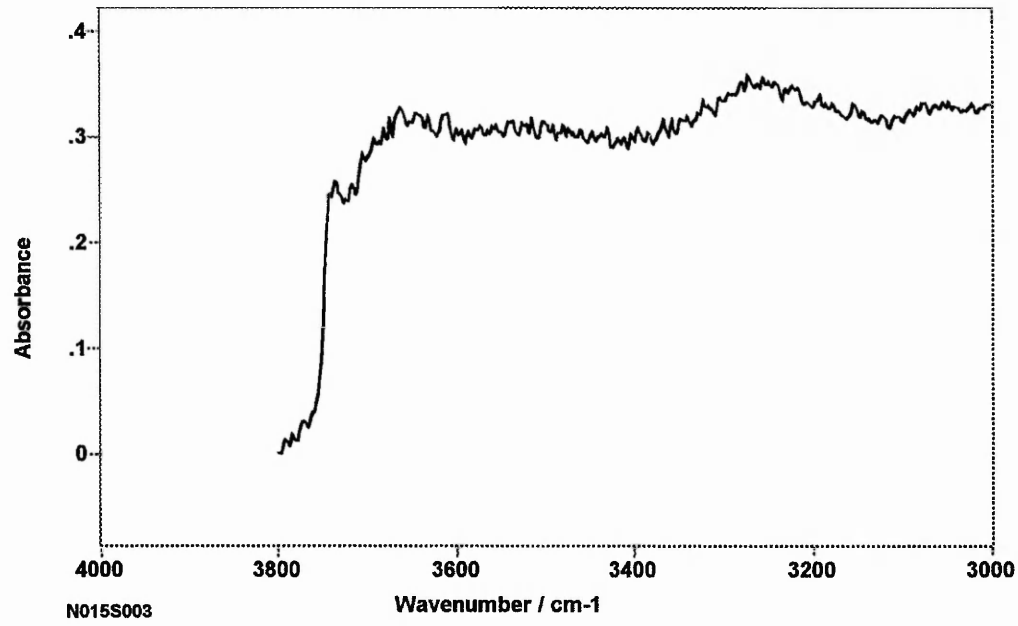

The FTIR spectra of pyridine adsorbed on H-MOR-12.5 (Fig 7.21.11) shows the sample to be in the purely protonic form. There are large numbers of Bronsted sites and there is no evidence of Lewis acid sites. The 1546 cm^{-1} Bronsted bound pyridine adsorption band is relatively broad, and a small amount of pyridine desorption is seen at each temperature increment above 100 °C. These observations demonstrate that the Bronsted sites present in the sample have a range of acid strengths, although are generally strong. When H-MOR-12.5 interacts with heptane at elevated temperature (Fig 7.21.13) a band at ~ 1585 cm^{-1} is observed in the FTIR spectra, which can be assigned to coke formation. From this 'coke band' it is clear that coke deposition on the sample increases as the temperature is increased. The lowest temperature at which it is observed is 150 °C. Above this temperature the coke band steadily grows with each temperature increment until 300 °C. Even at 300 °C there is only a small coke band, but as the temperature is increase from 300°C to 350°C there is a large increase in coke deposition.

The –OH region of the FTIR spectra (Fig 7.21.14) is not very well defined for this sample. The absorption band at 3741 cm^{-1} is assigned to terminal silanol groups, and is typical of zeolites and silicas.[1-5] The broad band centred around 3660 cm^{-1} is assigned to –OH groups associated with extra-framework aluminium.[1,5,6] This band is often accompanied by a band at 3690 cm^{-1}, which is assigned to another type of Al-OH species, the nature of which is a subject of discussion. There is no sign of the band at ~3600 cm^{-1} which is assigned by many authors to Bronsted sites.[1,4-7]

The IR hydroxyl region of mordenites is complex. The absorption band of bridging hydroxyl, which is assigned by most authors to Bronsted sites, has been shown to consist of two overlaid components. A high frequency component at around 3612 cm^{-1}, due to hydroxyls vibrating in the main channels, and a low frequency component at around 3585 cm^{-1} due to hydroxyls vibrating in the side pockets.[5,6,9] Several deconvolutions of this complex hydroxyl band have been suggested in the literature.[5.6.8-13] The lack of observable Bronsted OH stretch

may be related to the range of Bronsted strengths observed in the pyridine FTIR. Bronsted sites of different strengths will have slightly different OH stretching frequencies. This may broaden the OH stretch absorption band making it difficult to differentiate from the background signal. In addition the OH region of this spectrum is not well defined, possibly as a result of the low outgasing temperature. The band between 3400 and 3200 cm^{-1} can be assigned to the normal OH stretching vibrations of adsorbed water.[4,8]

In the microadsorption experiments H-MOR-12.5 performed well, and the 50 % breakthrough point was not reached until ~330 minutes (Fig 7.21.12). This corresponds to an adsorption capacity of ~1.9 wt %.

7.21.2 Cu-H-MOR-12.5

Fig 7.21.21 FTIR – Pyridine region and tabulated band areas

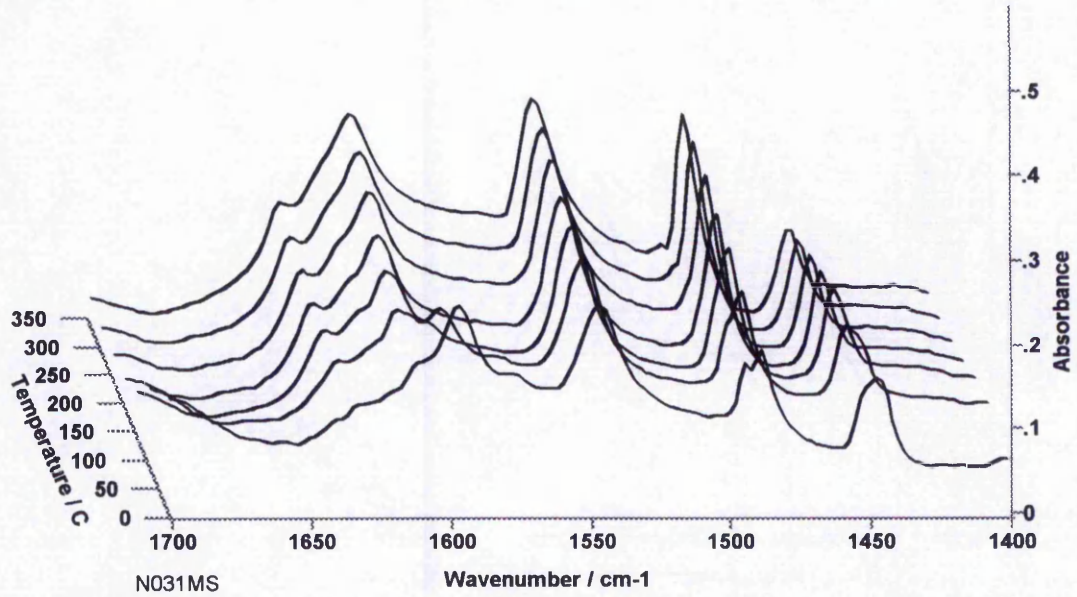

	Temperature / C	*25*	*100*	*150*	*200*	*250*	*300*	*350*
Assignment	cm-1							
Physisorbed	1446	1.16	0.33					
Lewis	1450	5.48	5.59	5.48	4.70	4.37	4.48	3.98
L + B	1492	6.91	7.47	9.13	9.96	9.68	9.85	7.19
Bronsted	1546	9.96	12.61	14.16	14.27	12.72	11.62	11.62
Physisorbed	1598	7.74	2.21					
Lewis	1608	1.66	2.77	7.19	8.85	9.40	11.06	11.06
Bronsted	1633	0.55	0.83	1.11	1.11	1.11	1.11	1.11

Fig 7.21.22 Microadsorption breakthrough vs time

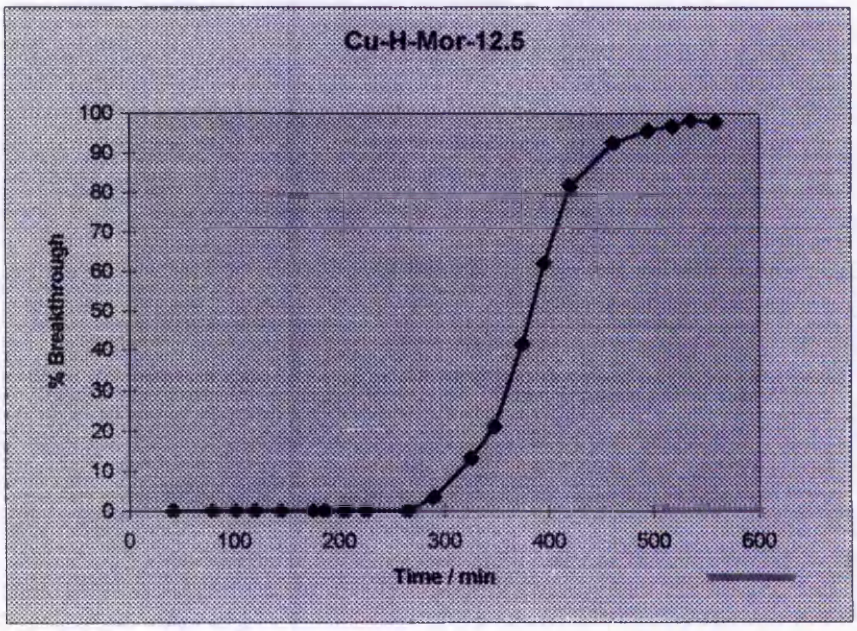

Fig 7.21.23 FTIR - Heptane coking experiment

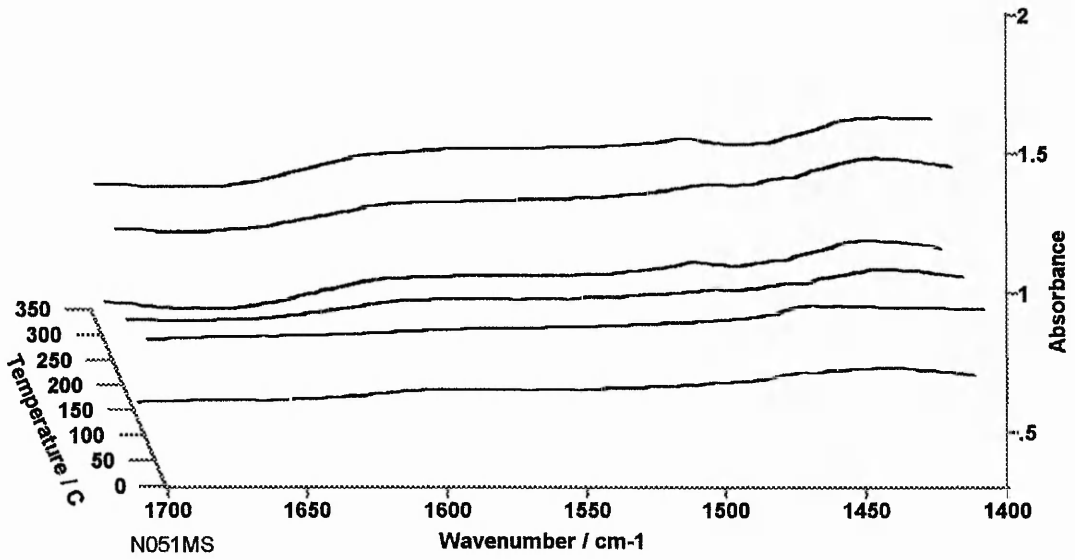

Fig 7.21.24 FTIR – OH Region

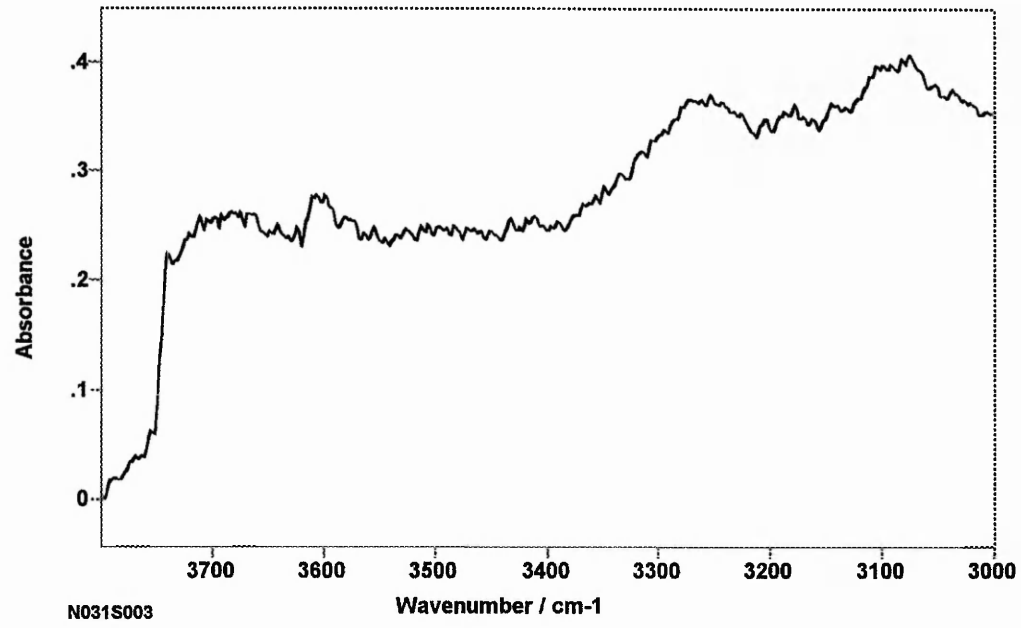

When the H-MOR-12.5 sample is ion exchanged with Cu^{2+}, to form Cu-H-MOR-12.5, the pyridine adsorption FTIR spectra are altered significantly (Fig 7.21.21). An absorption band is observed at 1450 cm^{-1} which is assigned to pyridine adsorbed on Lewis acid centres, in this case Cu Lewis centres, introduced by the ion-exchange. The Cu exchanged sample retains a significant number of Bronsted acid sites. It is unclear whether these Bronsted acid sites are the result of only partial ion exchange of the original H-mordenite, or whether an acidic $[Cu\text{-}OH]^+$ species is present. In theory ion-exchange with Cu^{2+} should remove 2 Bronsted sites for every Cu^{2+} Lewis site created, leading to a reduction in the total number of acid sites. However it has been shown that high temperature treatment of Cu^{2+} exchanged mordenite can lead to reduction of the Cu^{2+} to Cu^+ [7], although much higher temperatures were used than in this work, together with over-exchanged zeolites. As this sample has undergone a single exchange, with a relatively dilute Cu^{2+} solution (0.05M $Cu(NO_3)_2$), and a low outgasing temperature has been used, partial exchange appears to be the most likely explanation for the large number of Bronsted sites

The ratio of Bronsted band areas to Lewis band areas is approximately 3:1 over most of the temperature range studied. When the differing extinction coefficients for the two bands are considered (L / B = 1.33) [14], then the true ratio of Bronsted to Lewis sites is in the region of 3.5 – 4.0. Assuming ion-exchange of Cu^{2+} replacing two Bronsted sites, this would mean approximately 30 – 40 % of the original Bronsted sites have been ion-exchanged.

Regardless of whether the copper is Cu^{2+} or Cu^+, the pyridine FTIR study shows that the total number of Bronsted sites in the Cu exchanged sample is higher than in the purely protonic sample, despite the fact that Lewis centres have been introduced. One possible explanation for this could be occlusion of some of the pores in H-MOR-12.5 by extra-framework aluminium species, which are removed by the aqueous ion-exchange procedure. Extra-framework species can be strongly acidic, but a dense aluminium rich phase would be expected to have a relatively small number of accessible sites compared to the zeolite. In the effectively one-

dimensional pore structure of mordenite a small amount of extra-framework material could prevent access to a large number of sites. Removal of the extra-framework Al would therefore lead to a large increase in the total number of accessible sites. This might explain why the number of pyridine accessible Bronsted sites increases upon ion-exchange, even though 30 – 40% of Bronsted sites have been converted to Lewis sites.

Further evidence for the removal of extra-framework Al can be gained from examination of the hydroxyl region of the FTIR spectra (Fig 7.21.24). In addition to the terminal hydroxyl band at 3741 cm^{-1} observed with the parent H-MOR-12.5, there is also an absorption band visible at 3605 cm^{-1}, assigned to bridging hydroxyl groups associated with Bronsted sites. This provides verification of the increase in the number of Bronsted sites, observed in the pyridine FTIR, as the band is absent in the parent H-mordenite. The band at 3660 cm^{-1}, assigned to hydroxyls on extra framework aluminium, is much less intense than in the parent H-MOR-12.5, and indicates a reduction in the amount of extra framework material.

The ion-exchanged Cu-H-MOR-12.5 sample did not reach 50 % breakthrough until ~380 minutes. This represents an improvement of 50 minutes over H-MOR-12.5, which is consistent with the findings of the FTIR study. It demonstrates that the increase in acid site density observed by FTIR is genuine.

In addition to a higher density of acid sites Cu-H-MOR-12.5 also has less of a tendency to form coke (Fig 7.21.23). No 'coke band' is observed by FTIR when Cu-H-MOR-12.5 interacts with heptane, even at 350 °C. This may be an additional factor leading to the improvement in microadsorption performance upon Cu ion-exchange. The lack of coke formation on Cu-H-MOR-12.5 in comparison with H-MOR-12.5 is unexpected, as both samples possess large numbers of Bronsted sites.

There are a number of different potential explanations for the difference in coking activity between the H-MOR-12.5 and Cu-H-MOR-12.5. Firstly the presence of

Lewis sites in Cu-H-MOR-12.5. Cracking reactions have been shown to predominantly take place on strong Bronsted sites. Selectivity towards coke formation is, however, enhanced by the presence of Lewis sites.[16] Hence coking relies on a combination of strong Bronsted and Lewis sites. Cu-H-MOR-12.5 has large numbers of Cu Lewis sites, introduced in the ion-exchange, as well as large numbers of strong Bronsted sites. The parent H-MOR-12.5 appears, from pyridine FTIR, to only contain Bronsted sites. Therefore if coking is caused by some sort of interplay between strong Bronsted and Lewis sites then the Cu exchanged sample would be expected to have a high activity for coke formation. However, the reverse of this is found to be true. It is possible that a very small number of Lewis sites are present in H-MOR-12.5. Insufficient to be detected by pyridine FTIR. If this is the case then the differing nature of Lewis sites may be important. Any Lewis sites present in H-MOR-12.5 will most probably be in the form of positively charged structural silicon atoms, closely associated with aluminium and caused by dehydration of Bronsted sites. Alternatively a small number of Na^+ sites may still be present if the mordenite was originally synthesised in the Na^+ form. In Cu-H-MOR-12.5 the Lewis sites are more likely to be associated with Cu cations balancing the charge on the lattice.

The ion-exchange procedure should remove any remaining Na^+ and re-hydrate Si based Lewis sites. It is possible that some forms of Lewis acid site play a role in coking and others do not. If a small number of Na^+ cations are present in H-MOR-12.5, it is probable that these sites are located in the side pockets rather than in the main channels. Makarova et al[6] have found that when partially exchanging Na-mordenite to H-Na-mordenite the H^+ ions exchange for Na^+ ions in the main channels first. As the 3607 cm^{-1} Bronsted OH band is a composite of bands from Bronsted OH in the main channels (3612 cm^{-1}), and the side pockets (3585 cm^{-1}), the band is first observed at 3612 cm^{-1}. It then shifts to lower frequency, as the Na^+ in the side pockets is exchanged and the 3585 cm^{-1} component of the absorption band is introduced. If Na^+ sites are present in the side pockets then they would not be detected by using pyridine as an FTIR probe molecule. The side pockets are inaccessible to pyridine. They may however be accessible to

small molecules produced by cracking reactions on strong bronsted sites, and hence could be involved in coking.

Another possible explanation is that there is some difference in the Bronsted sites present in the two samples. If Cu^{2+} ion-exchange preferentially exchanges the strongest Bronsted sites, which are involved in cracking reactions, then this could explain the reduction in coking activity. There is, however, no evidence for a reduction in the Bronsted site strength in the FTIR spectra. Alternatively the Bronsted sites found in the two samples could be fundamentally different, for instance the Bronsted sites in Cu-H-MOR-12.5 are $[Cu\text{-}OH]^{+}$. However, it is difficult to believe that all the Bronsted sites in Cu-H-MOR-12.5 are of this form. The band in the FTIR at 3605 cm^{-1} is typical of bridging OH associated with traditional Bronsted sites.

Another explanation could be that extra-framework species present in H-MOR-12.5, but not in Cu-H-MOR-12.5 are, in some way, responsible for the formation of coke. Extra-framework material can be acidic, and the combination of such material and strong Bronsted sites may lead to coke formation. However, highly acidic extra-framework Al should be observable by pyridine FTIR, but no Lewis acidity is observed for the H-MOR-12.5 sample.

It is clear that ion-exchanging H-MOR-12.5 to Cu-H-MOR-12.5 leads to an improvement in pyridine adsorption performance. The hydroxyl regions of the FTIR spectra show that extra-framework material has been removed from the structure during this procedure. A much greater number of pyridine accessible Bronsted acid sites are observed in the pyridine FTIR as well as Cu Lewis sites. At the same time the coking activity of the sample has been reduced. It is unclear whether the reduction in coking or the increased accessibility of the pore structure is the most important factor leading to the improvement in performance. Alternatively the Cu^{2+} acid sites introduced could simply be more effective for selective pyridine adsorption, although from the pyridine FTIR both the Cu Lewis and Bronsted sites appear to strongly acidic and capable of retaining pyridine at temperatures above that used in the microadsorption experiment.

7.21.3 Na-MOR- 6.4

Fig 7.21.31 FTIR - Pyridine region and tabulated band areas

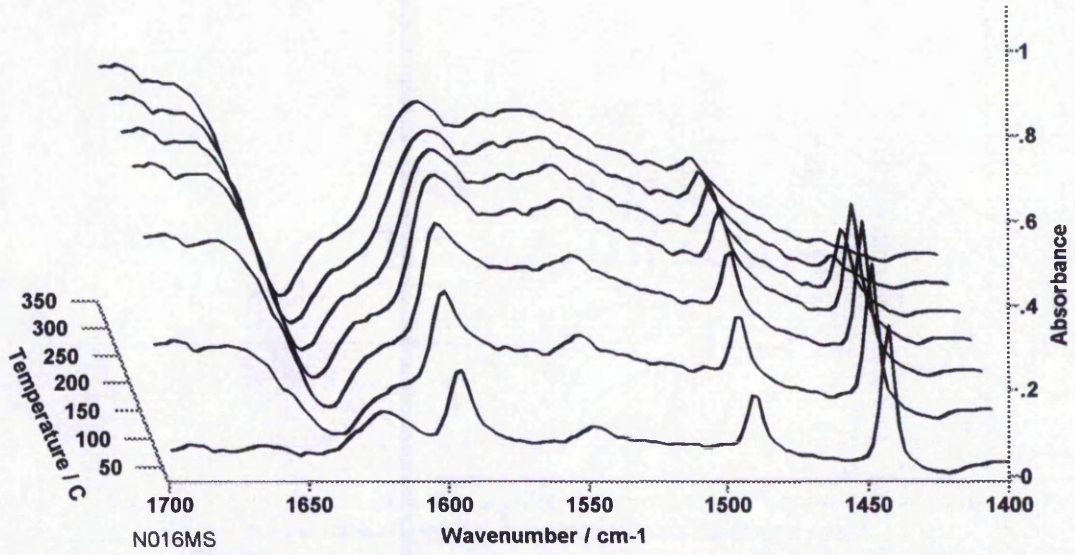

	Temperature / C	*25*	*100*	*150*	*200*	*250*	*300*	*350*
Assignment	cm-1							
Physisorbed	1446							
Lewis	1444	22.91	23.32	20.50	18.79	12.66	3.42	
L + B	1492	11.86	11.46	11.06	10.65	10.65	8.04	5.23
Bronsted	1546	4.22	4.32	4.22	3.72			
Physisorbed	1598							
Lewis	1595	16.08	19.10	19.10	15.88	11.66	10.05	10.05
Bronsted	1633	11.06	3.52	4.62	4.12	3.62	3.02	3.42

Fig 7.21.32 Microadsorption breakthrough vs time

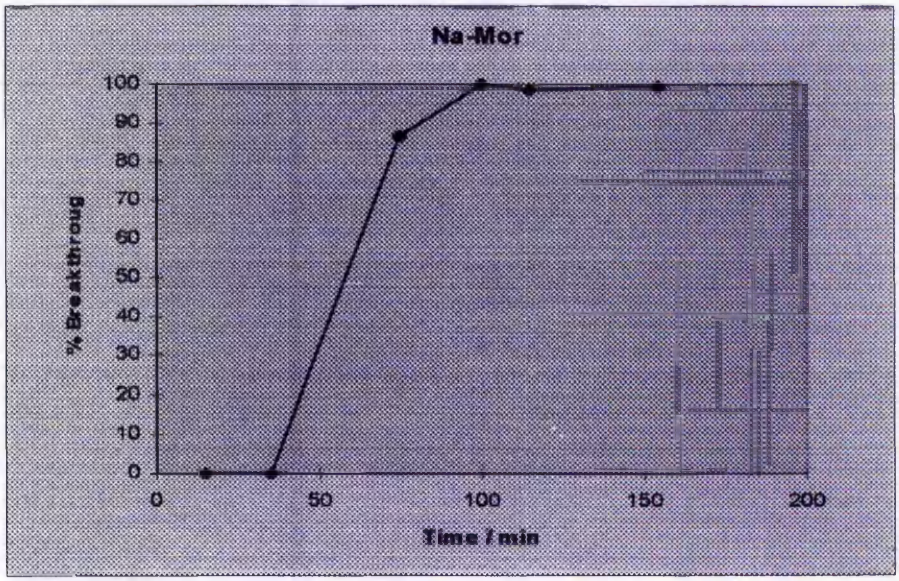

Fig 7.21.33 FTIR - Heptane coking experiment

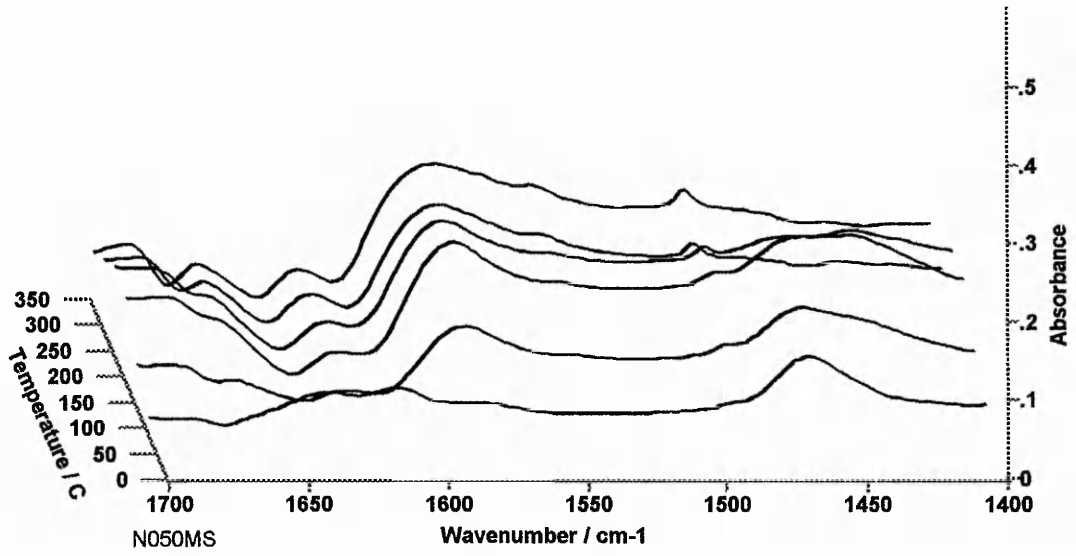

Fig 7.21.34 FTIR –OH Region

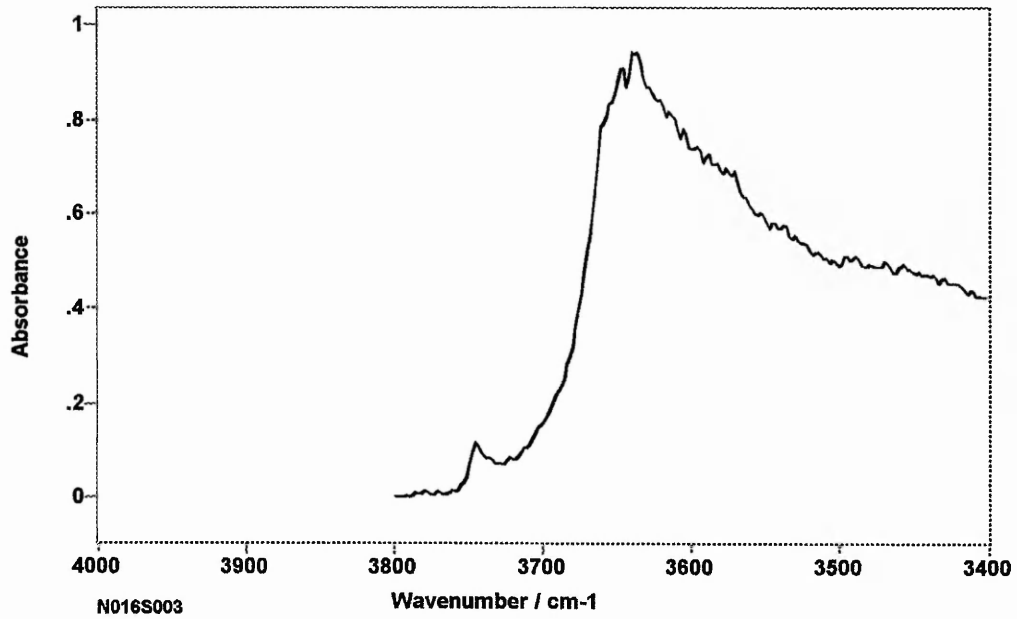

From the pyridine FTIR spectra of Na-MOR-6.4 (Fig 7.21.31) a very large number of Lewis acid sites are observed. At temperatures below 200°C the Lewis band area is > 20 absorbance units. However these Lewis sites are not very strong. The Lewis bound pyridine desorbs readily at temperatures above 200°C and is completely removed after 30 minutes evacuation at 350 °C. Further evidence for the weak acid site strengths can be obtained from the position of the V_{19b} and V_{8a} Lewis bound pyridine bands. These bands are at 1444 cm^{-1} and 1595 cm^{-1} respectively, which are among the lowest frequencies at which these absorption bands are observed. The low frequency is indicative of a weak acid - base interaction, i.e. a weak acid site, and this is typical of alkali metal exchanged zeolites.

As well as a very large number of Na Lewis sites there are a much smaller number of Bronsted acid sites shown by the small band at 1546 cm^{-1}. The broad nature of this band, coupled with regular pyridine desorption at each increment of temperature above about 150 °C, suggests that the few Bronsted sites available for pyridine adsorption have a wide range of acid strengths. However, they generally seem weak, as the band is not observed at 350 °C. The FTIR spectra of Na-MOR-6.4 interacting with heptane (Fig 7.21.33) show a large absorption feature developing at 1585 cm^{-1} with increasing temperature. This feature could be assigned to coke formation, although it is difficult to positively define this feature as an absorption band, especially when it is so evident at 100 °C.

The hydroxyl region of the Na-mordenite FTIR spectrum (Fig 7.21.34) is dominated by a very large absorption feature at around 3645 cm^{-1}. A small shoulder is visible around 3585 cm^{-1} and the ubiquitous terminal hydroxyl band is seen at 3740 cm^{-1}. For Na-mordenite, the band at 3645 cm^{-1} can be assigned to the stretching vibration of bridging OH groups (Bronsted sites) [6,17]. This band is shifted to higher frequency, compared to H-mordenites, which is probably a result of lower acid site strength in the Na^+ exchanged material. In this case the increased aluminium content may also contribute to a reduction in acid site strength, and hence the shift in the absorption. The high frequency of this band

therefore correlates well with the pyridine FTIR observation of generally weak Bronsted sites. The small shoulder at 3585 cm^{-1} is most likely assigned to more strongly acidic OH groups located in the side pockets. There does not appear to be any absorption associated with OH on extra framework Al, which is generally observed at 3660 cm^{-1} or 3690 cm^{-1}, but the bridging OH band extends to 3660 cm^{-1} and so a small Al-OH absorption band could be hidden.

In the microadsorption experiment 50 % pyridine breakthrough occurred after approximately 55 minutes on-line. This is much shorter than the breakthrough times for H-MOR-12.5 and Cu-H-MOR-12.5. Na-MOR-6.4 has a much greater number of acid sites, and therefore should have a higher adsorption capacity for pyridine. One possible explanation for the low adsorption capacity is the strength of the acid sites. All of the acid sites in Na-MOR-6.4 are relatively weak. The Na^+ sites appear to be uniformly weak, with virtually all adsorbed pyridine desorbing from these sites between 200 and 300°C. The Bronsted sites are also weak, but have a broader strength distribution. It is possible that only a small percentage of acid sites can retain pyridine at 200°C under the operating conditions of the adsorption experiment. The nature of these active sites (Lewis or Bronsted) is unknown as the FTIR shows pyridine desorbs from both types of site at similar temperatures. It is therefore possible that only one type of site is active for the selective adsorption of pyridine in the microadsorption experiment.

If the absorption feature at 1585 cm^{-1}, observed in the heptane FTIR spectra, is the result of coking, then coke formation may be another possible reason for the short breakthrough times. Na-MOR-6.4 has a very large number of acid sites, which are accessible to pyridine. The formation of coke inside the pores during a microadsorption experiment could have a large effect on the breakthrough time, either by blocking access to the sites directly, or by occluding the pores and preventing the diffusion of pyridine to the acid sites. If coke is blocking access to the acid sites directly then it is possible that one type of site (Lewis or Bronsted) is being selectively coked, allowing pyridine adsorption on just the remaining type of acid site.

It is obvious that of the large number of pyridine accessible acid sites observed by FTIR, only a small number are active for pyridine adsorption under the operational conditions of the microadsorption experiment. All of the acid sites in this sample are weak, and this may be the overriding factor limiting the adsorption performance. The apparent coke band formed upon interaction with heptane may be an additional factor, or could be more significant.

It seems likely that only one type of site is active for pyridine adsorption, either because only a small number of one type of site are strong enough, or because of some sort of selective coking. In view of the large number of Na^+ Lewis sites and much smaller number of Bronsted acid sites it seems most likely that it is the Bronsted sites that are active.

7.21.4 Cu-Na-MOR-#1

Fig 7.21.41 FTIR - Pyridine region and tabulated band areas

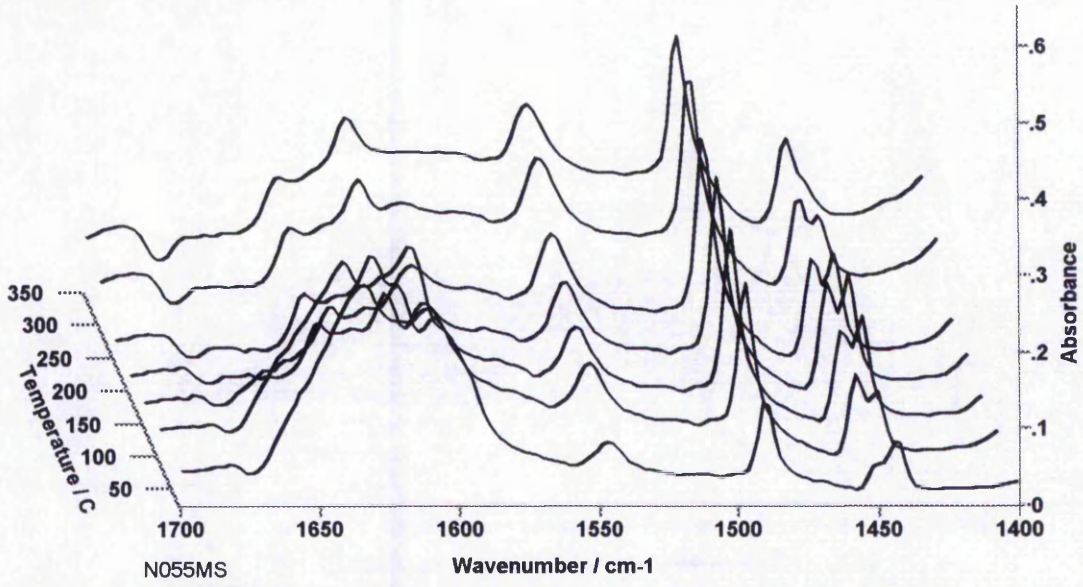

	Temperature / C	25	100	150	200	250	300	350
Assignment	cm-1							
Na Lewis	1442	3.10	2.18	5.44	5.72	5.27	2.63	0.06
Cu Lewis	1450	0.25	4.66	3.95	5.28	4.87	5.09	6.08
L + B	1492	4.24	8.48	9.46	10.66	11.66	11.48	10.37
Bronsted	1546	2.24	4.22	4.65	5.89	6.27	6.12	5.70
Physisorbed	1598							
Na Lewis	1594	0.29	0.34	1.09	1.60	1.43	0.46	
Cu Lewis	1608	7.39	5.43	2.10	1.89	1.78	1.88	2.73
Bronsted	1639	8.43	4.70	1.44	1.43	1.66	1.59	1.51

Fig 7.21.42 Microadsorption breakthrough vs time

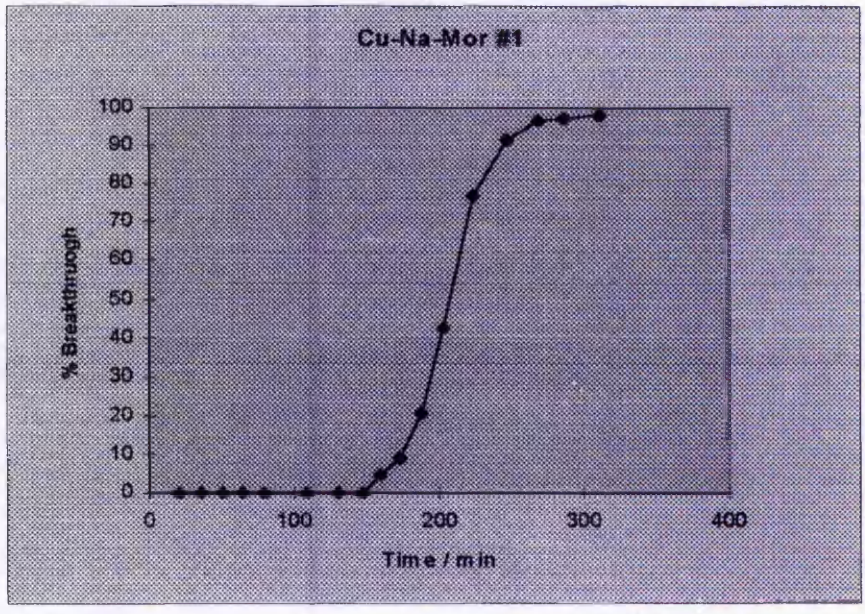

Fig 7.21.43 FTIR - Heptane coking experiment

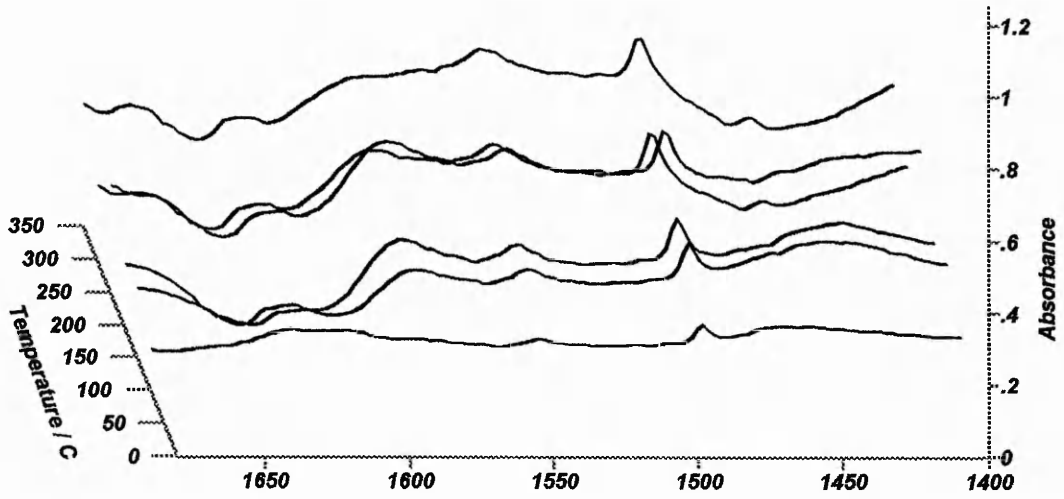

Absorbance / Wavenumber (cm-1)
File # 5 = N045M#6 @ 350

Fig 7.21.44 FTIR - OH Region

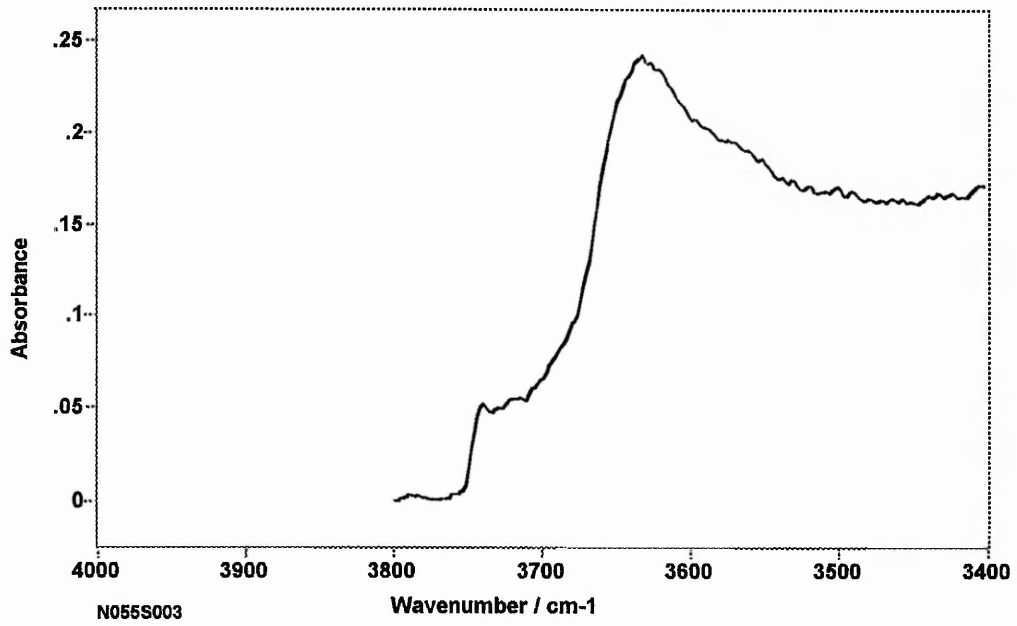

When Na-MOR-6.4 is ion-exchanged with Cu^{2+} to form Cu-Na-MOR-6.4-#1, an additional type of Lewis site is introduced. Cu-Na-MOR-6.4-#1 exhibits Bronsted and two types of Lewis acid site (Fig 7.21.41). The Bronsted sites are strong, with pyridine retained at 350°C. Two distinct bands are observed in the Lewis signature region. The band at 1442 cm^{-1} can be assigned to pyridine adsorbed on Na^{+} Lewis sites. Its position is very similar to the corresponding band in Na-MOR-6.4 and it is also accompanied by a low frequency V_{8a} absorption band at 1594 cm^{-1}. The band at 1450 cm^{-1} is assigned to pyridine adsorbed on Cu Lewis sites. The Na sites are weak, as evidenced by the low frequency of the absorption bands, and as with the Na-mordenite, pyridine is desorbed from these sites at 300°C and above. The Cu sites are much stronger, with no desorption of pyridine at 350°C. Cu-Na-MOR-#1 also has a large number of Bronsted sites (Fig7.21.41). The origin of these sites is unclear, as both Na and Cu ions should form Lewis sites. One possibility is that the Bronsted sites are formed via protonation from the aqueous ion exchange, although protonation would not be expected to achieve such a high level of exchange. Alternatively some sort of $[Cu\text{-}OH]^{+}$ species is responsible, although this is unlikely as these types of species are usually associated with over-exchanged zeolites. In this case a large number of Na^{+} sites are retained indicating only partial exchange.

From FTIR with heptane (Fig 7.21.43) there may be a small amount of coking at temperatures above 150°C although the spectra are not conclusive as the coke band appears to be reduced at 350°C. The shape of this potential coke band is similar to that observed for Na-MOR-6.4 interacting with heptane, but it is less pronounced. The absorption band at 1490 cm^{-1} can be assigned to background pyridine in the FTIR cell from previous experiments adsorbing on the sample.

The hydroxyl region of the spectrum of Cu-Na-MOR-6.4 #1 (Fig 7.21.44) is very similar to that of the parent Na-mordenite. The main absorption feature, assigned to Bronsted OH vibrations, has shifted to 3632 cm^{-1}. The position of this band is

typical for this type of material, indicating that the Bronsted sites are associated with bridging hydroxyl groups and not some sort of $[Cu\text{-}OH]^+$ species. The shift of 13 cm^{-1} to lower frequency indicates an increase in the strength of the Bronsted sites upon Cu exchange. This is entirely consistent with the pyridine FTIR spectra (fig 7.21.41). The terminal OH band at 3741 cm^{-1} and the shoulder at 3585 cm^{-1}, assigned to Bronsted sites in the side pockets, remain unchanged by the ion-exchange.

The introduction of Cu Lewis sites greatly improves the microadsorption performance (Fig 7.21.42). The 50 % breakthrough point is not reached until ~ 200 minutes on-line. Although this adsorption capacity is almost four times greater than Na-MOR-6.4, it is still significantly less that either H-MOR-12.5 or Cu-H-MOR-12.5 which both have a lower aluminium content.

Fig 7.21.45 Nitrogen adsorption isotherms for Cu-Na-MOR #1

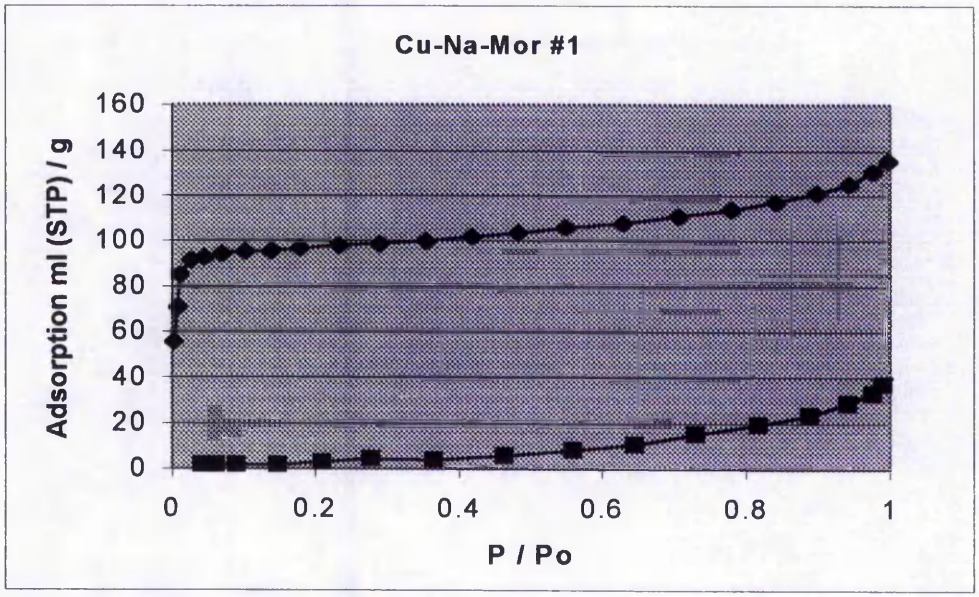

◆ - Isotherm before microadsorption experiment

■ - Isotherm after microadsorption experiment

The nitrogen adsorption isotherms in fig 7.21.45 show that after the microadsorption experiment the pore structure of Cu-Na-MOR #1 is inaccessible

to nitrogen. Adsorption of nitrogen on the external surface of the zeolite appears unchanged, but the micropore filling region of the isotherm (P/Po < 0.05) has been suppressed to virtually zero. It seems unlikely that this is the result of coke formation, as the post microadsorption FTIR (Fig 7.21.46) does not reveal a large coke band. However the FTIR coking experiments with heptane do suggest there is coke formation, and a small amount of coke located at or near the pore mouths could exclude nitrogen from the entire pore system.

Fig 7.21.46 FTIR - Pyridine region and tabulated band areas after a microadsorption experiment

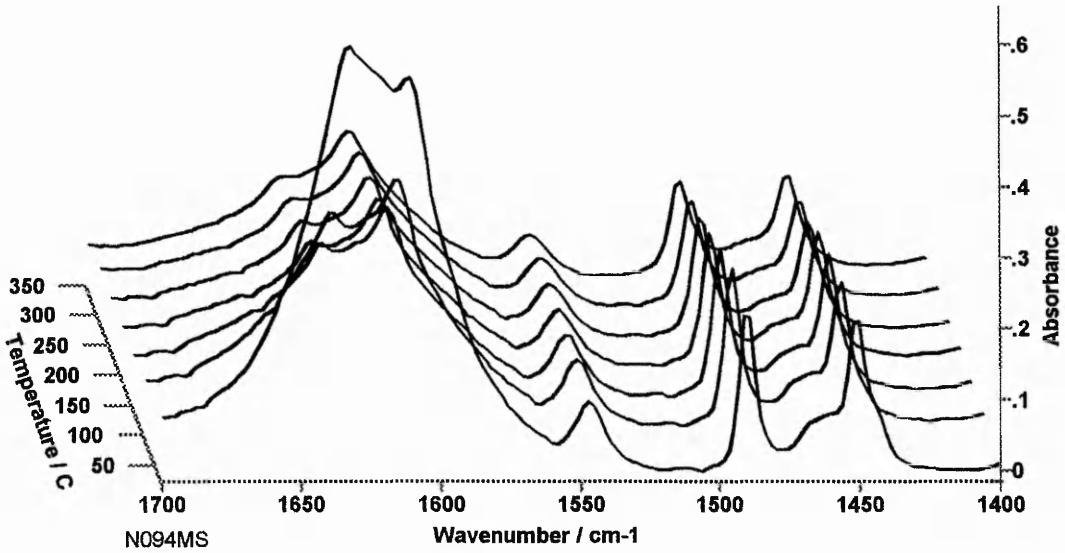

	Temperature / C	25	100	150	200	250	300	350
Assignment	cm-1							
Physisorbed	1446							
Lewis	1450	11.30	10.92	10.92	10.36	8.87	8.68	8.50
L + B	1490	13.26	13.45	12.79	11.76	11.20	10.27	9.34
Bronsted	1546	7.56	7.75	7.28	6.63	6.35	6.07	5.14
Physisorbed	1598							
Lewis	1610	7.75	7.28	7.00	6.63	6.54	6.63	6.16
Bronsted	1633	3.08	2.99	2.15	1.77	1.21	1.12	1.21

When Cu-Na-MOR-6.4-#1 is studied by FTIR after removal from the microadsorption apparatus (Fig7.21.46) the spectra are very similar to the spectra before the microadsorption experiment. The origin of the large feature around 1600 cm^{-1} at room temperature is unknown, but it could be due to residual hydrocarbon from the microadsorption experiment. The spectra show pyridine associated with both Bronsted and Cu Lewis sites, however Na Lewis sites have been eliminated by the microadsorption experiment. One possible explanation for the loss of the Na Lewis band at 1442 cm^{-1} is selective coking of the Na Lewis sites. The band areas for pyridine bound to the Bronsted and Cu Lewis sites are slightly larger after the microadsorption experiment (Fig 7.21.46) than before (Fig 7.21.41). This is probably due to a diffusion effect. The band areas in the FTIR before the microadsorption experiment grow with increasing temperature, up to around 200 °C. This means that it takes either extra time, or increased temperature, for the pyridine to reach many of the acid sites inside the pore system. In the FTIR study after the microadsorption experiment, much of the adsorbed pyridine will have originated from the microadsorption experiment, where pyridine had approximately 5 hours, at 200 °C, to diffuse through the structure and reach inaccessible sites. Consequently pyridine may be observed adsorbed to sites that were not probed effectively in the original FTIR experiment, explaining the increase in the pyridine band areas.

In a further experiment on Cu-Na-MOR-6.4-#1 the sample was allowed to interact with heptane vapour for 20 minutes at 350 °C in the FTIR transmission cell, before the start of a standard pyridine FTIR experiment (Fig 7.21.47). The resultant spectra are similar to those obtained with the standard procedure except that the 1442 cm^{-1} Na^{+} Lewis bound pyridine band is significantly reduced. This is therefore very similar to the spectra of the post microadsorption sample. In the original spectra (Fig 7.21.41) there are approximately equal amounts of pyridine adsorbed to Na and Cu Lewis sites at low temperature. In the heptane pre-activated sample the size of the Na Lewis bound pyridine band is approximately 25 % that of the Cu Lewis pyridine band. This is further evidence for the

effective elimination of Na^+ Lewis sites upon interaction with a hydrocarbon, possibly as the result of selective coking of these sites

Fig 7.21.47 FTIR - Cu-Na-MOR heptane pre-activation Pyridine region and tabulated band areas

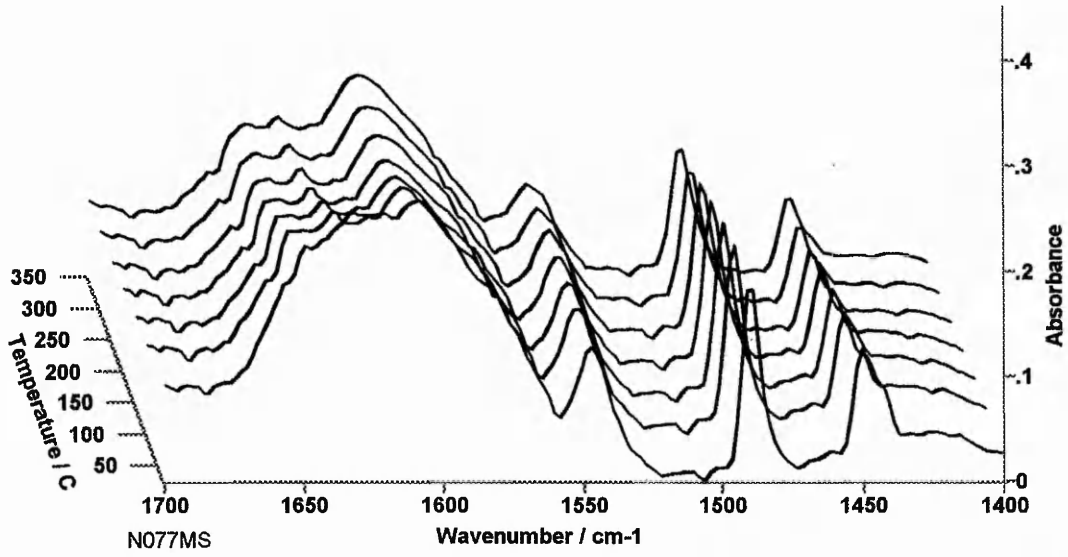

	Temperature / C	25	100	150	200	250	300	350
Assignment	cm-1							
Na Lewis	1444	1.66	1.49	1.41	1.24	0.83	0.41	
Cu Lewis	1450	5.79	5.13	4.72	4.47	4.30	4.14	4.06
L + B	1490	11.75	10.76	10.76	10.35	9.93	9.52	9.02
Bronsted	1546	8.77	8.44	8.28	8.28	7.45	6.62	5.71
Physisorbed	1598							
Lewis	1608	1.08	0.91	0.91	0.58	0.50	0.17	
Bronsted	1633	0.66	0.60	0.58	0.58	0.60	0.57	0.51

The introduction of Cu^{2+} Lewis sites along with Bronsted sites has led to a significant improvement in the microadsorption performance. The exact nature of the Bronsted sites is unknown, but protonation from the aqueous ion-exchange appears the most probable explanation, as the IR band at 3632 cm^{-1} in the OH region, is consistent with bridging hydroxyl groups (Si-OH-Al Bronsted sites). Although the coking studies are inconclusive, interaction with a hydrocarbon, in the FTIR cell or the microadsorption experiment, does effectively eliminate the Na^+ Lewis sites. The effect of this on the microadsorption result is unclear, as Na^+ acid sites do not appear to be very active for pyridine adsorption.

7.21.5 Cu-Na-MOR 6.4 #2

Fig 7.21.51 FTIR - Pyridine region and tabulated band areas

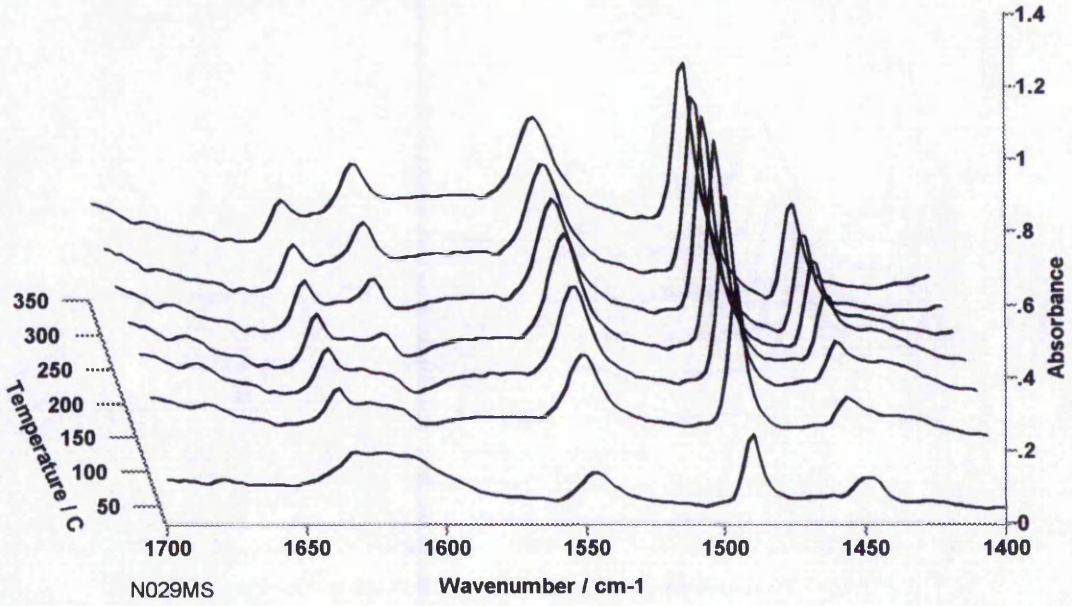

	Temperature / C	25	100	150	200	250	300	350
Assignment	cm-1							
Physisorbed	1446							
Lewis	1455	4.33	4.19	5.43	8.38	11.20	12.57	17.03
L + B	1492	10.92	21.77	28.71	34.27	32.90	33.59	32.21
Bronsted	1546	8.52	20.12	26.10	30.91	30.91	30.22	29.67
Physisorbed	1598							
Lewis	1608			0.69	2.06	3.91	7.49	8.86
Bronsted	1633	1.03	3.37	3.71	5.01	4.74	4.12	3.09

Fig 7.21.52 Microadsorption breakthrough vs time

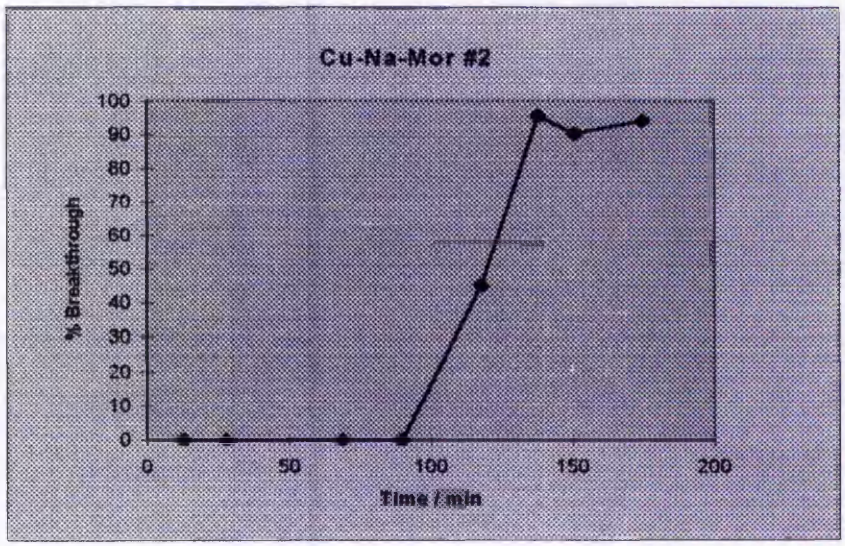

From the pyridine FTIR spectra of Cu-Na-MOR-6.4 #2 (Fig 7.21.51) it can be seen that there is no evidence of remaining Na sites. Only the Cu Lewis bound pyridine and Bronsted bound pyridine bands are observed at 1455 cm^{-1} and 1546 cm^{-1} respectively. The Na^+ cations have been completely ion-exchanged out of the mordenite structure. However the Na Lewis sites have not been completely replaced with Cu sites; there are very large numbers of Bronsted sites as well. The Bronsted bound pyridine band is large. It is larger than the Cu Lewis band at every temperature. At 150 °C the Bronsted band is almost five times the size of the Lewis band, and between 200 °C and 300 °C the Bronsted band area is over 30 absorbance units. The nature of these Bronsted sites is unclear. The more concentrated ion-exchange solution (0.3M) used to exchange this sample may have caused the sample to become 'over exchanged' and some of the Bronsted sites may be of the form $[Cu\text{-}OH]^+$. If water is present in the pores it can potentially be disproportionated by Cu^{2+} to form $[Cu\text{-}OH]^+$ and a H^+ Bronsted site.

In addition to the very large Bronsted band, the Cu-Na-MOR-6.4 #2 pyridine spectra have another unusual feature. The amount of pyridine adsorbed on both types of acid site increases with increasing temperature. This effect is observable in the V_{8a} ring vibration bands at 1608 cm^{-1} and 1633 cm^{-1}, as well as in the V_{19b} bands. There appears to be some sort of activated process governing the adsorption of pyridine onto both types of acid site. It is possible that the ion-exchange solution has partly de-aluminated the structure, leaving extra framework material in the pores. This would limit the ability of pyridine to diffuse through the pore structure and reach all of the acid sites. The effect is similar to that observed with Cu-Na-MOR-6.4 #1, but is less prominent here.

Despite the very large adsorption of pyridine seen in the FTIR spectra, the microadsorption study was not as successful as the Cu-Na-MOR-6.4 #1 sample. Pyridine broke through the adsorbent bed with 50 % of the feed concentration after 120 minutes.

Fig 7.21.53 FTIR - Heptane coking experiment

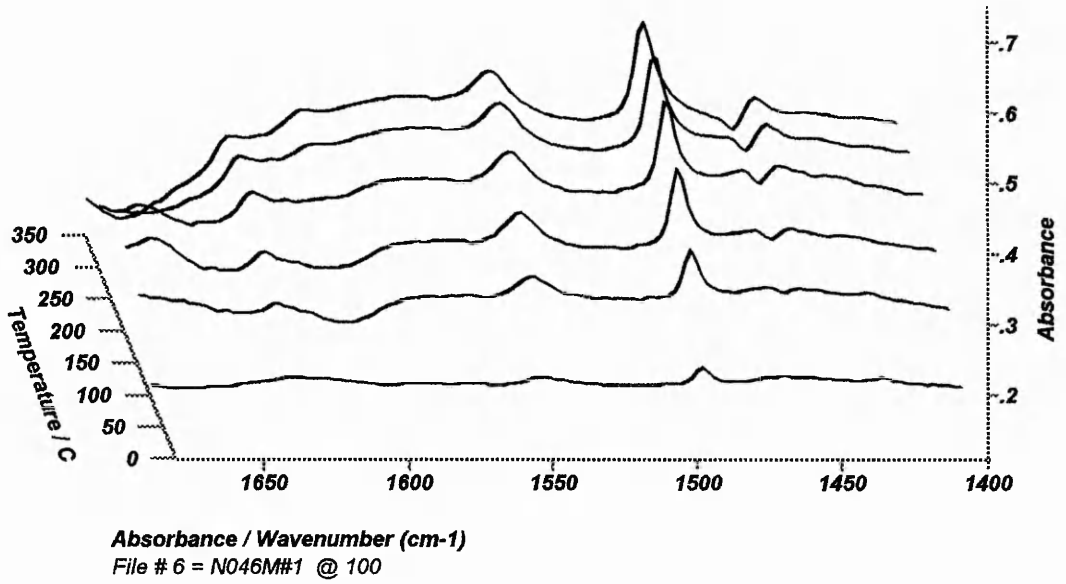

The interaction of Cu-Na-MOR #2 with heptane does not produce any strong absorbance bands that can be assigned to coke formation. The background pressure of pyridine adsorbing on the zeolite follows a similar profile to that in Fig 7.21.51 i.e. increasing adsorption at higher temperatures.

Fig 7.21.54 FTIR – OH Region

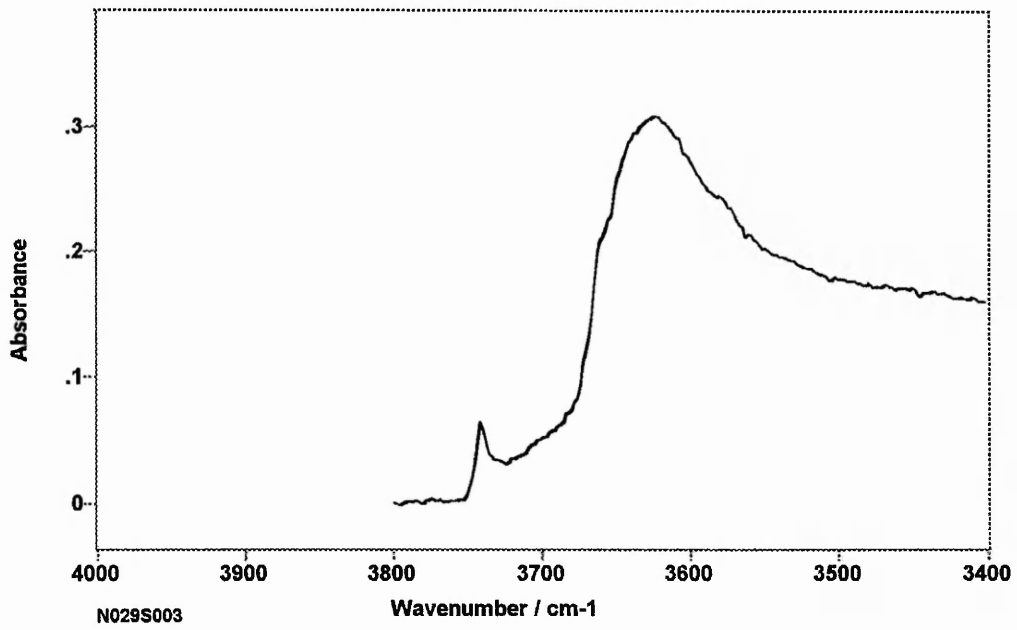

The FTIR hydroxyl region for Cu-Na-MOR-6.4 #2 (Fig 7.21.54) continues the trend from Na-MOR-6.4 and Cu-Na-MOR-6.4 #1. Upon Cu^{2+} ion-exchanging Na-MOR-6.4 to Cu-Na-MOR-6.4 #1, the bridging OH band moved to lower frequency, from 3645 cm^{-1} to 3632 cm^{-1}. Cu-Na-MOR-6.4 #2 is more extensively exchanged than Cu-Na-MOR-6.4 #1 and the bridging OH band is seen at 3623 cm^{-1}, 9 cm^{-1} lower than Cu-Na-MOR-6.4 #1 and 22 cm^{-1} lower than Na-MOR-6.4. This shift is consistent with literature values exchanging Na-mordenites to H-mordenites [6]. In this sample the Bronsted OH band is only 16 cm^{-1} removed from the standard position in H-mordenites of ~3607 cm^{-1}, although this value may be influenced by Si / Al ratio. In addition to the ever present terminal hydroxyl band at 3740 cm^{-1} there is a small shoulder on the bridging OH band at ~3660 cm^{-1}, which can be assigned to OH on extra-framework Al. If extra-framework material limits diffusion of pyridine through the pores then this might explain why the pyridine FTIR bands, in fig 7.21.51, increase in size with increasing temperature. Some of the acid sites are only accessed by pyridine later in the experiment, either because the extra time is required for diffusion, or because the high temperatures allow pyridine to reach sites that are inaccessible at room temperature.

Fig 7.21.55 FTIR - Pyridine region and tabulated band areas after a microadsorption experiment

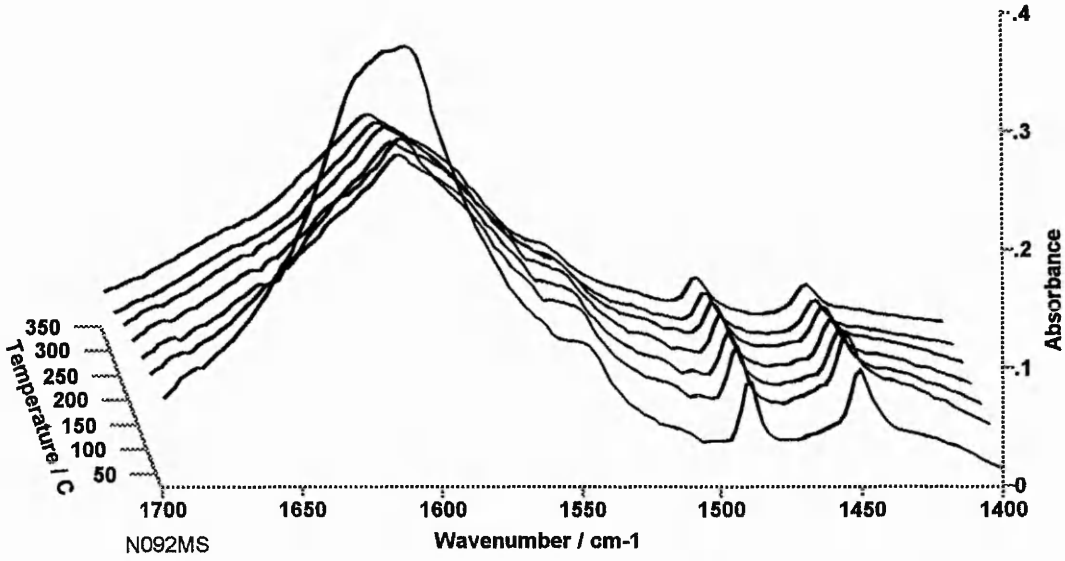

	Temperature / C	25	100	150	200	250	300	350
Assignment	cm-1							
Physisorbed	1446							
Lewis	1450	14.57	9.43	8.00	7.14	6.57	5.71	5.14
L + B	1490	10.29	9.14	7.71	7.14	6.86	6.29	5.43
Bronsted	1546	5.43	4.57	3.43	3.14	2.29	2.00	1.43
Physisorbed	1598							
Lewis	1610							
Bronsted	1633							

The most striking feature in the FTIR spectra of Cu-Na-MOR-6.4 #2 after a microadsorption experiment is a large, broad feature at ~ 1600 cm^{-1} (Fig 7.21.55). The origin of this band is uncertain. It is at a higher frequency than the typical position of a coke band, although there appears to be a shoulder on the low frequency side at ~ 1585 cm^{-1}. At room temperature there is an even more pronounced feature which disappears once the sample is heated to 100 °C. An almost identical absorption is observed with Cu-Na-MOR-6.4 #1, and is probably due to residual hydrocarbon re-adsorbing on the zeolite at room temperature. Pyridine is observed associated with both Lewis and Bronsted sites. This pyridine desorbs from both types of site steadily with increasing temperature. There is no

sign of the apparently activated uptake observed before the microadsorption study, although most of the pyridine present in this sample will have originated from the microadsorption experiment, rather than the pyridine dosed into the FTIR cell. Consequently this pyridine will have been adsorbed at 200°C, over a period of several hours, thus overcoming the diffusion limitations evident in the original pyridine FTIR experiment. Despite this, the pyridine band areas are all much smaller than in the original FTIR experiment. This means that many acid sites observed by FTIR, albeit mostly only at higher temperatures, become inaccessible to pyridine during the course of the microadsorption experiment.

Fig 7.21.56 Nitrogen adsorption isotherms for Cu-Na-MOR #2

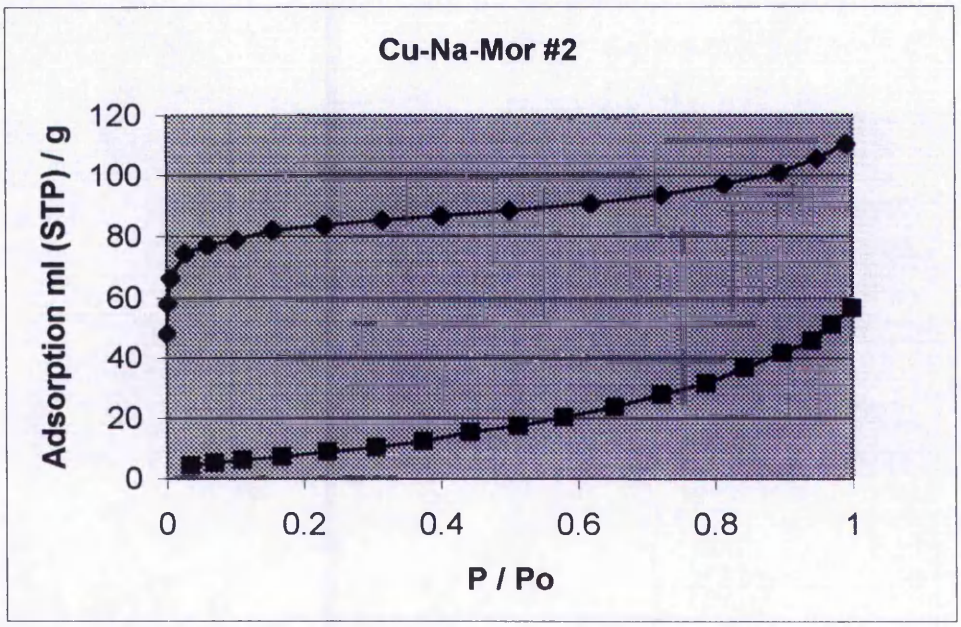

◆ - Isotherm before microadsorption experiment

■ - Isotherm after microadsorption experiment

The nitrogen adsorption isotherms for Cu-Na-MOR-6.4 #2 before and after a microadsorption experiment show that after the microadsorption study, the pore volume accessible to nitrogen is reduced to virtually nil. This is the same effect observed for Cu-Na-MOR–6.4 #1, and is possibly the result of coking, although the heptane FTIR spectra do not show the formation of a coke band. The pyridine FTIR bands in the spectra after the microadsorption experiment are much smaller

than in the original pyridine spectra, and this seems consistent with the N_2 adsorption isotherms. The accessibility of the pore structure has been reduced for both pyridine and nitrogen. In addition, although the heptane FTIR spectra do not show any sign of coke formation, the spectra after the microadsorption run show an absorbance at ~ 1600 cm^{-1} which might be due to coke.

The volume of adsorbed nitrogen in the two Cu-Na-mordenites, before the microadsorption, differs significantly. In Cu-Na-MOR-6.4 #1 (Fig 7.21.45) the micropore filling region of the isotherm (P / Po <0.05) accounts for approximately 90+ ml (STP) g^{-1} nitrogen uptake. In Cu-Na-MOR-6.4 #2 (Fig 7.21.56) this uptake is reduced to ~75 ml (STP) g^{-1}. The more concentrated $Cu(NO_3)_2$ ion-exchange used to prepare Cu-Na-MOR-6.4 #2 has obviously had a detrimental effect on the mordenite structure. The removal of framework Al may have led to occlusion of some of the pores by extra-framework material. The OH region of the FTIR spectra has shown there to be extra-framework Al present in the sample. This would explain the loss in pore volume seen in the N_2 adsorption isotherms and also the activated adsorption / diffusion limitation effect observed in the pyridine FTIR.

7.21.6 H-MOR-6.4

Fig 7.21.61 FTIR - Pyridine region and tabulated band areas

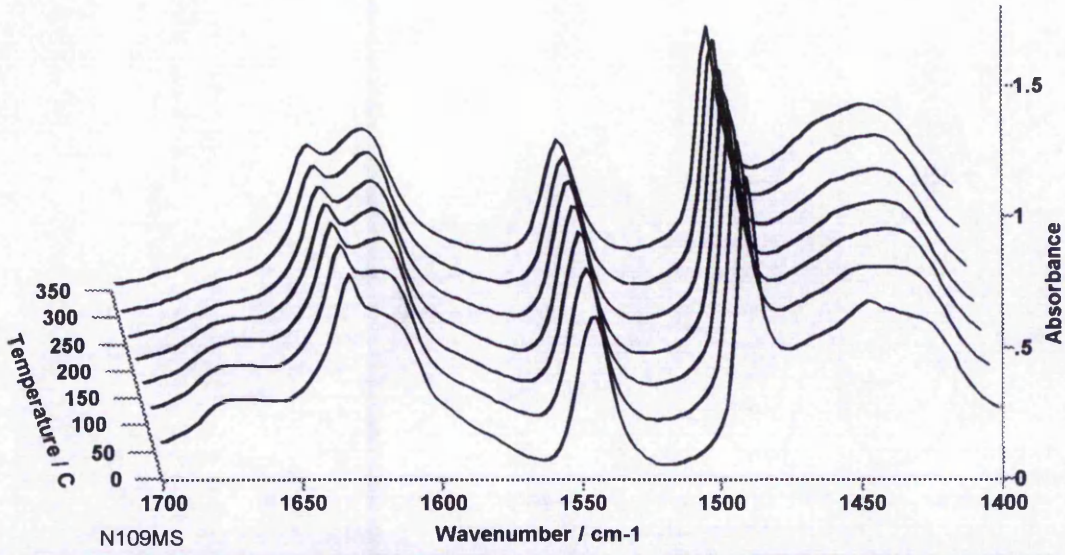

	Temperature / C	25	100	150	200	250	300	350
Assignment	cm-1							
Physisorbed	1446							
Lewis	1450	5.79	3.16	2.74	2.05	1.42	1.05	0.89
L + B	1490	37.37	37.89	37.37	35.26	35.79	35.26	32.63
Bronsted	1546	43.16	43.16	43.16	41.05	37.89	34.74	31.05
Physisorbed	1598							
Lewis	1612							
Bronsted	1631	11.37	10.84	9.79	9.47	8.42	7.37	7.47

Fig 7.21.62 Microadsorption breakthrough vs time

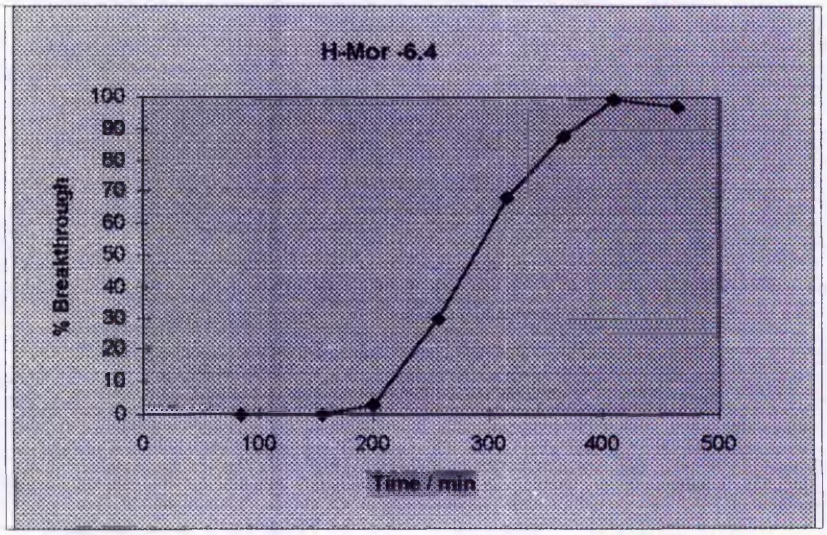

The H-MOR-6.4 sample has been successfully ion exchanged from the Na form. There is only evidence in the FTIR pyridine spectra (Fig7.21.61) of a very small number of Lewis acid centres. A much larger number of Bronsted sites are present. A small amount of pyridine desorbs from these Bronsted sites as the temperature is increased, but approximately 75 % of the peak band area is retained at 350 °C, indicating that most of these sites are strong.

Fig 7.21.63 FTIR – OH Region

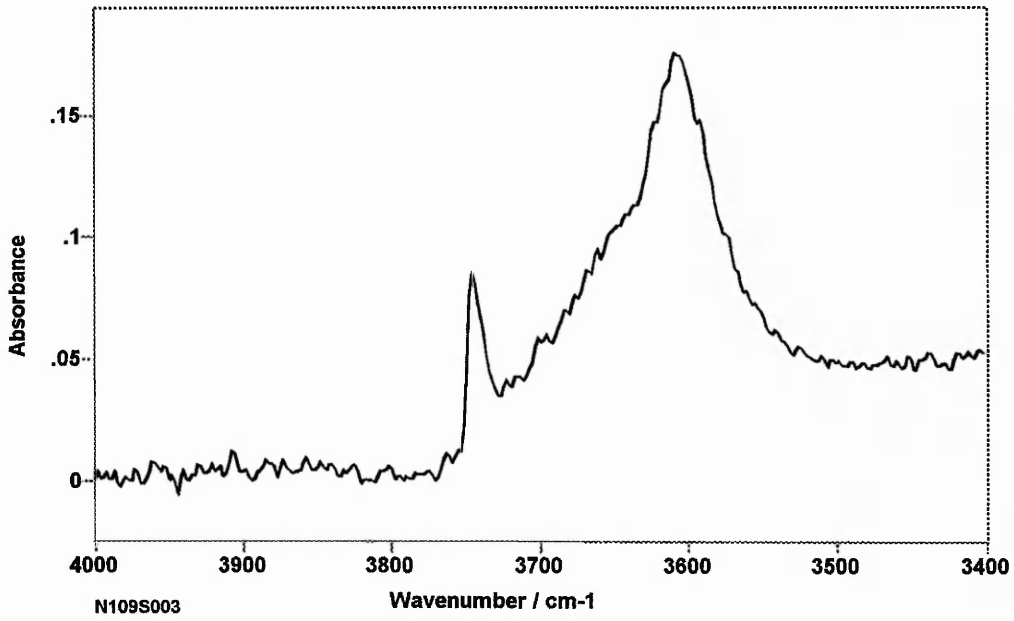

The FTIR hydroxyl region of H-MOR-6.4, shown in Fig 7.21.63, is similar to the other samples in this series. Like Cu^{2+} ion-exchange, H^{+} ion-exchange has shifted the bridging hydroxyl band to lower frequency. In this case the band has moved to 3607 cm^{-1} which is typical for H-mordenites. The shoulder at 3660 cm^{-1} indicates that there is extra-framework Al present in the sample.

Fig 7.21.64 Powder XRD pattern of H-MOR-6.4

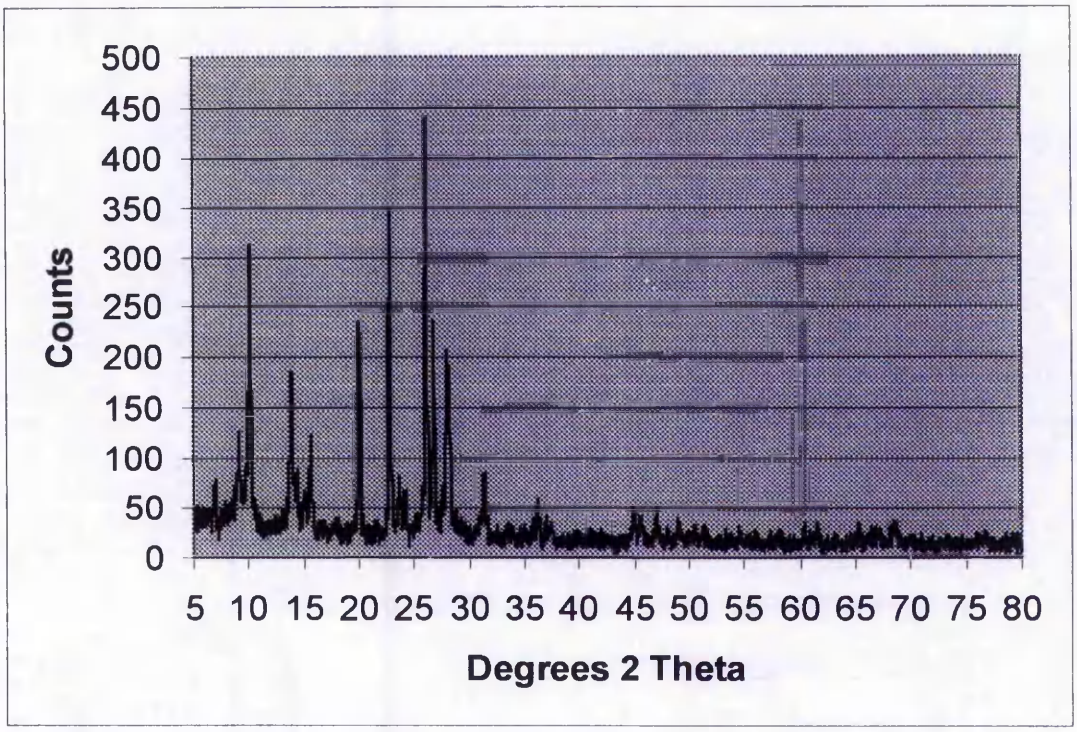

The powder x-ray diffraction pattern of H-MOR-6.4 in Fig 7.21.64 shows that there is an amorphous element present in the material. This is probably the extra-framework Al observed in the OH region of the FTIR spectra (Fig 7.21.63). The ion-exchange procedure appears to have had a detrimental effect on the structural integrity of the zeolite.

The microadsorption performance experiment (Fig 7.21.62) showed it to be a good adsorbent for pyridine at these temperatures, and the 50 % breakthrough point was reached after 280 minutes. However, this breakthrough time is 50 minutes shorter than the breakthrough time for H-MOR-12.5. H-MOR-6.4 has twice the aluminium content of H-MOR-12.5 and so in theory should have twice the number of acid sites, and a higher adsorption capacity. One possible reason for the lower than expected adsorption capacity is the extra-framework material observed in Figs 7.21.63 and 7.21.64. A small amount of amorphous extra-framework material can block adsorption to a large number of sites in the mordenite structure, because the pore system is effectively one-dimensional.

However, if extra-framework material was responsible for blocking pyridine from reaching acid sites, then this should be evident from the pyridine FTIR spectra. The Bronsted bound pyridine band areas for H-MOR-6.4 are far greater than for H-MOR-12.5, indicating that there are a much greater number of accessible sites. With such a large number of accessible sites before the microadsorption experiment then it is possible that a build up of coke during the experiment is responsible for the shorter breakthrough time.

Fig 7.21.65 Microadsorption breakthrough vs time for the regenerated sample

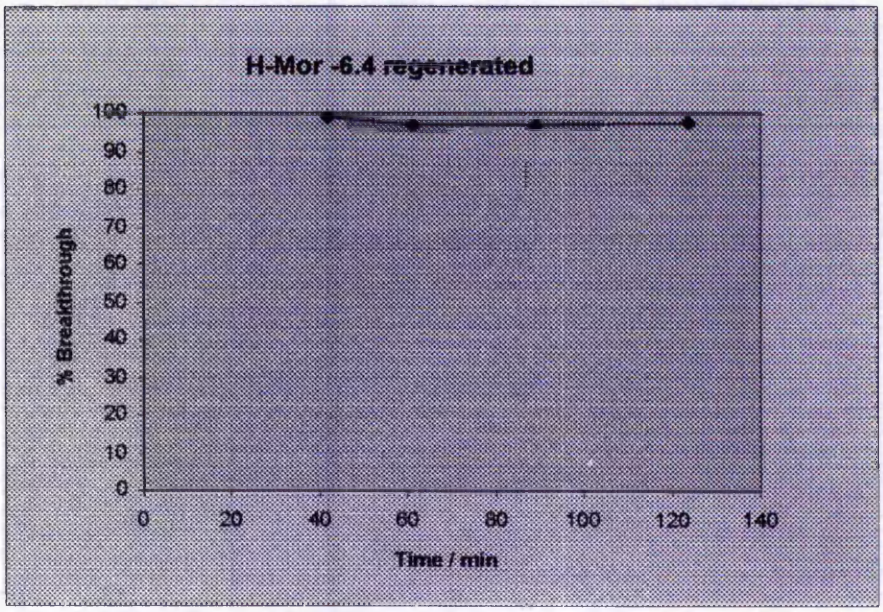

Fig 7.21.65 shows the microadsorption performance of H-MOR-6.4 after regeneration at 650 °C. It can clearly be seen that the adsorption capacity of the material has been reduced to virtually zero. The pyridine FTIR spectra after regeneration (Fig 7.21.66) demonstrate the same effect. Very little pyridine is adsorbed on the sample. The small amount of pyridine that is observed, may have originated from the first microadsorption experiment, i.e. the regeneration step failed to remove all of the pyridine after the first run. This would explain the

presence of a small amount of pyridine, in the FTIR spectra, when the adsorption capacity on the second run appears to be almost nothing. The spectra also show a broad feature at ~ 1580 cm^{-1} which could be assigned to coke. It is impossible to tell if the coke was formed during the microadsorption experiment, or during the regeneration step where the sample was heated to 650°C, possibly in the presence of residual hydrocarbon. The former seems likely, as this would explain the reduction in adsorption capacity in comparison with H-MOR-12.5. Coke formation in the regeneration step cannot be ruled out however, due to the high temperature.

Fig 7.21.66 FTIR - Pyridine region and tabulated band areas after two microadsorption experiments

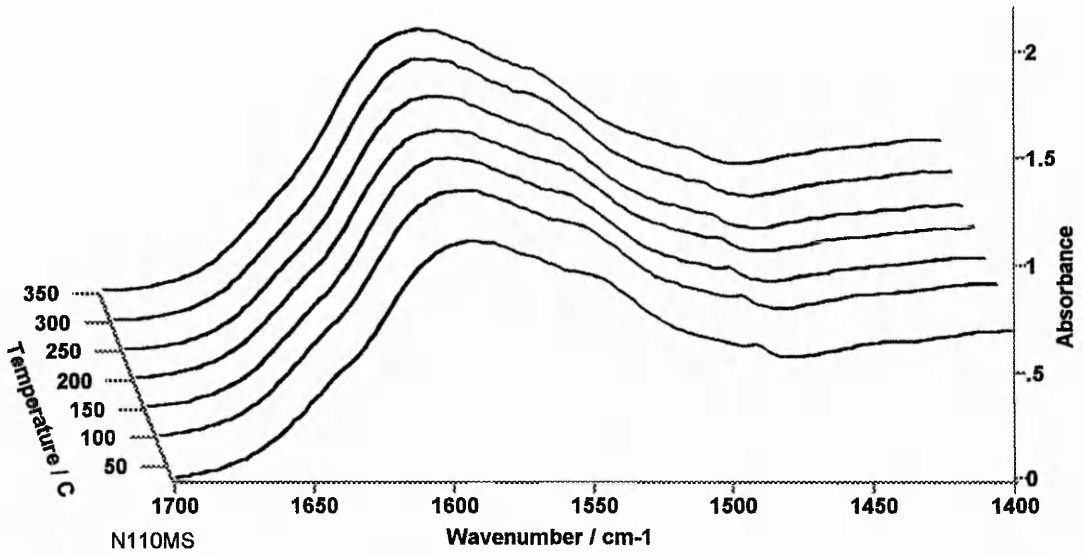

	Temperature / C	25	100	150	200	250	300	350
Assignment	cm-1							
Physisorbed	1446							
Lewis	1450	4.49	2.49	1.66	1.66			
L + B	1490	1.83	2.16	1.83	1.83	1.83	1.50	1.33
Bronsted	1546	9.97	6.64	6.15	5.65	4.82	4.82	4.65
Physisorbed	1598							
Lewis	1612							
Bronsted	1631							

Fig 7.21.67 Nitrogen adsorption isotherms for H-MOR –6.4

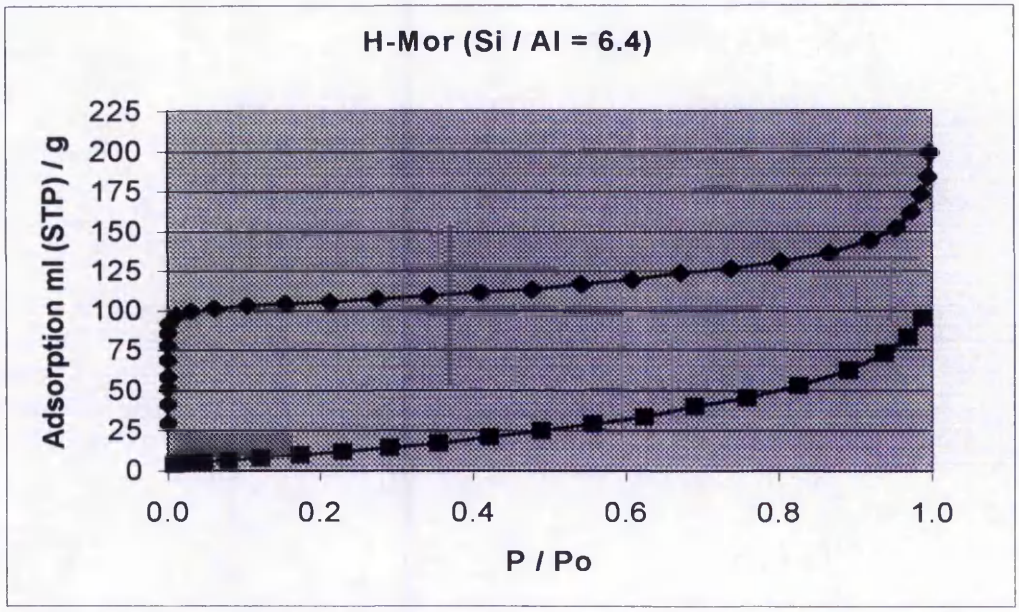

◆ - Isotherm before microadsorption experiment

■ - Isotherm after microadsorption experiment

The nitrogen adsorption isotherms for H-MOR-6.4 (Fig 7.21.67) are similar to those for the other mordenites. There is an almost complete loss in uptake in the micropore filling region suggesting that coke has built up in the pores and is preventing nitrogen physisorption. The micropore filling region of the isotherm is responsible for approximately 95 ml (STP) nitrogen uptake before the microadsorption experiment. This is slightly more than Cu-Na-MOR-6.4 #1 or Cu-Na-MOR-6.4 #2 which have been prepared from the same parent mordenite. Although the OH region of the FTIR spectra and the XRD pattern both show evidence for the presence of extra-framework material, this material does not seem to have a large effect on the pore volume accessible to nitrogen. This does not necessarily mean that the pores are as accessible for pyridine because pyridine is a much larger molecule than N_2.

7.22 ZSM-5 Samples

Fig 7.22.0 ZSM-5 samples used in this work

Sample	Si / Al ratio	Name
H-ZSM-5[(a)]	25	H-ZSM-5 #1
Cu-H-ZSM-5	25	Cu-H-ZSM-5
H-ZSM-5	25	H-ZSM-5 #2
H-ZSM-5	15	H-ZSM-5 #3

(a) The Parent ZSM-5 (of Cu-H-ZSM-5 and H-ZSM-5 #2)

7.22.1 H-ZSM-5 #1

Fig 7.22.11 FTIR – Pyridine region and tabulated band areas

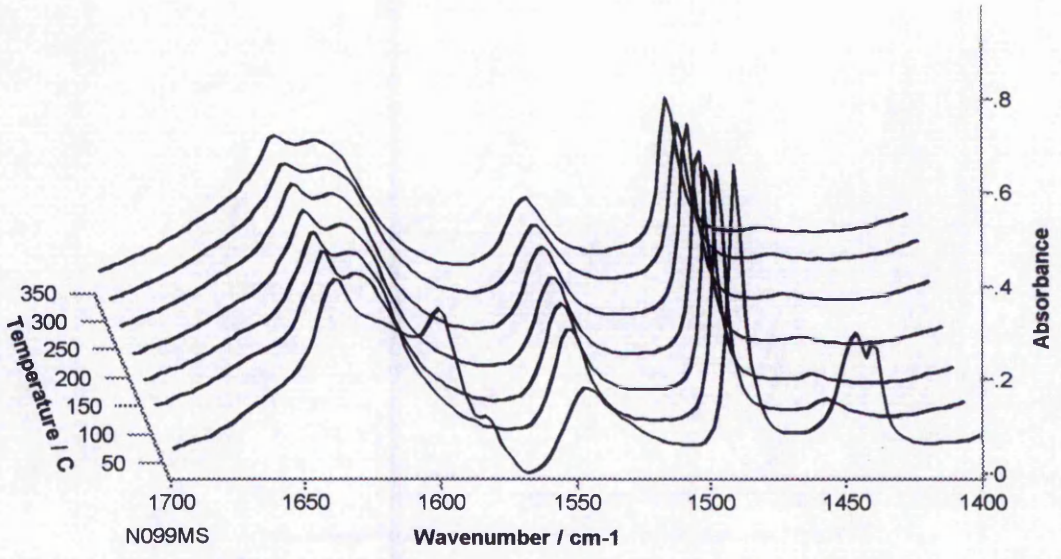

	Temperature / C	25	100	150	200	250	300	350
Assignment	cm-1							
Physisorbed	1446	10.52						
Lewis	1450	0.92	0.92	0.38	0.26	0.32	0.29	0.26
L + B	1491	14.05	11.27	10.87	10.40	9.83	8.61	8.67
Bronsted	1546	9.08	9.39	8.87	8.38	7.51	6.24	6.36
Physisorbed	1598	2.69						
Lewis	1621							
Bronsted	1639	4.16	2.72	2.40	2.28	1.85	1.59	1.45

As can be seen in Fig 7.22.11 the H-ZSM-5 #1 sample has a large number of relatively strong Bronsted acid sites and a much smaller number of Lewis acid sites. It is almost exclusively in the Bronsted form. Both the Lewis and Bronsted sites appear to be strong, and large proportions of both retain pyridine at 350°C. In the microadsorption study the 50 % breakthrough point was reached after ~ 220 minutes. The nitrogen adsorption isotherms (Fig 7.22.14), before and after microadsorption are very similar. There is only a very small reduction in the micropore-filling region after the microadsorption run. This is in stark contrast to the mordenites, which experienced a complete loss of N_2 accessible pore volume after a microadsorption experiment. The retention of the pore volume suggests that there has not been any coke formation inside the pore system. There is also a sharp uptake in the adsorption isotherm at P / Po > 0.9, in the post microadsorber sample, suggesting the formation of macropores. Whether this effect would become more significant if the sample was subjected to regeneration and re-use is unknown.

Fig 7.22.12 Microadsorption breakthrough vs time

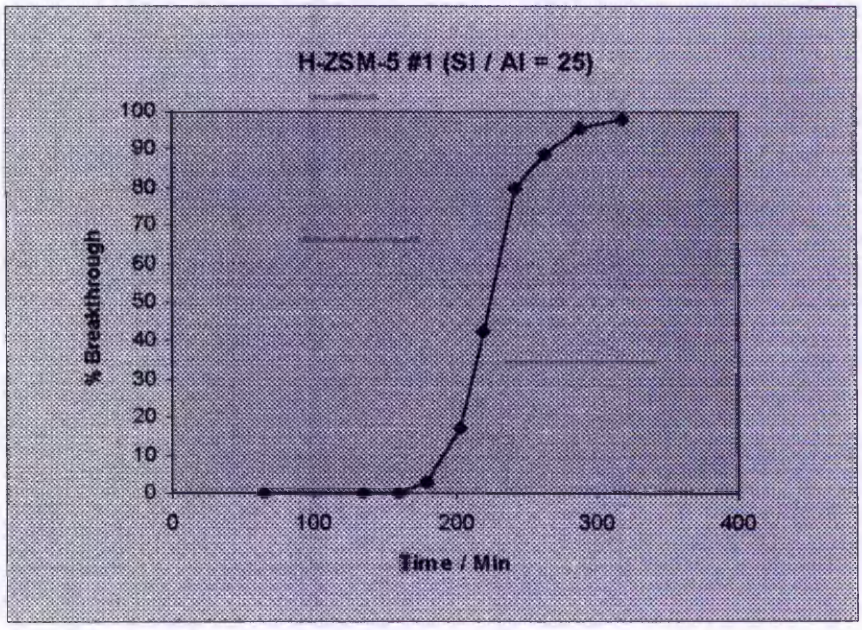

The FTIR examination of the sample after removal from the microadsorber (Fig 7.22.15) verifies the lack of coking. There is no band observed which could be assigned to coke, and the amount of pyridine adsorbed on to both types of site is almost identical to the spectra taken before microadsorption.

Fig 7.22.13 FTIR –OH Region

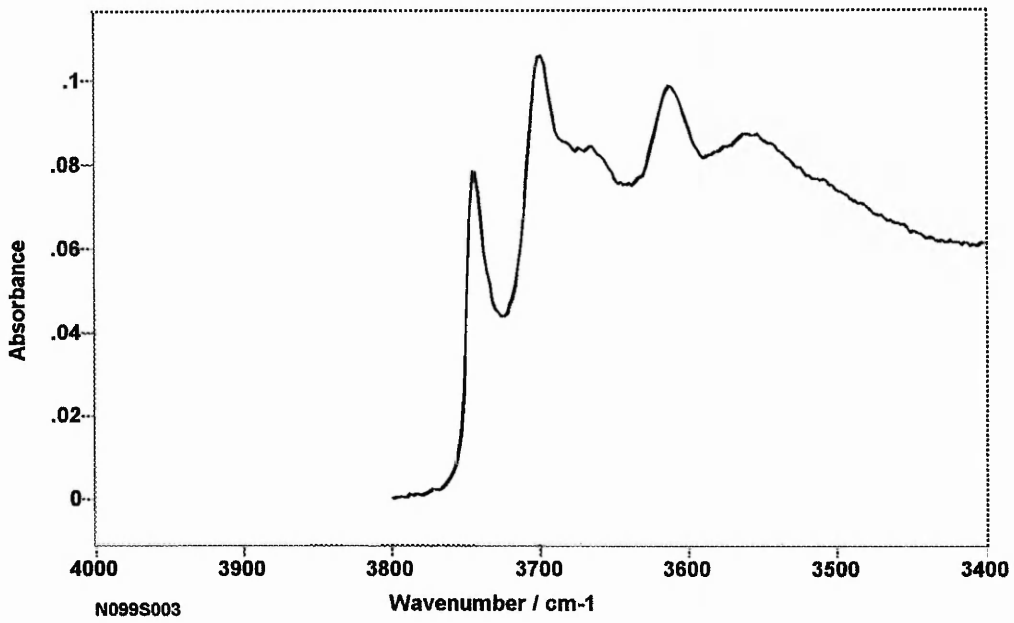

There are five absorption bands visible in the hydroxyl region of the FTIR spectrum, at 3745, 3700, 3665, 3612 and 3555 cm^{-1}. The band at 3745 cm^{-1} is the ubiquitous terminal silanol absorption. The bands at 3665 and 3612 cm^{-1} can be assigned to OH on extra-framework Al [18-20], and acidic bridging OH respectively [18,19,21,22]. The band at 3555 cm^{-1} is most likely due to hydrogen bonded Si-OH groups[21]. These may either be hydrogen bonded with other Si-OH groups, or with adsorbed water. Adsorbed water may still be present after outgasing due to the low outgasing temperature of 350°C, and may be responsible for the poorly resolved nature of the hydroxyl region in many samples. The nature of the groups giving rise to the absorption at ~3700 cm^{-1} is somewhat unclear. Warecka et. al.[21] have assigned an absorption at 3690 cm^{-1} to Al^{3+}-OH, and have not observed a band at ~3660 cm^{-1}. Other authors have reported a band at ~3660 cm^{-1} as OH on extra-framework Al, and not observed an absorption at ~3690 [18-20]. In

mordenites a similar band at 3690 cm^{-1} has been assigned to an alternative type of extra-framework Al-OH, the exact nature of which is the subject of discussion [1].

Fig 7.22.14 Nitrogen adsorption isotherms for H-ZSM-5 #1

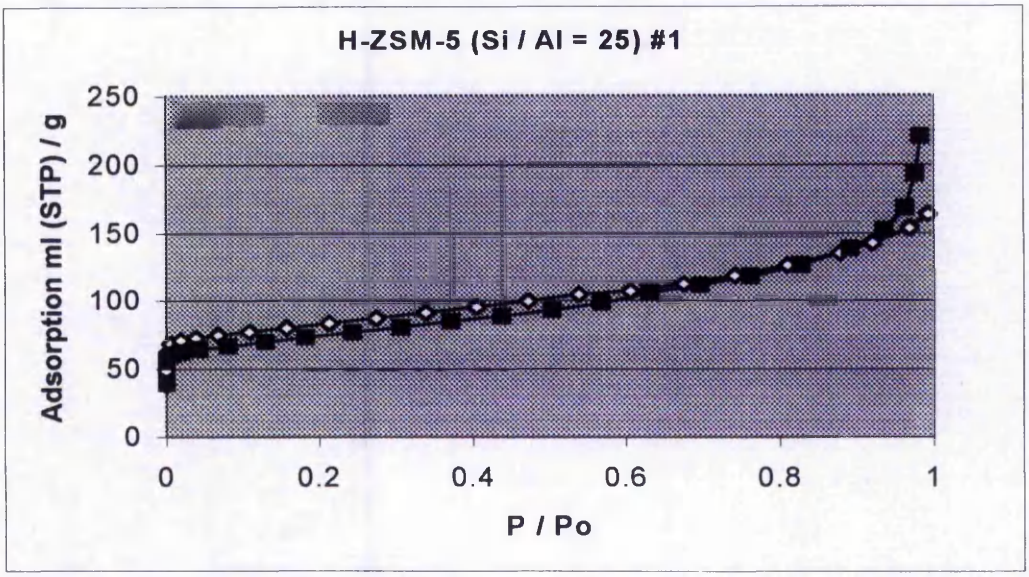

◊ isotherm before microadsorption experiment
■ Isotherm after microadsorption experiment

Fig 7.22.15 FTIR - Pyridine region and tabulated band areas after a microadsorption experiment

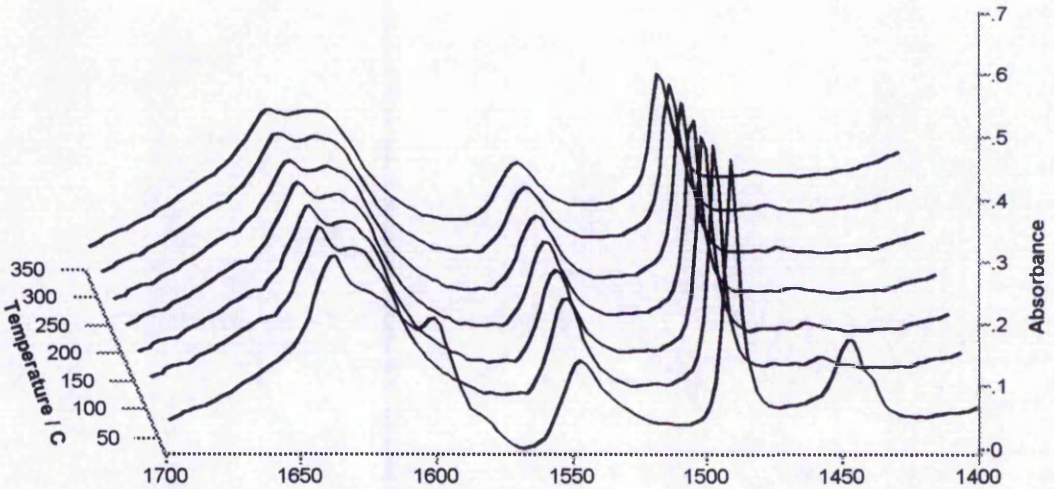

	Temperature / C	25	100	150	200	250	300	350
Assignment	cm-1							
Physisorbed	1446	6.45						
Lewis	1450	0.37	0.37	0.29	0.17	0.17	0.17	0.17
L + B	1491	12.81	10.95	10.83	10.12	9.13	8.26	7.73
Bronsted	1456	8.80	9.26	8.72	7.93	7.23	6.32	5.66
Physisorbed	1598	2.27						
Lewis	1621							
Bronsted	1639	3.47	2.64	2.19	2.07	1.61	1.32	1.12

7.22.2 Cu-H-ZSM-5

Fig 7.22.21 FTIR – Pyridine region and tabulated band areas

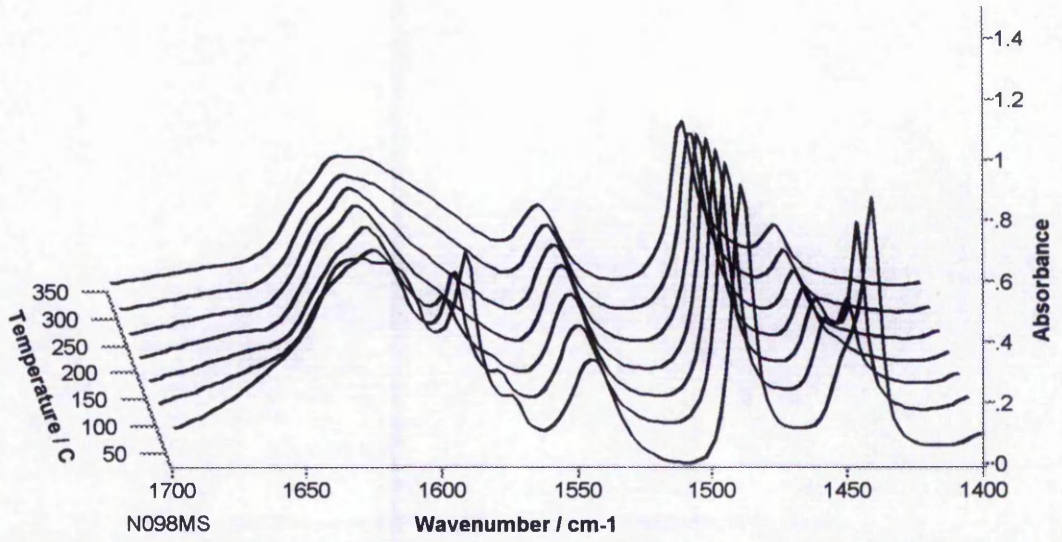

	Temperature / C	25	100	150	200	250	300	350
Assignment	cm-1							
Physisorbed	1446	8.38	5.88	2.25				
Lewis	1450	5.08	5.08	5.08	3.89	3.05	2.40	2.19
L + B	1491	12.50	11.28	10.64	10.42	9.86	9.17	8.43
Bronsted	1545	6.67	6.27	6.21	5.80	5.20	3.95	3.24
Physisorbed	1598	3.75	2.36	0.69				
Lewis	1610							
Bronsted	1639							

Fig 7.22.22 Microadsorption breakthrough vs time

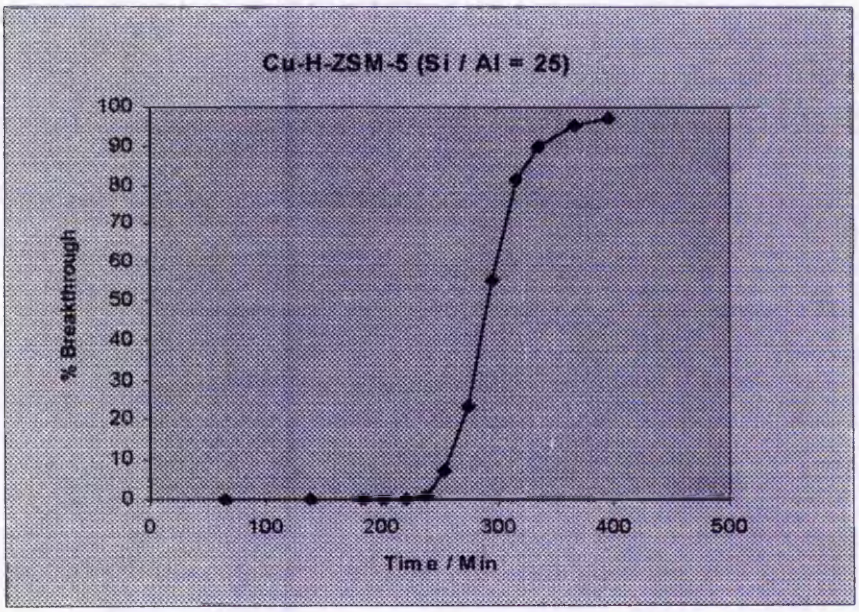

When the parent H-ZSM-5 #1 is exchanged with Cu^{2+} a significant number of Lewis acid sites are introduced. However there is still a greater amount of Bronsted acidity than Lewis. Therefore it appears that less than half of the Bronsted sites have been exchanged with Cu^{2+}, although if two H^{+} sites are exchanged with one Cu^{2+} site then more than half of the Bronsted sites may have been exchanged (assuming one Cu^{2+} site adsorbs one pyridine molecule). Alternatively some sort of $[Cu\text{-}OH]^{+}$ species is operating. This seems less likely, as a single ion-exchange with 0.05M Cu^{2+} was used, hence partial exchange is quite reasonable. The microadsorption performance shows a significant improvement upon ion-exchange, and the 50 % breakthrough time is increased to ~290 minutes. The improved performance could be due to Cu Lewis sites being better adsorption sites that Bronsted. However another explanation can be drawn from the nitrogen adsorption isotherms (Fig 7.22.23).

Fig 7.22.23 Nitrogen adsorption isotherms for Cu-H-ZSM-5

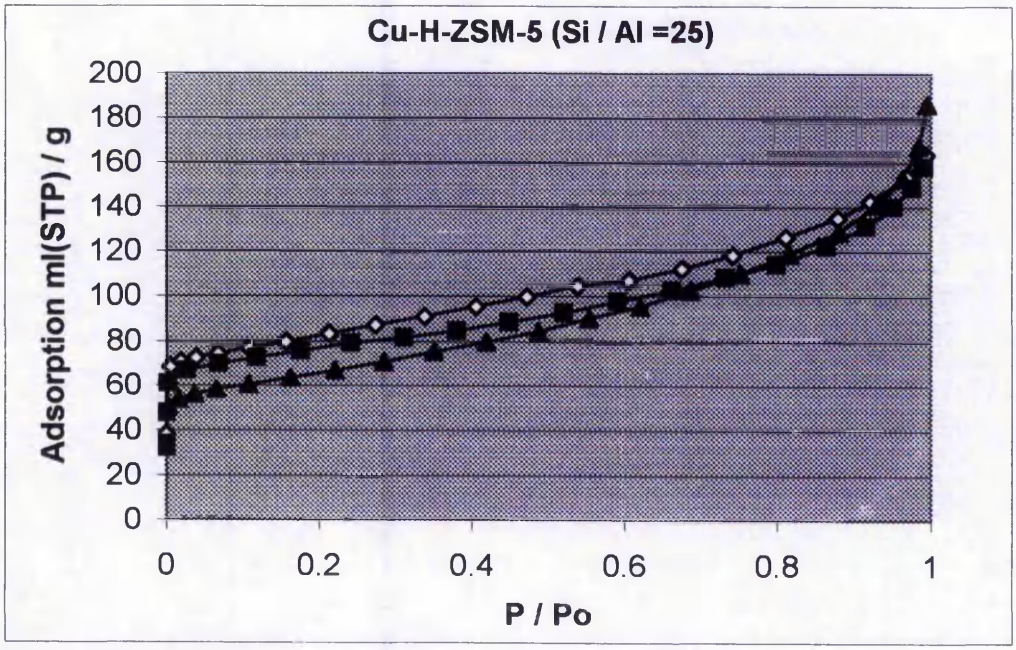

■ Before Cu^{2+} exchange

◊ After Cu^{2+} exchange and calcination (Cu-H-ZSM-5)

▲ After microadsorption experiment

Upon ion-exchange the volume of nitrogen adsorbed in the micropore filling region (P / Po < 0.05) increases. This could be due to removal of extra-framework material from the pores during the ion-exchange. Pyridine would therefore be able to access acid sites, within the pores, that were previously blocked by the presence of extra-framework material. If extra-framework material were present, external to the pores, then removal of this would also lead to an improvement in performance. This external extra-framework material would contribute mass to the sample but it would not contribute to the pore volume or be as active for pyridine adsorption as the porous zeolite structure.

Fig 7.22.24 FTIR –OH Region

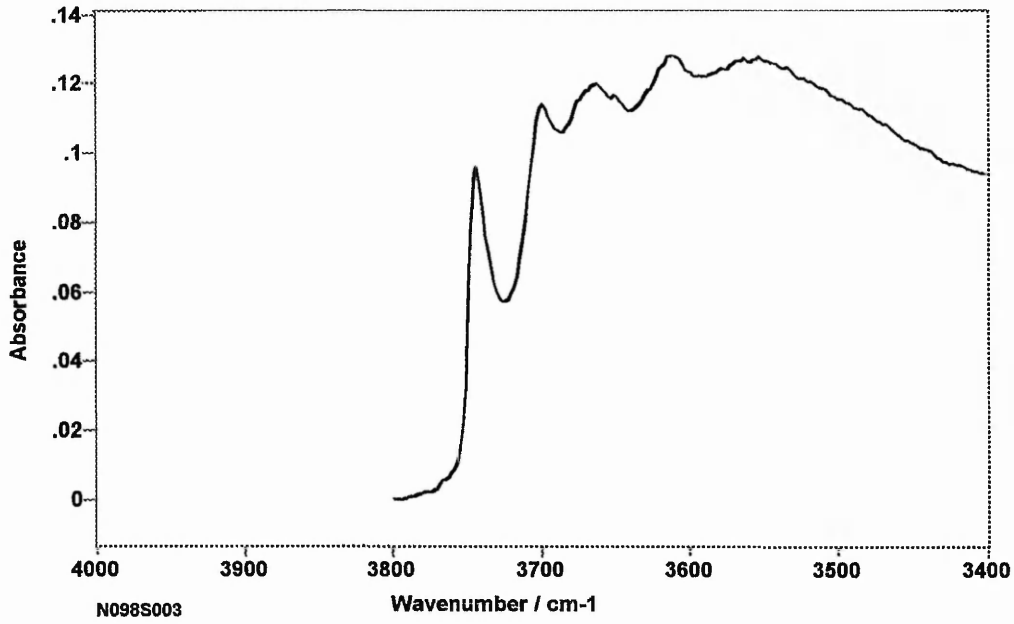

Examination of the FTIR hydroxyl region (Fig 7.22.24) supports this theory. Although the OH region is not as well resolved as in H-ZSM-5 #1, the absorption band at ~3700 cm^{-1} is particularly suppressed. The band at 3700 cm^{-1} can be assigned to Al-OH species, and so its suppression indicates the removal of extra-framework material. The band at 3612 cm^{-1} is also suppressed by the ion-exchange, and this can be explained by the replacement of Bronsted sites with Cu^{2+} sites.

Neither the nitrogen adsorption isotherm (Fig 7.22.23), nor FTIR study (Fig 7.22.25) after microadsorption, show any evidence of coking. There is no apparent 'coke band' and the pyridine adsorption bands are very similar in size before and after the microadsorption experiment. There is also only a small reduction in the pore volume accessible to nitrogen. As in the parent H-ZSM-5 sample there is a sharp uptake in the adsorption isotherm at P / Po > 0.9 in the post microadsorber sample indicating the possible formation of macropores.

Fig 7.22.25 FTIR - Pyridine region and tabulated band areas after a microadsorption experiment

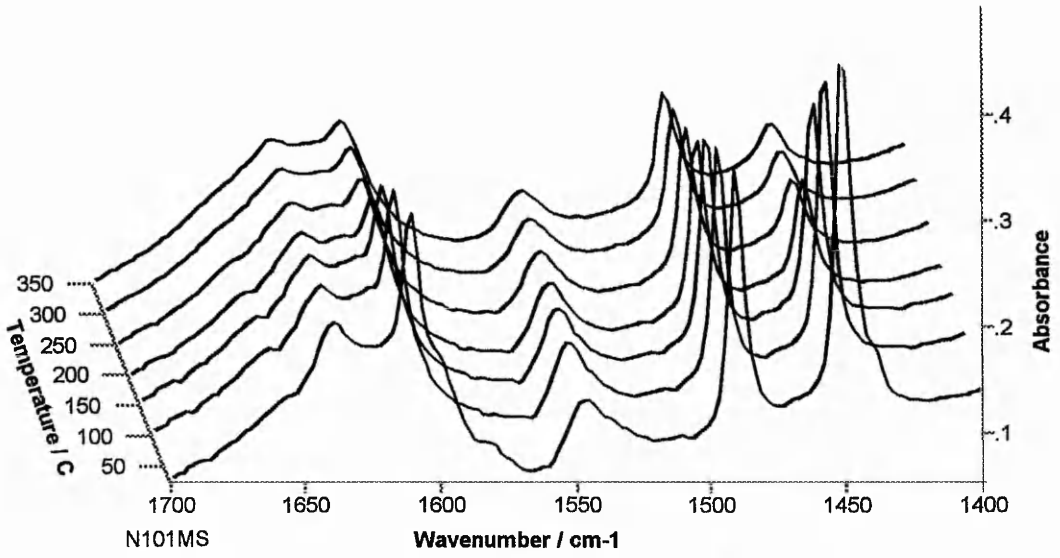

	Temperature / C	25	100	150	200	250	300	350
Assignment	cm-1							
Physisorbed	1446	17.87	11.09	6.52				
Lewis	1450	5.28	5.28	5.28	5.28	3.91	3.78	3.52
L + B	1491	12.00	10.24	9.46	8.35	7.50	6.91	6.72
Bronsted	1546	5.87	6.20	5.94	5.61	4.89	4.17	3.78
Physisorbed	1598	1.89	0.65					
Lewis	1610	5.87	5.02	4.17	3.00	2.61	2.48	2.41
Bronsted	1639	2.61	1.83	1.70	1.57	1.37	1.11	1.04

7.22.3 H-ZSM-5 #2

Fig 7.22.31 FTIR – Pyridine region and tabulated band areas

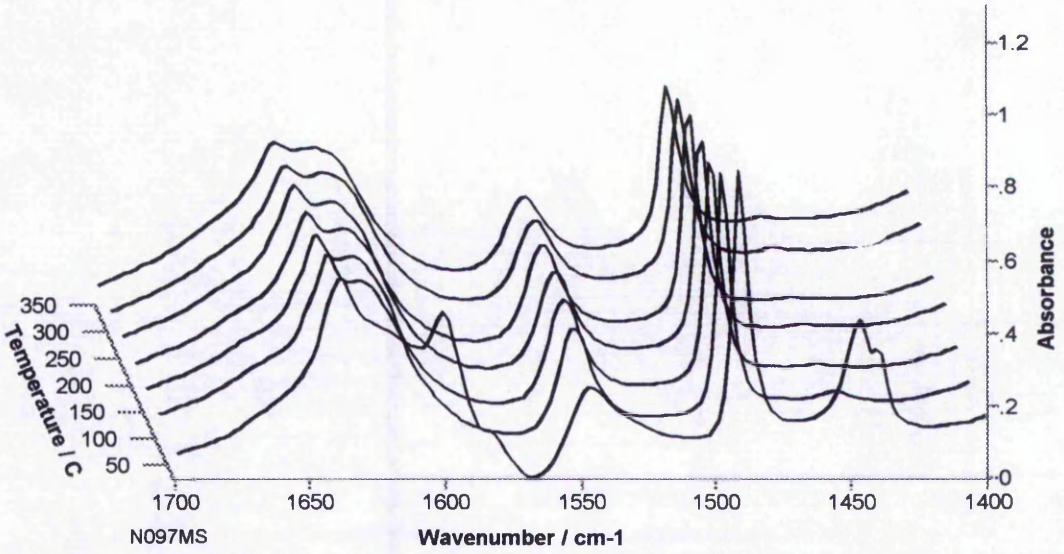

	Temperature / C	25	100	150	200	250	300	350
Assignment	cm-1							
Physisorbed	1446	9.05						
Lewis	1450	0.68	0.68	0.20	0.18	0.23	0.23	0.23
L + B	1491	13.05	10.92	10.56	10.52	10.63	9.61	9.05
Bronsted	1546	11.28	9.61	9.32	8.73	8.59	7.24	6.67
Physisorbed	1598	3.03						
Lewis	1621							
Bronsted	1639	4.98	3.17	2.87	2.49	2.49	1.92	1.76

Fig 7.22.32 Microadsorption breakthrough vs time

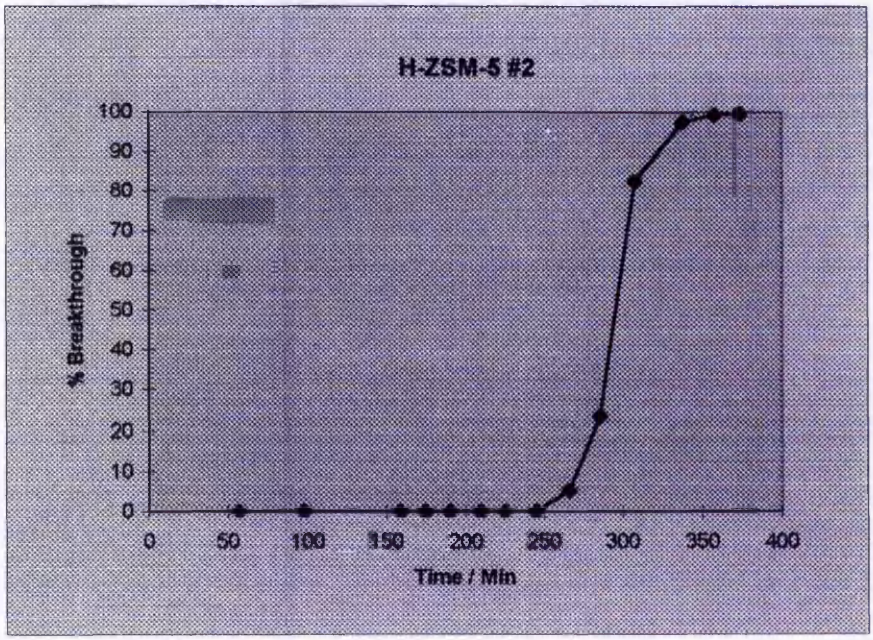

When H-ZSM-5 #1 is exchanged to H-ZSM-5 #2 the effect is very similar to the Cu^{2+} exchange. In this case, different types of acid site cannot explain changes to the adsorption properties of the sample. The zeolite appears to be almost completely protonic (Fig 7.22.31). The relative distribution of acid sites between Lewis and Bronsted is virtually unchanged from the parent sample. The total number of sites, however, appears to be very slightly higher after ion-exchange. From the nitrogen adsorption isotherms (Fig 7.22.34) it is observed that the pore volume of the zeolite available for N_2 physisorption is increased after the ion-exchange. This is the same effect that was observed in the Cu exchanged sample, but it is even more pronounced here, and is probably due to the removal of extra-framework material. Further evidence for this conclusion can be gained from examination of the hydroxyl absorbance bands (Fig 7.22.33). The hydroxyl region of the spectrum is not well resolved, but the 3614 cm^{-1} band remains prominent whilst the 3665 and 3700 cm^{-1} bands, associated with extra-framework material, have almost disappeared.

Fig 7.22.33 FTIR –OH Region

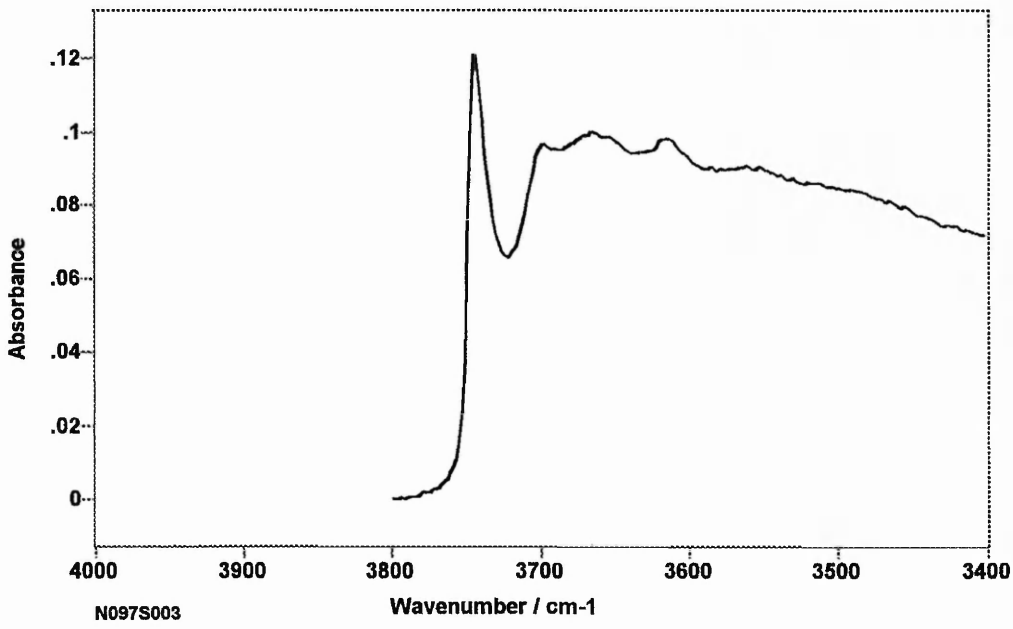

There is only a small reduction in the N_2 accessible micropore volume in the post microadsorption material. This combined with the absence of a 'coke band' in the FTIR study (Fig 7.22.35) indicates the resistance of this sample to coke formation. As in H-ZSM-5#1 and Cu-H-ZSM-5 there is a sharp uptake in the adsorption isotherm at P / Po > 0.9 in the post microadsorber sample, indicating the formation of much larger pores (Fig 7.22.34).

Fig 7.22.34 Nitrogen adsorption isotherms for H-ZSM-5 #2

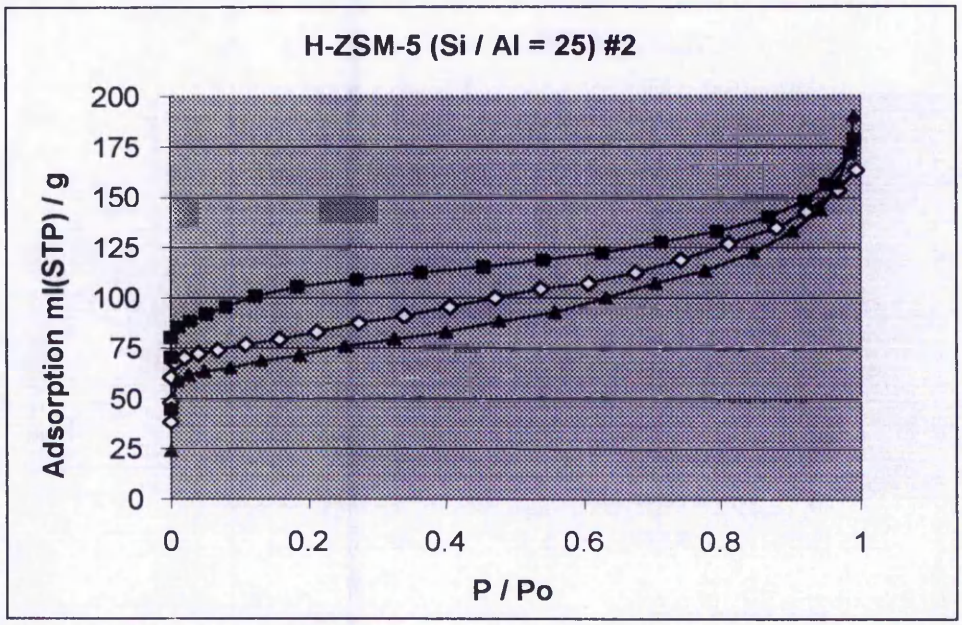

◊ Before NH_4^+ exchange; ■ After NH_4^+ exchange and calcination (H-ZSM-5 #2); ▲ After microadsorption experiment

The result of the microadsorption experiment was a 50% breakthrough time of ~ 295 minutes (Fig 7.22.32) which is almost identical to the Cu exchanged sample. It seems likely that the most important factor at work here is not the nature of the adsorption site but the quality of the pore system. Cu^{2+} and Bronsted sites appear to be equally effective for the selective adsorption of pyridine under the chosen experimental conditions. This demonstrates the importance of comparing samples with similar histories. In theory the Cu^{2+} ion exchange should lead to a reduction in the number of acid sites, and hence adsorption capacity, as one Cu^{2+} should exchange for 2 H^+ cations. It is unclear why this is not the case.

Fig 7.22.35 FTIR - Pyridine region and tabulated band areas after a microadsorption experiment

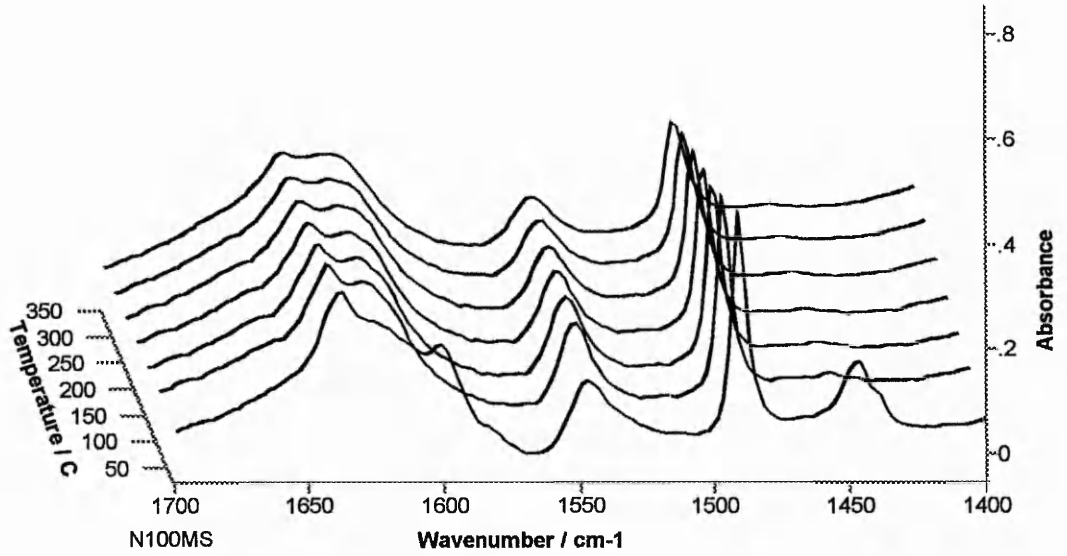

	Temperature / C	25	100	150	200	250	300	350
Assignment	cm-1							
Physisorbed	1446	6.93						
Lewis	1450	0.40	0.40	0.31	0.18	0.18	0.18	0.18
L + B	1491	13.78	11.78	11.64	10.89	9.82	8.89	8.31
Bronsted	1456	9.47	9.96	9.38	8.53	7.78	6.80	6.09
Physisorbed	1598	2.44						
Lewis	1621							
Bronsted	1639	3.73	2.84	2.36	2.22	1.73	1.42	1.20

The two comparable samples (H-ZSM-5 #2 and Cu-H-ZSM-5) have virtually identical breakthrough times. One possibility is that one Cu^{2+} can adsorb two pyridine molecules. Alternatively Cu^{2+} may have been reduced, due to thermal treatment, to Cu^{+} giving rise to an increase in the total numbers of sites. This type of process however generally requires much higher outgasing temperatures than used here [18]. A $[Cu\text{-}OH]^{+}$ species is another possibility, but this species would be expected to generate some sort of Bronsted site. There are a very large number of Lewis sites in Cu-H-ZSM-5, which cannot be associated with Cu in this form. There are also no additional bands in the OH region of the Cu-H-ZSM-5 FTIR spectra which could be assigned to such species.

7.22.4 H-ZSM-5 #3

Fig 7.22.41 FTIR – Pyridine region and tabulated band areas

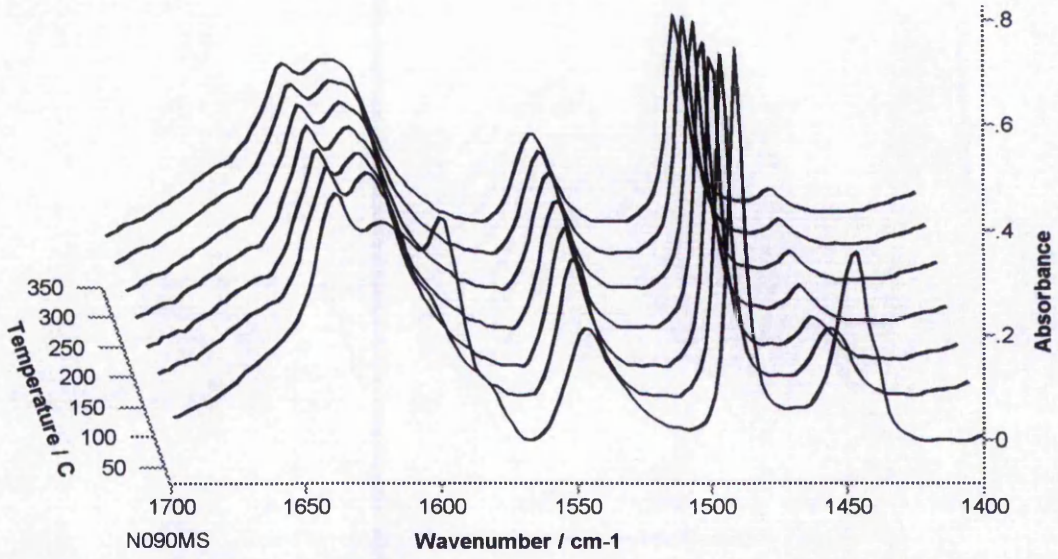

	Temperature / C	25	100	150	200	250	300	350
Assignment	cm-1							
Physisorbed	1446	27.62						
Lewis	1455	1.79	1.72	1.11	1.02	0.97	0.88	0.79
L + B	1492	31.12	28.71	26.22	23.98	23.22	21.08	19.23
Bronsted	1546	15.14	17.56	14.44	13.69	13.48	11.35	10.09
Physisorbed	1598	1385						
Lewis	1621							
Bronsted	1639	7.26	6.71	6.22	5.42	4.33	3.84	2.98

Fig 7.22.42 Microadsorption breakthrough vs time

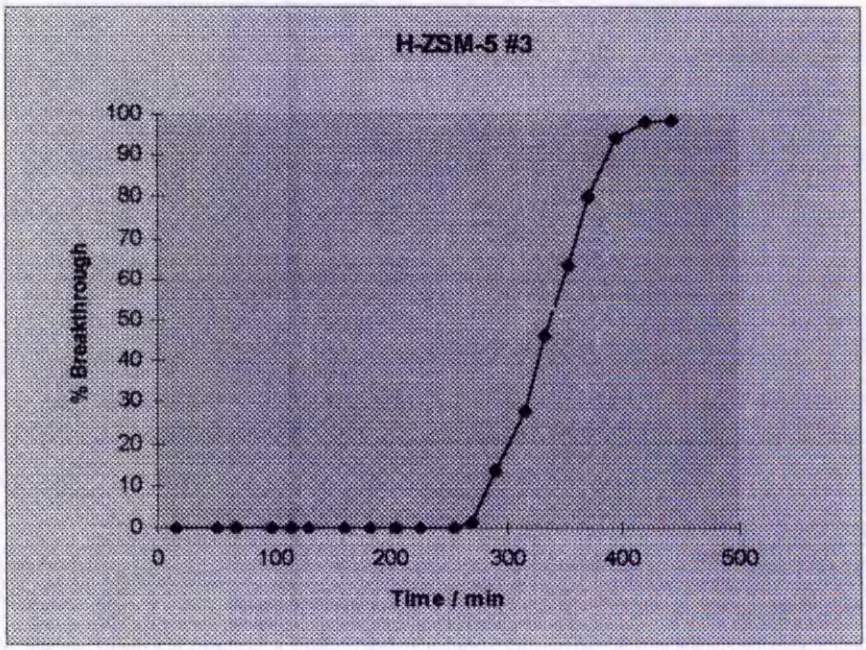

Another H-ZSM-5 (H-ZSM-5#3), with a higher aluminium content (Si / Al = 15) has also been studied. The conventional wisdom is that a zeolite with a higher aluminium content will contain more acid sites, and therefore will be a better adsorbent for basic molecules like pyridine. H-ZSM-5 #3 has not been ion-exchanged, and so it is only really comparable to H-ZSM-5 #1. The pyridine FTIR spectra (Fig 7.22.41) show the sample is in the Bronsted form, with a large number of Bronsted sites and relatively few Lewis sites. The microadsorption 50% breakthrough point was not reached until ~ 330 minutes which is equivalent to 1.9 wt % pyridine adsorption. This is higher than any of the other ZSM-5 samples. As with many of the samples studied the FTIR hydroxyl region is not perfectly resolved. As well as terminal silanol and hydrogen bonded silanol absorption bands at 3741 and 3555 cm^{-1}, there are bands assigned to acidic OH and two types of Al-OH at 3614, 3664 and 3700 cm^{-1} respectively. The acidic bridging OH band at 3614 cm^{-1} is prominent, and this is consistent with the large number of Bronsted sites observed by pyridine FTIR. The band at 3664 cm^{-1} is also quite pronounced, and confirms the presence of extra-framework Al.

Fig 7.22.43 FTIR –OH Region

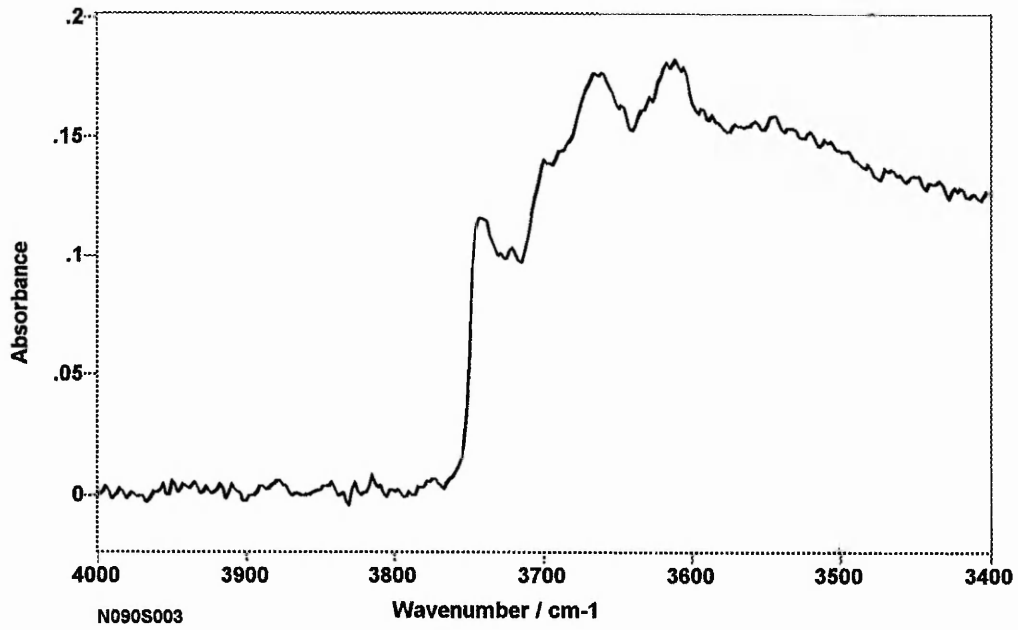

This sample is therefore similar to H-ZSM-5 #1, except for the increased aluminium content. It seems likely that if it were carefully ion-exchanged, the microadsorption performance would improve in an analogous manner to H-ZSM-5 #1. Despite the presence of extra-framework material it still has the highest number of pyridine accessible acid sites. This fact is inferred by the microadsorption breakthrough time, but is also observed directly by the pyridine FTIR. The pyridine absorption bands are larger than for any other ZSM-5 sample studied. The simple explanation is the higher aluminium content, and subsequent increase in the population of acid sites.

7.23 Zeolite X Si / Al <2

Fig 7.23.01 FTIR – Pyridine region and tabulated band areas

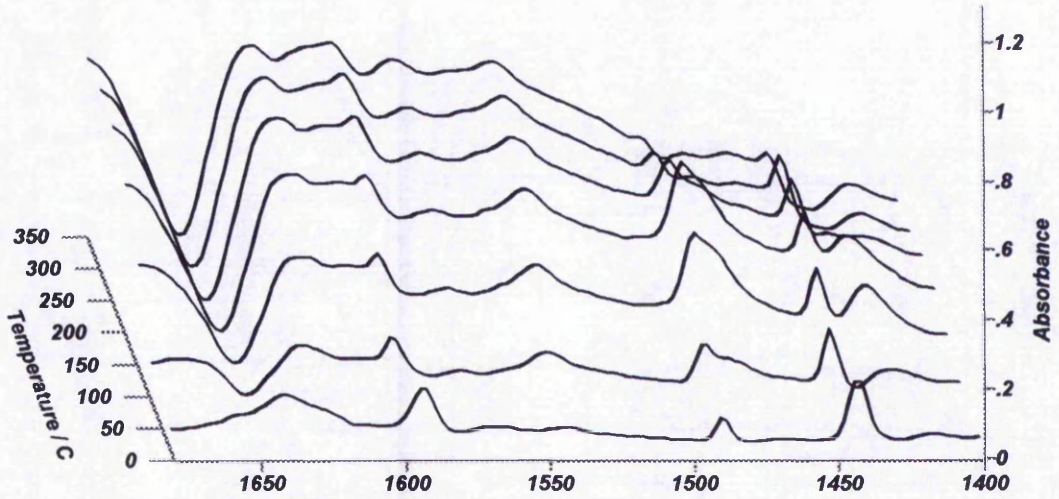

Absorbance / Wavenumber (cm-1)
File # 5 = N019M#7 @ 350

	Temperature / C	*25*	*100*	*150*	*200*	*250*	*300*	*350*
Assignment	cm^{-1}							
Physisorbed	1446	2.9286						
Lewis	1442	6.1013	5.7352	4.2099	3.5387	4.3929	3.2947	2.0317
L + B	1492	2.593	9.1519	23.795	25.015	9.7621	2.0134	0.8969
Bronsted	1547	1.8304	9.1519	12.203	12.203	10.372	6.1623	1.5863
Physisorbed	1592	5.4912						
Lewis	1600	3.6608	3.2337	2.8676	2.5015	3.6608	3.5387	2.8066
Bronsted	1639							

Fig 7.23.02 Microadsorption breakthrough vs time

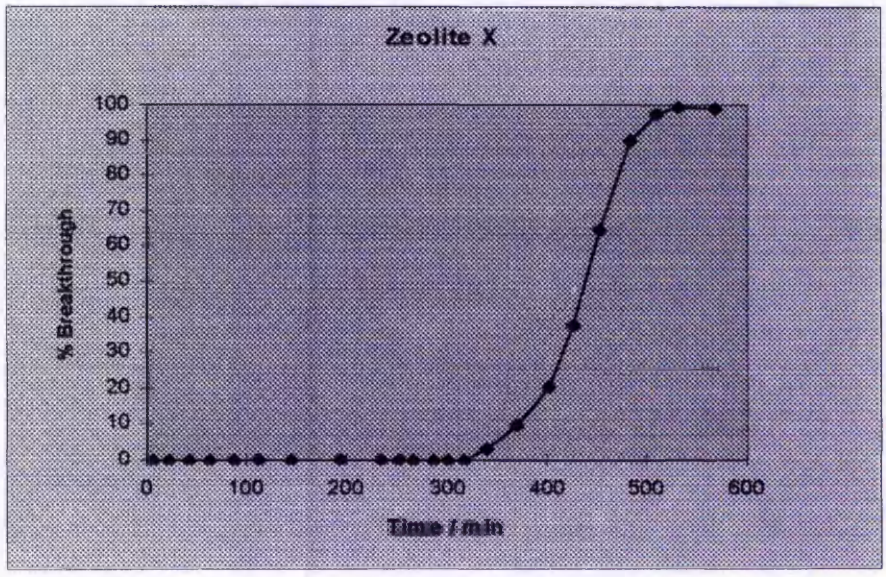

Fig 7.23.03 FTIR - Heptane coking experiment

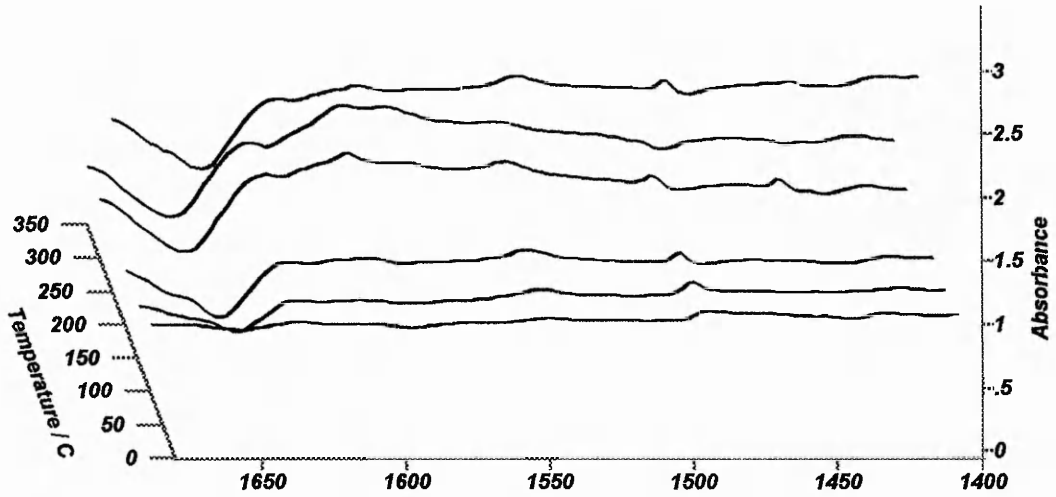

Absorbance / Wavenumber (cm-1)
File # 3 = N043M#1 @ 100

In a last series of experiments the adsorption properties of zeolite X were studied. Zeolite X is one of the most aluminium rich zeolites, and has pores more than large enough to accommodate pyridine. High aluminium zeolites are generally in an alkali metal exchanged form, often Na^+, which is the form of this material. The FTIR experiments do not look particularly promising. Although the sample does not appear to coke in the heptane FTIR experiment (Fig 7.23.03), the pyridine adsorption bands are relatively small (Fig 7.23.01). Both Lewis and Bronsted sites are present, but both are only weakly acidic, and there is notable desorption from both types of acid site as the temperature is increased. The wavenumbers of the Lewis bands are typical of the Na^+ sites found in Na-MOR-6.4.

The acidic hydroxyl bands generally associated with faujasite type zeolites, are located at ~3640 and ~3550 cm^{-1} [23-27]. The high frequency band is due to acidic OH vibrating in the large 'supercages', and the low frequency band is due to acidic OH located in sterically less accessible cavities (sodalite cages and hexagonal prisms) [23-25]. These bands are not observed in this sample. The FTIR hydroxyl region exhibits two very large absorption bands at 3695 and 3624 cm^{-1} (Fig 7.23.04). These two absorption bands are more commonly associated with

de-aluminated faujasites. The precise nature of the groups giving rise to these bands is a subject of discussion. A band at 3695 cm^{-1} has been assigned to the interaction of Na^+ with residual water[24,28], although it is only observed after high temperature evacuation. However, a similar band at 3690 cm^{-1} has been assigned to extra-framework Al-OH groups [27]. Kubelkova et. al.[29] have assigned bands at 3620 and 3630 cm^{-1}, in de-aluminated zeolite Y, to weakly or non acidic hydroxyl, and strongly acidic framework hydroxyls respectively. The nature of the band at 3624 cm^{-1} is therefore unclear.

One thing all of these bands have in common is that they are associated with dealumination of the faujasite structure. This provides strong evidence that the zeolite X has undergone a significant degree of dealumination prior to the FTIR experiment, possibly during the outgasing step where the sample was heated to 335°C. Zeolite X has a very high aluminium content, which has a detrimental effect in the stability of the framework. It may not be possible to out-gas the sample, under conditions sufficient to remove adsorbed water, without damaging the framework and removing Al. This may be especially true if the adsorbed water is partly responsible for stabilising the structure. The outgasing procedure in the microadsorption experiment is performed at the same temperature as in the FTIR cell. Therefore the sample tested in the microadsorption experiment should have been in a similar condition to the sample in the FTIR, and hence the FTIR spectra will represent the sample studied.

From the pyridine FTIR spectra, it is apparent that at least some of these hydroxyls are acidic, as a large amount of pyridine is adsorbed on some type of Bronsted sites. These Bronsted sites are not very strong, although aluminium rich zeolites like zeolite X are not generally considered to have many strongly acidic sites.

In the microadsorption experiment the 50 % breakthrough time was ~430 minutes. This is the best performance by any sample studied and correlates to an adsorption capacity of nearly 2.5 wt %. Which of the two types of site are active for the selective adsorption of pyridine is unknown. Both the Bronsted and Lewis sites

are relatively weak, but in the pyridine FTIR, they both retain pyridine at the operating temperature of 200°C. In Na-MOR-6.4 the Na sites appear to be eliminated by coke deposition, and so Bronsted sites are most likely to be responsible for the microadsorption uptake. It is possible that a similar process is operating in 13X, although there is no evidence of coking from the heptane FTIR.

Fig 7.23.04 FTIR –OH Region

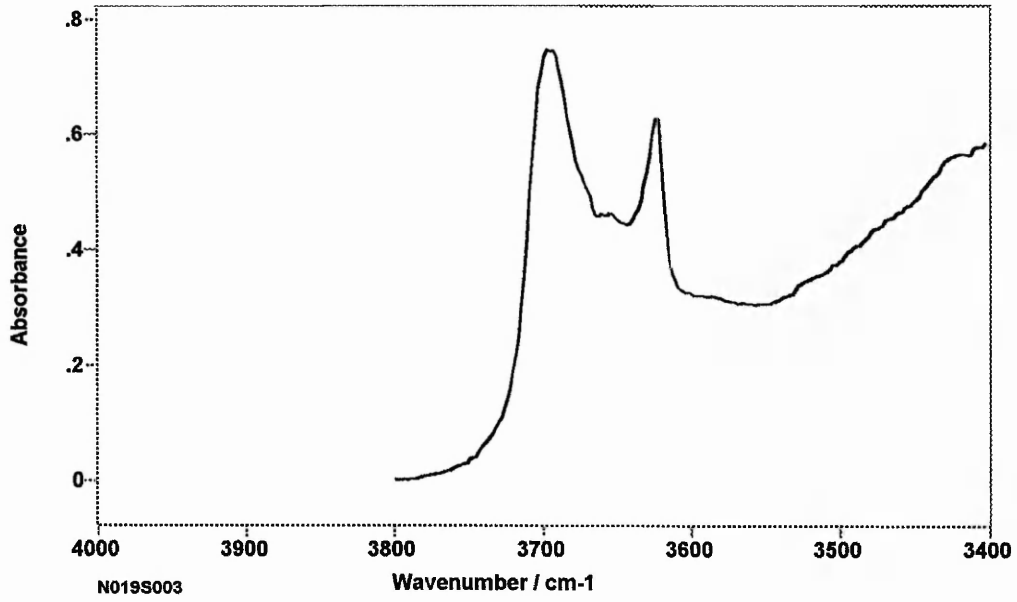

Zeolite 13X has been the most successful selective pyridine adsorbent studied. It has successfully adsorbed 2.5 wt% pyridine, despite having a large amount of extra-framework material. The large pores of the faujasite structure must be able to accommodate this extra-framework material and still allow pyridine to diffuse to acid sites. The very high aluminium content of the zeolite means that if only a small percentage of acid sites were retained after dealumination, there may still be sufficient to adsorb a relatively large amount of pyridine in the microadsorption experiment. Alternatively, acid sites associated with the extra-framework material may be directly involved.

Several attempts were made to ion-exchange zeolite X with NH_4^+ and Cu^{2+} ions. In each case the zeolite lattice collapsed and pyridine adsorption was much lower than the parent zeolite.

7.3 Summary

7.31 Mordenites

Fig 7.31.01 Band areas at 200°C and 50% breakthrough times for the mordenite samples

Sample	Lewis	Lewis / Bronsted ratio[a]	Bronsted	50% Breakthrough time (mins)
H-MOR-12.5	-	-	5.01	330
Cu-H-MOR-12.5	4.7	0.25	14.27	380
Na-MOR-6.4	18.79	3.80	3.72	55
Cu-Na-MOR-6.4 #1	5.72 +5.28[b]	1.40	5.89	200
↳ after microadsorption	10.36	1.17	6.63	-
↳ after C_7 pre-activation	1.24 + 4.47[b]	0.52	8.28	-
Cu-Na-MOR-6.4 #2	8.38	0.20	30.91	120
↳ after microadsorption	7.14	1.71	3.14	-
H-MOR-6.4	2.05	0.04	41.05	280
↳ after microadsorption	1.66	0.22	5.65	-

(a) Normalised using relative molar extinction coefficients from ref 14

(b) Na Lewis sites + Cu Lewis sites

Fig 7.31.01 summarises the breakthrough times and FTIR pyridine band areas at 200 °C for the mordenite samples. The correlation between pyridine FTIR data and breakthrough times is very difficult to resolve. Cu-Na-MOR-6.4 #2 and H-MOR-6.4 have very large adsorbed pyridine bands at 200 °C, but their microadsorption breakthrough times are relatively short. A number of factors seem to be influencing the microadsorption performance.

Fig 7.31.02 and Fig 7.31.03 show the pyridine desorption profiles, for the Lewis and Bronsted sites respectively, in the mordenite samples. The y-axis scale on the two graphs is different, with the Bronsted bound pyridine graph (Fig 7.31.03) having twice the range of the Lewis graph (Fig 7.31.02). This is indicative of the very high numbers of Bronsted sites present in some of the mordenite samples.

Fig 7.31.02 Pyridine Temperature Programmed Desorption Profiles for the mordenite samples (Lewis acid sites)

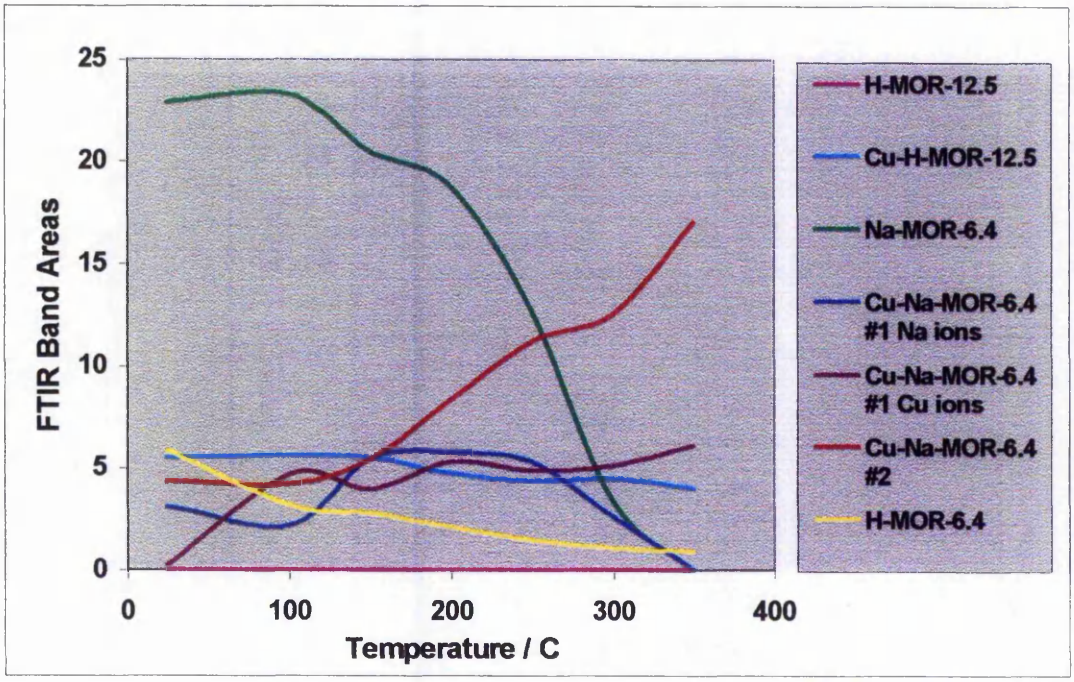

The parent H-MOR-12.5 has virtually no Lewis acid sites, demonstrating that it is almost exclusively in the 'H' form. The sample does have Bronsted sites, although not as many as some of the other mordenite samples. The Bronsted sites are strong, with pyridine being retained on nearly all the sites at 350 °C. The microadsorption breakthrough time of 330 minutes is the second longest of all the mordenite samples. This is unexpected, as the sample appears to contain only a relatively small number of acid sites. At 200 °C only Na-MOR-6.4 has fewer Bronsted sites. In addition H-MOR-12.5 has been shown to generate coke when interacting with heptane at elevated temperatures, and an OH stretching band, associated with extra-framework Al, is visible in the FTIR spectra. This sample

performed very well in the microadsorption study despite having relatively few pyridine accessible acid sites, extra-framework material and a propensity to form coke.

Ion exchanging H-MOR-12.5 with Cu^{2+} to form Cu-H-MOR-12.5 introduces a significant number of Lewis acid centres. These acid sites are strong, and there is little desorption of pyridine even at 350 °C. Unexpectedly the number of Bronsted sites has also increased. These Bronsted sites are also strong and there is virtually no desorption of pyridine in the temperature range studied. The OH region of the FTIR spectra show that the extra-framework material present in the parent sample has been removed, possibly by the aqueous ion-exchange procedure. The heptane FTIR experiment shows that this sample also has much less of a tendency to form coke. As would generally be anticipated the combination of many more acid sites, less extra-framework Al and less coke formation has led to an improvement in the microadsorption performance. The 50% breakthrough time has been increased to 380 minutes.

Fig 7.31.03 Pyridine Temperature Programmed Desorption Profiles for the mordenite samples (Bronsted acid sites)

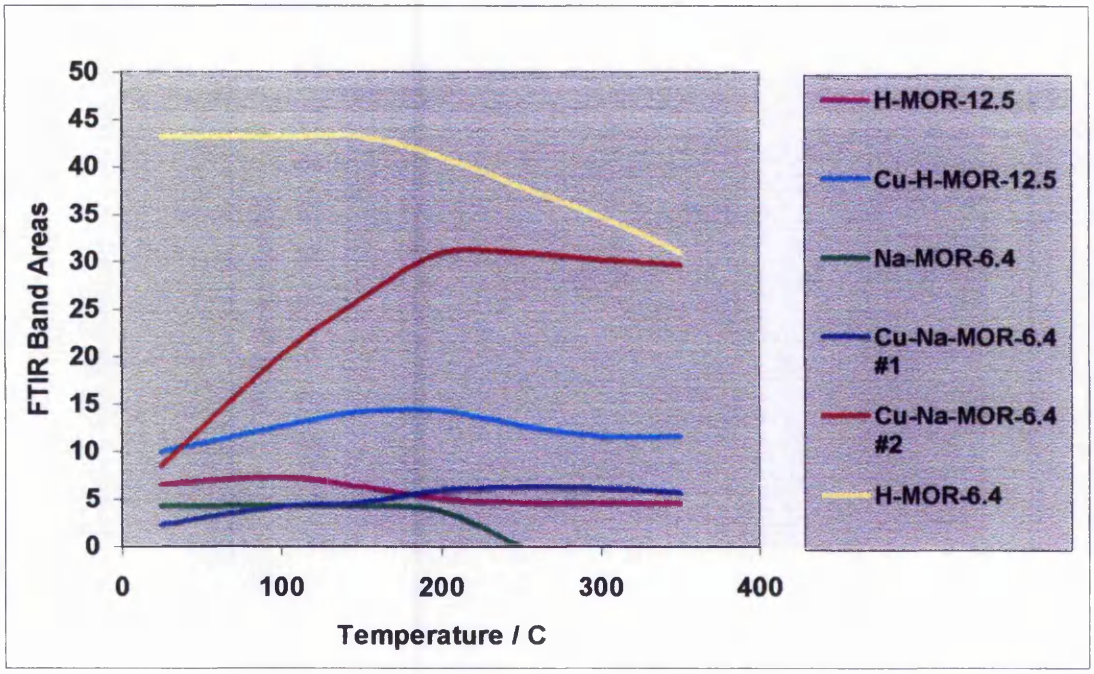

Perhaps the most striking feature of Fig 7.31.02, is the very large amount of Lewis bound pyridine on Na-MOR-6.4 at low temperatures, and the rapid desorption above 200 °C. Whereas the Lewis sites in Cu-H-MOR-12.5 are probably associated with Cu cations, the Lewis sites in Na-MOR-6.4 are Na sites, and these are only weakly acidic. There is complete desorption from these sites by 350 °C. The much smaller number of Bronsted sites are also only weakly acidic and follow a similar desorption profile. The microadsorption breakthrough time of 55 minutes is the shortest of all the mordenite samples. The most likely explanation for this is simply the weak nature of both the Bronsted and Lewis acid sites. The heptane FTIR coking study is inconclusive, but does suggest that there may be some coke deposition when the sample is exposed to a hydrocarbon at elevated temperature. The assessment of extra-framework Al from the FTIR OH region is also inconclusive due to the high frequency of the bridging OH band. It is therefore unclear whether coking, or extra-framework material influence the microadsorption breakthrough time, or if the weak acid sites is the primary factor.

Cu-Na-MOR-6.4 #1 and #2 are both derivatives of Na-MOR-6.4, prepared by ion-exchanging with Cu^{2+}. Cu-Na-MOR-6.4 #1 has been partially exchanged, and has a mixture of Na and Cu Lewis sites. As in Na-MOR-6.4 the Na sites are weak, with pyridine being completely desorbed by 350 °C. The Cu sites are stronger, retaining pyridine at 350 °C. In addition, the sample has a similar number of Bronsted sites, which are also strong. The nature of these Bronsted sites is unknown, as both Cu and Na should form Lewis sites, but there is a band in the FTIR spectra at 3632 cm^{-1} which can be assigned to acidic bridging OH. The amount of pyridine adsorbed on all three types of site increases with increasing temperature. For the Cu sites this increase continues throughout the temperature range studied and there is more adsorbed pyridine on Cu sites at 350 °C than at any other temperature. The pyridine bound to Na and Bronsted sites reaches a maximum at around 200 and 250 °C respectively. Above this temperature the Bronsted bound pyridine is stable, but pyridine is desorbed from the Na sites due to their weak nature. This increase in adsorption at higher temperatures indicates some sort of diffusion limitation, i.e. many of the acid sites only become

accessible to pyridine at higher temperatures. This might be due to occlusion of some of the pores by extra-framework material, although there is no evidence for extra-framework material in the FTIR spectra. Interestingly, the sum of the Cu, Na and Bronsted sites is less than the number of Na sites present in Na-MOR-6.4, indicating that pyridine may be excluded from many acid sites even at the highest temperature used in this study. The microadsorption performance is improved in comparison with the parent Na-MOR-6.4, with the 50% breakthrough time almost quadrupling to 200 minutes. Although the FTIR spectra after the microadsorption experiment show little evidence for coke formation, the FTIR coking experiment with heptane does show the introduction of a band at ~1585 cm^{-1} which can be assigned to coke. In addition the post microadsorption spectra show very little pyridine bound to Na Lewis sites. A further experiment where the sample was 'pre-activated' with heptane at 350 °C, before a pyridine FTIR experiment, confirmed that the Na Lewis sites were effectively deactivated for pyridine adsorption by this treatment. This suggests selective coke formation on the Na sites making them inaccessible to pyridine. As with the other mordenite samples, N_2 adsorption isotherm data has shown a complete suppression of the micropore filling region, after the microadsorption experiment, indicating that the internal pore volume of the zeolite is inaccessible to nitrogen.

Cu-Na-MOR-6.4 #2 has been more extensively exchanged than Cu-Na-MOR-6.4 #1 and there are no remaining Na acid sites observed by FTIR. There are a very large number of Bronsted sites present in this sample. This is unexpected, as exchanging Na-mordenite to Cu-mordenite should exchange Na^+ Lewis sites for Cu^{2+} Lewis sites. Considering the differing extinction coefficients there are more than twice as many Bronsted sites as Lewis. Both the Lewis and Bronsted sites exhibit the same diffusional effect seen with Cu-Na-MOR-6.4 #1. The amount of adsorbed pyridine increases with increasing temperature. The Lewis bound pyridine increases with each temperature increment to a maximum at 350 °C, but there may be more sites that become accessible at even higher temperatures. The Bronsted bound pyridine reaches a maximum at 200 °C, as is the case with Cu-Na-MOR #1, and is then stable to 350 °C. The exact nature of the Bronsted sites

is unknown, and it is possible that some sort of $[Cu\text{-}OH]^+$ species is involved. There is a band in the hydroxyl region of the spectra at 3623 cm^{-1}, which can be assigned to acidic bridging hydroxyls, so at least some of the Bronsted sites are of this form. The microadsorption breakthrough time of 120 minutes is shorter than that of Cu-Na-MOR-6.4 #1. The reason for this is unclear, considering the very large number of pyridine accessible acid sites, although the FTIR reveals the presence of extra-framework aluminium and coke formation in the post microadsorption sample.

H-MOR-6.4 has also been ion-exchanged from Na-MOR-6.4. There are relatively few Lewis acid sites remaining, indicating a high level of exchange. These Lewis sites are probably associated with Na cations, and seem weak, although at least some of these sites are stronger than those in Na-MOR-6.4. Around 20% retain pyridine at 350 °C. Either these Lewis sites are not Na^+ cations i.e. are generated by the dehydration of Bronsted sites, or the introduction of H^+ sites has increased the strength of the remaining Na Lewis centres. The later seems more likely. There are a very large number of Bronsted acid sites, as might be expected for a zeolite in the H^+ form. Many of these sites are strong and approximately 75% retain pyridine at 350 °C. FTIR has identified extra-framework Al present in the material, and this is consistent with the amorphous element observed by XRD. Despite this there are no signs of the diffusional problems effecting the other samples exchanged from Na-MOR-6.4. Lewis bound pyridine desorbs steadily with each increment above room temperature, whilst Bronsted bound pyridine is stable to 150 °C, and then there is a small desorption with each temperature increment. The microadsorption performance (280 minutes) is much improved over the other Na-MOR-6.4 derived samples. After regeneration at 650 °C the microadsorption capacity is reduced to virtually zero. The pyridine FTIR spectra of the sample, after the second microadsorption experiment, are consistent with the low adsorption capacity. Very little pyridine is observed adsorbed on the sample, and there is a large absorption feature that can be assigned to coke formation. The nitrogen adsorption isotherm after the microadsorption

experiments is also consistent with the loss in adsorption capacity, as the internal pore volume is inaccessible to nitrogen.

7.32 ZSM-5s

Fig 7.32.01 and Fig 7.32.02 show the pyridine desorption profiles, for the Lewis and Bronsted sites respectively in the ZSM-5 samples. The y-axis scale on the two graphs is different, with the Bronsted bound pyridine graph (Fig 7.32.02) having a larger range. This is because the Cu-H-ZSM-5 is only partially exchanged whereas the other samples are almost exclusively in the H form.

Fig 7.32.01 Pyridine Temperature Programmed Desorption Profiles for the ZSM-5 samples (Lewis acid sites)

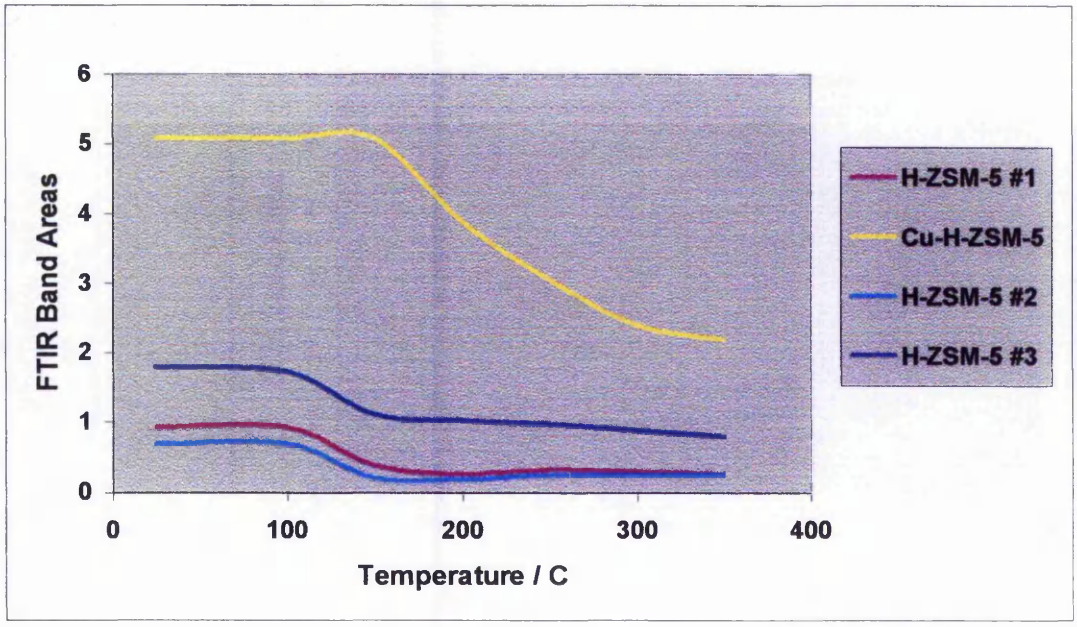

The profile of pyridine desorption from the Lewis sites is very similar for all the ZSM-5 samples. Adsorbed pyridine is stable to 100 °C, but then in all four ZSM-5 samples there is significant desorption between 100 and 150 °C. With the H-ZSM-5s the remaining Lewis bound pyridine is stable to 350 °C. With Cu-H-ZSM-5 there is a small amount of further desorption at each temperature

increment. In all cases approximately 50% of the pyridine observed at room temperature is still present at 350 °C. The desorption profiles indicate that in all samples approximately 50% of the Lewis sites are of weak strength, but the remaining sites are all strongly acidic.

The profile of desorption from Bronsted acid sites is also similar for each of the ZSM-5 samples. A small amount of pyridine desorbs at each temperature increment, leaving approximately 60 –70% retained at 350 °C. The increase in Bronsted bound pyridine at 100 °C may indicate a diffusion limitation, but if this was the case the effect should be observed for the Lewis bound pyridine. It is possibly due to difficulties measuring the integrated band area accurately.

Fig 7.32.02 Pyridine Temperature Programmed Desorption Profiles for the ZSM-5 samples (Bronsted acid sites)

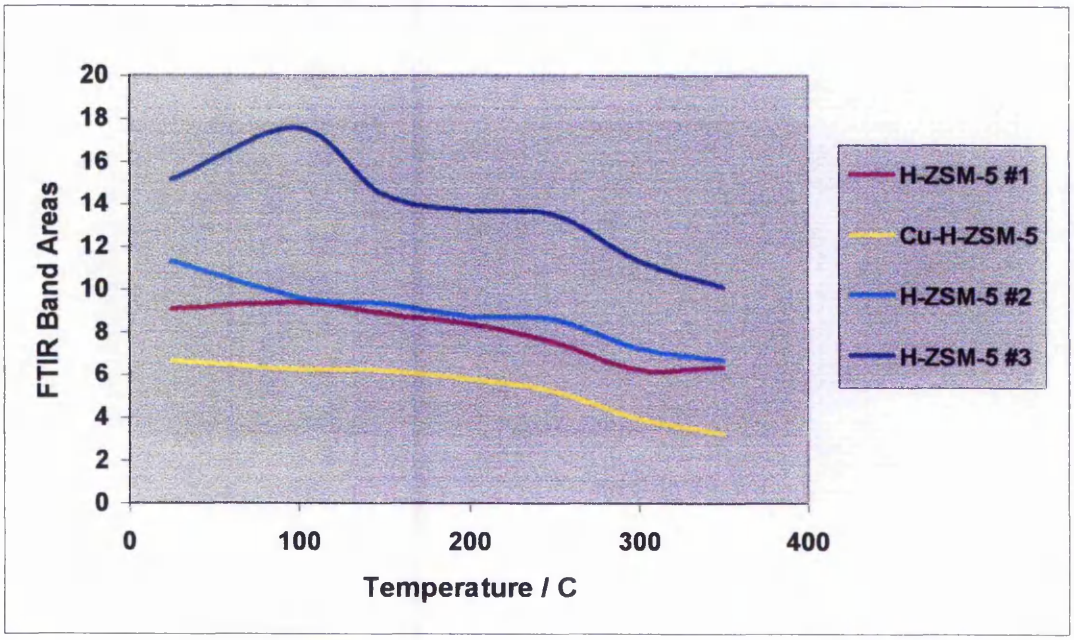

Cu-H-ZSM-5 has by far the greatest number of Lewis sites, but also has the least Bronsted sites. This is expected, since the Cu^{2+} ion exchange should form Cu Lewis sites at the expense of Bronsted sites. The three H-ZSM-5s have similar ratios of Lewis to Bronsted sites, but H-ZSM-5 #3 has more acid sites, of both

types, than the other two. This is simply a result of the higher aluminium content of this sample (Si / Al = 15). H-ZSM-5 #2 and the parent H-ZSM-5 #1 have very similar numbers of both types of site. H-ZSM-5 #2 has marginally fewer Lewis sites, but a slightly higher number of Bronsted sites. This may be due to the ion exchange procedure, re-hydrating Lewis sites to Bronsted sites, or possibly removing a small number of cations, which give rise to Lewis sites.

Fig 7.32.03 summarises the breakthrough times and FTIR pyridine band areas at 200 °C for the ZSM-5 samples. There is a very good correlation between the band areas and breakthrough times, indicating that for these samples, pyridine FTIR is an excellent technique for the characterisation of adsorption properties.

Fig 7.32.03 Band areas at 200°C and 50% breakthrough times for the ZSM-5 samples

Sample	Si / Al ratio	Lewis	Lewis / Bronsted ratio (a)	Bronsted	50% Breakthrough time (min)
H-ZSM-5 #1	25	0.26	0.02	8.38	220
Cu-H-ZSM-5	25	3.89	0.50	5.8	290
H-ZSM-5 #2	25	0.18	0.015	8.73	295
H-ZSM-5 #3	15	1.02	0.06	13.69	330

(a) Normalised using relative molar extinction coefficients from ref 14

H-ZSM-5 #1 performed well in the microadsorption experiment. The 50% breakthrough time of 220 minutes corresponds to an adsorption capacity of ~ 1.3 wt %. Ion exchanging H-ZSM-5 in an aqueous solution of Cu^{2+} or NH_4^+ led to an increase of 70 – 75 minutes in the breakthrough time, regardless of the exchanging cation. In ZSM-5, both Bronsted and Cu sites appear to be very effective for the selective adsorption of pyridine. The improvement in performance may be attributed to the removal of extra-framework material. Removal of extra-framework material from the pores will allow pyridine to diffuse through the

pores more easily, and will expose previously inaccessible acid sites. Removal of extra-framework material, which is external to the pore structure, will also improve performance because it will contribute to the mass of the zeolite, and if it does not contribute to pyridine adsorption, then this will reduce the wt % adsorption value. H-ZSM-5 #3 has a higher aluminium content than the other ZSM-5 samples studied and consequently has a larger number of acid sites. With the exception of the size of the absorption bands the FTIR spectra are similar to the other H-ZSM-5 samples. The larger numbers of acid sites are responsible for an increase in the breakthrough time to 330 minutes. This sample has not been ion exchanged and so should only be directly compared to H-ZSM-5 #1. Ion exchanging this sample may lead to an improvement in performance analogous to that observed with H-ZSM-5 #1.

FTIR studies with heptane, and post microadsorption FTIR spectra show no indication of coke formation in any of the ZSM-5s. In addition, nitrogen adsorption isotherms after the microadsorption experiments show very little loss in pore volume. The pore structures are still highly accessible to N_2.

7.33 Zeolite X

Fig 7.33.01 Pyridine Temperature Programmed Desorption Profiles for Zeolite X

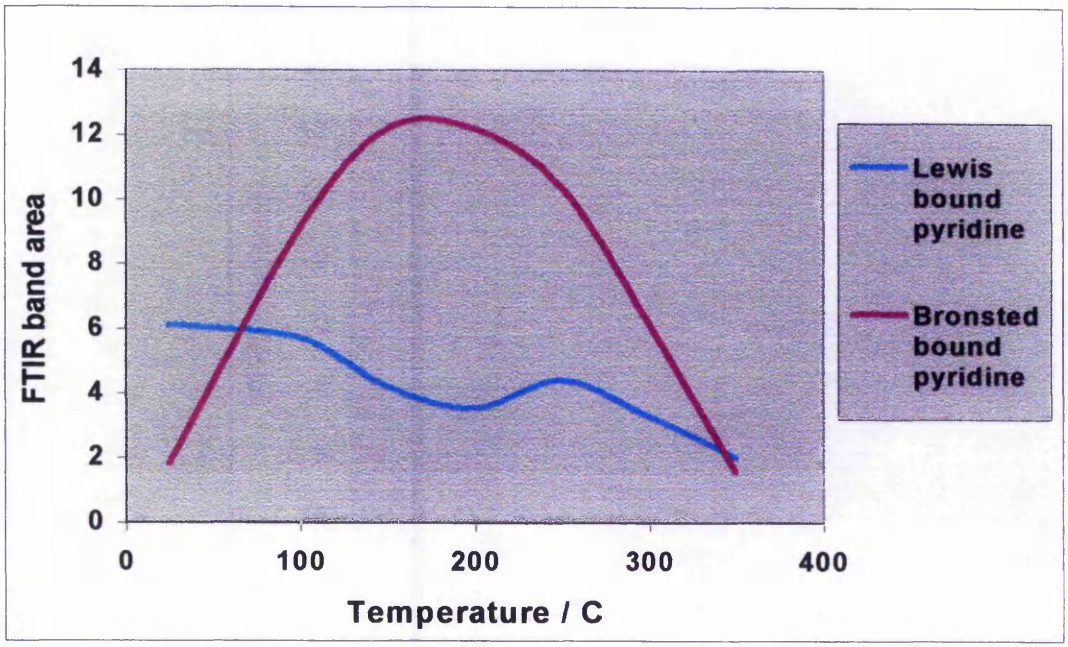

Fig 7.33.01 shows the pyridine TPD profiles for zeolite X. Lewis bound pyridine desorbs with each temperature increment, indicating that these sites have a range of acid site strengths. The Lewis sites are generally weak, with only one third of the pyridine present at room temperature being retained at 350°C. The stepwise desorption profile and increase at 250°C may be due to difficulties measuring the integrated band area accurately. The Bronsted bound pyridine desorption profile is unusual. There is a six-fold increase in Bronsted adsorbed pyridine between 25°C and 200°C, but all of this additional pyridine then desorbs by 350°C. There appears to be a large number of weak Bronsted acid sites, from which pyridine is desorbed by 350°C, and a much smaller number of stronger Bronsted sites. The increase in adsorbed pyridine as the temperature is raised from 25°C to 200°C could be due to extra-framework material limiting the diffusion of pyridine through the pore structure. Examination of the FTIR hydroxyl region indicates the sample has undergone extensive dealumination. Alternatively it could be caused by the displacement of adsorbed water, by pyridine, as the temperature is

caused by the displacement of adsorbed water, by pyridine, as the temperature is increased. As the sample has undergone dealumination the nature of the Bronsted sites is unknown. There are no bands in the FTIR OH region that can be assigned to traditional Bronsted sites. Despite the loss of structural integrity, the sample performed very well in the microadsorption study. The 50% breakthrough time of 430 minutes corresponds to a pyridine adsorption capacity of ~ 2.5 wt%, which was the highest recorded for any sample studied.

Fig 7.33.02 Band areas at 200°C and 50% breakthrough time for 13X

Sample	Lewis	Lewis / Bronsted ratio (a)	Bronsted	50% Breakthrough time (min)
13 X	3.54	0.22	12.2	430

(a) Normalised using relative molar extinction coefficients from ref 14

Fig 7.33.02 shows the band areas at 200°C for zeolite X, as well as the 50% breakthrough time. These band areas are not particularly large in comparison with some of the other samples, and so the FTIR pyridine study cannot account for the high adsorption capacity. Zeolite X is clearly subject to other factors, which influence the adsorption capacity, under the conditions of the microadsorption experiment.

7.4 Conclusions

Fig 7.4.01 is a plot of 50% breakthrough time vs Si / Al ratio. With the exception of the four mordenites with Si / Al ratio 6.4, there is a reasonably good trend of increasing breakthrough time with decreasing Si / Al ratio. These samples are the Na-mordenite and its derivatives. The Na-mordenite itself has a large number of Na^+ acid sites. The weak nature of these sites may be the single most important factor limiting the adsorption capacity. The samples derived from Na-mordenite have been ion exchanged to various degrees of substitution, but even those samples where Na appears to have been completely removed, and replaced with much stronger sites, fail to perform to the level of the trend-line.

Fig 7.4.01 50% Breakthrough times vs Si / Al ratios for the zeolite samples

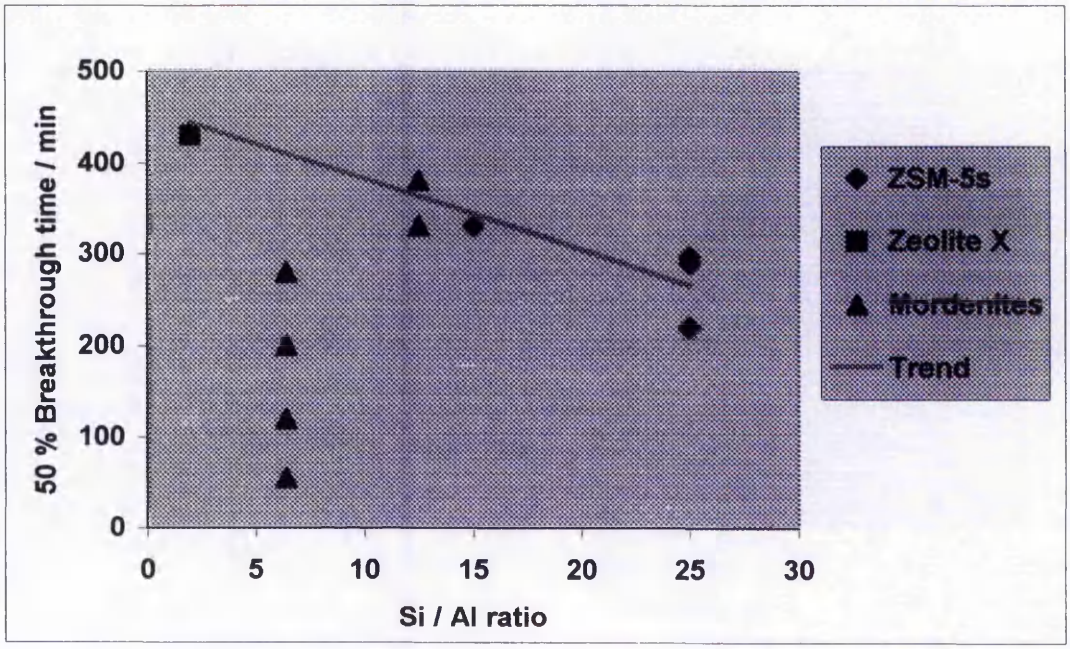

These Na-mordenite derived samples all exhibit very large adsorbed pyridine bands in the pyridine FTIR spectra, and this is consistent with the low Si / Al ratio. These bands are much larger than those in the higher silica mordenites, but the microadsorption breakthrough times are much shorter, indicating much lower adsorption capacities under the chosen experimental conditions. The most likely

source of this deficit is probably coke formation. The nitrogen adsorption isotherms confirm that after the microadsorption experiment the accessible pore volume is virtually zero. Coking is a very complex phenomenon, which is not yet fully understood. Extra-framework material may also play a role, as it is undoubtedly present in many of these materials. The one-dimensional pore structure of mordenite is very sensitive to extra-framework material and coke deposition. A small amount of either can block access to a very large number of sites. The effective elimination of Na^+ sites after interaction with a hydrocarbon suggests that they may be involved in coking. The relatively poor performance of the Na-mordenite derived samples supports this idea. The other two mordenites (H-mordenite and Cu-H-mordenite) fit well with the general trend, despite some extra-framework material and coke formation. In this case extra-framework material has been removed by aqueous ion exchange which resulted in increased adsorption capacity.

The mordenite structure does not appear to be a good choice for the selective adsorption of pyridine. There is nothing fundamentally wrong with the structure, and H-MOR-12.5 and Cu-H-MOR-12.5 have performed well. However mordenite appears to be very sensitive to other factors. The presence of Na^+ ions, even in very small quantities has a profoundly detrimental effect on the performance. All the samples derived from the Na-mordenite appear to generate coke, to the extent that the pore volumes become inaccessible to nitrogen. A further complicating factor is the inability of pyridine to enter the side pockets in the mordenite pores. Hence the pyridine FTIR spectra only probe the straight pore channels, and the nature of acid sites in the side pockets is unknown. As mordenites have been shown to ion exchange in the main channels first, this means that the extent of exchange cannot be determined by pyridine FTIR.

With careful control of the counterbalancing cations and extra-framework material mordenites might have some potential for selective adsorption of base molecules. However it is difficult to imagine them being successfully regenerated at high temperatures without a large amount of coke build up. The structure appears to be

prone to coke formation, whilst at the same time is very sensitive to the presence of coke.

The ZSM-5 zeolite structure has proven itself to be highly resistant to coke formation. The two dimensional pore structure appears to be much better suited to applications involving hydrocarbons than the effectively one-dimensional structure of mordenite. After the microadsorption experiments the pore volumes are still highly accessible. Small amounts of extra-framework Al do not have a major effect on performance, although removal through aqueous ion exchange does increase adsorption capacity slightly. In ZSM-5, Cu^{2+} and H^{+} acid sites are both effective for pyridine adsorption. The use of pyridine as an FTIR probe molecule is a very useful characterisation technique for ZSM-5. Pyridine can reach all of the acid sites and the spectral data correlate well with the microadsorption results. Highly crystalline ZSM-5s with Si / Al ratios of less than 15, could be very promising for this type of application.

High aluminium zeolites also appear to show a lot of potential. Their relatively weak acid site strength reduces the likelihood of coking, and the large numbers of acid sites confer high adsorption capacities. Zeolite X has proven to be an effective pyridine adsorbent, even when extensively de-aluminated. As Na^{+} Lewis sites do not appear to be effective, it may be beneficial to generate a high aluminium zeolite in the H^{+} form. Zeolite X is probably unstable in the H^{+} form and so zeolite Y is potentially very interesting. Zeolite Y has the same three dimensional pore structure as zeolite X (faujasite) but has a slightly higher Si /Al ratio. Zeolite Y should be more stable than Zeolite X and so could be studied in the H^{+} form without the extensive dealumination that affected zeolite X in this study.

7.5 References

1) Borade, R. B. and Clearfield, A., *Studies in surface science and catalysis, Vol. 84., Zeolites and Related Microporous Materials: State of the Art 1994,* Weitkamp, J., Karge, H. G., Pfeifer. H. and Hölderich, W., (Eds)., 661.

2) Jacobs, P. A. and von Ballmoos, R., *J. Phys. Chem.*, 1982, **82**, 3050.

3) Chu, C. T. W. and Chang, C. D., *J. Phys. Chem.*, 1985, **89**, 1569.

4) Mohamed, M. M. and Vansant, E. F., *J. Mater. Sci.*, 1995, **30**, 4834.

5) Zholobenko, V. L., Makarova, M. A. and Dwyer, J., *J. Phys. Chem.*, 1993, **97**, 5962.

6) Makarova, M. A., Wilson, A. E., van Liemt, B. J., Mesters, C. M. A. M., de Winter, A. W. and Williams, C., *J. Catal.*, 1997, **172**, 170.

7) Koroda, Y., Konno, S., Yoshikawa, Y., Maeda, H., Kubozono, Y., Hamano, H., Kumashiro, R. and Nagao, M., *J. Chem. Soc. Faraday Trans.*, 1997, **93** (11), 2125.

8) Maache, M., Janin, A., Lavalley, J. C. and Benazzi, E., *Zeolites*, 1995, **15** (6), 507.

9) Wakabayashi, F., Kondo, J., Wada, A., Domen, K. and Hirose, C., *J. Phys. Chem.*, 1993, **97**, 10761.

10) Borida, S., Lamberti, C., Geobaldo, F., Zecchina, A., Turnes Palomino, G. and Otero Areán, C., *Langmuir*, 1995, **11**, 527.

11) Geobaldo, F., Lamberti, C., Ricchierdi, G., Bordiga, S., Zecchina, A., ., Turnes Palomino, G. and Otero Areán, C., *J. Phys. Chem.*, 1995, **99**, 11167.

12) Wakabayashi, F., Kondo, J., Domen, K. and Hirose, C., *Bull. Natn. Sci. Mus. Tokyo Ser.E*, 1994, **17**, 19.

13) Wakabayashi, F., Fujuno, T., Kondo, J.N., Domen, K. and Hirose, C., *J. Phys. Chem.* 1995, **99**, 14805.

14) Emeis, C. A., *J. Catal*, 1993, **141**, 347.

15) Corma, A., Grande, M. S., Gonzales-Alfaro, V. and Orchilles, A. V., *J. Catal.* 1996, **159**, 375.

16) Abbot, J. and Guerzoni, F. N., *Appl. Catal. A,* 1992, **85**, 173.

17) Koroda, Y., Yoshikawa, Y., Konno, S., Hamano, H., Maeda, H., Kumashiro, R. and Nagao, M., *J. Phys. Chem.*, 1995, **99**, 10621.

18) Anpo, M., Matsuoka, M., Shioya, Y., Yamashita, H., Giamello, E., Morterra, C., Che, M., Patterson, H. H., Webber, S., Ouellette, S. and Fox, M. A., *J. Phys. Chem.*, 1994, **98**, 5744.

19) Flego, C., Kiricsi, I., Perego, C. and Bellussi, G., *Cat. Lett.*, 1995, **35**, 125.

20) Beck; K., Brunner; E. and Staudte B., *Z.Phys.Chem.(Munich)*, 1995, **190**, 1 1-8.

21) Warecka, G., Rumplmayr, G. and Lercher, J. A., *Mikrochim. Acta [Wien]*, 1988, **2**, 101.

22) Jacobs, P. A. and von Ballmoos, R., *J.Phys.Chem.* 1982, **86** (15), 3050.

23) Echoufi, N. and Gélin, P., *Cat. Lett.*, 1996, **40**, 249.

24) Borade, R. B., Adnot, A. and Kaliaguine, S., *J. Chem. Soc. Faraday Trans.*, 1990, **86**(23), 3949.

25) Blackmond, D. G. and Goodwin, J. G. Jr., *J. Catal.*, 1982, **78**, 34.

26) Mitani, Y., Tsutsumi, K. and Takahashi, H., *Bull. Chem. Soc. Jpn.*, 1983, **56**(6) 1917.

27) Datka, J., Sulikowski, B. and Gil, B., *J. Phys. Chem.*, 1996, **100**(27), 11242.

28) Fritz, P. O. and Lunsford, J., *J. Catal.*, 1989, **118**, 85.

29) Kubelkova, L., Seidl, V., Novakova, J., Bednarova, S. and Jiru, P., *J. Chem. Soc. Faraday Trans.*, 1984, **80**, 1367.

Chapter 8 Conclusions

The materials studied in this work have a wide range of pyridine adsorption capacities at the conditions employed. However, all the materials were successful, at least for some short time. At least one out of every class of material studied reduced the concentration of pyridine in the simulated stream from 10 ppm to below the analytical detection limit of ca. 0.2 ppm. This illustrates the adsorbent vs hydrotreating debate. Further incremental decreases in nitrogen concentrations achieved through hydrotreating will become exponentially more difficult and possibly expensive. Adsorbent systems as studied in this work, almost inherently reduce the nitrogen concentration to zero. As the concentration of the target molecule decreases, adsorbents become increasingly cost effective whilst the reverse is true for catalytic systems such as hydrotreating. If the movement towards a requirement for lower nitrogen levels in catalytic reformer feed continues, then it may only be a matter of time before adsorbent systems are retrofitted in refineries between the hydrotreating and reforming units.

At the chosen operational temperature of 200 °C, metal sulfates supported on silica gels were found to have quite low adsorption capacities; up to 0.3 wt % pyridine. This is due to a low density of strong acid sites that can retain pyridine at this temperature. Several factors influence the acid site density and hence microadsorption performance. These include the type of silica support, the loading of the sulfate and the type of sulfate used. The Acros silica gel is the most effective of the two silica supports studied. Differences in pore size, particle size and sulfate – support interactions cannot be discounted, but the higher surface area of the Acros gel is probably the primary factor influencing performance. The higher surface area will allow better dispersion of the sulfate. As might be expected the sulfate loading is another important factor. Increasing the sulfate loading increases the number of acid sites generated, regardless of the support, or sulfate used. $NiSO_4$ has proven to be more effective than $Al_2(SO_4)_3$, although it is possible that the 350°C pre-treatment is better suited to $NiSO_4$. Optimisation of these conditions for $Al_2(SO_4)_3$ may improve its performance and restore parity with $NiSO_4$. The use of a larger surface area

support, and higher sulfate loadings, may also increase adsorption capacity for both metal sulfates.

Whilst there is much that can be done to optimise their performance, it is unlikely that their adsorption capacities will ever compete with some of the other samples discussed here. However they do offer a potentially simple method of regeneration, namely dehydration at 400+ °C, or re-hydration at low temperature. These procedures should destroy the acid character of the sulfate and release adsorbed bases.

Aluminas were also found to have low adsorption capacities. Modification with fluoride appears to improve their capacity slightly, but only up to 0.2 wt %. The effect of fluoriding the alumina is unclear. The addition of 1 wt% F^- has increased the number of weak Lewis sites, but removed the few Bronsted sites that were initially present. Increasing the fluoride loading to 14 wt% has introduced weak Bronsted sites, but has dramatically reduced the number of Lewis sites, (especially strong Lewis sites), and reduced the BET surface area slightly. Calcination at 1000°C, to convert γ-alumina to α-alumina, dramatically reduced the BET surface area from ~ 80 m^2g^{-1} to ~ 5 m^2g^{-1}. This reduced the adsorption capacity to virtually zero, and appears to be the single most important factor controlling performance. Samples calcined at 600°C have very similar breakthrough times regardless of fluoride addition. Optimisation of surface area and fluoride loading may yield some improvement in performance, but aluminas are unlikely to compete with some of the other materials in this study.

Amorphous silica-aluminas have been shown to be moderately successful as selective adsorbents for pyridine. Samples with 10 and 25% Al_2O_3 have adsorption capacities of ~ 0.6 wt%, indicating that the optimum composition probably lies between these two values. Higher alumina samples have reduced numbers of both Bronsted and Lewis acid sites. The reduction in the number of Bronsted sites is particularly striking, indicating that as the Al_2O_3 content is increased, the structure becomes increasingly like that of alumina, which generally displays only Lewis acidity. In addition, increasing incorporation of alumina, reduces the mean acid site strength and

lowers BET surface area. The surface area appears to be one of the most important factors influencing the microadsorption performance. There is a close correlation between surface area and breakthrough time. Increasing the surface areas of these materials may lead to a significant increase in adsorption capacity. There is also potential for optimisation of the SiO_2 / Al_2O_3 ratio, which is another important variable.

In many ways MCM-41 can be considered a high surface area silica-alumina, and their pyridine adsorption performances are consequently improved in comparison with amorphous silica-aluminas. They seem to achieve the goal of intermediate acidic strength; strong enough to retain pyridine at the chosen temperature, but not strong enough to activate the hydrocarbon stream and become covered with coke. Acid site density and breakthrough times increase with increasing aluminium content, despite a reduction in the BET surface areas. This appears to be the most important factor influencing adsorption capacity. NH_4^+ ion exchange and calcination also improves microadsorption performance by increasing the number of Lewis acid sites, although the number of strong Bronsted sites is reduced. The large mesopores allows pyridine to diffuse through the structure freely, even when N_2 adsorption isotherms show the pore volume to be reduced by the ion exchange procedure. The best breakthrough time of 175 minutes corresponds to an adsorption capacity of approximately 1.0 wt%. After successful regeneration and re-use this material was only slightly less effective on the second run (within experimental error of the first run). The regeneration (at 650°C) has partly collapsed the mesoporous structure. Further regeneration procedures might lead to increased structural collapse, and failure of the adsorbent.

Future improvements in the synthesis of MCM-41 materials, allowing greater incorporation of aluminium, without loss of surface area and structural stability, may make these materials very attractive for selective adsorption applications. Improved structural stability in aluminium containing samples will improve their resistance to high temperature regeneration. At the same time incorporation of greater amounts of aluminium, with increased surface areas, may improve their adsorption capacities.

Zeolites have the highest adsorption capacities of all the materials studied: up to 2.5 wt %. Important factors in their performance are the Si / Al ratio, the nature of the acid sites, the integrity of the pore structure as well as the shape of the pore structure. As a general trend, the number of acid sites and breakthrough times increase with increasing aluminium content. The high alumina zeolite X had the highest adsorption capacity. However, certain zeolite structures are subject to other factors influencing the adsorption performance.

The mordenites studied have a wide range of breakthrough times. The high silica mordenites performed well, with adsorption capacities of over 2 wt%. Cu^{2+} ion exchange had the effect of removing extra-framework Al and reducing coking, which led to an improvement in microadsorption performance. The higher aluminium mordenites, which in theory should have more acid sites and higher adsorption capacities, failed to perform anywhere near as well as might be expected, especially considering the large amount of adsorbed pyridine observed in the pyridine FTIR spectra. These samples were all derived from Na-mordenite. Sodium Lewis sites have been shown to be inactive for pyridine adsorption, under these experimental conditions, probably as a result of coke deposition. In addition Na^+ Lewis sites are generally only weakly acidic. Consequently the original Na-mordenite only had a low adsorption capacity. Ion exchange with Cu^{2+} or H^+ (via NH_4^+) led to significant improvement, but not to the level of the other mordenites, even when FTIR showed all the Na^+ sites to be removed. Nitrogen adsorption isotherms showed that in all these samples, the accessible pore volume had been reduced to almost zero by the microadsorption experiment. This may be as a result of coke formation, the presence of which has been confirmed by FTIR.

By contrast, the pore structure of ZSM-5 appears to be highly resistant to coke formation. These samples performed well in the microadsorption experiments. The performance was also consistent with their Si / Al ratios, and with the pyridine FTIR results. Nitrogen adsorption isotherms showed the pore structure to be highly accessible after the microadsorption experiments, and no evidence of coke formation was observed by FTIR. The two dimensional pore structure appears to be much better suited to applications involving hydrocarbons than the effectively one-

dimensional structure of mordenite. Ion exchange led to an improvement in performance, irrespective of the exchanging cation, due to removal of extra-framework material.

Pyridine FTIR studies on zeolite X did not show a large amount of adsorbed pyridine, suggesting a low adsorption capacity. In addition FTIR has shown the zeolite X to be extensively de-aluminated. Despite this, and the fact that most of the acid sites were Na^+ Lewis sites, which are ineffective in mordenites, the microadsorption performance was the best of any sample studied. It is possible that only the relatively small number of Bronsted sites are active for pyridine adsorption in this sample.

In general, zeolites have the strongest acid sites of all the materials studied. The high pore volumes and well dispersed acid sites mean that they have very high adsorption capacities for pyridine. However, the high acid strength also makes them prone to coking. Coking is a complex phenomenon, and the nature of the acid sites is an important factor. This is demonstrated by the widely differing breakthrough times for the mordenite samples. The pore structure is also an important factor. The mordenite structure appears to be prone to coke formation, although this is dependent on the cations present. The effectively one-dimensional pores also seem to be very sensitive to this coke formation (and to extra-framework material). The ZSM-5 structure is highly resistant to coke formation, possibly because the 10 membered pores are too small for coke species to form. The two dimensional pores also make ZSM-5 less sensitive to extra-framework material, as pyridine can find an almost infinite number of routes to diffuse from one point in the structure to any other. The pore size does potentially present a problem for use in an industrial application. Basic nitrogen compounds larger than pyridine, i.e. quinoline or heavily substituted quinolines may not be able to enter the pore system of ZSM-5 due to their size. The larger, three dimensional, pore structure of zeolite X has also proven to be effective. The large supercages appear to be able to accommodate extra-framework material without blocking access to adsorbing molecules. Coke formation does not seem to be a problem although this may be a result of the relatively weak acid sites. As Na^+ Lewis sites do not appear to be effective, it may be beneficial to generate a high aluminium zeolite in the H^+ form. Zeolite X is probably unstable in the H^+ form and so zeolite Y

is potentially very interesting. Zeolite Y has the same three dimensional pore structure as zeolite X (faujasite) but has a slightly higher Si /Al ratio. Zeolite Y should be more stable than Zeolite X and so could be studied in the H^+ form without the extensive dealumination that affected zeolite X in this study.

The other porous materials used in this study have much larger pores than zeolites. MCM-41, Amorphous silica-alumina and supported metal sulfates all have mesopores. These pores are all much larger than the dimensions of a pyridine molecule, so pyridine can diffuse through the pores with ease, even if the pore structure is not well defined, and extra-framework material is present. None of these samples appear to generate coke, but this is probably due to the weak acid sites and not the pore structures. At higher temperatures these mesoporous materials might generate coke, although the large pores would probably be able to accommodate coke and still allow pyridine to diffuse through the structure.

FTIR of adsorbed pyridine has proven to be an extremely useful technique to characterise solid acid materials. With the exception of some of the zeolites, which are subject to additional factors other than acid site density and strength, the pyridine FTIR spectral data has been consistent with the microadsorption breakthrough measurements. The use of a Flame Thermionic (Nitrogen Phosphorous) detector in conjunction with G.C. has proven to be a sensitive and reliable method of analysing very low levels of organic nitrogen. The system could be developed for use with a real hydrocarbon stream such as naphtha to quantify and speciate the organic nitrogen compounds. The use of this analytical technique in combination with a bench-top microadsorption apparatus has been very effective in assessing potential basic nitrogen adsorbents.

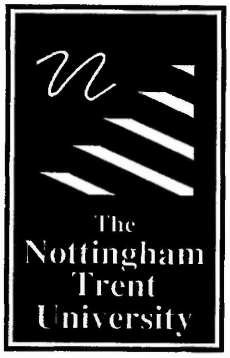

Libraries &
Learning
Resources

The Boots Library: 0115 848 6343
Clifton Campus Library: 0115 848 6612
Brackenhurst Library: 01636 817049